Chemical polarization of the liquid-liquid interface towards controlled cocrystallization

Magdalena Kaliszczak

Ecole Doctorale Chimie - Mécanique - Matériaux- Physique (C2MP) ED 606

Laboratoire de Chimie Physique et Microbiologie pour les Matériaux et l'Environnement (LCPME)

Thèse

Présentée et soutenue publiquement pour l'obtention du titre de

DOCTEUR DE l'UNIVERSITE DE LORRAINE

Mention : CHIMIE

Par **Magdalena KALISZCZAK**

Sous la direction de Grégoire Herzog

POLARISATION CHIMIQUE DE L'INTERFACE LIQUIDE-LIQUIDE VERS UNE COCRISTALLISATION CONTRÔLÉE

12 décembre 2022

Membres du jury :

Directeur(s) de thèse :	M. Grégoire HERZOG	Dr, Chargé de Recherche au LCPME, Université de Lorraine
Président de jury & Rapporteur :	M. Frédéric KANOUFI	Dr, Directeur de Recherche, ITODYS, Université Paris Cité
Rapporteur :	Mme T Jane STOCKMANN	Prof, Memorial University of Newfoundland, Canada
Examinateurs :	M. Enrique ESPINOSA	Prof, CRM2 Université de Lorraine, Nancy
	Mme Encarnacion TORRALBA-PEÑALVER	Dr, ICMPE, Université Paris-Est Créteil, Val de Marne

PhD School Chimie - Mécanique Matériaux- Physique (C2MP) ED 606

Laboratoire de Chimie Physique et Microbiologie pour les Matériaux et l'Environnement (LCPME)

Thesis

Presented and publicly defended for the title of

DOCTOR OF THE UNIVERSITY OF LORRAINE

Mention: CHEMISTRY

By **Magdalena KALISZCZAK**

Supervised by Grégoire Herzog

CHEMICAL POLARIZATION OF THE LIQUID-LIQUID INTERFACE TOWARDS CONTROLLED COCRYSTALLIZATION

Planned defence day: 12 December 2022

Jury members:

Supervisor:	M. Grégoire HERZOG	Dr, Chargé de Recherche au LCPME, Université de Lorraine
President of the jury:		
Reviewers:	M. Frédéric KANOUFI	Dr, Directeur de Recherche, ITODYS, Université Paris Cité
	Mme T Jane STOCKMANN	Prof, Memorial University of Newfoundland, Canada
Examiners:	M. Enrique ESPINOSA	Prof, CRM2 Université de Lorraine, Nancy
	Mme Encarnacion TORRALBA-PEÑALVER	Dr, ICMPE, Université Paris-Est Créteil, Val de Marne

ACKNOWLEDGEMENT

Firstly, I would like to thank my supervisor, Grégoire Herzog, for his advice, guidance and opportunities he gave me during my PhD work. His help during my research was invaluable and for that I am very grateful.

I would also like to express my thanks to all the people who contributed to this work: Manuel Dossot for help in Raman analysis, Pierrick Durand for PXRD and thermal analysis, Emmanuel Wenger for SCXRD analysis, Marc Hébrant for help in HPLC analysis and Imane Bamou and Marina Teresa Garcia Atance for help in experimental work. Also, many thanks to the team in Australia: Damien Arrigan and Franca Jones who were always willing to discuss and give their advice. I would like to thank Claire Genois, our lab technician, for always keeping the chemical stocks up to date, and Mariela Brites Helu, for trainings in SEM and 3D printing, Gérard Paquot and Patrick Bombardier for their technical support when mechanical problems occurred during my experiments. Many thanks Marie Tercier, Christelle Charbaut and Sandrine Lemoine for their help with administrative matters. I would also like to thank the other members of my ELAN team: Alain Walcarius, Mathieu Etienne and Liang Liu who offered advice and ideas, I always appreciated their useful comments during the group meetings.

In addition, many thanks to my younger colleagues in the laboratory: Joanna Roginska, Ranine El Hage, Julius Gajdar, Madjid Tarabet, Harpeet Sighn, Gustavo Salazar, Qiao Liu, Jessie Hollywood and Clara Richart, who were always there to help, with whom we spent time both in the laboratory during lunches and outside the laboratory during trips and ‘aperos’.

And finally, I would like to thank my family and friends in Poland who have helped me during these three years, I am very grateful to you. Especially my mum, my dad, my sister who supported me from afar and visited me when they could and my husband who was with me and supported me every day.

Table of contents

RESUME

La cristallisation est un processus impliquant la nucléation et la croissance pour former des matériaux solides qui joue un rôle crucial dans de nombreuses industries (pharmaceutique, chimique et alimentaire) et dans de nombreux phénomènes naturels . La nucléation est l'étape cruciale de la cristallisation car c'est la formation de la nouvelle phase qui décide de la forme et de la distribution de la taille des cristaux. Le contrôle de la sursaturation et de la température de nucléation, la sélection du solvant, la présence d'additifs, l'application d'un champ externe ou la modification de la surface peuvent conduire à une nucléation sélective. De cette façon, la formation du polymorphe souhaité est possible.

La plupart des produits pharmaceutiques se présente sous forme solide, par exemple sous forme de capsules, de comprimés et de suppositoires. Les propriétés physicochimiques des médicaments sont cruciales pour leur efficacité et ces propriétés dépendent des différents états cristallins. On estime que 80 % des médicaments présentent un polymorphisme. La recherche de méthodes de cristallisation innovantes est un sujet d'intérêt constant de l'industrie pharmaceutique car la plupart des médicaments se présente sous des formes cristallines dont les polymorphes peuvent avoir un point de fusion, une solubilité, une vitesse de dissolution, une stabilité thermique, une biodisponibilité, une toxicité ou une hygroscopicité différents. Un autre problème rencontré dans le développement des médicaments est la mauvaise stabilité dans l'eau des ingrédients pharmaceutiques actifs (API) solides, qui entraîne des problèmes de fabrication et de stockage.

Les cocristaux pharmaceutiques est une classe moderne de substances pharmaceutiques, qui peut améliorer les propriétés des médicaments. Les cocristaux sont des matériaux cristallins structurellement homogènes contenant deux ou plusieurs composants présents en quantités stœchiométriques définies. Les cocristaux pharmaceutiques peuvent incorporer des molécules invitées pharmaceutiquement acceptables dans un réseau cristallin avec l'API, sans affecter l'activité pharmacologique du médicament. La formation de cocristaux peut améliorer les propriétés du médicament, sans altérer leur comportement pharmacologique. Les cocristaux peuvent être formés par des interactions non covalentes (par exemple, des liaisons hydrogène) entre des groupes fonctionnels tels que l'acide carboxylique-amide et l'alcool-pyridine, les forces de van der Waals et l'empilement π-π. Les conservateurs, excipients, vitamines, minéraux, acides aminés, biomolécules ou autres médicaments peuvent être utilisés comme coformeurs. La

cocristallisation entraîne l'apparition de nouvelles phases polymorphes. Leur formation dépend de la méthode choisies et des solvants utilisés. Le choix du polymorphe est important en raison de ses propriétés physico-chimiques dans le processus de développement du médicament, de sa biodisponibilité et des questions de propriété intellectuelle. La formation contrôlée de cocristaux est un objectif important dans le développement de médicaments. Ce travail a utilisé l'électrochimie à l'interface entre deux liquides non miscibles (ITIES) pour contrôler la formation de cocristaux.

Dans la première partie, le comportement électrochimique de la caféine a été étudié au moyen de la voltampérométrie cyclique (CV) et de la voltampérométrie à courant alternatif (ACV). La caféine est un alcaloïde purique, qui a un effet stimulant sur le système nerveux et est utilisée pour renforcer l'action des médicaments analgésiques et antipyrétiques. La caféine est instable dans un environnement humide et a tendance à se transformer en hydrates instables. Elle est utilisée comme un composé modèle dans les essais de cocristaux avec des acides carboxyliques, puisque de tels cocristaux sont connus pour améliorer les propriétés physiques de la caféine. En CV, le signal électrochimique enregistré est généré par le transfert d'espèces ioniques à travers l'interface. Le transfert des espèces ioniques est induit par l'application d'une différence de potentiel de Galvani ($\Delta_o^w\phi$) à travers l'interface. Si un potentiel standard positif est appliqué à l'interface, il provoquera un excès de cations dans la phase aqueuse et un excès d'anions dans la phase organique. La charge enregistrée est proportionnelle à la quantité d'espèce ionique mais la différence de potentiel à laquelle un transfert est observé, donne une indication de la nature de l'espèce ionique transférée. Ainsi, les cations transférés de la phase aqueuse à la phase organique et les anions transférés de la phase organique à la phase aqueuse donnent lieu à un courant positif et, à l'inverse, les anions transférés de la phase aqueuse à la phase organique et les cations transférés de la phase organique à la phase aqueuse donnent lieu à un courant négatif. La caféine est un cation hydrophile donc, elle a été transférée à un potentiel hautement positif. Le transfert de la caféine ($CaffH^+$) a été vérifié à différents pH et le pH 2 a été choisi comme étant le plus optimal pour la formation de cocristaux. L'expérience de contrôle a prouvé que le 1-hydroxy-2-naphtoïque (1H2N) ne transfère pas à l'ITIES. L'ACV a fourni des informations sur l'influence de la composition de la phase aqueuse et organique. Lorsque $\Delta_o^w\phi$ a augmenté vers des valeurs plus positives, la capacité était plus élevée lorsque $CaffH^+$ seul, 1H2N seul et 1H2N et $CaffH^+$ étaient présents dans la phase aqueuse. Ces résultats suggèrent que ces deux molécules sont actives au niveau interfacial.

Dans la deuxième partie, la cocristallisation de Caff et 1H2N a été étudiée à l'ITIES sous polarisation chimique. L'interface a été polarisée par l'ajout d'anions hydrophobes à la phase organique. De cette façon, une cocristallisation sélective a été obtenue, confirmé par la diffraction des rayons X et la spectroscopie Raman. Un système biphasique a été étudié avec de la caféine dissoute dans la phase aqueuse et du 1H2N dissous dans la phase organique. L'interface a été polarisée chimiquement en dissolvant différents sels dans la phase organique. On a constaté que la polarisation de l'interface favorisait la formation d'une phase plutôt que l'autre.

Afin de connaître la structure cristallographique et les phases polymorphes, les cocristaux ont été examinés par diffraction des rayons X sur monocristal (SCXRD). Les phases détectées dans les cocristaux correspondaient aux cocristaux de Caff :1H2N déjà publiés dans le Cambridge Crystallographic Data Centre (CCDC). Les mesures ont montré l'existence de deux phases cristallographiques : I et II. Ces complexes cristallisaient dans le groupe spatial monoclinique P21/n avec une quantité stœchiométrique de $CaffH^+$ et 1H2N. $CaffH^+$ et 1H2N ont interagi par liaison hydrogène entre les groupes carbonyle et imidazole. La SCXRD est une technique puissante pour la détermination de la structure cristallographique, cependant elle n'est pas représentative de la totalité d'un échantillon car un seul cristal est nécessaire pour l'analyse. Par conséquent, afin de connaître la structure représentant l'ensemble de l'échantillon, les cocristaux en poudre ont été analysés par diffraction des rayons X sur poudre (PXRD). On a constaté que la forte polarisation de l'interface favorisait la phase I par rapport à la phase II. Les analyses PXRD des poudres recueillies pour des concentrations de 30 mM et de $CaffH^+$ saturé ont montré que la phase I prédominait dans l'échantillon lorsque l'interface était polarisée positivement, tandis que la phase II était plus présente dans l'échantillon référence. Les molécules conformères incorporent le cocristal en croissance des deux côtés de l'interface, en raison d'un gradient de concentration, qui peut être contrôlé par la différence de potentiel. À pH = 2, la caféine est protonée et, par conséquent, chargée positivement. La différence de potentiel élevée a provoqué le transfert de la caféine cationique, et a conduit à la concentration localement sursaturée et donc à la cocristallisation à l'interface liquide-liquide. Lorsque l'interface était polarisée avec le potentiel le plus bas, la formation de cocristaux était inhibée. Lorsque l'interface est polarisée positivement, la prédominance de la phase I augmente avec la concentration croissante de caféine dans la phase aqueuse, ce que nous n'avons pas observé dans les expériences de contrôle. Les spectres Raman ont montré une différence significative dans les bandes caractéristiques entre les cocristaux de

Caff: 1H2N et les réactifs, confirmant que les matériaux de départ n'étaient pas présents dans le produit collecté à l'interface. Deux pics distincts peuvent être observés aux longueurs d'onde de 1378 cm^{-1} et 1648 cm^{-1}. Le déplacement du pic à 1378 cm^{-1} par rapport à la caféine pure est dû à la liaison hydrogène entre le cycle imidazole de la caféine et le groupe carboxyle de 1H2N, tandis que le déplacement Raman à 1648 cm^{-1} est causé par le pic d'étirement C=O impliqué dans la liaison hydrogène intermoléculaire dans l'acide naphtoïque. Les décalages obtenus dans la région 1300-1800 cm^{-1} sont caractéristiques d'un complexe 1 :1 avec des liaisons hydrogène entre les deux molécules, ce qui est cohérent avec les résultats de l'analyse en diffraction des rayons X (DRX).

En effet, les analyses des poudres recueillies par DRX pour une concentration de 30 mM et de Caff saturé ont montré que la phase I était prédominante dans l'échantillon lorsque l'interface était polarisée, alors que la phase II était plus présente dans l'échantillon de référence. De plus, dans chaque échantillon, il y a une petite impureté provenant de la poudre de caféine, mais il n'y a aucun résidu de 1H2N, et des autres sels présents dans le système. Des potentiels interfaciaux positifs ont favorisé la formation d'une forme polymorphe de cocristal de Caff: 1H2N et un potentiel négatif a inhibé la cocristallisation à l'interface liquide-liquide. Cette approche du contrôle électrochimique de la cocristallisation ouvre de nouvelles possibilités pour le développement de médicaments.

Dans la troisième partie, la mesure simultanée des variations de potentiel (ΔE) et de courant (I) à l'interface liquide-liquide, polarisée en utilisant des cations tétraalkylammonium (TAA^+) comme ion commun, a été rapportée. Il s'agit du contrôle du potentiel interfacial par la dissolution d'un ion commun dans chaque phase, sans utiliser d'électrodes. En faisant varier initialement la concentration de l'ion commun dans les phases aqueuses ou organiques, on peut modifier la différence de potentiel. La distribution des ions entre les phases produit une différence de potentiel électrique entre les phases. Divers rapports de concentration de tétraméthyl-, tétraéthyl- et tétrapropylammonium (TMA^+, TEA^+ et TPA^+) ont été dissous dans les deux phases. Ces systèmes biphasiques ont ensuite été utilisés pour vérifier que la différence de potentiel interfacial mesurée correspondait aux calculs théoriques. Ce dispositif expérimental a ensuite été utilisé pour étudier le processus de cocristallisation interfaciale de $CaffH^+$ hydrophile et cationique avec 1H2N lipophile. La présence de caféine dans la phase aqueuse a conduit à des valeurs de courant plus élevées, causées par le transfert de charge interfacial. De telles variations de courant ont été

observées aussi bien en l'absence qu'en présence de 1H2N dans la phase organique. L'analyse du bruit du courant électrochimique a montré une nette différence entre les cellules dans lesquelles les cocristaux sont formés et celles dans lesquelles la cocristallisation est empêchée, soit par un potentiel négatif, ou par l'augmentation du pH. La méthode ECN est un outil puissant pour suivre les changements qui se produisent aux ITIES dans les expériences sur les ions communs par la mesure simultanée du potentiel et du courant. Le bruit électrochimique (EN) est une méthode couramment utilisée dans les études de corrosion, qui permet la mesure simultanée du courant et du potentiel pour identifier les différents types d'événements de corrosion. Nous proposons ici de suivre simultanément les changements de courant et de potentiel associés aux événements de cocristallisation à une interface liquide-liquide polarisée par un ion commun dissous dans chaque phase. L'EN a été appliquée pour mesurer le potentiel et le courant de manière synchrone. Les cellules électrochimiques ont été placées dans une cage de Faraday mise à la terre. Les mesures ont été effectuées pendant 1 heure pour permettre à la répartition des ions d'atteindre l'équilibre à l'interface liquide/liquide. Les mesures ont été commencées juste après la préparation des cellules électrochimiques. Le potentiel est stable dans le temps et sa valeur diminue avec le rapport $\frac{c^o_{TAA^+}}{c^w_{TAA^+}}$. Des résultats similaires ont été obtenus pour les trois ions, TMA^+, TEA^+ et TPA^+, ce qui indique que le transfert n'est pas basé sur le potentiel de transfert formel, mais sur le rapport de concentration de TAA^+ dans chaque phase.

Dans la partie suivante de l'étude, les solutions étant bien définies et conformes à la théorie, nous avons mis en place la cellule électrochimique avec une solution saturée de Caf comme phase aqueuse et 1H2N comme phase organique dans les conditions suffisantes pour transférer la caféine. Ici, la formation de cristaux à l'interface a été observée. En l'absence de caféine, les valeurs de la moyenne quadratique du courant (I_{rms}) sont très faibles tout au long de l'expérience, ce qui suggère qu'il n'y a pas de transfert de charge interfacial. Lorsque la caféine est présente dans la phase aqueuse, les valeurs I_{rms} sont plus élevées, que le 1H2N soit présent ou non dans la phase organique. Comme expérience de contrôle, le courant et le potentiel ont été mesurés en présence de caféine et de 1H2N mais lorsque le potentiel interfacial est négatif, ce qui est défavorable à la formation de cocristaux de caféine : 1H2N. Les valeurs I_{rms} dans ces conditions expérimentales sont similaires à celles observées en l'absence de caféine confirmant que les valeurs I_{rms} élevées sont liées au transfert de charge de la caféine, lorsque le potentiel d'interface est positif. Dans la

cellule électrochimique, lorsque les cocristaux sont créés, l'impédance du bruit (R_{sn}) à basse fréquence diminue dans les premiers 1000 s, ce qui peut être attribué à la création du complexe Caff/1H2N et au faible bruit du courant. Après ces temps, la résistance faiblit, ce qui peut être lié à l'absorption du complexe au niveau des ITIES. Contrairement à une cellule dans laquelle le complexe n'est pas formé, la variation de la R_{sn} ne change pas de manière significative au cours d'une expérience. L'impédance de bruit a des valeurs plus faibles au début, parce que la croissance ou l'absorption du cocristal sur le LLI n'a pas lieu - la caféine est transférée et le courant a des valeurs plus élevées. En outre, les valeurs PSD_I (Densité Spectrale de Puissance du courant) lorsque des cocristaux sont formés sont inférieures d'un ordre de grandeur à celles de l'expérience avec l'absence de 1H2N dans la cellule électrochimique. Ceci est dû à la formation de complexes provoquant les changements à l'interface liquide-liquide qui retiennent le transfert de caféine. Le signal s'estompe plus rapidement lors de la formation du cocristal car la caféine entre en réaction avec 1H2N et leur adsorption à l'ITIES. En revanche, en l'absence de 1H2N, la caféine continue à être transférée vers la phase organique. Ceci suggère que le transfert de caféine est responsable du PSD_I.

Dans la dernière partie, des cocristaux ont été formés sur les ITIES selon les conditions choisies par la méthode des plans d'expériences Différents facteurs ont été testés : électrolytes en phase aqueuse, divers solvants et sels appliquant un potentiel positif. Le plan d'expériences est la partie de la statistique appliquée dans laquelle des études contrôlées sont planifiées, menées, analysées et interprétées. L'objectif est d'évaluer les facteurs qui contrôlent la valeur d'un paramètre ou d'un groupe de paramètres. Avec le plan d'expériences, nous pouvons manipuler un certain nombre de facteurs d'entrée et examiner leur impact sur la sortie souhaitée (réponse). La formation de cocristaux de Caff : 1H2N cocristaux à une interface eau-huile a été étudiée en préparant une série de flacons dont les conditions expérimentales varient. Les cocristaux ont été collectés à l'interface, séchés à l'air et analysés par DRX pour vérifier les différences dans le contenu de la phase I et II. Dans tous les flacons, l'interface était positivement polarisée, impliquant toutefois différents sels imposant un potentiel élevé (KTPBCl, KTB et LiTB) et divers solvants en phase organique (1,2-dichloroéthane (DCE) et le mélange anisole: trifluorotoluène (A:TFT)). L'analyse DRX a montré les conditions permettant d'obtenir une phase I et une phase II presque pures. L'étude des ΔE et I simultanés et de la tension interfaciale a prouvé que le potentiel appliqué influence la cinétique du processus de cocristallisation. Des valeurs de ΔE plus faibles ont été mesurées lorsque KTPBCl

était présent dans le flacon, ce qui signifie une cinétique de transfert plus lente de $CaffH^+$. Le potentiel appliqué influence la cinétique du processus, car des cristaux de différentes phases ont été obtenus.

Il a été prouvé que la tension interfaciale fournit des informations importantes sur la nature des solvants et des électrolytes utilisés pour les mesures et son impact sur la cinétique qui contrôle les processus qui se produisent aux ITIES. Les différences dans les valeurs de tension interfaciale entre DCE et le mélange A:TFT suggèrent que non seulement la composition des phases joue un rôle dans la tension superficielle mais aussi le choix du solvant. La tension interfaciale a diminué avec l'augmentation de l'hydrophobie du cation organique (TB^- > $TPBCl^-$). En comparant les résultats des mesures de tension superficielle à ceux obtenus par l'analyse DRX, nous voyons que lorsque la phase I pure a été obtenue, la tension superficielle est beaucoup plus élevée que lorsque la phase II pure a été obtenue. Les cocristaux de la phase I se sont formés dans la cellule lorsque nous avions alors LiCl en phase aqueuse et KTPBCl en phase organique. Les deux cations Li+ et K^+ et l'anion Cl^- ont des propriétés chaotropiques. Ils ont provoqué le mélange des solvants à l'ITIES ce qui a conduit à un accès plus facile de $CaffH^+$ à 1H2N et à la création des cocristaux du côté organique de l'interface. Dans d'autres cas, les anions et les cations présents dans la phase aqueuse et organique ont créé des conditions plus kosmotropes. Il existe une corrélation importante entre la tension de surface et les mesures de capacité. L'augmentation de la capacitance dans le LiCl peut être causée par la présence de Cl^- plus chaotrope dans la phase aqueuse. Il a étendu la couche de largeur des solvants mélangés (eau/DCE) et le $CaffH^+$ a pénétré l'interface. De plus, la tension interfaciale plus élevée dans les flacons avec KTPBCl que KTB et LiTB pourrait avoir favorisé la cocristallisation de la phase I plutôt que de la phase II. Tandis que les mesures de la tension interfaciale ont montré que les effets de Cl^-, $CaffH^+$ et $TPBCl^-$ et du 1,2-dichloroéthane pourraient favoriser la phase I polymorphe préférentielle tandis que la forme II semble être favorisée par $SO4^{2-}$, TB^- et le mélange Anisole : TFT. Le plan d'expérience a indiqué que le sel organique est le facteur ayant un impact actif sur la cocristallisation aux ITIES.

ABSTRACT

Controlled formation of cocrystals is an important objective in drug development. This work used the electrochemistry at the interface between two immiscible liquids (ITIES) to control the formation of cocrystals. In the first part, the electrochemical behaviour of caffeine was investigated by means of cyclic voltammetry (CV) and alternating current voltammetry (ACV). The caffeine is the hydrophilic cation thus, it transferred at highly positive potential. Transfer of caffeine (Caff) was verified at various pH and the pH 2 was chosen to be the most optimal for the cocrystals formation. The control experiment proved that 1-hydroxy-2-naphthoic (1H2N) did not transfer at ITIES. ACV provided the information about the influence of the aqueous and organic phase composition. When $\Delta_o^w\phi$ increased to more positive values, capacitance (C) was higher when $CaffH^+$ alone, 1H2N alone and both 1H2N and $CaffH^+$ were present in the aqueous phase. These suggest that these two molecules are interfacially active.

In the third part the simultaneous measurement of potential (ΔE) and current (I) variations at the ITIES, which were polarised using tetraalkylammonium cations as a common ion was reported. Various concentration ratios of tetramethyl-, tetraethyl-, and tetrapropylammonium were dissolved in both phases. Such biphasic systems were then used to verify that the interfacial potential difference measured fit the theoretical calculations. This experimental set-up was next used to probe the interfacial cocrystallisation process of hydrophilic and cationic $CaffH^+$ with lipophilic 1H2N. The presence of caffeine in the aqueous phase led to higher current values, caused by interfacial charge transfer. Such current variations were observed both in the absence and in the presence of 1H2N in the organic phase. Analysis of the electrochemical current noise showed a clear difference between cells in which cocrystals are formed and those in which cocrystallisation is hindered, either by a negative potential or by a change in pH. The EN method is a powerful tool to follow the changes occurring at ITIES in common ion experiments by simultaneous measurement of potential and current.

In the last part, cocrystals were formed on the ITIES according to the conditions chosen by the design of experiments (DoE) method. Various factors were tested: electrolytes in the aqueous phase, various solvents and salts applying positive potential. The XRD analysis showed the conditions to obtain almost pure Phase I and almost pure phase II. Study of simultaneous ΔE and I and the interfacial tension proved that the applied potential influences the kinetics of the

cocrystallization process. The interfacial tension measurements showed that effects from Cl^-, $TPBCl^-$ and 1.2-dichloroethane might favour the preferential phase I polymorph while SO_4^{2-}, TB^- and a:TFT might favour phase II formation. DoE method indicated organic salt as the factor having an active impact on cocrystallization at ITIES.

FREQUENTLY USED ABBREVIATIONS

1H2N – 1-hydroxy-2-naphthoic acid

BA^+ – bis(triphenylphosphoranyldiene) ammonium cation

$CaffH^+$ – caffeine cation

Caff: 1H2N – cocrystals of caffeine and 1-hydroxy-2-naphthoic acid

CE – counter electrode

CV – cyclic voltammogram

DCE – 1.2-dichloroethane

EN – electrochemical noise

ITIES – interface between two immiscible solvents

RE – reference electrode

SEM – scanning microscopy

TEA^+ – tetraethylammionium cation

TMA^+ – tetramethylammonium cation

TPA^+ – tetrapropylammonium cation

$TPBCl^-$ – tetrakis (4-chlorophenyl) borate anion

TB^- – tetrakis (pentafluorophenyl) borate

$\Delta_o^w\phi$ – standard transfer potential

`

1. INTRODUCTION

This chapter introduces the subjects of my PhD, defines terms that are frequently used and introduces the main aspects to be studied in the thesis.

1.1. General interest for crystallization

Crystallisation is a process involving nucleation and growth to form solid materials. This process plays a crucial role in many industrial and natural processes such as pharmaceutical, chemical and food industries. Nucleation is the crucial stage in crystallization and it is the formation of the new phase which decides about the form and crystal size distribution. The control of the supersaturation and nucleation temperature, solvent selection, presence of the additives, application of an external field or surface modification can lead to selective nucleation. In this way, the formation of the desired polymorph is possible.[1], [2] As the crystallization occurs in many different environments, it sometimes has an undesirable outcome. For example, the formation of inorganic barium sulphate in offshore oil production. This crystallisation limits the rate and extent of oil recovery. Sulphate-rich seawater mixes with barium-rich aquifer water, a supersaturated environment is created which leads to crystallisation of barium sulphate ($BaSO_4$) in rock pores or in the pipeline.[3] Nucleation on such water-oil phases is often heterogeneous and this nucleation is a practical problem in the crystallisation process.

Crystallization is the most efficient method to separate and to purify active pharmaceutical ingredients (API). It is the final and critical process in drug manufacturing.[4] In the pharmaceutical industry, there are crystallizations from the solution, from melt and from the gas phase. The quality of a pharmaceutical product is assessed in terms of purity, size distributions, polymorphism, and mechanical strength of the crystal, morphology and residual solvent. The control of these properties is controlled by the choice of solvent, supersaturation conditions, mixing, geometry of the crystallizer, seeding and external control.[5]

Most of pharmaceutical products are in solid forms e.g. capsules, tablets and suppositories. The physiochemical properties of medicines are crucial in their efficacy and these properties depend on different crystalline states. It is estimated that 80% of drugs show polymorphism.[6] The search for innovative crystallisation methods is a subject of constant interest of the pharmaceutical industry as most drugs appear in crystalline forms whose polymorphs may have different melting

point, solubility, dissolution rate, thermal stability, bioavailability, toxicity or hygroscopicity [7]–[11]. An additional issue encountered in drug development is the low stability in humid environments of the solid APIs, resulting in manufacturing and storage problems.[12]

There is a need in the pharmaceutical industry for high-throughput technologies for predicting crystal structures and which will allow *in situ* screening and testing of new crystal forms. Crystal engineering is a way of designing crystals with desired physiochemical properties. The physicochemical properties can be improved by changing the physical forms of the drug through the formation of polymorphs, salts[17], hydrates, amorphous, solvates[18], cocrystals, etc.[19] Among the methods of improving drug forms are cocrystals (Figure 1.1).[20]

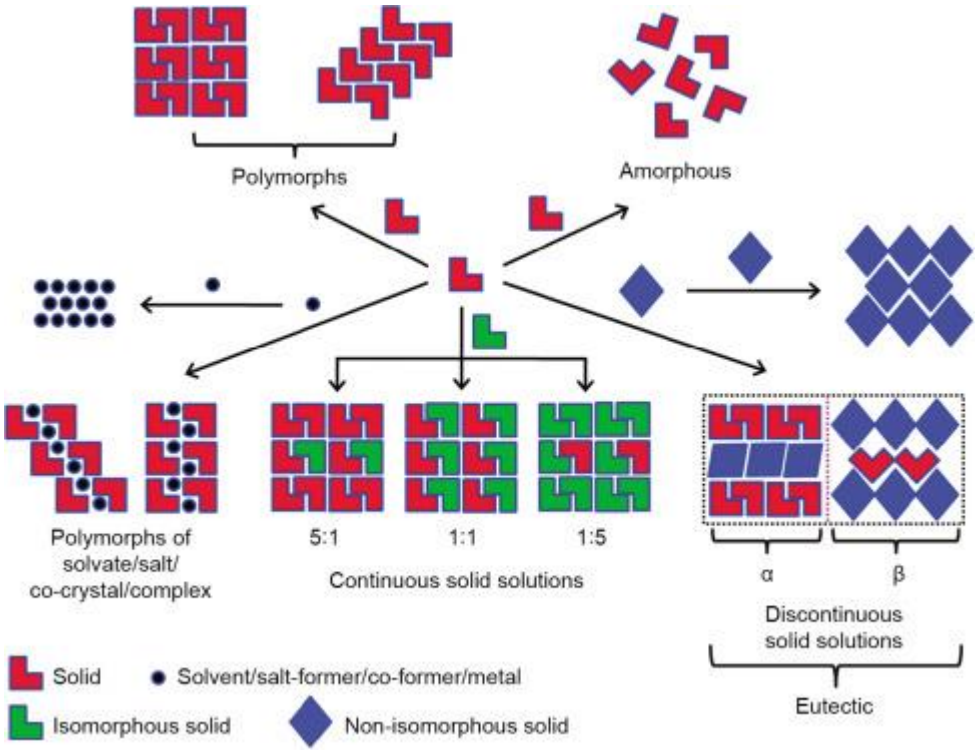

Figure 1.1: Pharmaceutical solids structural diversity.[20]

1.2. Cocrystals and methods of cocrystallization

A drug cocrystal is a modern class of pharmaceutical substances, which can improve drugs properties. They have gained great popularity and interest because of their potential in making multicomponent and improved drugs.[21] Pharmaceutical cocrystals may contain two or more

guest molecules recognized as safe (e.g. preservatives, excipients, carboxylic acids) or another drug incorporated with the API in the crystal lattice in definite stoichiometric amounts, without affecting the pharmacological activity of the drug.[22], [23] Figure 1.2 present structural relationship in cocrystals between API and cocrystal conformer (CFF).

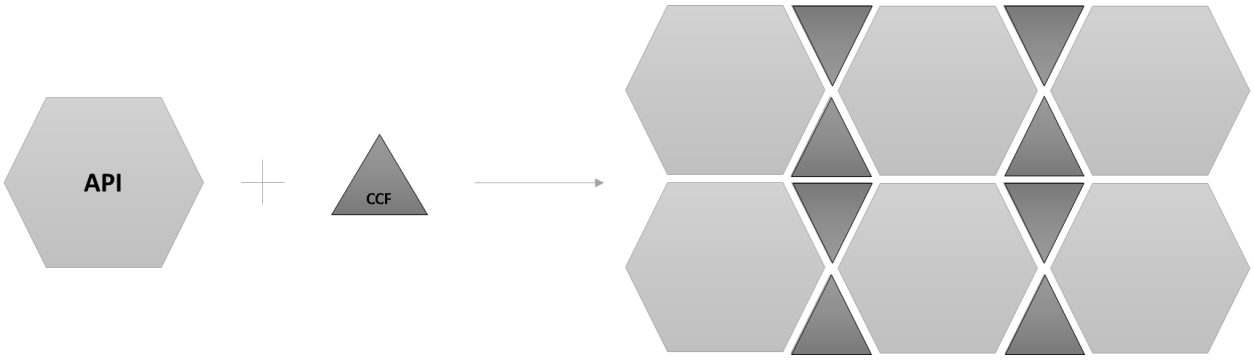

<u>Figure 1.2:</u> Schematic illustration of structural relationships in cocrystals.[9] *API – active pharmaceutical ingredient, CCF – cocrystal conformer.*

Cocrystals can be formed by non-covalent interactions (e.g. hydrogen bonds) between functional groups such as carboxylic acid–amide and alcohol–pyridine, van der Waals forces and π-π stacking [10], [24]. The most common hydrogen bond in cocrystals are presented on Figure 1.7. Several mechanochemical methods such as grinding in presence or absence of solvents[25] and solvent based methods: e.g. solvent evaporation, solvent cooling, cocrystallisation from melt, different types of grinding and slurrying, anti-solvent cocrystallisation,[26] and liquid-liquid crystallization[27] are used to form cocrystals. Cocrystallisation results in the appearance of new polymorphic phases[28]. Their formation depends on the method of cocrystal formation[10], [29] and the solvents used[30]. The polymorph selection is important due to the physiochemical properties in drug development process, bioavailability and patent issues. On the market there are commercially available cocrystals of drugs with carboxylic acids like ertugliflozin with L-pyroglutamic acid (Steglaro)[31], with another drug which consists of valproic acid and sodium valproate (Depakote)[32], escitalopram-oxalate (Seroplex)[33] or celecoxib with tramadol (Seglentis) [34].

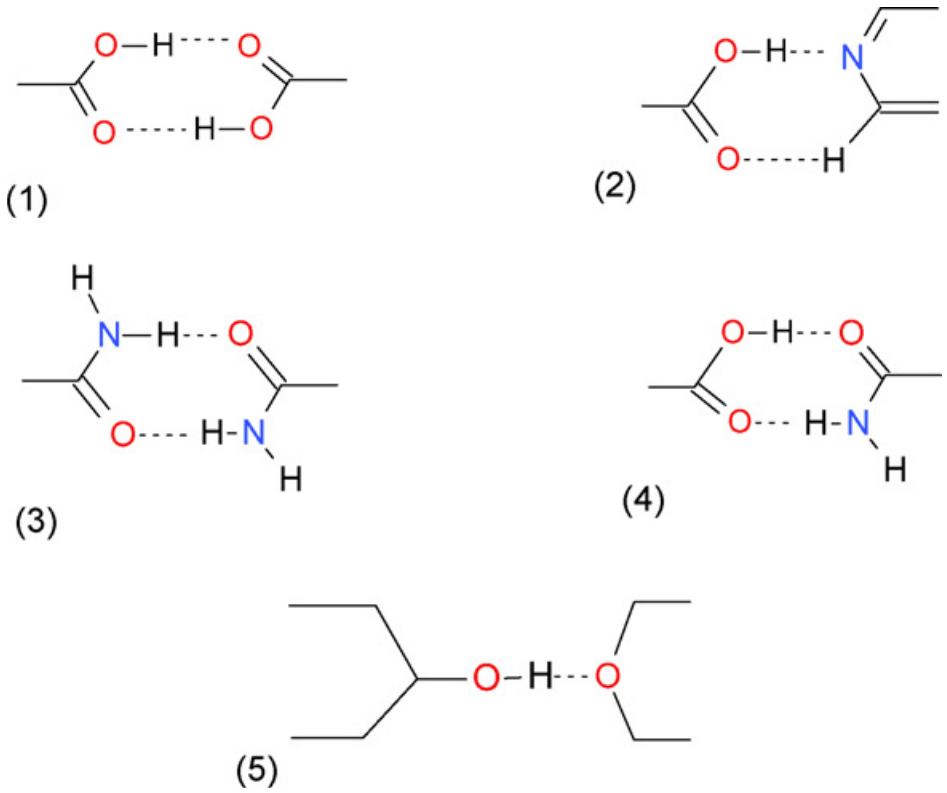

Figure 1.3: The most common hydrogen bonds utilised in cocrystal engineering. (1) carboxylic acid homosynthon, (2) carboxylic acid – pyridine heterosynthon, (3) amide homodimer, (4) carboxylic – amide heterosynthon, (5) alcohol - ether heterosynthon[22].

1.2.1. Properties and cocrystals of caffeine

Caffeine (Caff) is a bitter, white crystalline powder. It is a purine alkaloid, which has a stimulating effect on the nervous system and is used to reinforce analgesic and antipyretic drugs action.[12] Usually, Caff is extracted from plans e.g. guarana, yerba mate, coffee, cacao[35]. In medicine, Caff is used as an analgesic adjuvant in fatigue, apnea or drowsiness treatment.[36] Caffeine is a weak base, with a pKa around 10 [37]. Therefore, the salt formation is an issue because of the difference between the caffeine pKa and the pKa of the suitable ion is not big enough[20]. Generally it exists in two anhydrous forms α and β which at atmospheric humidity convert to a nonstoichiometric hydrate.[12], [38], [39] Caffeine is often used as a model compound in cocrystal studies with carboxylic acids, since such cocrystals are known to improve its physical properties. There are many examples of cocrystals of caffeine with various coformers and they are presented

in Table 1.1. In the table are listed: name of the cocrystal conformer, method of cocrystallization and reference.

Table 1.1: Examples of the most representative cocrystal coformers for caffeine and methods of obtaining them and reference.

Cocrystal coformer	Method of cocrystallization	Reference
1-hydroxy-2-naphthoic, 3-hydroxy-2-naphthoic acid, 6-hydroxy-2-naphthoic acid	Slow evaporation	[39]
	Cocrystallization at solvent interfaces	[27]
2-hydroxy-1-naphthoic acid	Solution-mediated phase transformation (SMPT) slurrying	[40]
Adipic acid	Solution-mediated phase transformation (SMPT) slurrying	[41]
Citric acid	Liquid assisted grinding	[42]
	Slurrying	[24]
D, L-tartaric acid	Liquid Assisted grinding	[43]
Dapson	Liquid assisted grinding, spray drying, solvent evaporation	[44]
Gallic acid	Non-photochemical laser-induced nucleation	[45]
Glutaric acid	Solvent Drop Grinding	[46]
	Liquid assisted grinding	[38]
	Slow evaporation	[12]
	Slow evaporation	[47]

	Ionic liquid-assisted grinding	[48]
Hydroxybenzoic acid	Slurrying	[49]
L-malic acid	Liquid assisted grinding	[50]
Maleic acid	Grinding	[51]
	Solution and grinding methods	[12]
Malonic acid	Solution and grinding methods	[12]
Nicotinamide	Cooling crystallization	[52]
Oxalic acid	Solution precipitation and by solid-state grinding	[12]
	Extrusion	[53]
	Laser irradiation	[54]
Succinic acid	Liquid assisted grinding, slow evaporation,	[55]
Urea	Milling	[56]

The cocrystals of caffeine were formed with various coformers listed in Table 1.1. These studies resulted in many polymorphic forms. Their properties and the factors influencing the formation of the selected polymorph have been the subject of many studies. The cocrystals of caffeine with a series of dicarboxylic acids e.g. glutaric, oxalic, maleic and malonic were prepared and their relative hydration (RH) stability was studied by varying the humidity conditions.[12] The two polymorphic forms (Form I and form II) of glutaric acid were found and they were obtained in grinding, slurrying or solution cocrystallization.[48] The formation of these polymorphic forms were further investigated and the influence of solvent used for liquid-assisted grinding was found. The use of non-polar solvents e.g. heptane, or hexane resulted in Form I while the presence of solvents like acetonitrile, water or chloroform leaded to Form II formation.[38] Other studies of caffeine and maleic acid also proved the importance of solvent selection. Cocrystals with

stoichiometry 2:1 were obtained in ethyl acetate [51] when 1:1 was obtain by grinding with toluene [12]. In some screening method only one polymorphic form was obtained e.g. caffeine and adipic acid cocrystals, regardless of the solvent used for SMPT slurring technique [41]. The cocrystals of caffeine and three naphthoic acids were obtained during slow evaporation from acetonitrile. For all three hydroxyl-2-naphthic acid only one polymorphic form 1:1 was found; however, unusual dimers were formed due to hydroxyl-caffeine heterosynthons [39]. Interestingly, other forms were found during interfacial cocrystallization of the same components and it will be discussed in Chapter 1.2.2.

1.2.2. Cocrystals of caffeine at liquid-liquid interface

The first attempts to crystallize caffeine with hydroxyl-2-naphthoic (xH2N) acids were carried out at non-polarised water-organic interface.[27] The three xH2N were studied as a coformers: 1-hydroxy-2-naphthoic acid (1H2N), 3-hydroxy-2-naphthoic acid (3H2N) and 6-hydroxy-2-naphthoic acid (6H2N) which can boost the stress lowering effect.[57] The experimental conditions and structure of the caffeine and coformers are shown in Figure 1.4. The polymorphism of the cocrystals was studied in different solvents, temperature and while stirring. Changing solvents resulted in different polymorphic forms for the three coformers. The more polar solvents favoured form I (1:1). Temperature accelerated the formation of interfacial cocrystals, while mixing changed the stoichiometry and, in the case of 3H2N and 6H2N, resulted in the formation of form II than form I.

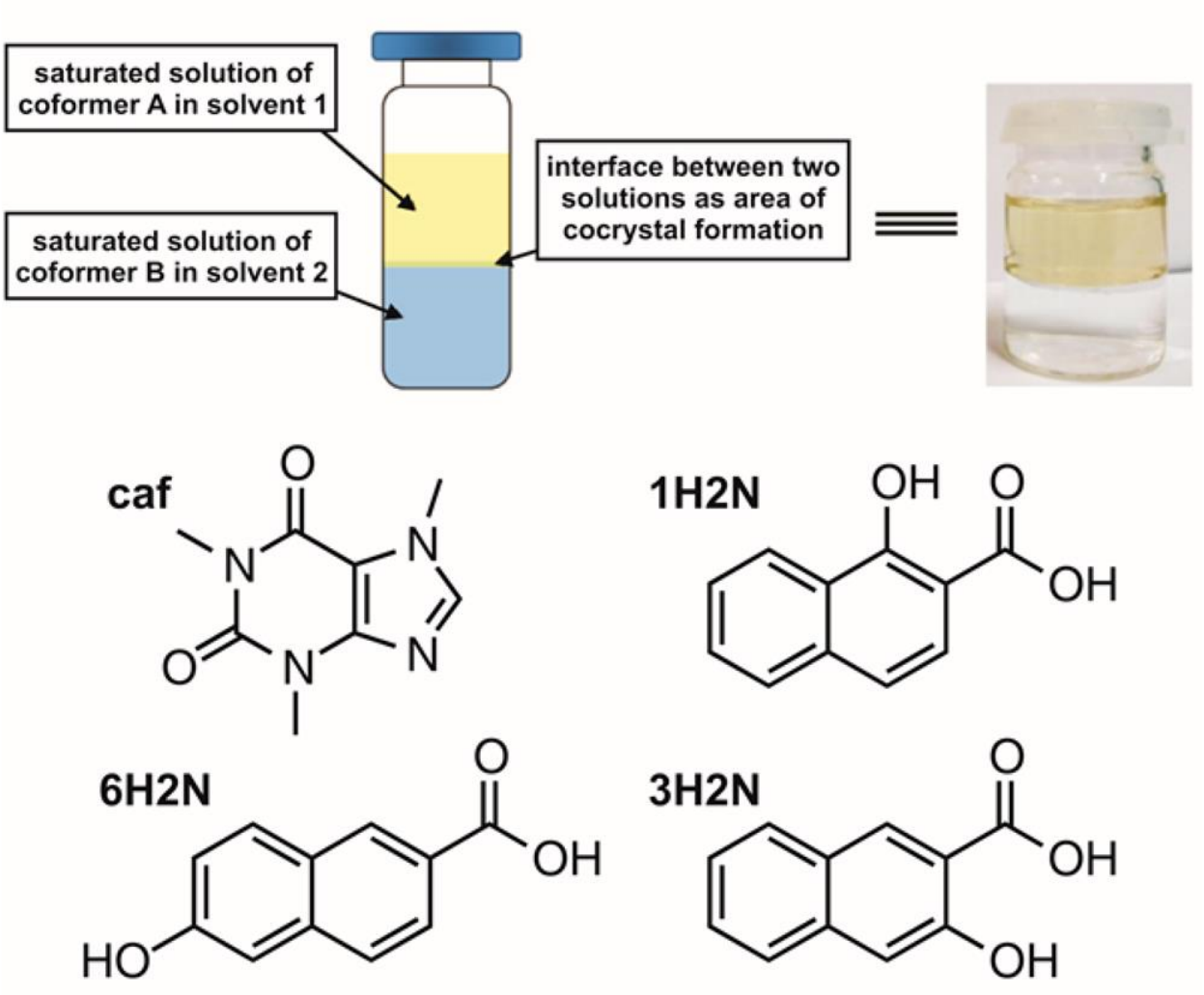

<u>Figure 1.4:</u> The experimental conditions and structure of the caffeine and coformers.[27]

The control of polymorphism is now crucial in cocrystal research, and methods are being sought for the selective synthesis of specific crystalline materials. Screening methods for controlled cocrystallisation are therefore necessary. Caffeine (Caff) and 1-hydroxy-2-naphthoic acid (1H2N) were chosen as the API and conformer, respectively as a model drug in cocrystals studies. The chemical structure of chosen components is presented on Figure 1.5.

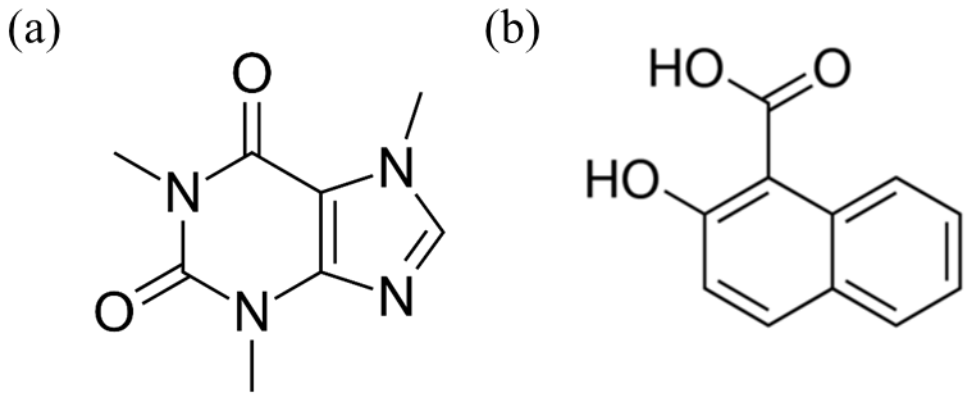

Figure 1.5: Chemical structure of the API caffeine (a) and cocrystal conformer 1-hydroxy-2-naphthoic acid (b).

1.3. Electrochemistry at the Interface between Two Immiscible Electrolyte Solutions (ITIES)

In this research we studied the Interface between Two Immiscible Electrolyte Solutions (ITIES).[58] An ITIES is formed between two immiscible liquid solvents containing electrolytes. The first solvent is generally water, and the second one is a polar organic solvent which is characterized by a moderate or high dielectric permittivity, which is important for partial dissociation of electrolytes. The most commonly used solvents are polar organic solvents like nitrobenzene (NB)[59], 1.2-dichloroethane (DCE), which are characterized by relative permittivity in range 10-15[60]. Other solvents such as *o*-nitrophenyloctylether (NPOE) [15], 2-octanone, 2-heptanone[61], acetophenone[62], 1.4-dichlorobutane, 1.6-dichlorohexane (1.2-DCH)[63] dichlorobenzene[64] and recent ionic liquids (RTIL) are also suitable, but expensive and difficult to use[65]. Since the commonly used DCE or NB are toxic and carcinogenetic, the latest research applies trifluorotoluene (TFT) as a non–cancerogenic and not expensive solvent for ITIES experiments. The dielectric constant (ε) (9.2 at 20 °C) and density of TFT (1.19 gmL^{-1}) are comparable to those of DCE (10.3 at 20 °C and 1.25 g/mL, respectively)[66]. The standard transfer potential $\Delta_o^w\phi$ of ions transferred across the water/TFT interface can be determined and compared with those at the water/DCE interface. The linear relationship between the standard Gibbs energies $\Delta G_{tr,i}^{0,w\to o}$0, w→o) allows to extrapolate it for other ions. In addition to the increase in the use of

TFT, more environmentally friendly organic solvents such as anisole[67] or the well-known oils such as avocado oil, coconut oil and walnut oil have also begun to be considered[68], [69]. Anisole has lower ε (4.3 Fm^{-1}) than DCE (10.4 Fm^{-1}) and TFT (9.2 Fm^{-1}) and its phenyl group allows to interact with the cations and biologic substances, thus anisole can be used to mimic biological reactions and drug distribution studies. The linear correlation between with standard potentials at water/DCE and water/anisole interface was found. Avocado oil, coconut oil and walnut oil are free from toxicity, not expensive and easily accessible. However, they are limited due to the high viscosity which slows down the mass transfer at ITIES and that are not yet well studied. Both phases contain an electrolyte salt that is soluble just in one of the phases but not in the other.[70] The composition of the phases is very important so that we can observe the results of the experiments. The water phase comprises a hydrophilic electrolyte like LiCl or Li_2SO_4, while an organic solvent contains a highly hydrophobic electrolyte e.g. bis(triphenylphosphoranyldiene) ammonium (BA^+) in combination with tetrakis(4-chlorophenyl)borate ($TPBCl^-$), or tetrakis(4-fluorophenyl)borate (TB^-)[71].

Aqueous and organic electrolyte solutions have ionic conductivity due to mobile charge carriers, allowing them to reach equilibrium through ion transfer across this interface. The advantage of using such electrolyte solutions at ITIES is that the ionic conductivity of the two phases produces an electrical potential difference at the interface.[72] Therefore, in some electroanalytical applications, the ITIES can replace the working electrode in classical electrochemistry and give the possibility to detect ionic species which are not detectable in redox processes. This is done by monitoring the current generated during the transfer of ions across the liquid-liquid interface, from one phase to another.

1.3.1. Simple ion transfer at ITIES

The electrochemical signal is generated by the transfer of ionic species through the interface. This transfer is induced by the application of a Galvani potential difference across the interface. That is, to provide the ions with the Gibbs energy needed to move from one phase to another by polarizing the interface based on the Galvani potential difference defined by the equation (1.1)[58], [73]:

$$\Delta_o^w\phi = \Delta\phi(w) - \Delta\phi(o) = \Delta_o^w\phi_i^0 + \frac{RT}{z_iF} ln \frac{a_i(o)}{a_i(w)} \quad (1.1)$$

And in case of diluted solutions:

$$\Delta_o^w\phi = \Delta_o^w\phi_i^0 + \frac{RT}{z_iF} ln \frac{c_i(o)}{c_i(w)} \quad (1.2)$$

Where $\Delta_o^w\phi$ – the Galvani potential difference; $\Delta_o^w\phi_i^0$ – standard transfer potential of the ion I; z_i – charge of i; a_i – activity in each phase, c_i – concentration in each phase.

When the Galvani interfacial potential difference changes (through the application of an external potential by the reference electrodes present in each phase), there is a transfer of ions from one phase to the other in order to maintain the equilibrium described by Eq. (1.1). Each ion passing through the interface produces a current which is recorded by the counter electrode present in both phases[70], [74], [75].

1.3.2. Assisted ion transfer at ITIES

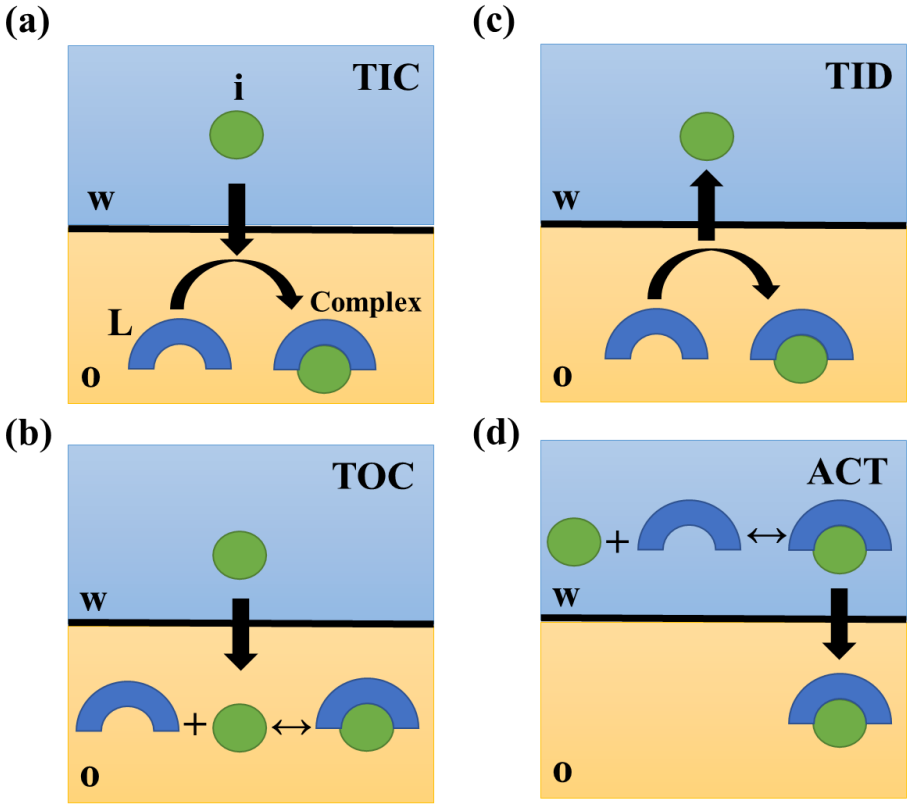

Figure 1.6: The four mechanisms of possible assisted ion (i) transfer reactions. (a) TIC – transfer by interfacial complexation; (b) TID – transfer by interfacial dissociation; (c) TOC – transfer followed by interfacial complexation; (d) ACT – aqueous complexation followed by transfer of the complex. L - ligand, i - ion, w – aqueous phase, o – organic phase.

Assisted (facilitated) ion transfer involve not only the transferring ion (i), but also neutral ligand (L) that are distributed on the surface or that can be distributed on either side of the interface[58]. The assisted ion transfer reaction is quite complex, so four mechanisms are proposed to describe the processes involved (Fig 1.6): transfer by interfacial complexation (TIC), transfer by interfacial dissociation (TID), transfer followed by organic phase complexation (TOC) and aqueous complexation followed by transfer of the complex (ACT). [76]

Nernst-like equation (Eq. 1.1) can be adapted for assisted ion transfer when we assume that[77]:

$$L_{org} + (i_{aq}) \leftrightharpoons L_{aq} - (i_{org}) \tag{1.3}$$

For above reaction the association constant is defined by:

$$K_a = \frac{a_{L-(i)}^{org}}{a_L^{org} a_{(i)}^{aq}} \tag{1.4}$$

The $\Delta_o^w \phi$ for the facilitated ion transfer can be written in the form of equation:

$$\Delta_o^w \phi = \Delta_o^w \phi_{L-(i)}^0 + \frac{RT}{z_{(i)}F} ln \frac{a_{L-(i)}^{org}}{a_{(i)}^{aq}} \tag{1.5}$$

With the standard transfer potential of ligand, $\Delta_o^w \phi_{L-(i)}^0$:

$$\Delta_o^w \phi_{L-(i)}^0 = \Delta_o^w \phi_{(i)}^0 + \frac{RT}{z_{(i)}F} \ln(K_a a_L^{org}) \tag{1.6}$$

First assisted ion transfer was reported for the transfer of K^+ from the aqueous phase to a nitrobenzene containing dibenzo-18-crown-6 ionophore via complexation of these ions.[78] The ionophores present in the organic phase lowered the Gibbs energy of transfer and facilitated the transfer of potassium. This study was followed by facilitated ion transfer studies of other elements, including Fe(II) and (III), Ni(II) and Zn(II) involving o-phenanthroline and o,o'-bipyridine and heavy metals i.e. cadmium and lead [79]. Interesting example of TIC and TID is

facilitated proton transfer. In presence of piroxicam and its derivatives, H^+ transfer through complexation and decomplexation at the ITIES.[80]

1.3.3. Electron transfer at ITIES

Electron transfer reactions concern the study of electron transfer between two redox species across the ITIES, with one species dissolved in either phase. They are based on the redox reaction between the oxidised redox form in one phase and the reduced form in the other. However, they are rarely used in analytical applications, as it is more interesting from an analytical point of view to study ions electrochemically at the ITIES.[59] The electron transfer in comparison with ion transfer can be studied by many external techniques such as SECM[81], in situ UV-Vis spectroscopy[82] or fluorescence spectroscopy[83] and recently by computational simulations[84]. The first reports of electron transfer at ITIES was made for the redox couple $Fe(CN)_6^{3-}/Fe(CN)_6^{4-}$ in aqueous phase and ferrocene in the organic phase.[85] Since then a lot of studies about the mechanism of this transfer were cried out. The electron transfer may occur spontaneously or by control of the potentiostat.[86]–[88] Interfacial electron transfer was the first step of electrosynthesis of PEDOT (poly(3,4-ethylenedioxythiophene) films at ITIES.[89] Under the positive polarization there was the exchange of electrons between EDOT in the organic phase and Ce^{4+} oxidant in aqueous phase, generating $EDOT^+$. This cationic form adsorbed at the ITIES under the negative potential and it was followed by the autocatalytic electron transfer between above-mentioned redox couple. This process is presented in Figure 1.7.

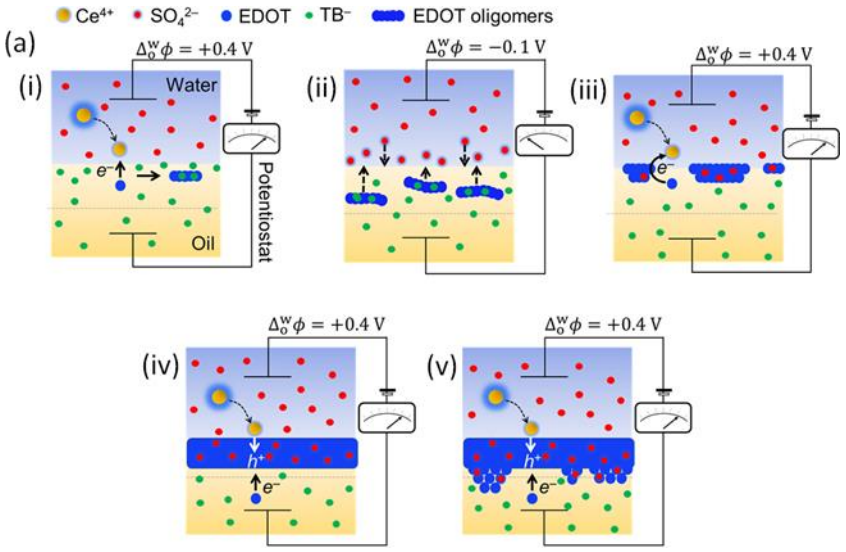

Figure 1.7: PEDOT formation by the electron transfer at ITIES in five steps electrosynthesis.[89]

1.3.4. Potential window for the transfer of ions

The interfacial potential is controlled by a potentiostat and it is applied through the reference electrodes in each phase. With Pt counter-electrodes, one in the aqueous and one in the organic phase, the current variation linked to charge transfer across the liquid−liquid interface is recorded.[90] When a hydrophilic salt is dissolved in the aqueous phase and a hydrophobic salt is dissolved in the organic phase, the interface is polarizable. Thus, if we want to polarize the interface, without changing the chemical composition of the phases, it is necessary to apply an external potential. This creates a potential window (Fig. 1.8) that allows the interface to be polarized to the point where the applied Galvani potential difference is enough to transfer the ion.[73] If a positive $\Delta_o^w\phi$ is applied to the interface, it will cause an excess of cations in the water phase and an excess of anions in the organic phase. The interface will be polarized until the Galvani potential difference reaches the standard transfer potential of hydrophilic or hydrophobic ion. The ion of choice is the hydrophilic lithium cation that has a high positive formal ion transfer potential (0.610 V)[91], or hydrophobic $TPBCl^-$, whose formal ion transfer potential is even larger. With Li^+ in the aqueous phase and $TPBCl^-$ in the organic phase, the use of positive potential will cause the transfer of lithium ions from the aqueous into the organic phase. Therefore, if we want to transfer a particular cation, it must possess less positive standard potential than Li^+. At the negative

end of the potential window, Cl^- or SO_4^{2-} is chosen by default in the aqueous phase. When we use sulphate ion in the aqueous phase, then the window will be limited by the transfer of this anion. Therefore, as above, we must place in the organic phase a hydrophobic cation with a standard potential more negative than SO_4^2 (-0.600 V) like BA^+.[73] Figure 1.8 shows the cyclic voltammogram recorded at a polarizable interface between the aqueous solution of LiCl and the organic solution of BATPBCl. An area between two dashed lines is the polarizable part of the interface called the potential window. It is limited by supporting electrolyte ion transfer – Li^+ at the positive $\Delta_o^w\phi$ and Cl^- at the negative $\Delta_o^w\phi$.

Standard transfer potential $\Delta_o^w\phi_i^0$ is related to the standard Gibbs energy of transfer $\Delta G_{tr,i}^{0,w\to o}$ from phase *w* to phase *o* according to Equation (1.3):

$$\Delta_o^w\phi_i^0 = \frac{\Delta G_{tr,i}^{0,w\to o}}{z_i F} \tag{1.6}$$

$\Delta G_{tr,i}^{0,w\to o}$ results from the difference in the standard molar Gibbs energy of solvation of ions in the two phases. Ions with a large positive $\Delta G_{tr,i}^{0,w\to o}$ are hydrophilic and they transfer at a positive $\Delta_o^w\phi$. On the contrary, ions with a large negative $\Delta G_{tr,i}^{0,w\to o}$ are hydrophobic and they transfer at negative $\Delta_o^w\phi$.[70] For that reason, the hydrophilic ions are transferred from the aqueous to organic phase when the required transfer potential ($\Delta_o^w\phi > \Delta_o^w\phi_i^0$) is applied by the electrodes. Thus, the transfer $Li_{aq}^+ \to Li_{org}^+$ occurs at a positive potential, while $Cl_{aq}^- \to Cl_{org}^-$ at a negative potential. The opposite is true for hydrophobic ions in the organic phase. $TPBCl_{org}^- \to TPBCl_{aq}^-$ generate a current during the positive forward scan. Meanwhile $BA_{org}^+ \to BA_{aq}^+$ generate a current through the transfer during the negative forward scan.[71], [92]

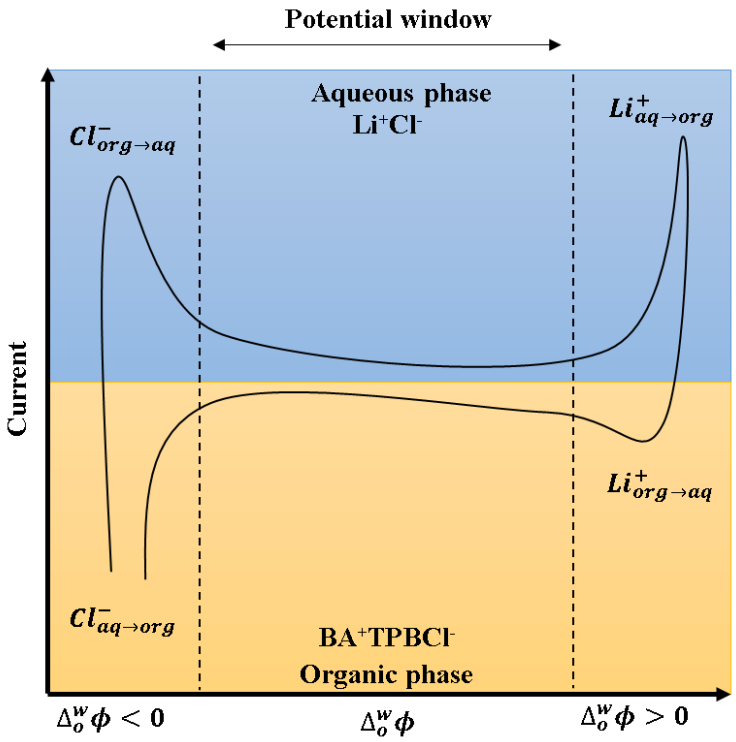

Figure 1.8: Blank cyclic voltamogram at the ITIES. Aqueous phase consisted of 10mM LiCl and a 10mM BATPBCl in organic phase. The forward scan was from a less positive to a more positive potential.

The charge recorded is proportional to the amount of ionic species but the potential difference at which a transfer is observed, gives an indication of the nature of the ionic species transferred. Therefore, cations transferred from aqueous to organic phase and anions transferred from organic to aqueous phase give raise to the positive current and contrariwise anions transferred from organic to aqueous phase give raise to the positive current and contrariwise anions transferred from aqueous to organic and cations transferred from organic to aqueous give raise to the negative current.[59] For these effects to be noticeable, they must be within the potential window.

1.3.5. Chemical polarization of the ITIES through common ion experiments

The interfacial potential can be controlled by a potentiostat but it can also be set through the dissolution of a common ion in each phase, without the use of electrodes. The so called 'shake-flask' approach is implemented to erase some uncertainties in kinetic parameters. Here, both phase electrolytes contain a common ion in different concentrations and the interface is polarized because

ions can freely migrate between the phases. Distribution of the ions between phases produces an electric potential difference between the phases. By initially varying the concentration of the common ion in aqueous or organic phases, we can alter the potential difference and the structure of the electrical double layers.[93] Ideally, the current occurring at the ITIES due to the transfer of a common ion should not change the interfacial potential difference. According to Nernst-like equation (1.2) the potential distribution relies on the ions separated between two immiscible phases.

In the case of the common ion approach, $\Delta_o^w\Phi$ is set by the concentration of a common species, *i*, in each phase.[94] If for instance, an ion like TMA^+ (tetramethylammonium) is dissolved in two adjusted phases (Fig. 1.9), the distribution of that ion causes a polarization of the interface. The Galvani potential difference is named now a distribution potential and is defined by Equation (1.2). In systems comprising the complex formation or ion association can apply this procedure. In such systems the ion partition equilibrium is shifted to favour one phase over the other. To keep the electro neutrality, this shift is compensated by the redistribution of other ions.[70]

The undeniable advantage of using common ion experiments is the greater possibility of approaching realistic conditions and the possibility of creating biomimetic systems. These 'shake flasks' experiments that enable analyses that are difficult to perform using a potentiostat, such as liquid-liquid extraction [95], the study of interfacial ion distribution [93], monitoring electrodeposition at the liquid-liquid interface [96] or biomimetic reduction of oxygen [97].

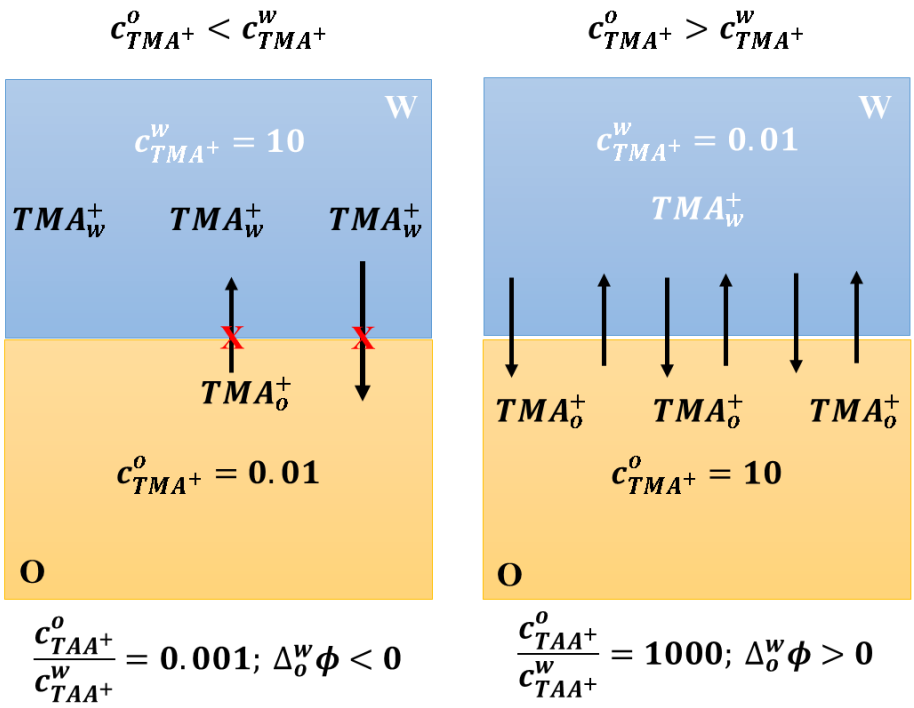

Figure 1.9: The ion distribution for TMA^+ (tetramethylammonium) as a common ion in aqueous and organic phase.

However, when the interface is polarised by the common ion approach, monitoring the potential and current associated with any chemical reactions is challenging. Such reactions can be followed visually [98], [99] and by the use of analytical methods (e.g. UV-vis absorption spectroscopy). Recently, potential changes at the ITIES have been monitored by open circuit potential (OCP) measurements and concentrations were calculated based on the Nernst-like equation shown as (1.2). The extraction of tetraalkylammonium chloride salts from an aqueous phase to the organic phase (DCE) was explained by examining the OCP at the water/DCE interface [100]–[102]. Current changes occurring in emulsions on the ITIES were also followed using chronoamperometry [103]. Current spikes associated with single microdroplets fusion events at the polarised interface were detected and quantitatively analysed. The number of ions present in a single droplet was calculated directly from the charge of the corresponding spike. Yet, this method focused on current analysis – a separate study of single fusion events through OCP was later reported.[104]

1.3.6. Assemblies at ITIES

In recent years, the liquid-liquid interface has been used as a tool to control the formation of different types of assemblies e.g. supramolecular [105]–[107], gold nanoparticles [108][88], phospholipids,[109] mesoporous silica [110], porphyrin [111]–[113], proteins [114]–[116] and polyamides [117]. The accumulation of nanostructures at the liquid-liquid interface is interesting from theoretical and experimental approach because these assemblies can act as encapsulants and have unusual optical, magnetic and electronic properties. These properties are the effect of dense arrangement in a two-dimensions. By creation of such assemblies of copolymers, dendrimers and surfactants, it is possible to decrease the interfacial tension.[118]–[120] Small molecules i.e. 5,10,15,20-tetrakis(4-sulfonatophenyl) porphyrin (H6TPPS), mellitic acid (MA) and 5,10,15,20-tetrakis(4-sulfonatophenyl)-21H,23H-porphine manganese(III) chloride (MnH4TPPS) were investigated as nanofibrous supramolecular structures stabilized the surfactants at the water-oil interface.[106] In another study it was proved that the formation of high molecular weighs polymers by interfacial polymerization is more efficient than in solution [107]. The liquid-liquid interface has proven to be an interesting approach for self-assembly of gold nanoparticles (AuNP).[88] The assembly was formed due to the low surface tension at water-propylene carbonate (PC) interface in the absence of promoters. The liquid nature of the interphase promotes self-healing, making the resulting nanofilms homogeneous at room temperature.[108], [121] The ITIES allowed the control of the interfacial electric field and thus manipulation of electrochemical activity [87] and physical position [122] of AuNP. The modification of the ITIES can increase its selectivity. Therefore, the formation of mesoporous silica was performed at a micro liquid-liquid interface. The ITIES allowed to control the interfacial potential and transfer of CTA^+ (cetyltrimethylammonium cation) from organic to aqueous phase that worked as a catalyst for the condensation of hydrolysed tetraethoxysilane (TEOS) molecules.[110] Interesting observation was that analysis of the cubes present on the Figure 1.10 are the crystals of sodium chloride (NaCl), which come from background electrolyte returning to the aqueous phase. Such modification increased the stability of the ITIES and further characterization.[123] Functionalization of the ITIES with solid materials that are not conductive and act as ion exchange membranes may be used in devices such as lithium batteries or fuel cells.[113] Using ion transfer at the ITIES, 1.6-DAH (polyamide) films were obtained and were easy to remove.[117]

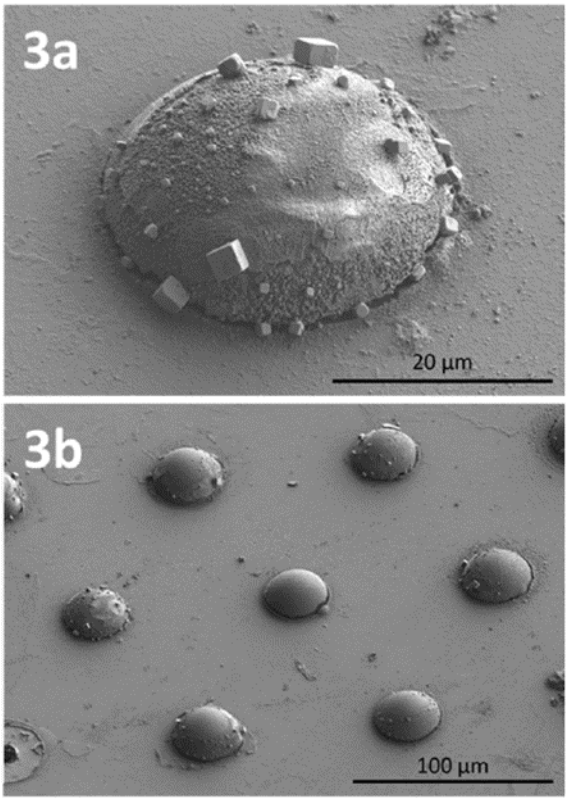

Figure 1.10: SEM images of µITIES modified with silica deposits. NaCl crystals are visible in morphological analysis.[110]

The functionalization of ITIES with biological molecules and its similarity to cell membranes allows the mimicking of biological systems. Several examples of its use in this way will be presented. Enhancement of the ITIES with biological molecules and its phospholipids (present in biological membranes) allowed to mimic biological systems. Interaction between model phospholipid DMPC (1.2-dimyristoyl-sn-glycero-3-phosphocholine) with H^+ and Li^+ was studied at water-chloroform interface.[109] DMPC facilitated the transfer of these cations at ITIES and catalytic transfer of H^+ to convert the solar energy was proposed as potential application. Biological application of ITIES was also used to form the porphyrins which are part of chromophores in photosynthetic organisms. The soft interfaces in contrary to solid-liquid interfaces present macro-scale homogeneity in particle-surface interactions, uniform absorption at ITIES[111] and reproducibility and self-healing properties[112]. Functionalization of the ITIES allowed to study the mechanism taking place in inner mitochondrial membrane. Change of the

cytochrome c (Cyt c) environment lead to modification of conformational plasticity and by the control of the potential toward water-TFT interface the adsorption of Cyt c was achieved and its interaction with lipid membrane was investigated.[114]

1.3.7. Crystallization at liquid-liquid interface

The recent studies have shown that an electric field applied across a biphasic system of miscible solvents resulted in the formation of inorganic crystals [124], [125], organic crystals[126] and metal organic frameworks [127], [128]. The crystallization of inorganic calcium sulphate was performed at the immiscible water-dodecane and water-octane interfaces.[124] SO_4^{2-} was in the aqueous phase and Ca^{2+} in the organic phase and the formation of $CaSO_4$ was achieved. Additionally, the micro liquid-liquid interface allowed the application analytical methods to follow the gypsum-anhydrite transformation. Then, the application of electric field at nanointerface allowed the control of crystallization of another inorganic salt – calcium carbonate ($CaCO_3$) [125]. Combination of experimental and simulation results confirmed that the applied voltage was the driving force for the crystallisation.

In other works, the crystallization of the organic compound – bicalutamide was monitored at nanointerface in real time.[129] Under the influence of the applied electric field, the water mixed with the DMSO containing protonated bicalutamide in the tip of the nanopipette. The solution became locally supersaturated and nucleation occurred. The crystallization of bicalutamide occurred at a negative potential so the applied bias had an influence on the crystallization at liquid-liquid interface. In other works, the water-oil interface was used to crystallize proteins [126]. Lysozyme was crystallizing at the interface between water and various organic solvents. The protein was dissolved in the aqueous phase. Some solvents such as parafilm and silicone oil inhibited the nucleation. When the solvents containing halogens supported crystallization at the interface due to the partial solubility in water and higher polarity than the others. It was noticed that at these active solvents first the film is formed, which is followed by the crystallization. Additionally, the water-DCE interface was polarized and the applied potential influenced the number of lysozyme crystals (Figure 1.11).

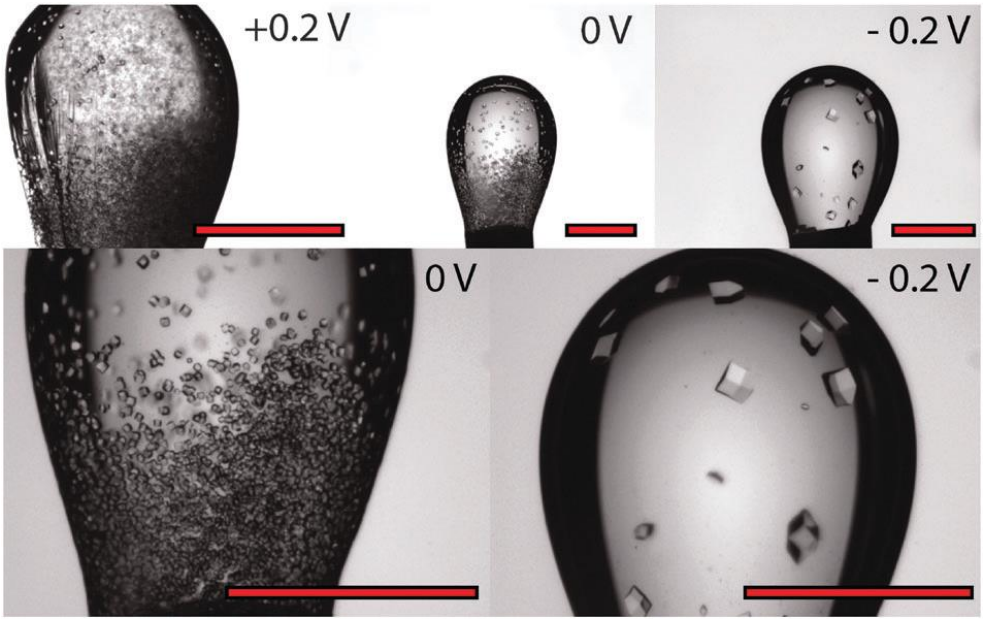

Figure 1.11: Lysozyme crystallization on the polarised water-DCE interface. Scale bars are 1.47 mm.[126]

1.4. Outline of the PhD work

In the third chapter the electrochemical properties of Caff and 1H2N were examined by means of Cyclic Voltammetry (CV), as well as the influence of the other components (LiCl, Li_2SO_4, BATB and BATPBCl) of the two phases on interfacial interactions by AC Voltammetry.

In the fourth chapter, the cocrystallization of Caff: 1H2N at the water-DCE interface was carried out. The interface was chemically polarized to study the influence of the applied potential on the cocrystals formation and polymorphic forms selection. The complexes formed at the liquid-liquid interface were analysed by single crystal X-ray diffraction (SCXRD), powder X-ray diffraction (PXRD), scanning electron microscopy (SEM) and Raman Spectroscopy.

The fifth chapter describes simultaneous measurements of the potential (ΔE) and current (ΔI) at the liquid-liquid interface. Firstly, a system was created in which the potential corresponds to theoretical values in order to use it for electrochemical cells containing caffeine and 1H2N. Analysis of the electrochemical noise (EN) provided information on the effect of applied potential and indicated differences in the electrochemical cells when the cocrystals were formed at interphase and when the conditions imposed stopped cocrystallization.

In the sixth chapter the composition of the aqueous and organic phases was changed according to the design of experiments (DoE) method. The resulting cocrystals were analysed by XRD. The new conditions were investigated by simultaneous potential and current analysis, and the surface tension between phases was studied by pendant drop experiments. In this way, the factors that have the greatest influence on the formation of the various polymorphs were found.

2. MATERIALS AND METHODS

This chapter provides information on all the experimental, and instrumental details employed during the research. First, chapter 2.1 provides a complete list of the chemicals used. Next, in chapter 2.2 are the fabrication and synthesis protocols for the salts used during the experiments. Finally, chapter 2.3 describes the electrochemical setup used during the electrochemistry at ITIES, and the other instrumentation used in this work.

2.1. Chemicals

Information on the chemical name, purity, abbreviation, CAS number, molar mass, source and function listed for each chemical used in this research in Table 2.1.

Chemicals are divided into the following sections:

- Aqueous and organic electrolytes
- Interfacial active species
- Solvents
- Other compounds

The procedure for manufacturing the compounds shown in italics in the table will be presented in chapter 2.2.

Table 2.1: List of chemicals used in the study

Aqueous and organic electrolytes						
Name	**Additional information**	**Abbreviation**	**CAS regulatory number**	**Molar mass g mol^{-1}**	**Source**	**Function**
Lithium chloride	≥ 99.0%	LiCl	7447-41-8	42.39	Sigma-Aldrich	Aqueous phase electrolyte
Lithium sulfate	≥ 98.5%	Li_2SO_4	10377-48-7	109.94	Aldrich	Aqueous phase electrolyte

Hydrochloric acid	1 mol L^{-1}	HCl	7647-01-0	36.46	VWR Chemicals	pH adjusting
Sulfuric acid	95.0-97.0 %	H_2SO_4	7664-93-9	98.08	Sigma-Aldrich	pH adjusting
Nitric acid	68.0-70.0%	HNO3	7697-37-2		Sigma-Aldrich	pH adjusting
Bis(triphenylphosphoranylidene)ammonium tetrakis(4-chlorophenyl) borate	-	BTPPATPBCl	-	995.59	Synthesed	Organic phase electrolyte
Interfacial active species						
Caffeine powder	Lab Grade	Caff/$CaffH^+$	58-08-2	194.19	Fisher Scientific	Studied drug, API
1-hydroxy-2-naphthoic acid	99.0%	1H2N	86-48-6	188.18	Aldrich	Cocrystal coformer
Bis(triphenylphosphoranylidene)ammonium chloride	97%	BTPPACl	21050-13-5	574.03	Sigma-Aldrich	Component changing the interphase potential; organic electrolyte preparation
Potassium tetrakis(4-chlorophenyl) borate	≥ 98.0%	KTPBCl	14680-77-4	496.11	Sigma-Aldrich	Component changing the interphase potential; organic electrolyte preparation
Tetramethylammonium chloride	≥98.0%	TMACl	75-57-0	109.6	Fluka	CV reference; interfacial active species in

						aqueous phase in common ion experiments
Tetraethylammonium chloride	≥99.0%	TEACl	56-34-8	165.7	Fluka	CV reference; interfacial active species in aqueous phase in common ion experiments
Tetrapropylammonium chloride	98%	TPACl	5810-42-4	221.81	Aldrich	CV reference; interfacial active species in aqueous phase in common ion experiments
Tetramethylammonium tetrakis(4-chlorophenyl) borate	-	TMATPBCl	-	531.21	Synthesed	Interfacial active species in aqueous phase in common ion experiments
Tetraethylammonium tetrakis(4-chlorophenyl) borate	-	TEATPBCl	-	587.31	Synthesed	Interfacial active species in aqueous phase in common ion experiments
Tetrapropylammonium tetrakis(4-chlorophenyl) borate	-	TPATPBCl	-	643.42	Synthesed	Interfacial active species in aqueous phase in common ion experiments
Piroxicam	≥ 98%,	Pir/PirH+	36322-90-4	331.34	Sigma-Aldrich	Studied drug, API
Piroxicam tetrakis(4-	-	PirH+-TPBCl-	-	789.45	Synthesed	Studied drug's salt, API

chlorophenyl) borate						
Sildenafil citrate	≥ 99%	$SilH^+$	171599-83-0	666.70	AlfaAesar	Studied drug, API
Sildenafil tetrakis(4-chlorophenyl) borate	-	$SilH^+$-TPBCl	-	930.71	Synthesed	Studied drug's salt, API
Diclofenac free acid	≥ 98%	DFA	15307-86-5	296.15	AlfaAesar	Studied drug, API
Ketoprofene	≥ 98%	Ket	22071-15-4	254.28	SIGMA	Studied drug, API
Solvents						
Water	18.2 MΩ cm	H_2O	7732-18-5	18.02	Ultrapure device from Elga Purelab	Aqueous phase solvent
1, 2-dichloroethane	> 99.5%	DCE	107-06-2	98.96	Sigma-Aldrich	Organic phase solvent
Trifluorotoluene	99%	TFT	98-08-8	146.11	Sigma-Aldrich	Organic phase solvent
Anisole	99% anhydrous	A	100-66-3	108.14	Aldrich	Organic phase solvent
Methanol	> 98%	MeOH	67-56-1	32.04	Carlo Erba	Solvent
Acetone	> 99.8%	ActOH	67-64-1	58.08	Carlo Erba	Solvent
Other compounds						
Iron (III) chloride	97%	$FeCl_3$	7705-08-0	162.20	Fisher Scientific	Silver wire oxidation

Chlorotrimethyl silane	(≥ 98.0% (GC)	-	75-77-4	108.64	Sigma-Aldrich	Glassware silanization

2.2. Standard transfer potentials

In this chapter, the standard transfer potentials of ions used in the work as references (TMA, TEA, and TPA) or in shake-flask experiments are listed.

Table 2.2: Standard transfer potentials, $\Delta_o^w\phi^0$, of ions in 1,2-DCE.

Ion	$\Delta_o^w\phi^0$ / **V**	**Reference:**
Li^+	0.610	[91]
Cl^-	-0.491	[130]
K^+	0.534	[91]
TEA^+	0.044	[131]
TPA^+	-0.090	[132]
TMA^+	0.160	[133]
TPB^-	0.307	[91]
$TPBCl^-$	0.590	[134]
TB^-	0.700	[135]

2.3. Protocols

A priori the salts of selected drugs were prepared in the reaction of metathesis.

Table 2.3: Metathesis reaction of selected salts with tetrakis (4-chlorophenylborate)

Salt	**PiroxicamH$^+$-tetrakis(4-chlorophenyl borate)**	**SildenafilH$^+$-tetrakis(4-chlorophenyl borate)**	**Tetraalkylammonium-tetrakis(4-chlorophenylborate)**	**Bis(triphenylphosphoranylidene)ammonium tetrakis(4-chlorophenyl) borate**
Abbreviation	**PirH$^+$-TPBCl**	**SilH$^+$-TPBCl**	**TAA$^+$-TPBCl**	**BTPPATPBCl**
1	Piroxicam (0.5 g) was dissolved in 250 mL MeOH and K^+TPBCl^- (0.676 g) was dissolved in 20 mL 2:1 MeOH: H_2O solution.	Sildenafil citrate (0.5 g) and K^+TPBCl^- (0.522 g) were dissolved in 10 and 20 mL 2:1 MeOH: H_2O solution, respectively.	TAACl (0.110 g of TMACl, 0.166 g of TEACl and 0.222g of TPACl) and K^+TPBCl^- (0.500 g) were dissolved in 10 and 20 mL 2:1 MeOH: H_2O solution, respectively.	BTPPACl (1.157 g) and K^+TPBCl^- (1.000 g) were dissolved in 10 and 20 mL 2:1 MeOH: H_2O solution, respectively.

2	The pH of $PirH^+$ solution was changed to 2 (pH = 2) by adding 2 mL of 37 % HCl.	The K^+TPBCl^- solution was added while stirring to solution of $SilH^+$, forming a white precipitate. The stirring was continuing for 2 h.	The K^+TPBCl^- solution was added dropwise while stirring to solution of TAACl, forming a white precipitate. The stirring was continuing for 2 h.	The K^+TPBCl^- solution was added dropwise while stirring to solution of BTPPACl, forming a white precipitate. The stirring was continuing for 2 h.
3	The acidic solution of $PirH^+$ and the solution of K^+TPBCl^- were mixed and mixed on magnetic stirring around 30 min. Methanol was removed by using rotary evaporator.	The solution was then filtered under vacuum for about 30 minutes, in this way the solvent was removed. The product obtained was transferred to a dry beaker, then covered with aluminium foil and kept in a desiccator overnight.		

4	The reaction product was then dissolved in acetone and the solution was filtered under gravity using filter paper. The beaker was covered with parafilm and holes were made to allow the acetone to evaporate.
5	The crystals were washed with a 1:1 mixture of Acetone: H_2O, filtered under vacuum and placed overnight in a desiccator.
6	The obtained crystals were stored in a refrigerator, with the sample vial covered with aluminium foil to prevent degradation caused by exposure to light.

2.4. Instrumentation

Information about the instrumentation used in the research will be dissected in this chapter.

2.4.1. Electrochemical measurements

Information about the electrochemical techniques used in the research will be dissected in this chapter.

2.4.1.1.Electrochemical setup

All measurements were performed in a custom made four-electrode glass cell with an interface area of ~1.13 cm^2. Platinum mesh was used as the counter electrodes. Ag/AgCl and Ag/Ag_2SO_4 wires as reference electrodes in both phases (Fig. 2.1). To avoid exposure to the aqueous phase, the organic phase counter electrode was previously covered with borosilicate glass. The Ag/AgCl electrodes were home made by oxidation of silver wire in a saturated $FeCl_3$ solution and Ag/Ag_2SO_4 were made by the electrochemical oxidation of silver. Two sets of reference and counter electrodes were present, one for the aqueous phase and one for the organic phase. A more detailed explanation of the electrochemical system was given in Chapter 1.3.

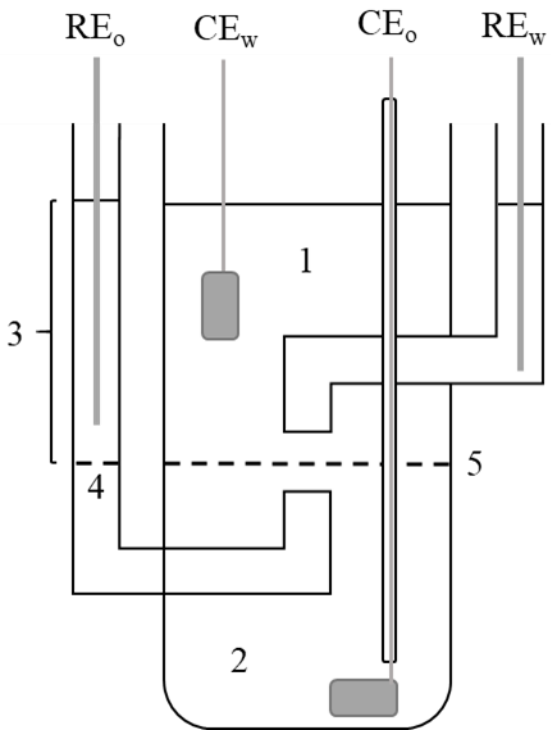

<u>Figure 2.1:</u> Four-electrode electrochemical cell. CE_o and CE_w correspond to the organic and aqueous counter electrode and RE_o and RE_w represent the organic and aqueous reference electrodes, respectively. 1 – aqueous phase (w); 2 – organic phase (o); 3 – organic reference phase (w'); 4 – LLI between the organic and organic reference phases; 5 – ITIES.

2.4.1.2.Cyclic Voltammetry

The potential difference across the water/organic solvent interface was controlled with an Autolab potentiostat PGSTAT302N or PGSTAT-100 controlled by NOVA software (Version 2.1). Examined compounds were dissolved in aqueous and/or organic phase electrolyte solution before filling the cell. –1,2-DCE was used as an organic solvent in each experiment. The volume added to the cell in each phase was always exactly 2.5 mL. The organic phase reference electrode (RE_o) was immersed in its aqueous reference solution of LiCl and BACl. Cyclic voltammograms were plotted using the Galvani scale so that the results were comparable. The standard potential was calculated based on the half-wave potential $\left(\Delta E^{1/2}\right)$ of TMA^+[133], TEA^+[131] and TPA^+[132]

and obtained by adding a predetermined concentration of the chloride salt of TAA^+ to the cell for each experiment. The Galvani potential difference ($\Delta_o^w\phi$) was calculated according to the equation:

$$\Delta_o^w\phi + \Delta_o^w\phi_{TAA^+}^0 = \Delta E + \Delta E_{TAA^+}^{1/2}, \quad (2.1)$$

Where ΔE is the potential difference between the reference electrodes and the $\Delta_o^w\varphi_{TAA^+}^0$ is the standard transfer potential of TMA^+, TEA^+ or TPA^+ as given in Table 2.1.

The pH was adjusted by addition of HCl, HNO_3 and LiOH. All measurements were carried out at room temperature (25 °C). Scan rate was $5mVs^{-1}$.

Scheme 2.1: The general electrochemical cell configurations

Electroche-mical cell:	**Ref 1:**	**(w)**	**(o)**	**(w')**	**Ref 2:**	**Information:**
1	Ag/AgCl	5 mM LiCl x mM HNO3	1 mM X 10 mM BATPBCl	10 mM BACl 10 mM LiCl	AgCl/Ag	X = Pir, $PirH^+$-$TPBCl^-$ x = 0, 0.1, 10
2	Ag/Ag2SO4	5 mM Li2SO4 x mM H2SO4	1 mM SilH+-TPBCl- 10 mM BATPBCl	10 mM BTTPACl 10 mM LiCl	AgCl/Ag	x = 0, 0.1, 10

3	Ag/Ag2SO4	1 mM Sil- 5 mM Li2SO4 x mM H2SO4	10 mM BATPBCl	10 mM BTTPACl 10 mM LiCl	AgCl/Ag	x = 0, 0.1, 10
4	Ag/AgCl	x mM Ket- 10 mM LiCl 10 mM LiOH	10 mM BATPBCl	10 mM BACl 10 mM LiCl	AgCl/Ag	x = 1
5	Ag/AgCl	x mM Dic- 10 mM LiCl 10 mM LiOH	10 mM BATPBCl	10 mM BACl 10 mM LiCl	AgCl/Ag	x = 1
6	Ag/AgCl	1 mM $CaffH^+$	10 mM BATPBCl	10 mM BACl	AgCl/Ag	x = 0, 10, 0.1

		10 mM LiCl y mM x		10 mM LiCl		X = HCl, LiOH
7	Ag/AgCl	1 mM 1H2N 10 mM LiCl 10 mM HCl	10 mM BATPBCl	10 mM BACl 10 mM LiCl	AgCl/Ag	
8	Ag/AgCl	x mM $CaffH^+$ 10 mM X	y mM 1H2N 10 mM Y	10 mM BACl 10 mM LiCl	AgCl/Ag	x = 0, 1 X = LiCl, Li_2SO_4 y = 0, 1 Y = BATPBCl, BATB

A more detailed explanation of the electrochemical system will be described in following Chapters.

2.4.1.3.Alternating Current (AC) Voltammetry

AC voltammetry experiments were run using an Autolab potentiostat PGSTAT302N or PGSTAT-100 controlled by NOVA software (Version 2.1). Parameters for the AC experiments were as follows: interval time – 0.125 s, frequency (f) – 1 Hz, step potential – 5 mV, amplitude (A): 10 mV RMS. The potential region was scanned at phase angles of 0° and 90°. The phase shift (ϕ) was calculated from the currents obtained at phase angles $i_{90°}$ and $i_{0°}$, using the following equation[136]:

$$\Phi = tan^{-1}\frac{i_{90}}{i_0} \quad (2.4)$$

The total impedance (Z) was calculated as follows:

$$Z = \frac{A}{\sqrt{i_{90}^2 + i_0^2}} \quad (2.5)$$

It includes real (Z_{Re}) and imaginary (Z_{Im}) parts:

$$Z_{Re} = Zcos\Phi \quad (2.6)$$

$$Z_{Im} = Zsin\Phi \quad (2.7)$$

The real part is related to the resistance of the solution and the imaginary part of the impedance expresses the interfacial capacitance (C), which can then be calculated:

$$C = \frac{1}{\omega Z_{Im}} \quad (2.8)$$

where $\omega = 2\pi f$. C can then be plotted as a function of the applied interfacial potential difference.

2.4.2. X-ray diffraction

The PXRD measurements were performed using a Panalytical X'Pert Pro diffractometer equipped with a Cu tube, a Ge (111) incident-beam monochromator (Kα1 = 1.5406 Å), 0.02 rad Soller slits, programmable divergence and anti-scatter slits, the irradiated area was fixed to 10mm x 10mm and an X'Celerator fast detector. The X'Celerator detector was used as "scanning line detector (1D)" with 2.122° active length. The resulting powder was characterized on a 200 μm thick zero

background X-ray holder because of relatively small amounts of powder (10-50 mg). Data collection was carried out in the scattering angle range 3–50° with a 0.0167° step over 4 hours.

The single crystal X-ray diffraction (SCXRD) measurements were performed using a Rigaku Oxford Diffraction 4-circles SuperNova diffractometer with a microfocus Molybdenum anode X-ray source (wavelength Mo ($K\alpha_1$, α_2) = 0.71073 Å) and an Atlas CCD detector. The cell parameters determination was carried out at room temperature.

2.4.3. Raman Spectroscopy

Experimental Raman scattering spectra were collected at 295 K on a Renishaw inViaTM Qontor® confocal microspectrometer, equipped by a laser wavelength of 532 nm, a grating of 1200 grooves per mm, a CCD detector cooled at -70°C and an Edge filter allowing spectral acquisition until 70 cm^{-1}. The laser beam was focused on the sample by an 80X objective with a long working distance of 7 mm and a numerical aperture of 0.90. Excitation irradiance at the sample was about 1000 $W.cm^{-2}$, which avoided any laser heating of the sample. Exposure time was 2 seconds and 5 spectra were averaged for increasing signal-to-noise ratio. Raman spectra were collected in step scan mode from 70 to 3200 or 3600 cm^{-1} depending on the sample. The final spectral resolution was closed to 3 cm^{-1} using this grating. At least 10 spectra were collected for each sample and we checked that the spectra were identical, indicating that the samples were quite homogeneous.

Density-functional theory (DFT) calculations (performed by Manuel Dossot) were made by the method of the DFT calculation at B3LYP 6311G++ (3d, 3p) level in gas phase. They were used to optimize the geometry of caffeine and 1H2N molecules, and the cocrystal involving a 1:1 complex between these two components. Vibrational spectra were calculated once the geometry was optimized, and no negative frequency was obtained, indicating a good convergence of the calculations. The aim was to compare the Raman active vibrational modes obtained experimentally and by a computational quantum mechanical modelling method. DFT computation and correction of the calculated vibrational wavenumbers by the following quadratic scaling function:

$$\bar{\sigma}_{scaled} = -0.0000104\bar{\sigma}_{calc}^2 + 0.9894\bar{\sigma}_{calc} \quad (2.20)$$

Where $\bar{\sigma}_{scaled}$ is the corrected Raman shift in cm^{-1}, and $\bar{\sigma}_{calc}$ calc is the calculated DFT Raman shift.

2.4.4. Thermal analysis

Thermal analysis was carried out using Differential scanning calorimetry (DSC). Thermograms were recorded in a nitrogen atmosphere using a differential scanning calorimeter equipped with a high sensitivity HSS8 probe from Mettler-Toledo. The heating rate was 10 $Kmin^{-1}$. Samples were prepared in 40 µl aluminum pans. The 10 mg of the powder was accurately weighted for each sample. The range of temperature was from -100°C to 350°C.

2.4.5. Multi-well crystallisation apparatus

A multi-well crystallisation home-made device (commercial equivalent ANACRISMAT) allowed the analysis of the interface in the 2 mL vials. They were stored in a thermostat to maintain a constant room temperature. The vials were placed on a motorised XY table, above the Nikon Eclipse TE2000 microscope equipped with a CCD camera. Labview software allowed observation on screen and manual or automatic acquisition of images. Image acquisitions were performed in sequences both automatic and periodic (30 minutes and 16 h).

2.4.6. Scanning Electron Microscopy (SEM)

Scanning electron microscopy micrographs were obtained using a JEOL JCM-6000 (acceleration voltage of 15 kV).

3. ELECTROCHEMICAL PROPERTIES OF SELECTED IONIC DRUG

In this chapter, cyclic and AC voltammetries were used to determine the electrochemical behaviour of the molecules of interest at the interface formed between an organic phase to an aqueous phase. The ITIES allowed the application of an external potential that can induce the transfer of the ionic species through the interface[58]. Preceding the preparation of co-crystals, it was necessary to perform the screening of the API and coformers, which comply with both: (i) the regulations of the creation of pharmaceutical cocrystals as well as with (ii) the rules governing the electrochemistry at ITIES. The studied drugs were already examined in the topic of pharmaceutical cocrystals formation[27], [40], [137]–[143]. For the purpose of the study, four drugs with low solubility in water (piroxicam, sildenafil, diclofenac and ketoprofene) and one with high solubility in water (caffeine) and chemical structure proper for creation of cocrystals were selected. Features that were mainly considered were: (i) water solubility, (ii) amphiphilic properties with $0 < \log P < 3$, (iii) electrical charge and (iv) selected chemical groups to create cocrystals. The most promising ion was caffeine and its electrochemical behaviour will be discussed at the ITIES. The electrochemical behaviour of the other ions envisaged are given in Appendix 1.

A priori the salts of selected drugs were prepared in the reaction of metathesis, as described in Table 2.3 in the Chapter 2.3. The metathesis reaction was first carried out because the original aim was to transfer poorly soluble drugs such as piroxicam and sildenafil from the organic phase to the aqueous phase. In the nonpolar phase, these drugs exist in a neutral form. The metathesis reaction yielded a salt with $TPBCl^-$ as a counter ion. Thus, the drugs studied could be soluble in the organic phase in an ionic form.

Table 3.1: Chemical parameters of the chosen drugs (N – neutral, C – cation, A – anion).

Drug name	**Abbreviation**	**pKa**	**Charge**	**Log P**	**Water solubility [mg L^{-1}]**	**$\Delta_o^w\phi$ [V]**	**Reference**
Piroxicam	Pir	1.86 5.46	+/+-/-	N: 3.06	23	C: 0.016	[80]
Sildenafil	Sil	6.78 9.12	+/N/-	N: 3.75	433	C: -0.005 A: -0.115	[144]
Diclofenac	DFA	3.99	N/-	3.24	2.37	-0.124	[145]
Ketoprofen	Ket	3.88	N/-	3.12	5.1	-0.270	[146]
Caffeine	$CaffH^+$	10.4, 14	+	-0.1	21700	0.390	[37], [147]
1-hydroxy-2-naphthoic acid	1H2N	3	N		0.228	-	[57]

3.1. Electrochemical behaviour of the selected lipophilic cationic drugs

Previous studies on the behaviour of piroxicam at the liquid-liquid interface have shown that in the presence of piroxicam in aqueous or organic phase there is no actual drug transfer but we witness the facilitated proton transfer[80]. Such transfer takes place via an interfacial complexation-decomplexation mechanism. However, in the previous studies were carried out using piroxicam salt and its derivatives and no attempt to create the salt was performed. PH^+TPBCl^- was obtained in metatheses reaction described in Table 2.3 in the Chapter 2.3.

3.1.1. Cyclic voltammetry study of piroxicam (Pir) transfer

Cyclic voltammetry was performed in electrochemical cell 1 Scheme 2.1. 1 mM of piroxicam salt (Pir) was added to the organic phase (Electrochemical cell 1 X = Pir). We adjusted pH to be acidic to select the conditions needed for the transfer of $PirH^+$. Firstly, taking a look at the results with neutral form of piroxicam (Fig. 3.1a), we could observe that the peaks do not correspond to the conditions fulfilled by peaks that genuinely represent a transfer to ITIES and was higher than characteristic peak-to-peak separation (59 mV) for the ion transfer at the LLI. In addition, the peaks were not constant when changing pH. In the Figure 3.1b. We observed that $\Delta_o^w\phi$ increased with pH, suggesting that no direct $PirH^+$ ion transfer was taking place in the potential window. The phenomenon that we observe here was indeed due to the facilitated proton transfer at ITIES[80].

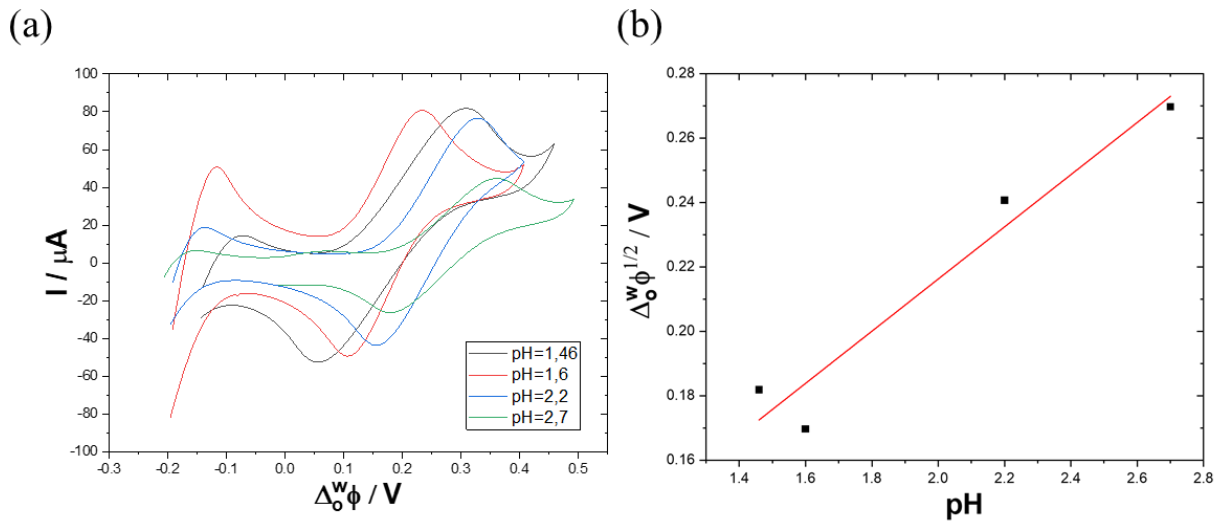

<u>Figure 3.1:</u> (a) Cyclic voltammogram of Pir at the liquid-liquid interface at various pH. (b) $\Delta_o^w\phi$ dependence on the pH. Concentration of piroxicam in the organic phase = 1 mmol L^{-1}. Electrochemical cell 1 in Chapter 2.4.1.2; X = Pir. Scan rate: 5 mVs^{-1}.

In Figure 3.2a cyclic voltammograms after the addition of 1mM piroxicam – PH^+TPBCl^- to the organic phase (Electrochemical cell 1 Scheme 2.1 X = PH^+TPBCl^-) are drawn. Analogically, peaks do not have a corresponding 59 mV difference between maximum and minimum current, indicating the irreversible charge transfer at the ITIES. We could observe that the $\Delta_o^w\phi$ increased with pH (Fig. 3.2b), suggesting that no $PirH^+$ ion transfer was taking place in the potential window

due the facilitated proton transfer. Piroxicam as well as his the salt PH^+TPBCl^- did not transfer across the interface and remained on the organic side of the interface throughout the potential window.

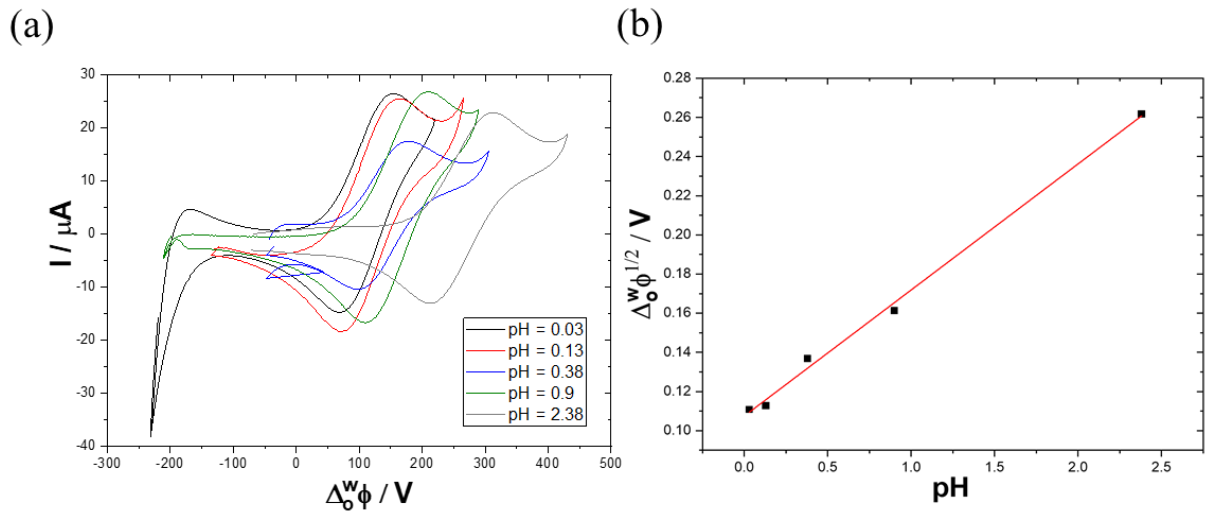

Figure 3.2: (a) Cyclic voltammogram of $PirH^+$ at the liquid-liquid interface at various pH. (b) $\Delta_o^w\phi^{1/2}$ dependence on the pH. Electrochemical cell 1 in Chapter 2.4.1.2; X = $PirH^+TPBCl^-$. Scan rate: 5 mVs^{-1}.

3.1.2. Cyclic voltammetry study of Sil and $SilH^+$-$TPBCl^-$

In this chapter, we presented electrochemical transfer experiments of $SilH^+$-$TPBCl^-$ on ITIES and monitored the effect of pH on the behaviour of the cation across ITIES. $SilH^+$-$TPBCl^-$ was examined in the 0 < pH < 2 range according to the electrochemical cell 2 Scheme 2.1 and the following transfer potentials are outlined in the Figure 3.3a. The effect of pH on the ion transfer at the ITIES was studied in the view of obtaining a constant standard potential. Firstly, taking a look at the results of transfer of $SilH^+$ from organic to the aqueous phase (Fig. 3.3a black, red, blue and green lines) we observed a decrease of standard potential along with increasing pH (Fig. 3.3b), suggesting that proton facilitated transfer was taking place in the potential window. $SilH^+$ did not also transfer across the interface from the aqueous to organic phase throughout the potential window (Figure 3.3a grey line) what does not correspond to the data contained in the following article [144].

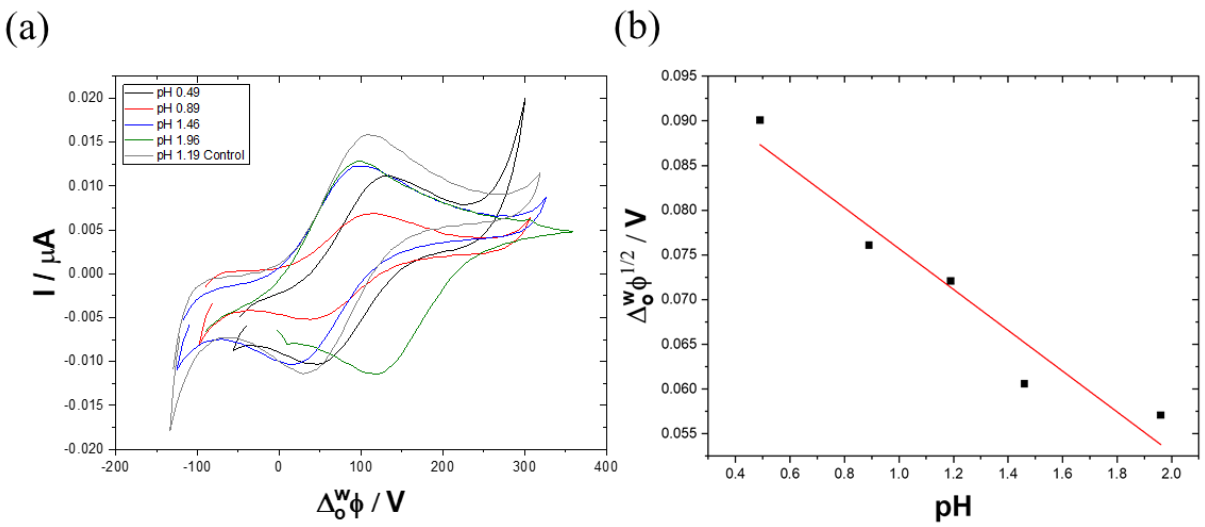

Figure 3.3: (a) Cyclic voltamogram of SilH$^+$-TPBCl at various pH: 0.49; 0.89; 1.46; 1.96 (Electrochemical cell 3) and 1.19 (Electrochemical cell 4 – control); (b) $\Delta_o^w\phi$ dependence on the pH. Scan rate 5mVs^{-1}.

To indicate if there is indeed a transfer of SilH$^+$ there is need to perform the experiments on the smaller scale –μITIES.

The selected lipophilic cationic drugs: piroxicam and sildenafil do not transfer at ITIES. The cocrystallizaion may be achieved by the use of the conformer which transfer at ITIES in aqueous phase.

3.2. Electrochemical behaviour of selected lipophilic anionic drugs

3.2.1. Cyclic voltammetry study of ketoprofen (Ket) transfer

Cyclic voltammetry was performed to verify the transfer of Ket$^-$ at the liquid-liquid interface (Fig. 3.4). Unlike the previous drugs, ketoprofen is a weak acid and will be tested as an anion at alkaline pH 10 (Scheme 2.1 Experimental cell 4). Ket$^-$ transfer from aqueous phase to organic phase was performed in electrochemical cell 3 in scheme 2.1. On Figure 3.4 we observed the transfer of Ket$^-$ at low electrochemical potential. The $\Delta_o^w\phi_{Ket^-}^{1/2}$ was hidden by the transfer of the anions creating

potential window. Therefore, it was calculated by subtraction of the baseline and its value was -0.260 V. The peak-to-peak separation corresponds to the classical value ~ 59 mV at the ITIES[148] which is expected for the reversible transfer of an ion with a single charge. Ketoprofen can be considered as an API for cocrystal formation as it transferred at the ITIES.

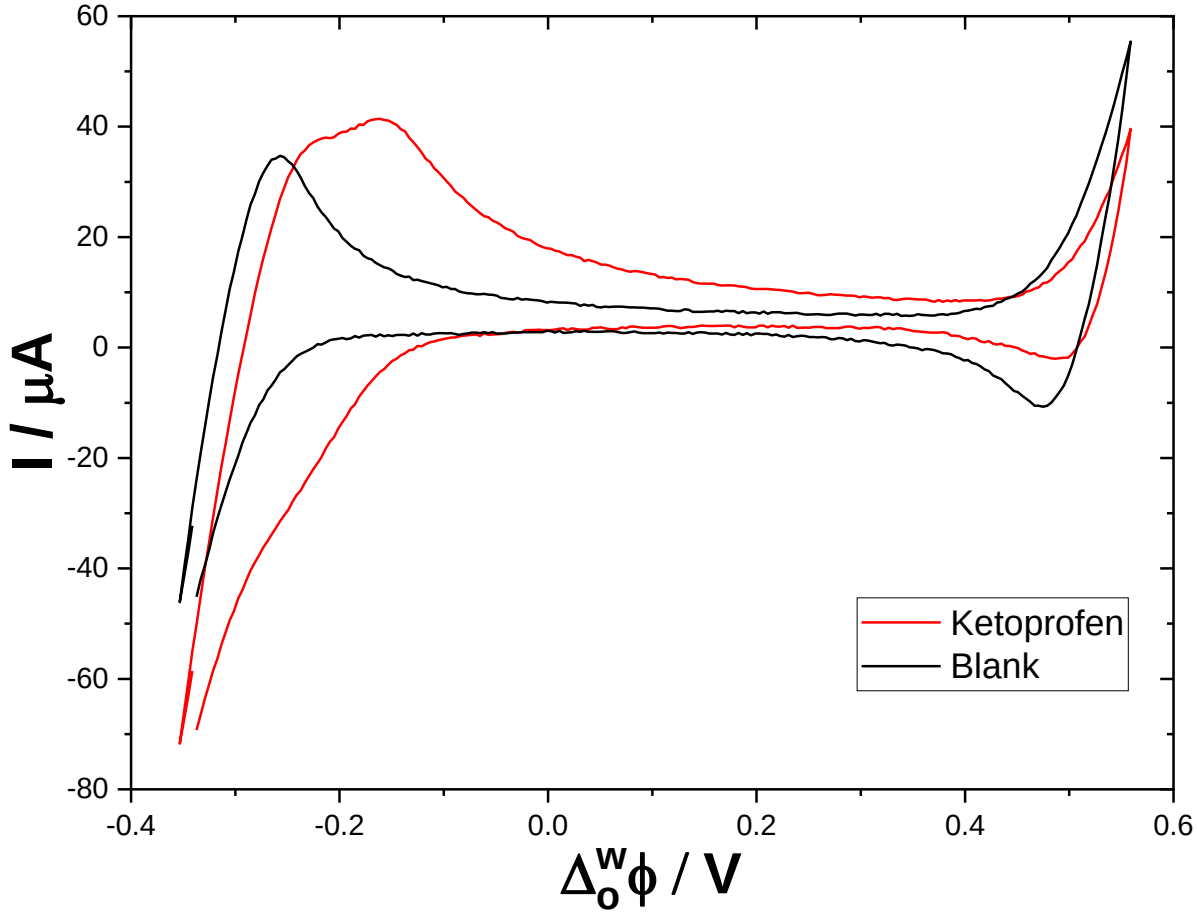

Figure 3.4: Cyclic voltammogram of Keoprofen$^-$ at pH 12 according to electrochemical cell 4. Scan rate 5mVs^{-1}.

Ketoprofen can be considered as an API for cocrystal formation as it transferred at the ITIES.

3.2.2. Cyclic voltammetry study of diclofenac (DFA) transfer

Cyclic voltammetry was performed to verify the transfer of DFA^- at the liquid-liquid interface (Figure 3.5). DFA represent similar properties as ketoprofen and it is a weak acid and it will be tested as an anion at alkaline pH. DFA^- transfer from aqueous phase to organic phase was performed in electrochemical cell 5 in scheme 2.1. On Figure 3.5 we observed the transfer of DFA^- at low electrochemical potential (below 0 V). The $\Delta_o^w\phi_{DFA^-}^{1/2}$ was -0.124 V. The peak-to-peak separation corresponds to the classical value ~ 59 mV at the ITIES[148] which is expected for the reversible transfer of an ion with a single charge. Diclofenac can be considered as an API for cocrystal formation as it transferred at the ITIES.

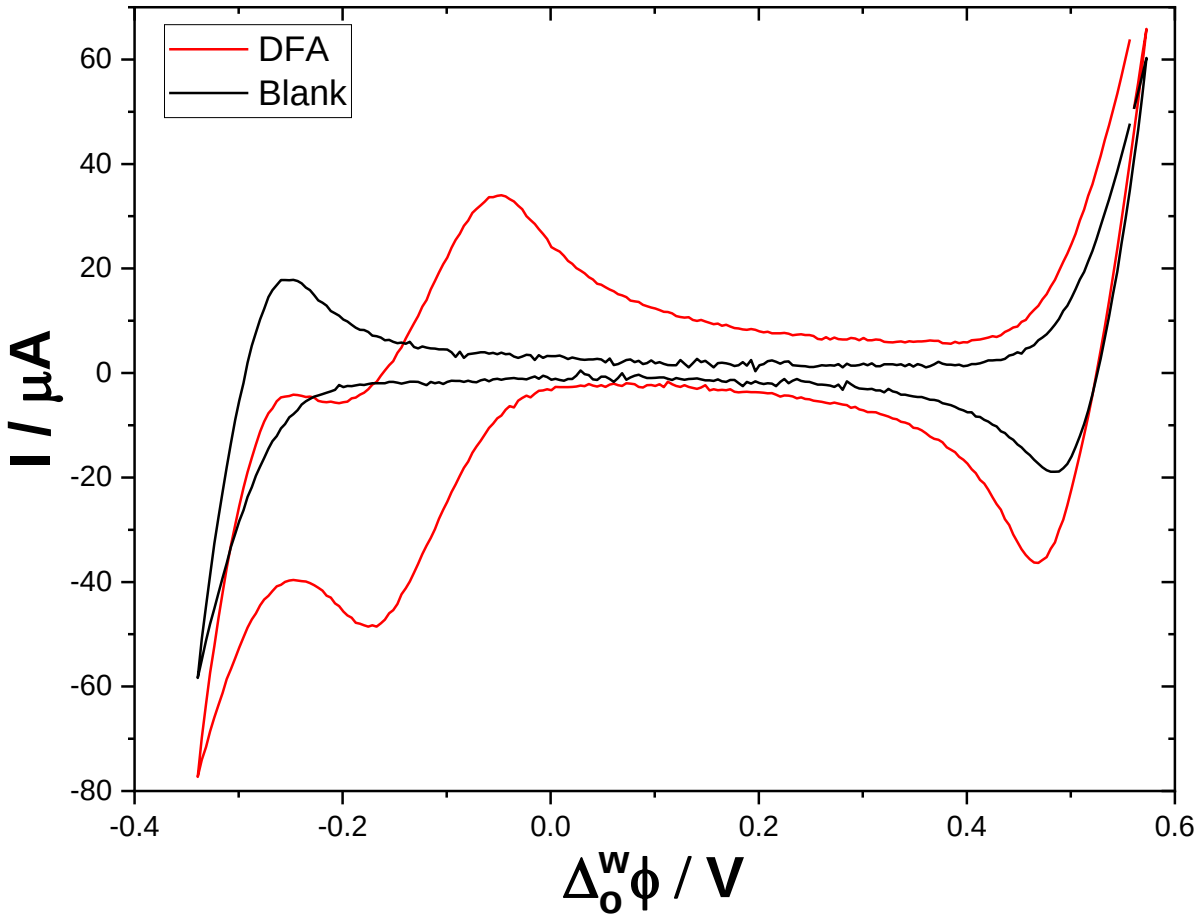

Figure 3.5: Cyclic voltamogram of DFA at pH 12 according to electrochemical cell 5 Scheme 2.1. Scan rate 5mVs^{-1}.

Diclofenac can be considered as an API for cocrystal formation as it transferred at the ITIES.

The selected lipophilic anionic drugs transfer at liquid-liquid interface. However, to obtain the cocrystals at ITIES the experiments with conformer in aqueous or organic phase need to be performed.

3.3. Electrochemical behaviour of hydrophilic cationic selected drug

3.3.1. Cyclic voltammetry study of caffeine transfer

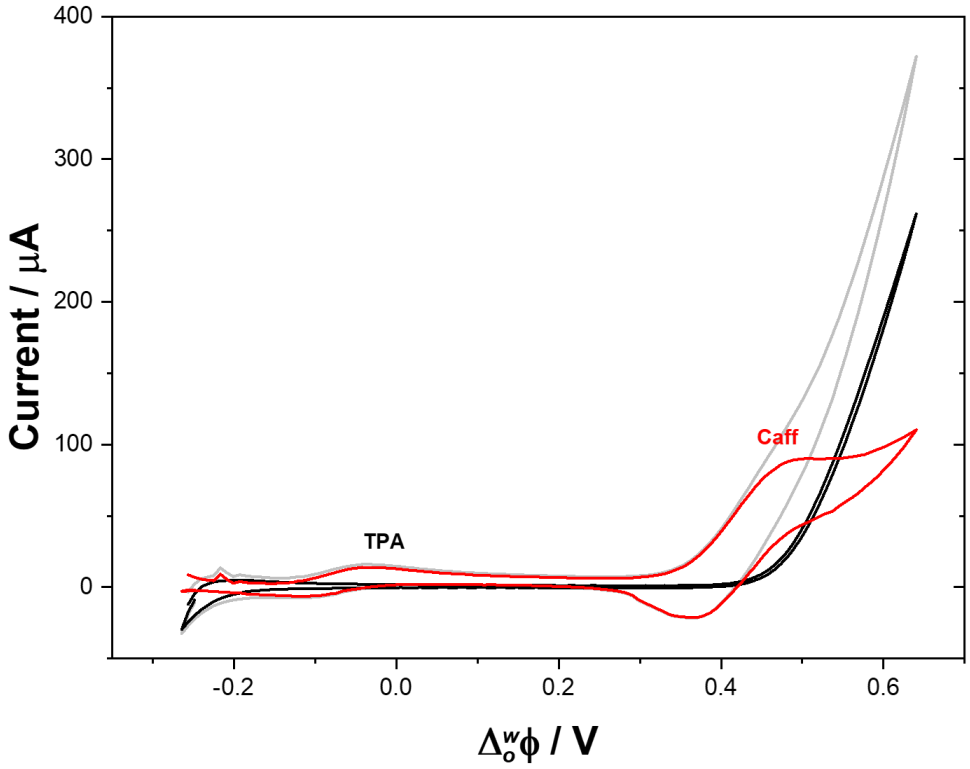

Figure 3.6: Cyclic voltammogram of caffeine transfer at the liquid-liquid interface before (grey) and after (red) subtraction of blank (black). Electrochemical cell 2. Insert image: control experiments confirming the absence of naphthoic acid transfer. Scan rate: 5 mVs^{-1}.

Cyclic voltammetry was performed to investigate the transfer of caffeine and 1H2N at the ITIES (Figure 3.6). The experimental part is described in Chapter 2.4.1. The transfer of caffeine was

performed in pH 2 to be sure that most of the caffeine is present in aqueous solution in the cationic form (electrochemical cell 6 Scheme 2.1). The peak indicating caffeine transfer ($\Delta_o^w\phi^{1/2} = 0.39$V) is visible when the baseline is subtracted due to the overlap of caffeine transfer with background electrolyte ion transfer (Li^+, H^+)[149]. The peak-to-peak separation corresponds to the classical value ~ 59 mV at the ITIES [148], which is expected for the reversible transfer of an ion with a single charge. Cyclic voltammetry showed that caffeine is transferred at high potentials, corresponding to the Nernst-like equation (Eq. 1.6), according to which hydrophilic cations are transferred at high interfacial potentials. On the Figure 3.6, the peak corresponding to the transfer of TPA^+ was also visible and used as a reference as explained in Chapter 2.4.

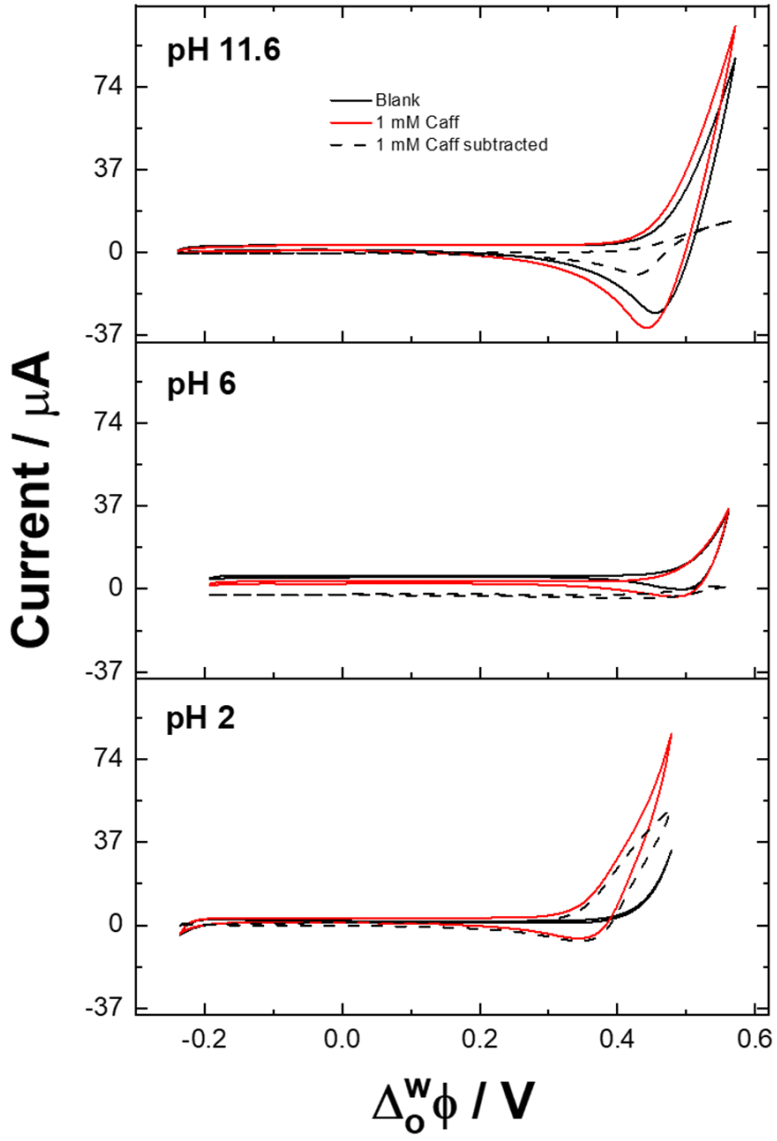

Figure 3.7: Cyclic voltammetry of caffeine transfer at various pH = 2, 6 and 11.6 according to the electrochemical cell 6 x = 10, X = HCl for pH 2, x = 0, X = - for pH 6 and x = 10, X = LiOH for pH 11.6. Scan rate 5mVs^{-1}.

The pH of the aqueous solution was varied to examine its effect on the transfer of caffeine (electrochemical cell 6 Scheme 2.1). At pH higher than 2 we did not observe such a big difference between the blank (black line) and when 1 mM of Caffeine was added to the cell (red line). Two explanations are possible here. First is that caffeine does not transfer at higher pH and the second is that the window is not sufficiently large to observe the caffeine transfer and it can be hidden by the transfer of very hydrophilic cations e.g. Li^+ and H^+ in case of lower pH [149]. Thanks to the studies of caffeine transfer at various pH we could choose the most suitable conditions for cocrytal formation at ITIES. The further experiments were carried out at pH 2 to be sure that most of the caffeine was protonated and the cationic caffeine was transferred at LLI.

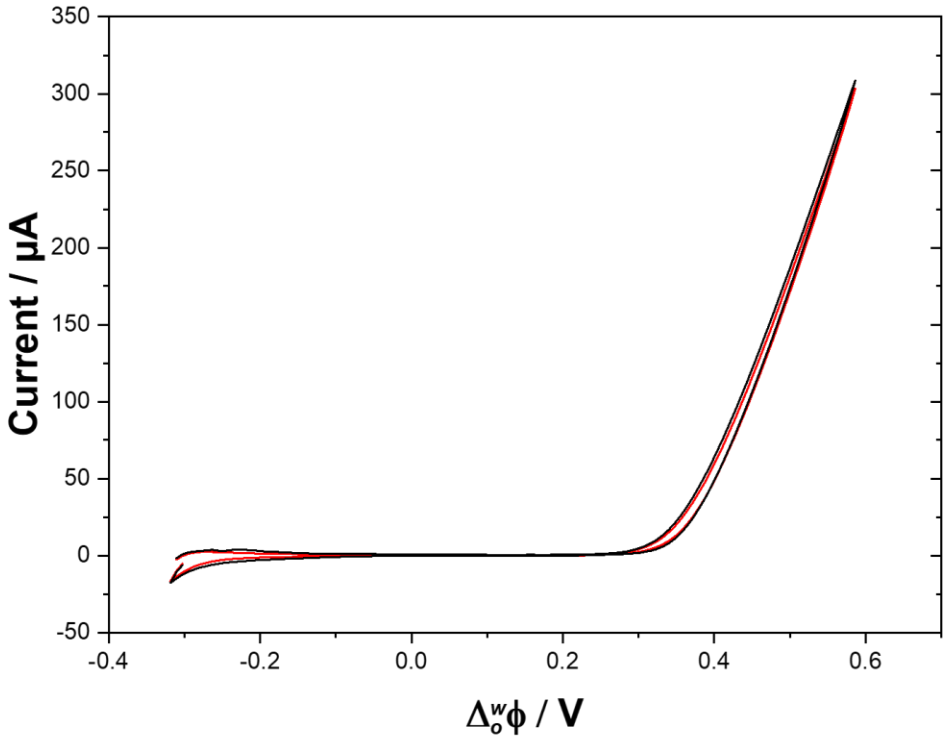

Figure 3.8: Cyclic voltammetry of 1H2N at pH = 2 according to the electrochemical cell 7. Scan rate 5mVs^{-1}. Blank line – blank, red line – 1 mM 1H2N.

1H2N was chosen as a drug conformer for API caffeine.[27], [40] The electrochemical behaviour of naphthoic acid was examined in the electrochemical cell 7 Scheme 2.1. Figure 3.8 indicated that no transfer of 1H2N was observed in the control experiments.

Because it does not transfer across the ITIES, 1H2N is a good candidate as a drug coformer for caffeine for the formation of cocrystals at the liquid-liquid interface.

3.3.2. Voltammetric investigation of the interfacial interactions between 1H2N and Caffeine

Possible interactions between $CaffH^+$ and 1H2N at the ITIES were investigated in different with various organic and aqueous background electrolytes (LiCl, Li_2SO_4, BA^+TPBCl^- and BA^+TB^-). Cyclic voltammograms in the four possible combinations of electrolytes are shown in Figure 3.9. When both $CaffH^+$ and 1H2N are present, the positive end of the potential window is limited by the presence of $CaffH^+$, whereas the negative end of the potential window is set by the presence of 1H2N. The fact that the electrochemical behaviour is the same in the presence or in the absence of 1H2N indicate that the transfer of $CaffH^+$ is not facilitated by 1H2N. AC voltammetry is more sensitive to phenomena taking place at the interface than cyclic voltammetry, so it was further used to characterise the interface when caffeine and 1H2N are present in the electrochemical cell.

In Figure 3.9, the AC voltammograms were recorded in the potential region where there was no background electrolyte ion transfer nor $CaffH^+$ transfer ($-0.15 < \Delta_o^w\phi < 0.15$ V). The differential capacitance (C) was calculated on the basis of AC voltammetry according to equations in Chapter 2.4.1. The potential of zero charge (pzc) was the potential for minimum capacity. Capacitance measurements are related to change in surface charge adsorbed at the liquid/liquid interface [114]. At more negative potentials, the negative charge (anions) is accumulated on the aqueous side of the interface and cations accumulate on the aqueous side of the interface at more positive potentials. The experiments were performed at neutral pH (pH = 6) to visualise the interaction of $CaffH^+$ with the anions present in organic phase. The parameters that have been considered are the difference in hydrophobicity of the anions present in the organic phase, and in lipophilicity of Cl^- and $SO4^{2-}$.

(a)

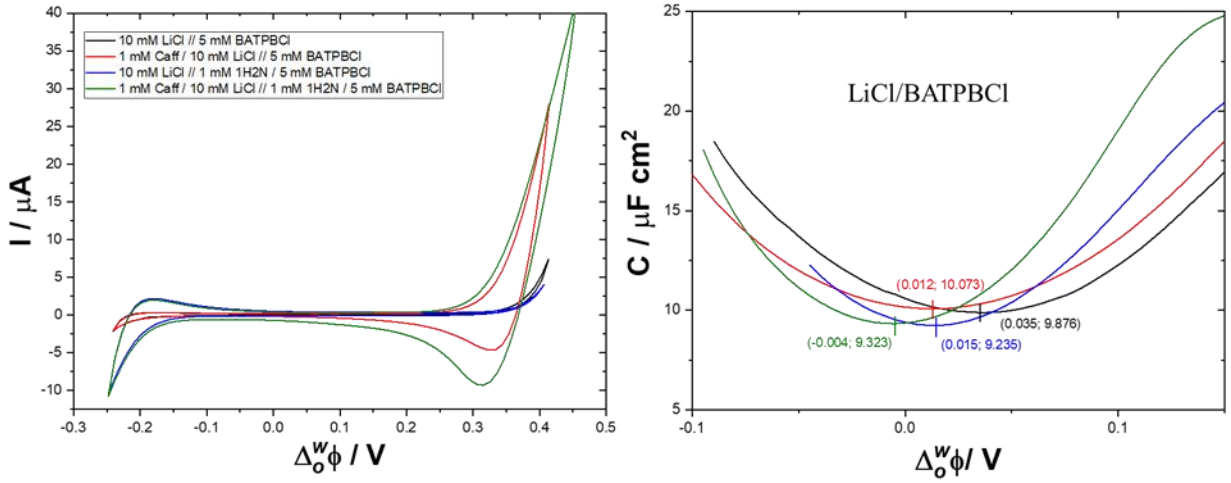
10 mM LiCl // 5 mM BATPBCl
1 mM Caff / 10 mM LiCl // 5 mM BATPBCl
10 mM LiCl // 1 mM 1H2N / 5 mM BATPBCl
1 mM Caff / 10 mM LiCl // 1 mM 1H2N / 5 mM BATPBCl
I / μA
$\Delta_o^w\phi$ / V
LiCl/BATPBCl
C / μF cm²
(0.012; 10.073)
(0.035; 9.876)
(-0.004; 9.323)
(0.015; 9.235)
$\Delta_o^w\phi$/ V

(b)

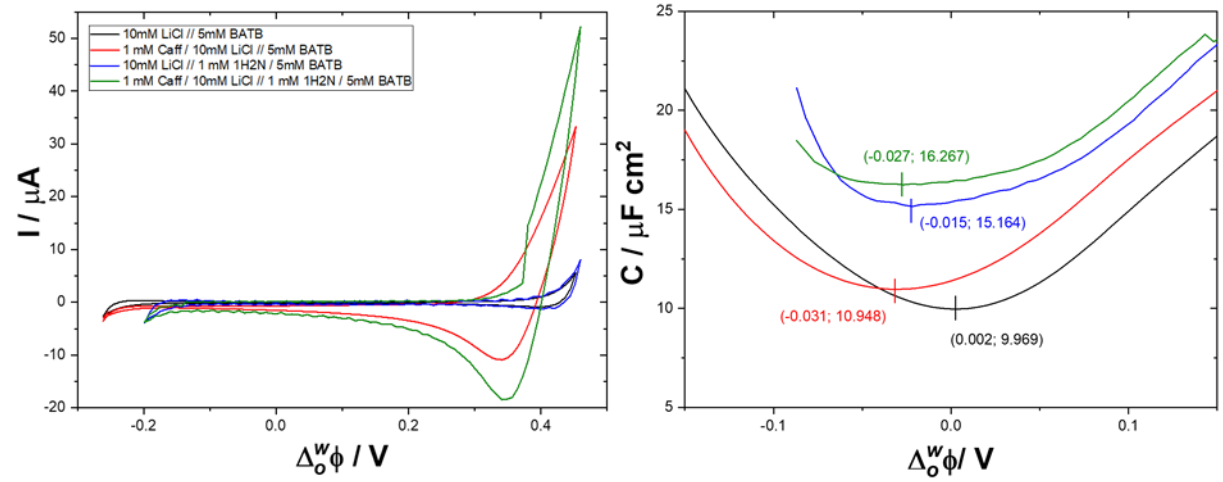
10mM LiCl // 5mM BATB
1 mM Caff / 10mM LiCl // 5mM BATB
10mM LiCl // 1 mM 1H2N / 5mM BATB
1 mM Caff / 10mM LiCl // 1 mM 1H2N / 5mM BATB
I / μA
$\Delta_o^w\phi$ / V
C / μF cm²
(-0.027; 16.267)
(-0.015; 15.164)
(-0.031; 10.948)
(0.002; 9.969)
$\Delta_o^w\phi$/ V

(c)

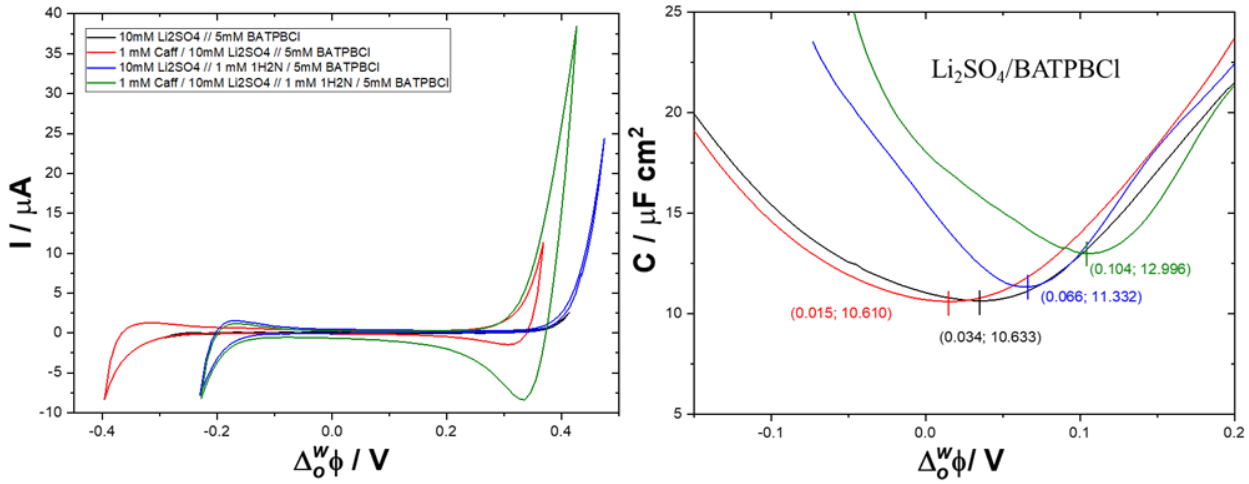

(d)

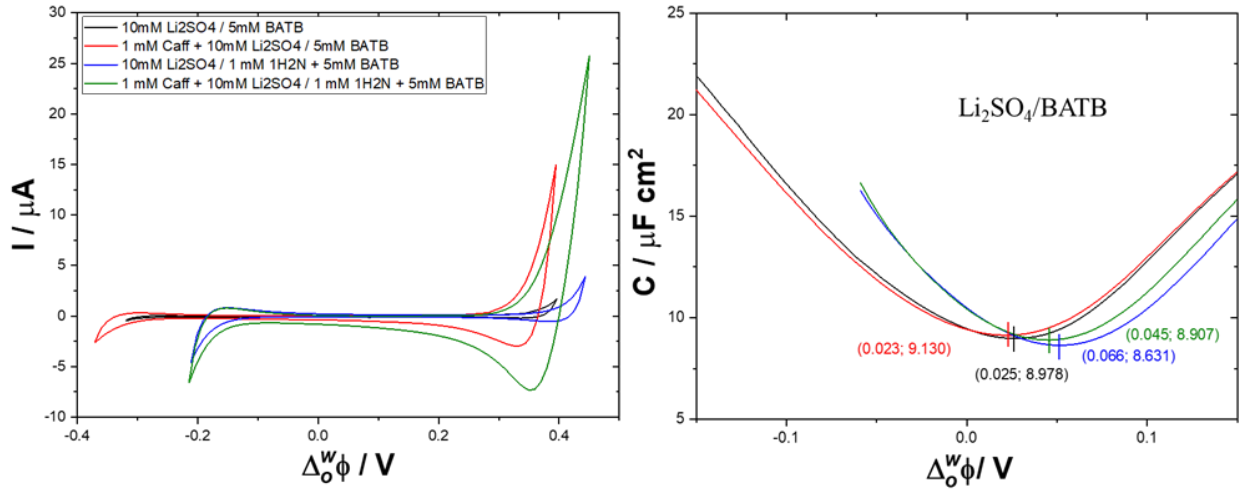

<u>Figure 3.9:</u> Potential dependence of the interfacial capacitance for various conditions and corresponding cyclic voltammograms according to Electrochemical cell 9. The experiments were performed at neutral pH (pH = 6).

When LiCl was used as a salt in the aqueous phase and the organic phase contained BATPBCl (Figure 3.9a), the pzc shifted to lower potential values from 0.035 to 0.012 V and (red line) with the addition of $CaffH^+$, to 0.015 V with the addition of 1H2N (blue line) and to -0.004 V when both 1H2N and $CaffH^+$ are present (green line). The capacitance at the pzc did not change

significantly between all the experimental conditions. However, when $\Delta_o^w\phi$ increased to more positive values, C was higher when $CaffH^+$ alone, 1H2N alone and both 1H2N and $CaffH^+$ were present in the aqueous phase. These results suggest that these two molecules are interracially active. 1H2N and $CaffH^+$ interacted through the interface, before $CaffH^+$ transfer. However, these interactions do not lead to a facilitated transfer of $CaffH^+$, as it was observed in cyclic voltammetry experiments.

When BATPBCl was replaced by the BATB in the organic phase, (Figure 3.9b), a similar behaviour of the pzc values was observed. The pzc shifted to lower potential values from 0.002 to -0.031 V and (red line) with the addition of $CaffH^+$, to -0.015 V with the addition of 1H2N (blue line) and to -0.027 V when both 1H2N and $CaffH^+$ are present (green line). However, the shift in pzc values was accompanied by an increase in capacitance. The differential capacitance values varied from 10.0 μFcm^{-2} (blank experiments), 10.9 μFcm^{-2} ($CaffH^+$) to 15.2μFcm^{-2} (1H2N) and 16.3 μFcm^{-2} ($CaffH^+$ and 1H2N).

Li_2SO_4 was then used as background electrolyte of the aqueous phase while the organic phase was comprised of 5 mM BATPBCl (Fig. 3.9c) or 5 mM BATB (Fig. 3.9d). When BATPBCl is used as background electrolyte, the pzc values increased with the addition of 1H2N from 0.034 to 0.066 V (in the absence of $CaffH^+$) and from 0.015 V to 0.104 V (in the presence of $CaffH^+$). Additionally, we observed the growth of capacitance. Its values varied from 10.6 μFcm^{-2} and 10.6 μFcm^{-2}, for the cells without 1H2N in the organic phase (black and red lines of Fig. 3.9c) to 11.3 μFcm^{-2} and 12.9 μFcm^{-2} (blue and green lines of Fig. 3.9c) for the cells where 1H2N was present in the organic phase. When the organic phase contained 5 mM BATB, we observed that the interface both in terms of pzc and capacitance was a lot let less disturbed by the addition of either $CaffH^+$, 1H2N or by the addition of both (Fig. 3.9d). Indeed, the pzc was, in the absence of 1H2N 0.025 V and 0.023 V (black and red lines of Fig. 3.9d) and was shifted in the presence of 1H2N to 0.066 V and 0.045 V (blue and green line of Fig. 3.9d), respectively. The capacitance decreased minimally comparing to the cells without 1H2N from 9.0 μFcm^{-2} and 9.1 μFcm^{-2} (black and red line) to 8.6 μFcm^{-2} and 8.8 μFcm^{-2} (blue and green line). The changing differential capacitance and pzc depended strongly on the composition of aqueous and organic phase. The various ion present in both phases tended to create ion pairing at ITIES between SO_4^{2-} and cations from organic phase.[150]

Another important remark is that the differences between differential capacitance and pzc values are more visible when 1H2N and $CaffH^+$ are in the vials. It suggested that there are interfacial interactions between these components.

The impact of the organic phase anion was also evident. When $CaffH^+$ was absent in aqueous phase, in case of BATPBCl (Fig. 3.9a and c) in the organic phase we observe bigger shift of pzc towards negative potential which is not noticeable in the cells with BATB (Fig. 3.9b and d). This indicates that positively charged caffeine adsorbed at the interface. This data agrees with these other studies of positively charged proteins[114], [116] and positively charged nanoparticles[151]. What is interesting this behaviour is not visible when 1H2N is present in the organic phase. Then, after $CaffH^+$ addition the potential shifts to more positive values. In this case we have the accumulation of negatively charged ions at ITIES and cations are repulsed from the interface.[152]

For the cells comprising BATPBCl in the organic phase, the capacitance attained smaller values in the experiment with Cl^- than SO_4^{2-} which is not in agreement with the previous work where there was no significant difference between these two anions [153]. In the cells with LiCl the differential capacitance and pzc have lower values for BATPBCl than in the cell with BATB[136], [153]. In the presence of Li_2SO_4 we had the reverse situation. The difference may come from ion pairing at the liquid-liquid interface. When $CaffH^+$ is presence in the aqueous phase, the capacitance is higher in the cells with BATB due to the possible ion pairing between the caffeine cation and TB^- anion[152]. In the blank experiment the differential capacitance seemed to be independent of the anions present in aqueous and organic phase.[153], [154] In the absence of 1H2N the differential capacitance differed less significantly at positive potentials than in the vials where 1H2N was a part of the organic phase.

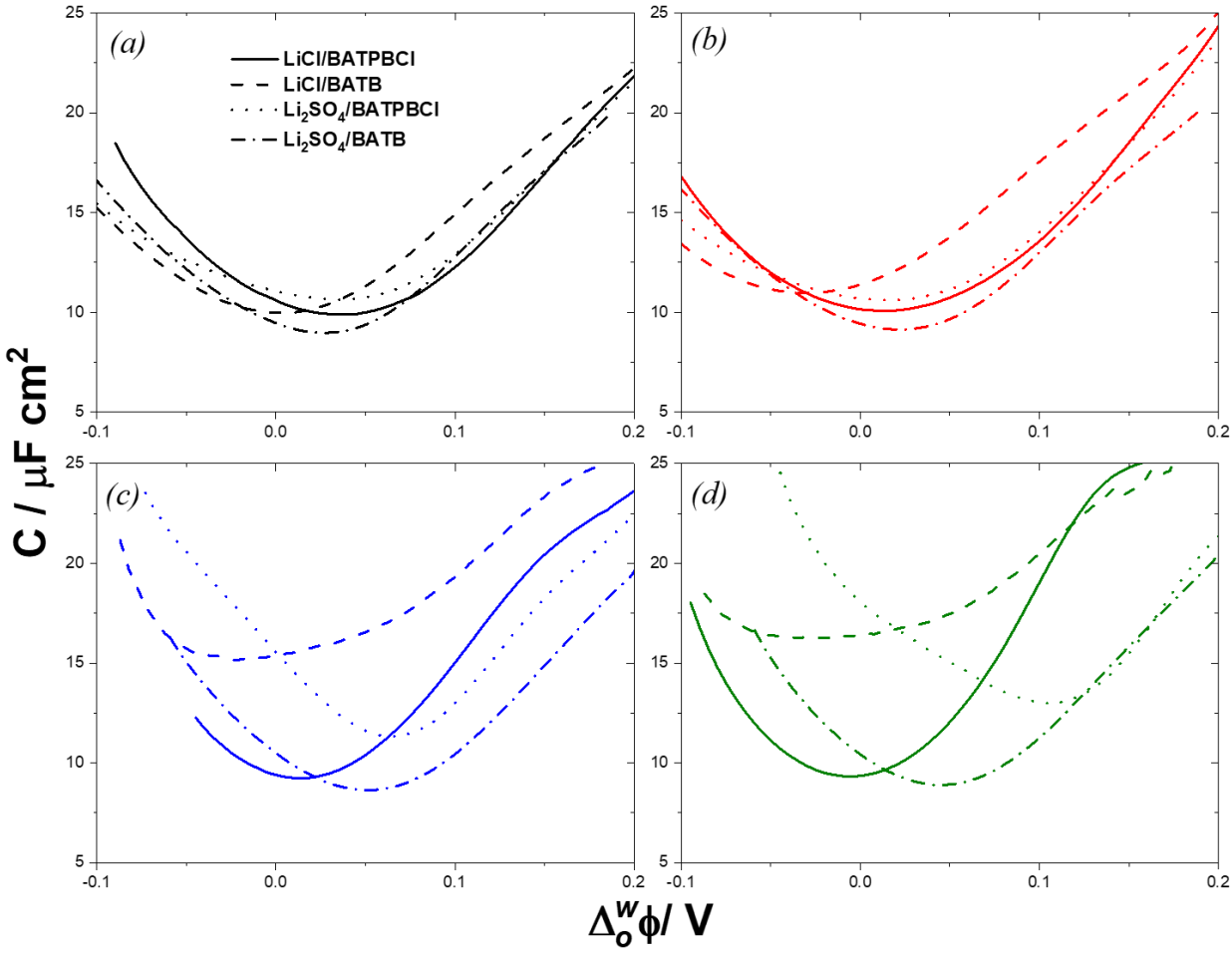

Figure 3.10: Potential dependence of the interfacial capacitance for various conditions according to Electrochemical cell 9: (a) blank (——), (b) Caff (——), (c) 1H2N (——), (d) Caff/1H2N (——). LiCl/BATPBCl (——), LiCl/BATB (- - -), Li_2SO_4/BATPBCl (···), Li_2SO_4/BATB (-·-·-).The experiments were performed at neutral pH (pH = 6).

For the electrochemical cells containing BATPBCl in the organic phase, the differences in capacitance are not in agreement with what was observed before that there was no significant difference between Cl^- and SO_4^{2-} [153], therefore the influence of other comportments must change the capacitance. In the electrochemical cells with LiCl the differential capacitance and pzc have lower values for BATPBCl than in the cell with BATB [136], [153]. In the presence of Li_2SO_4 we had the opposite situation. The difference may come from the ion pairing at the liquid-liquid interface involving anions in aqueous phase and cations in organic phase. When $CaffH^+$ is presence

in the aqueous phase, the capacitance is higher in the cells with BATB may be due to the possible ion pairing between the caffeine cation and TB^- anion [152].

According to Figure 3.10 b and c, there were more significant differences in the pzc and capacitance when 1H2N was part of the experiments than when there was only organic electrolyte present in organic phase (Fig. 3.10a and b). In the absence of 1H2N (Fig 3.10a), the pzc was lower than when 1H2N was present in the electrochemical cell (Fig 3.10b) which indicated that 1H2N played role in the interfacial phenomena. In the absence of 1H2N after addition of $CaffH^+$ (Fig 3.10b), the pzc shifted toward lower potential where in the presence of 1H2N its value increased (Fig 3.10d). Positively charged $CaffH^+$ in the aqueous phase caused the drop of the potential for minimum capacitance. The capacitance did not change significantly after the addition of $CaffH^+$ when there was no 1H2N in the organic phase (Fig 3.10b). On the contrary, in the presence of 1H2N and $CaffH^+$ there was a decrease in the capacitance in the cells with the Li_2SO_4 (dotted and dashed/dotted lines Fig 3.10d) indicating rise in the charge located at the interface.

3.4. Conclusion

This chapter provided information on the electrochemical behaviour of selected drugs at the ITIES. The results obtained proved that piroxicam, sildenafil did not transfer across the ITIES and therefore, are not the best candidates for the electrochemically controlled cocrystallization of drugs.

The chosen weak acids, ketoprofen and diclofenac were transferred across the ITIES at low potentials and seemed to be good candidates for the electrochemically controlled cocrystallization of drugs. However, due to the low solubility in water they will be further examined as the compounds of the organic phase.

Caffeine turned out to be the best candidate for the electrochemically driven cocrystallization. It is transferred across the ITIES and it is very water soluble. By verifying the behaviour of caffeine at different pHs, we chose pH 2 as the main and best conditions for further caffeine research. Additionally, 1-hydroxy-2-naphthoic acid, the suitable conformer for caffeine studies did not transfer at ITIES, which made it a suitable conformer for cocrystallization process.

The behaviour of $CaffH^+$ and 1H2N at the ITIES were followed by the series of cyclic and AC voltammetries experiments in various conditions of background electrolyte. The goal was to investigate the interaction at the ITIES between these compounds by use of various aqueous (LiCl, Li_2SO_4) and organic (BATPBCl and BATB) electrolytes. We remarked different behaviour of $CaffH^+$ in absence and in presence of 1H2N. The fact that the electrochemical behaviour is the same in the presence or in the absence of 1H2N indicate that the transfer of $CaffH^+$ is not facilitated by 1H2N. The increase of $\Delta_o^w\phi$ caused capacitance rise, when $CaffH^+$ alone, 1H2N alone and both 1H2N and $CaffH^+$ were present in the aqueous phase. These results suggest that these two molecules are interracially active. The differential capacitance and pzc also varied depending on the conditions used during the experiment. In the following chapter, the cocrystallisation of $CaffH^+$ and 1H2N will be investigated at an interface composed of LiCl as an aqueous electrolyte and BA^+TPBCl^- as an organic electrolyte.

4. ELECTROCHEMICALLY CONTROLLED COCRYSTALLISATION OF CAFFEINE: 1-HYDROXY-2-NAPHTHOIC ACID

We propose here the cocrystallisation of caffeine with organic carboxylic acids at the interface between two immiscible electrolyte solutions (ITIES). Electrochemistry at the ITIES has been harnessed in recent years for the electrogeneration of a variety of materials such as Au nanoparticle assemblies,[87] amorphous mesoporous silica,[155] porphyrin films,[111], [113] protein deposits,[116], [126] and polymer films.[117] In those previous studies, a potential difference, $\Delta_o^w\phi$, was applied across the oil-water interface. This electrical driving force triggered a charge transfer, either ion or electron transfer, across the interface and led to material electrodeposition at the interface. We have investigated here the control of cocrystallisation of two reagents of mismatch solubility by the imposed potential difference at the oil-water interface. The system comprised caffeine (Caff) as a hydrophilic compound present in the aqueous phase and 1-hydroxy-2-naphthoic acid (1H2N) as a coformer present in the oil phase, 1.2-dichloroethane (DCE). The effect of chemical polarisation of the oil-water interface on the polymorphism of the cocrystals formed was also explored.

4.1. Control of the interfacial potential difference by chemical polarization

On the Figure 4.1 the experimental set up is presented. It consisted of two immiscible solutions in order to form the interface. The aqueous phase was an acidic solution of 10 mM LiCl (pH = 2, acidified with HCl), and various concentrations of caffeine (x = 10, 30 mM and saturated solution). The organic phase (immiscible with water) was 1H2N in DCE. The components, the API – caffeine and its conformer 1H2N have a mismatched solubility i.e. the solubility of the acid in organic phase is high, while the solubility of caffeine is low in the contrary to the aqueous solution where the caffeine is very well soluble and 1H2N is insoluble. Following salts were added to the organic phase of the two-phase systems to chemically polarize the interface: BACl for a low potential and

KTPBCl for high potential. The ions present in the system are distributed in equilibrium between the aqueous and organic phases, resulting in a change of interfacial potential ($\Delta_o^w\phi$)[156], [157]. In case of negative potential (Fig 4.1 Vial 1 and 2), the standard transfer potential of BA^+ ($\Delta_o^w\phi^0_{BA^+}$ = -0.67V) is lower than the standard positive potential of caffeine ($\Delta_o^w\phi^0_{\text{Caff}^+}$= 0.39V) so caffeine will not transfer to the organic phase. However, when in the cell we placed KTPBCl (Fig 4.1 Vial 3) and standard transfer potential of K^+ is higher than the one of caffeine ($\Delta_o^w\phi^0_{\text{K}^+}$=0.53V) there is an ion exchange. This potential difference was measured by the open circuit potential (OCP) measurements: OCPs were -2.80 V (vial 1), 0.09 V (vial 2) and 0.57 V (vial 3). An additional biphasic system without salt imposing potential in organic phase was prepared as a control sample (Fig 4.1 Vial 4). The vials were left for 16h. The cocrystals were collected and any residual aqueous or organic solvent was left to evaporate.

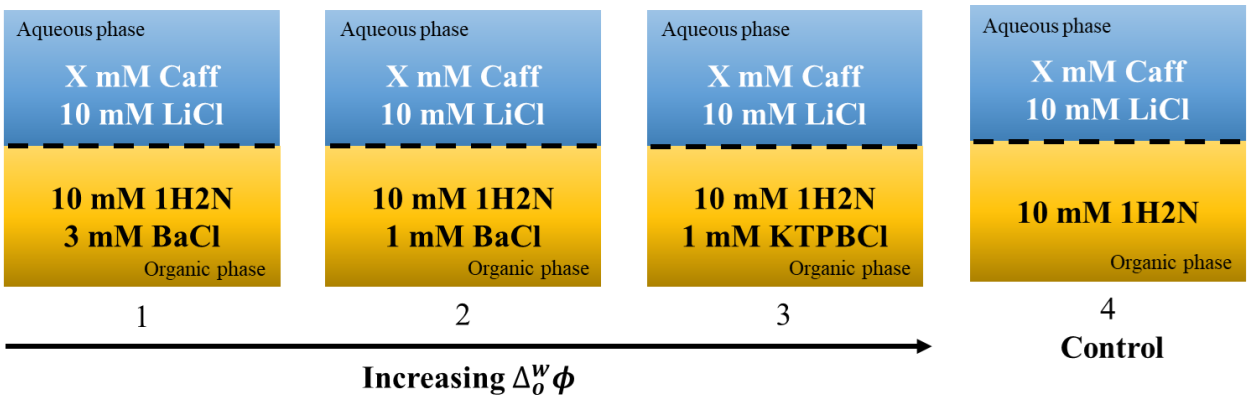

Figure 4.1: Experimental set up presenting chemical polarisation of the interface. BACl - Bis(triphenylphosphoranylidene)ammonium chloride; KTPBCl - potassium tetrakis(4-chlorophenyl) borate. The dashed line indicates the liquid-liquid interface.

4.2. Crystallisation of Caffeine: 1H2N at the polarised liquid-liquid interface

The formation of Caff: 1H2N cocrystals at a water-oil interface was investigated by preparing a series of vials of varying experimental conditions according to the description in Chapter 4.1.

Figure 4.2 shows images of vials containing aqueous caffeine solution and organic solution of 1H2N, respectively, and polarised by the addition of salts with corresponding experimental conditions below. The imposed potential difference increases from the negative potential on the left-hand side towards positive potentials on the right. Control experiment vials (Vials 4, 7, 10) were prepared in the absence of potential-imposing salts in the organic phase.

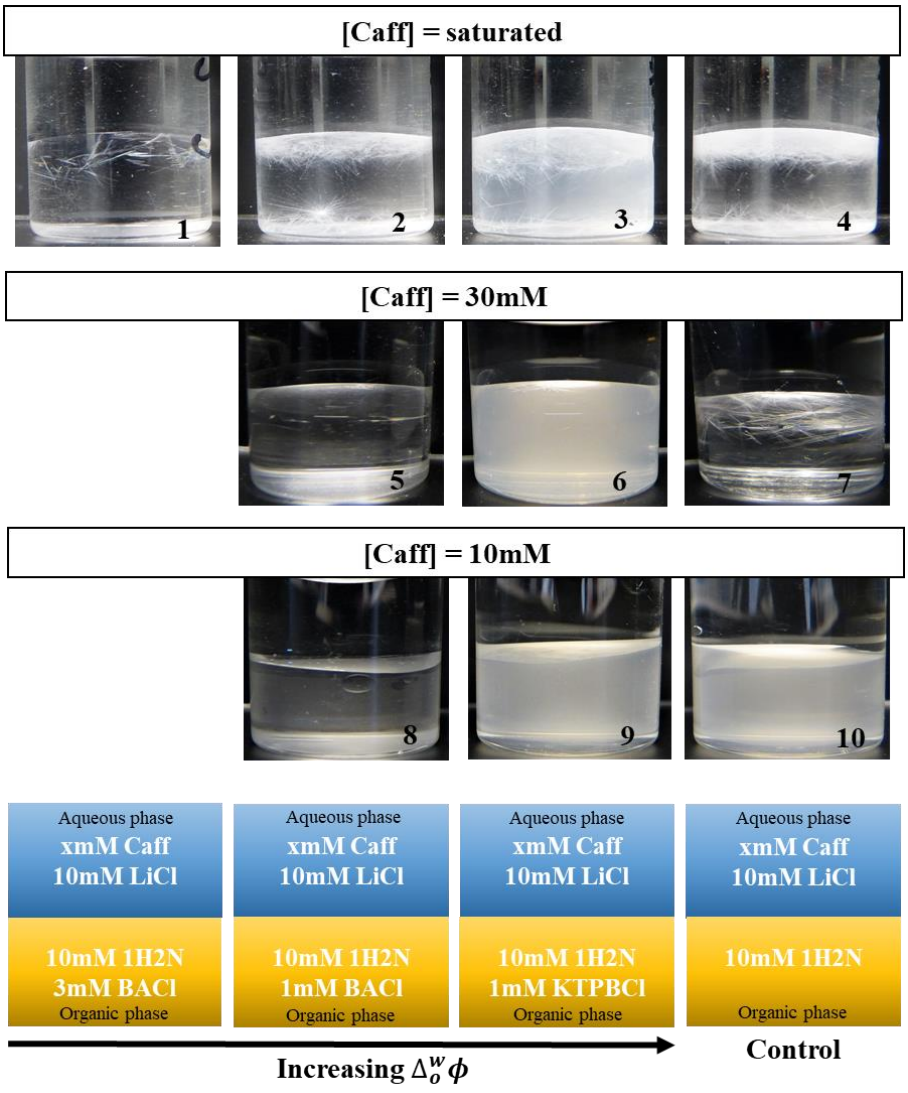

<u>Figure 4.2:</u> Photographs of aqueous-DCE biphasic systems for various concentration of caffeine ([Caff] = 10 mM, 30 mM and saturated solution) and different interfacial polarisations with corresponding experimental conditions below. Images were taken after the vials had been left at room temperature for 16 hours.

When the aqueous solution was saturated with $CaffH^+$, differences in the number of cocrystals forming at the interface were observed. We observe that the low interfacial potential hindered the transfer of $CaffH^+$ from the aqueous to the organic phase (Fig. 4.2 Vial 1). The observed number of crystals rose with increasing interfacial potential (Fig. 4.2 Vial 2 and 3). Differences in cocrystal formation due to changes in interfacial polarization were also visible at lower $CaffH^+$ concentrations. The formation of cocrystals was inhibited at the intermediate potential for 30 mM (Fig. 4.2 Vial 5) and 10 mM (Fig. 4.2 Vial 8) of $CaffH^+$ in aqueous phase. It was therefore not necessary to carry out experiments with a very negative potential, as was the case with the saturated $CaffH^+$ solution (Fig. 4.2 Vial 1). Additionally, with high interfacial polarisation and [Caff] = 10 mM, it was possible to collect cocrystals located at the interface, which was not achieved in the control experiment (Fig. 4.2 Vial 10). These outcomes suggest that the cocrystallisation of Caff: 1H2N can be controlled by changing the potential at the interface.

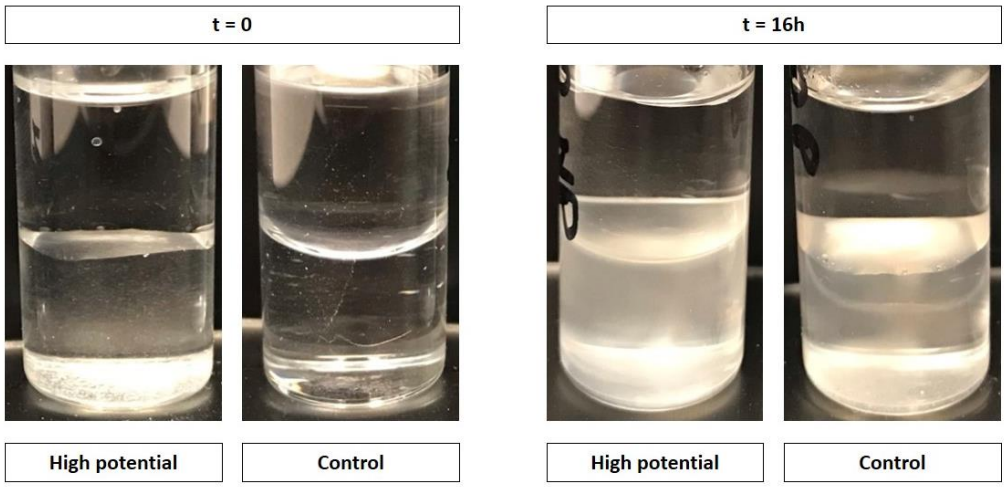

<u>Figure 4.3:</u> Photographs of aqueous-DCE biphasic systems for 10 mM $CaffH^+$ in aqueous phase, control and high polarisation. Images were taken after the vials had been left at room temperature for 16 hours.

Under these experimental conditions, $CaffH^+$ is a cation[149] and as shown before by cyclic voltammetry (Fig 3.6 Chapter 3.3) is transferred from the aqueous phase to the organic phase at a high potential ($\Delta_o^w\phi$ = 0.39V). In the high-potential vials, the cationic $CaffH^+$ was transferred to the organic phase, resulting in local supersaturation of the concentration, and consequent

cocrystallisation at the liquid-liquid interface. In fact, the blurred organic phase for [Caff] = 10 mM (Fig. 4.3) is attributed to the formation of Caff: 1H2N precipitates, which contrasts with the cells at time t = 0 when the vials were set.

4.3. Cocrystals characterization

4.3.1. Scanning Electron Microscopy – SEM

The cocrystals formed at the liquid-liquid interface, were collected and analysed by scanning electron microscopy (SEM). The images are presented on Figure 4.4. The higher potential favoured the formation of cocrystals at the interface. When it comes to the lower concentration of $CaffH^+$ in aqueous phase (10 mM and 30 mM), intermediate potential was sufficient to inhibit the cocrystal formation, whereas for saturated $CaffH^+$ solutions, even the lowest potential was required to hinder the cocrystallization process. SEM images showed that change in potential caused the differences between the cocrystal shape, size and quantity (Fig 4.4).

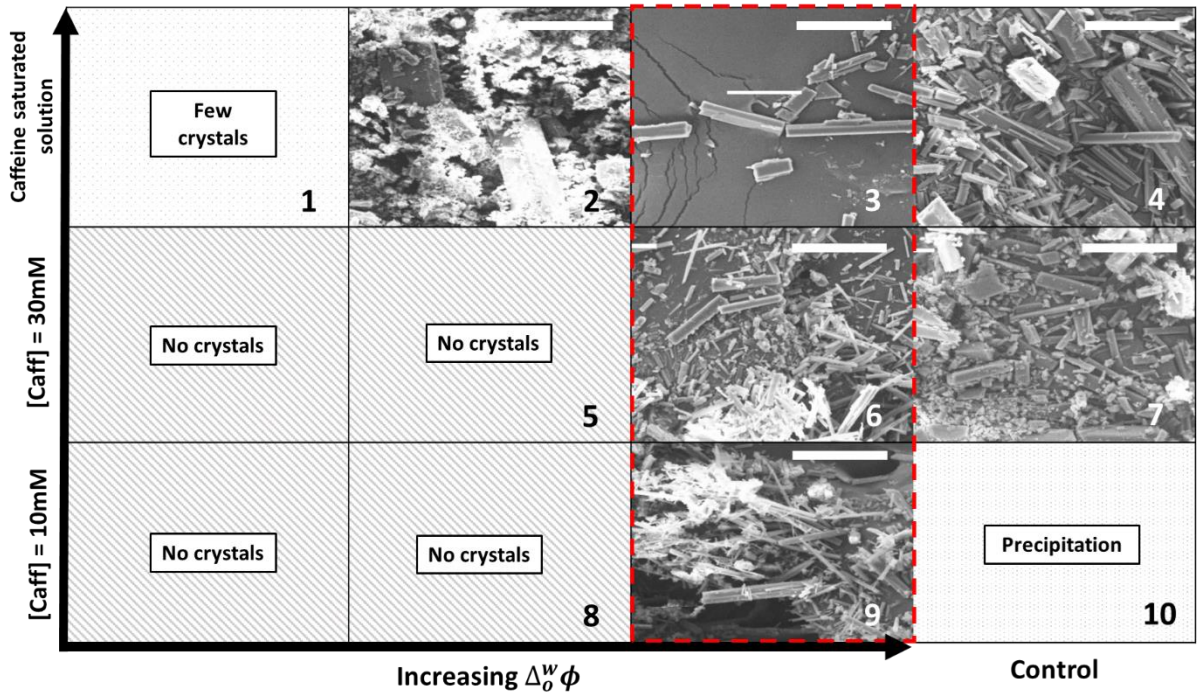

Figure 4.4: Scanning electron micrographs of the crystals obtained for different experimental

conditions with the indicated experimental vials. The crystals were collected after 16 h. Scale bar: 50 µm.

When a higher positive potential was applied, a large number of small crystals were formed, while when a less positive potential was applied, fewer crystals were formed. A similar effect was observed for electrodeposition of proteins at the ITIES.[126]

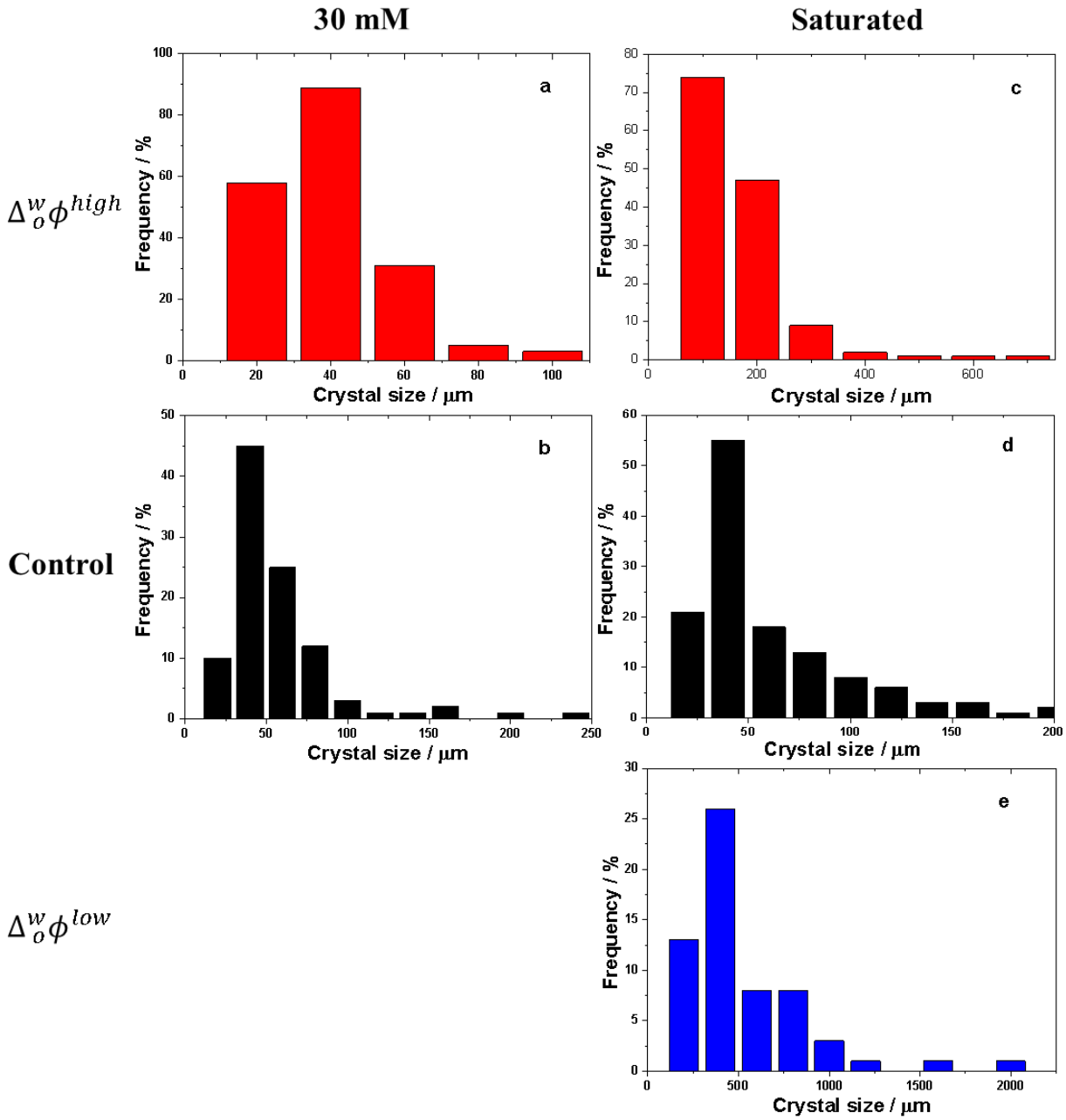

Figure 4.5: Crystal size distribution for (a) - 30 mM high polarisation (Fig. 4.2 Vial 6) and (b) -

control (Fig. 4.2 Vial 7) and (c) - saturated CaffH$^+$ concentration high polarization (Fig. 4.2 Vial 3), (d) - low polarization (Fig. 4.2 Vial 2) and (e) – control (Fig. 4.2 Vial 4).

The size and size distribution of the cocrystals were then analysed by SEM (Fig 4.4, Fig 4.5). In the vials with saturated solution of CaffH$^+$, the biggest cocrystals, with crystal sizes (426 ± 42) μm were obtained for the intermediate potential difference (Fig 4.4 and Fig 4.5 Vial 2). In the cells with higher potential the size of cocrystals were (121 ± 11) μm and larger than those found in the control experiment (50 ± 3) μm. This indicates the effect of the potential difference on the mass transport of CaffH$^+$ and cocrystal nuclei and thus on the size of the cocrystals. For 30 mM CaffH$^+$ concentration, the crystal size decreased at high potential (32 ± 1) μm, compared to control conditions (47 ± 3 μm). In the control experiment with 10 mM CaffH$^+$, the precipitate could not be collected and therefore no SEM analysis was performed.

4.3.2. X-ray diffraction

In order to know the crystallographic structure and polymorphic phases, the cocrystals were examined by single crystal X-ray diffraction (SCXRD). The cocrystals found at the interface were of the right shape and size to be analysed by SCXRD as described in Chapter 2.4.2. The phases detected in the cocrystals corresponded to the Caff:1H2N cocrystals already published in the Cambridge Crystallographic Data Centre (CCDC)[158] (Table 4.1 Figure 4.6). The measurements showed the existence of two crystallographic phases: I and II (Fig 4.7).

Such complexes crystallized in the monoclinic P21/n space group with a stoichiometric amount of CaffH$^+$ and 1H2N. CaffH$^+$ and 1H2N interacted by hydrogen bonding between the carbonyl and imidazole groups.[39] SCXRD is a powerful technique for crystallographic structure determination, however it is not representative of the entire contents of a product because only one crystal is needed for the analysis. Therefore, in order to know the structure representing the whole sample, the powdered cocrystals were analysed by Powder X-ray diffraction (PXRD), as described in Chapter 2.4.3. Phase I, Phase II and a minor contamination from caffeine powder were detected in all samples. None of the compounds initially present in the vials (LiCl, BACl, and KTPBCl) were visible in the PXRD diagram, as there were no 1H2N residues. All peaks presented in the

difractogram were thus well fitted and indexed only by phase I, phase II and caffeine. The high polarisation of the interface was found to favour phase I over phase II. PXRD analyses of the collected powders for concentrations of 30 mM (Figure 4.2 (a)) and saturated $CaffH^+$ (Fig 4.2 (b)) showed that phase I predominance was found in the sample when the interface was positively polarised (Fig. 4.2 Vial 6), while phase II was more present in the control sample (Fig. 4.2 Vial 7).

Table 4.1: Crystallographic data for phases I (CCDC 655956) and II (CCDC 1583505) of Caff: 1H2N cocrystals obtained by polarisation of the liquid-liquid interface[158].

	Phase I	**Phase II**
Crystal system	monoclinic	monoclinic
Space group	P21/n	P21/n
a/ Å	7.60	7.00
b/ Å	14.04	47.01
c/ Å	16.32	15.84
β /°	94.03	90.74
V/ Å³	1739	5217

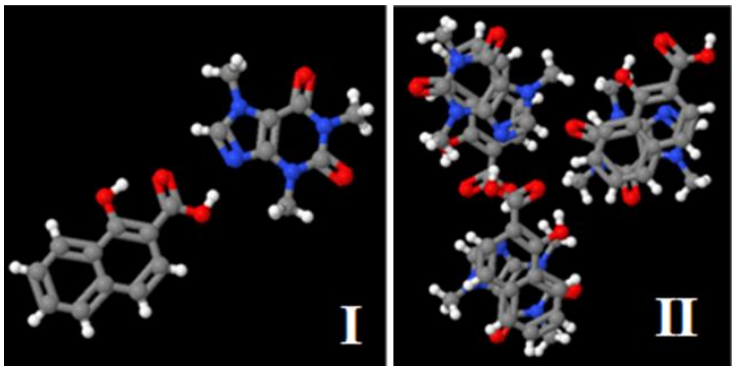

Figure 4.6: Chemical structures for phases I (CCDC 655956) and II (CCDC 1583505) of Caff: 1H2N cocrystals obtained by polarisation of the liquid-liquid interface[158].

Similar results were shown in the diffractograms of cocrystals collected in a sample with a saturated caffeine solution. The high potential resulted in crystals containing almost exclusively phase I. In the case of high caffeine concentration, a higher caffeine residue was also observed (Fig 4.7 (b)).

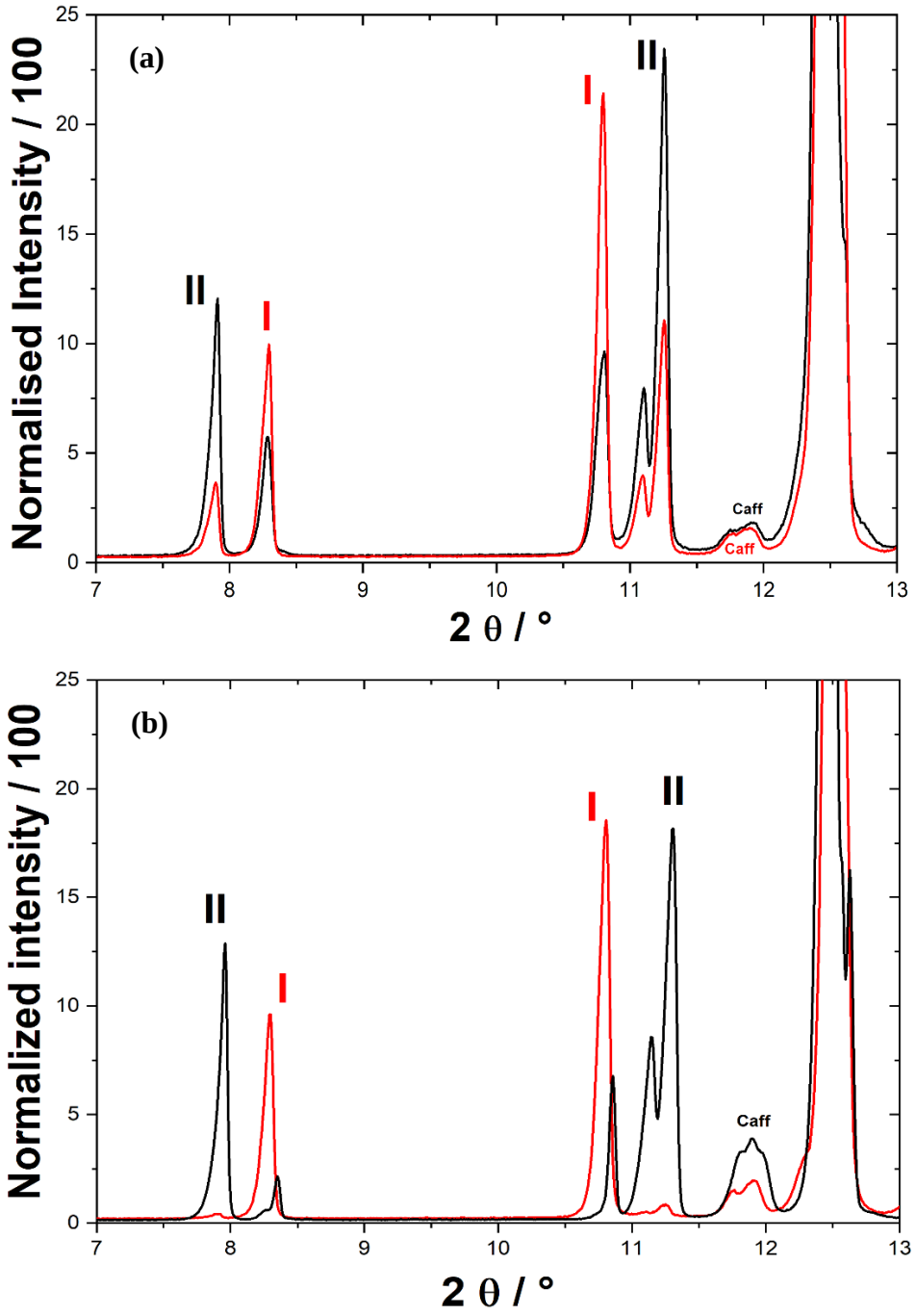

Figure 4.7: Diffractograms of cocrystal (Caff: 1H2N) powders obtained at the liquid-liquid interface for the 30 mM concentration of caffeine (a) and saturated concentration of caffeine (b) at high potential (red) and control (black). Roman numbers attributed the different peaks to the corresponding crystallographic phase, whereas Caff indicates the peak corresponding to the starting material.

We proposed semi-quantitative calculations to compare the phase ratios of the samples. The PXRD diagrams of a phase I and II mixture was simulated based on the CCDC files from the known structures of pure single-phase material. *The simulation of was carried out by Pierrick Durand.* Then we calculated the proportions of phases present in the cocrystals. The intensities of the peaks in the analyzed samples were normalized and compared with the normalized intensities of the pure single phases from the simulated phase I and II diffractograms. The results for various concentrations of caffeine are presented on Figure 4.8. When the interface was positively polarized, the predominance of phase I increase with rising caffeine concentration in the aqueous phase, which we did not observe in the control experiments. In addition, the unreacted caffeine content is lower when high potential is used (Fig. 4.9).

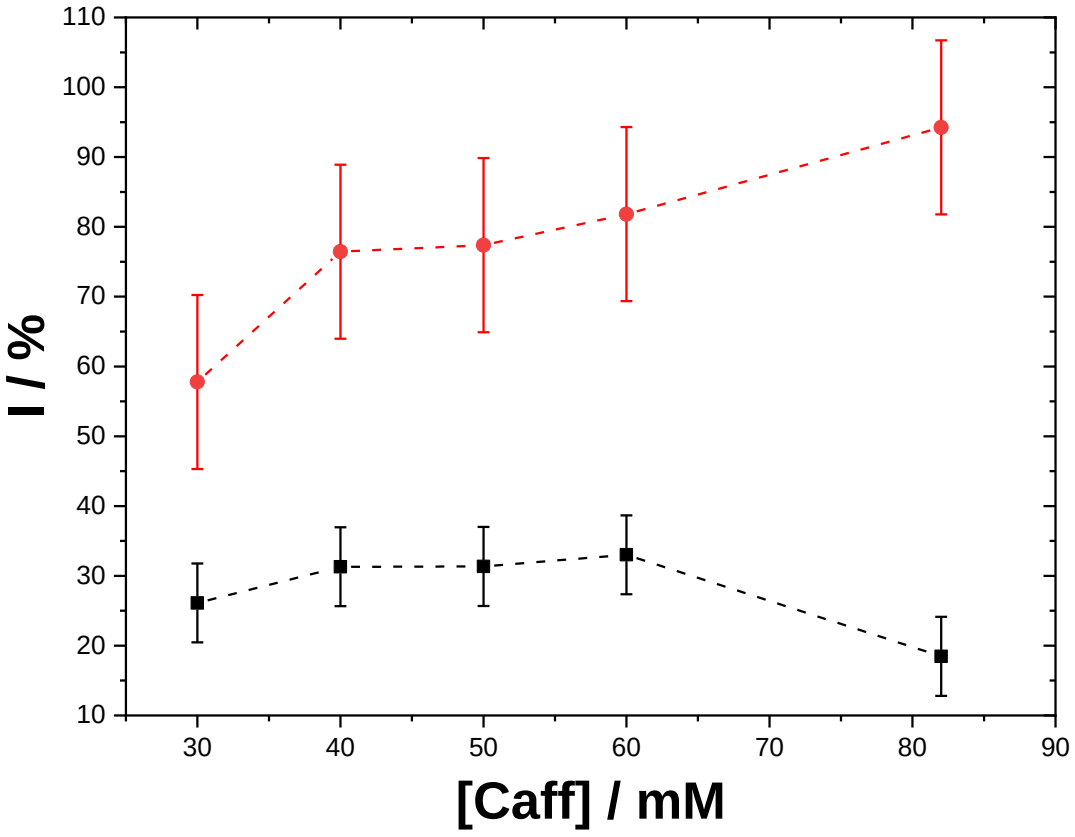

<u>Figure 4.8:</u> The Phase I % content dependence on caffeine concentration for high potential (red) and control experiment (black). Cocrystals caff: 1H2N obtained at the liquid-liquid interface for

caffeine concentration: 30mM, 40 mM, 50 mM, 60 mM and saturated. Error bars were determined as standard deviation.

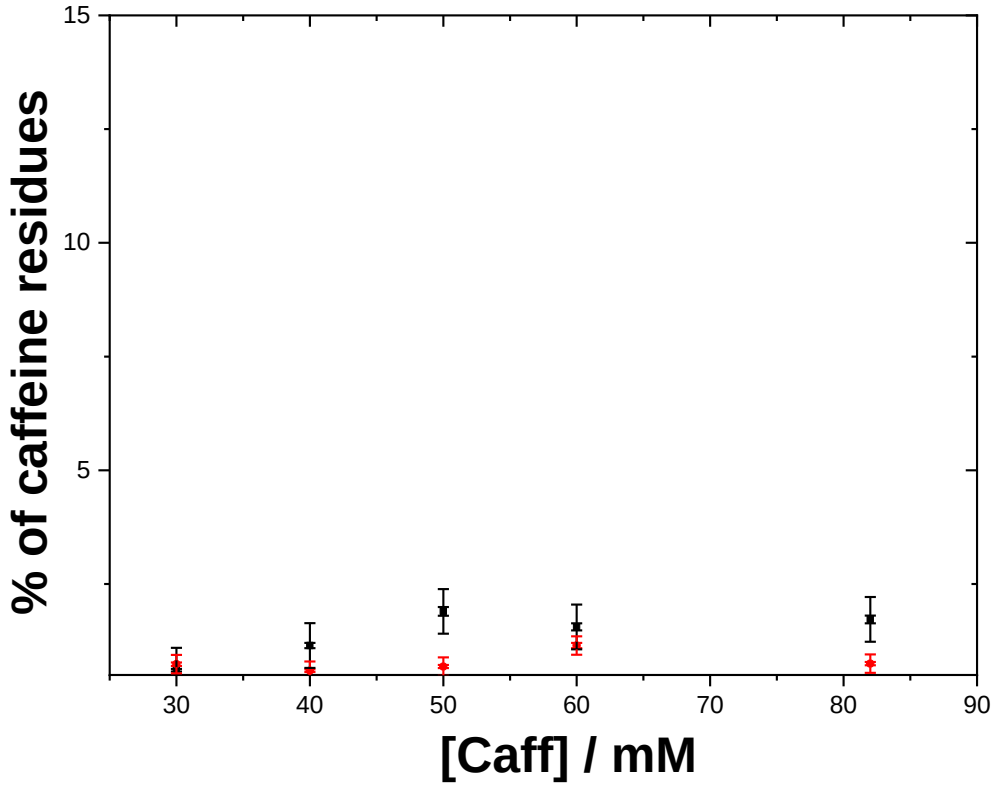

Figure 4.9: The content of the caffeine residues, depending on the caffeine concentration and the applied potential. The results correspond to caffeine residues found in the cocrystals Caff: 1H2N obtained at the liquid-liquid interface for Caffeine concentration = 30mM, 40 mM, 50 mM, and 60 mM and saturated at high potential (red) and control (black).

4.3.3. Thermal analysis

Thermal analysis was made by differential scanning calorimetry (DSC) for caffeine saturated solution and high potential and control experiment. The experimental conditions are described in Chapter 2.4.4.

Both phases represent endothermic events. However, we can observe that phase I has lower melting point (~190°C, Fig 4.10) than phase II due to the higher number of hydrogen bonds in the

Phase II (Fig 4.10). Similar results were obtained for the cocrystals of carbamazepine and nicotinamide (CBZ-NIC)[159] and caffeine and nitrobenzoic acid cocrystals[160]. Here, phase II represents 1:1 system, and the melting temperature is lower than for more complex Phase I. Thermal analysis of the cocrystals obtained at high potential (red line, Fig. 4.10) showed a characteristic melting point at 190°C, which corresponds to crystallographic phase I. Peak at 185.9 might come from sample impurities. For thermal analysis of the control cocrystals (black line, Fig. 4.10), there are two peaks that represent the two crystalline phases (phase I at 190.1 and phase II at 193.7°C). We can explain this as the phase transition and change in a melting point[160].

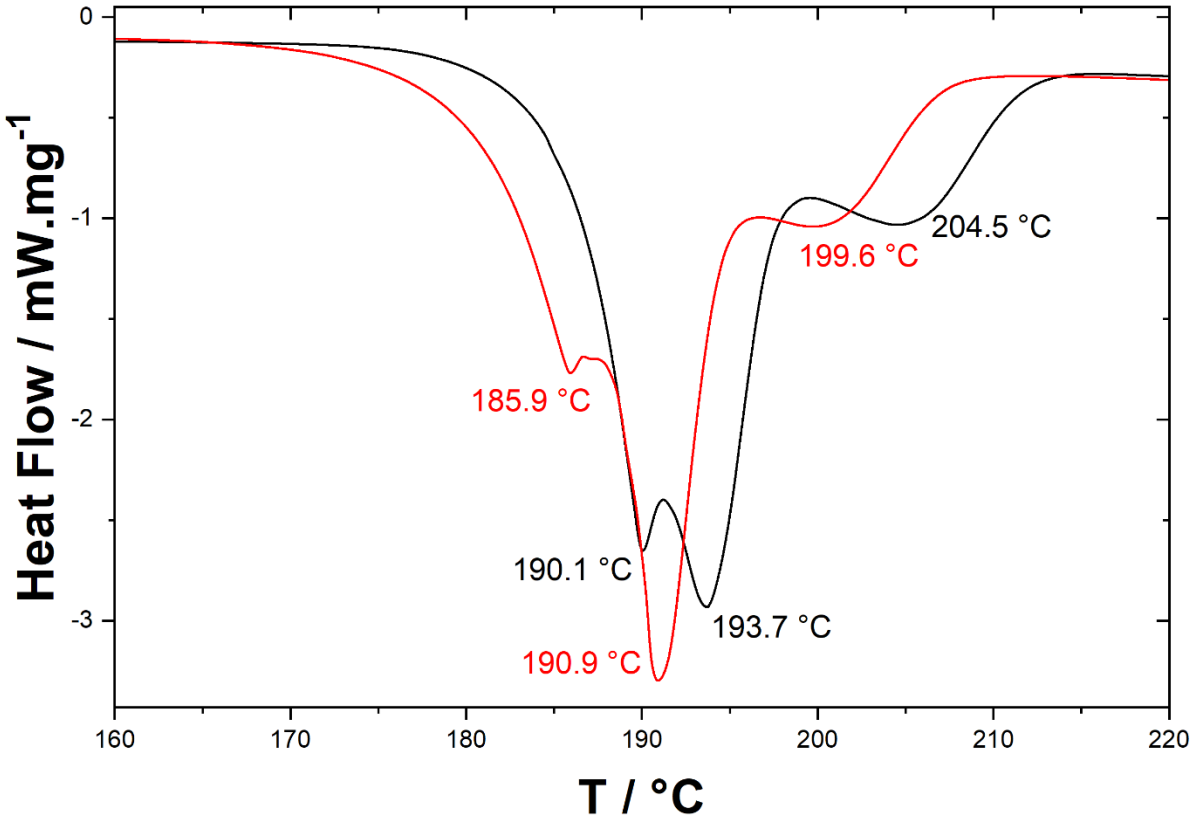

Figure 4.10: DSC heating curves for Caff: 1H2N cocrystals, obtained with caffeine saturated aqueous phase and at high positive polarization (red) and control experiment (black).

We do not observe any peaks at this temperature. On the contrary to 1H2N whose melting point was in the range of 195-200°C, and could be present in the sample but was not visible within the XRD.

4.3.4. Raman Spectroscopy

To complete the crystallographic information about the cocrystals we analysed them by Raman spectroscopy. The Raman spectrum of cocrystals in the range 1100-1800 cm^{-1} is shown in Figure 4.11. The sample was analysed according to the description in Chapter 2.4.3. The full Raman spectra are shown in Fig. 4.11. It should be added that the sample was analysed at three different locations, in different polarization modes in order to obtain statistically significant information about the composition of the sample. Raman peaks were assigned to theoretical spectra calculated using density functional theory (Fig. 4.13).

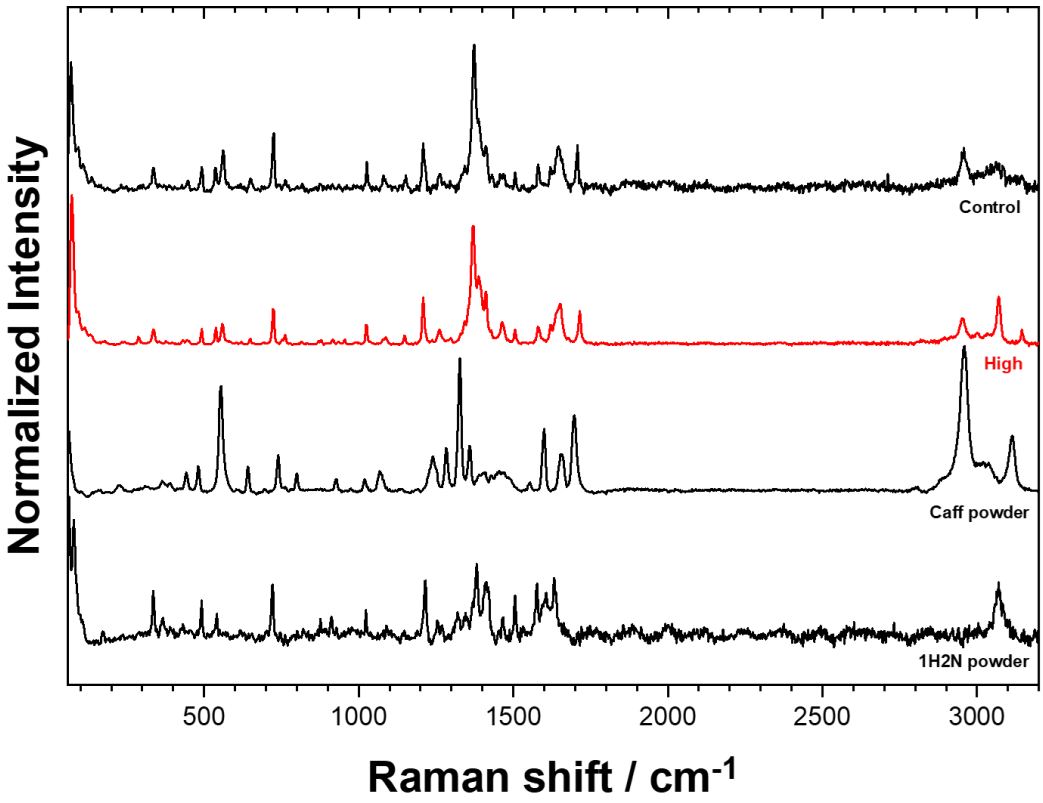

Figure 4.11: Raman spectra for Caff: 1H2N cocrystals (control and high polarization, [Caff] = saturated), caffeine and 1H2N.

Raman spectra showed a significant difference in characteristic bands between the Caff: 1H2N cocrystals and the reactants, confirming that the starting materials were not present in the product collected from the interface. Two distinct peaks can be observed in the Figure 4.12 at wavelengths of 1378 cm^{-1} and 1648 cm^{-1}. The shift of the peak at 1378 cm^{-1} compared to pure caffeine was due to the hydrogen bonding between the imidazole ring of caffeine and the carboxyl group of 1H2N,[12], [161] whereas the Raman shift at 1648 cm^{-1} is caused by C=O stretching peak involved in intermolecular hydrogen bonding in naphthoic acid.[162] The shifts obtained in the 1300-1800 cm^{-1} region are characteristic of a 1:1 complex with hydrogen bonds between the two molecules, which is consistent with the results of the XRD analysis.[39]

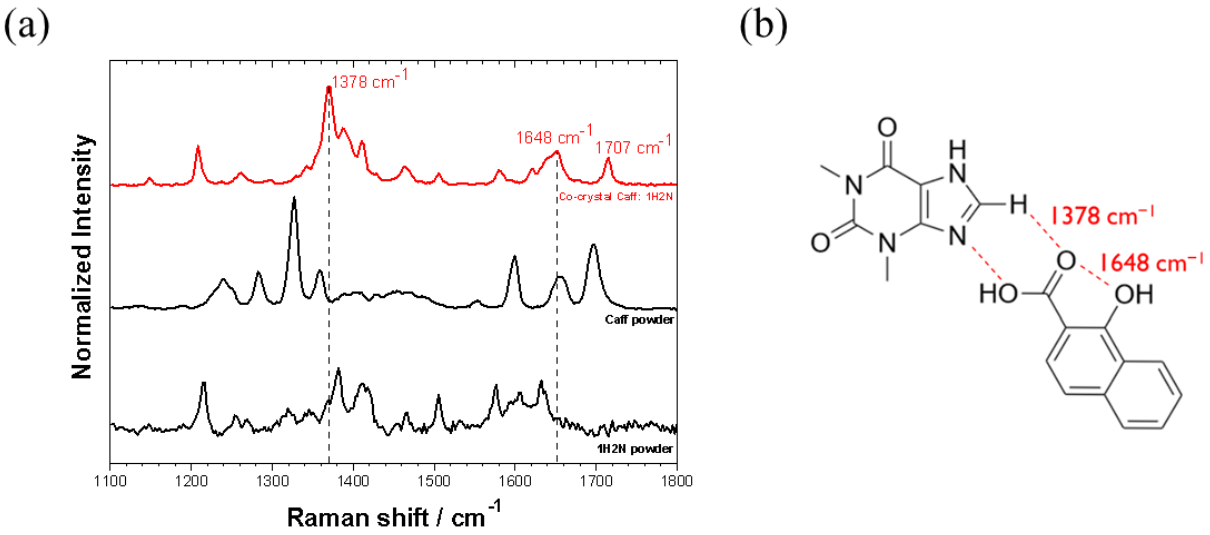

Figure 4.12: (a)Raman spectra for Caff: 1H2N cocrystals (obtained with caffeine saturated aqueous phase and at high positive polarization), caffeine and 1H2N; (b) depiction of hydrogen bonds in a cocrystal.

When we compare the Raman spectra, we see that the same bands are obtained, regardless of the experimental conditions (Fig 4.11). This means that the hydrogen bonds forming the cocrystals lead to the same displacements, although the cocrystals can be obtained in either Form I or Form II depending on the conditions of cocrystallisation. Raman spectra in this range is therefore not sensitive to the different molecular arrangement of the two forms.

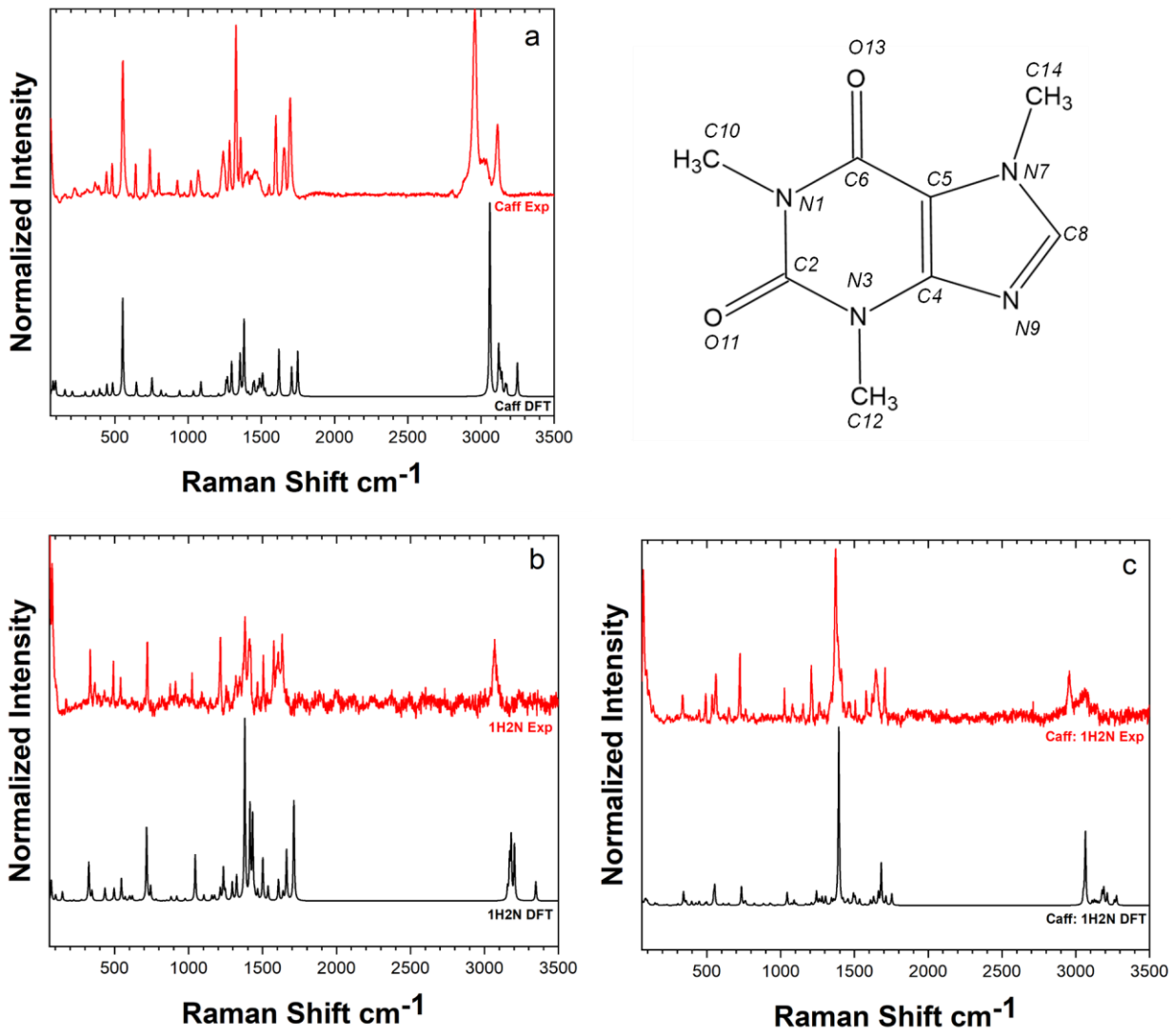

Figure 4.13: Experimental (red) and DFT calculated (black) Raman spectra for (a) Caff, (b) 1H2N, and (c) Caff: 1H2N (obtained at high polarization). Caffeine structure is also given along with the numbering of carbons atoms used in Table 4.2, 4.3 and 4.4.

The following figures report the comparison between experimental and theoretical Raman spectra for caffeine, 1H2N and the 1/1 cocrystal of these two molecules. Associated tables report the frequencies and the normalized Raman intensities, as well as the most important assignments for the two isolated molecules (caffeine and 1H2N). For caffeine, the assignment used the numbering of atoms indicated in Figure 4.13a. For the cocrystal structure, we have only assigned the most

important peaks featuring the frequencies strongly modified by hydrogen bonds. One can see that the theoretical spectra are in very good agreement with the experimental ones for the frequencies. It is less true concerning the Raman intensities, but this is well known for DFT calculations. Nevertheless, the agreement is acceptable.

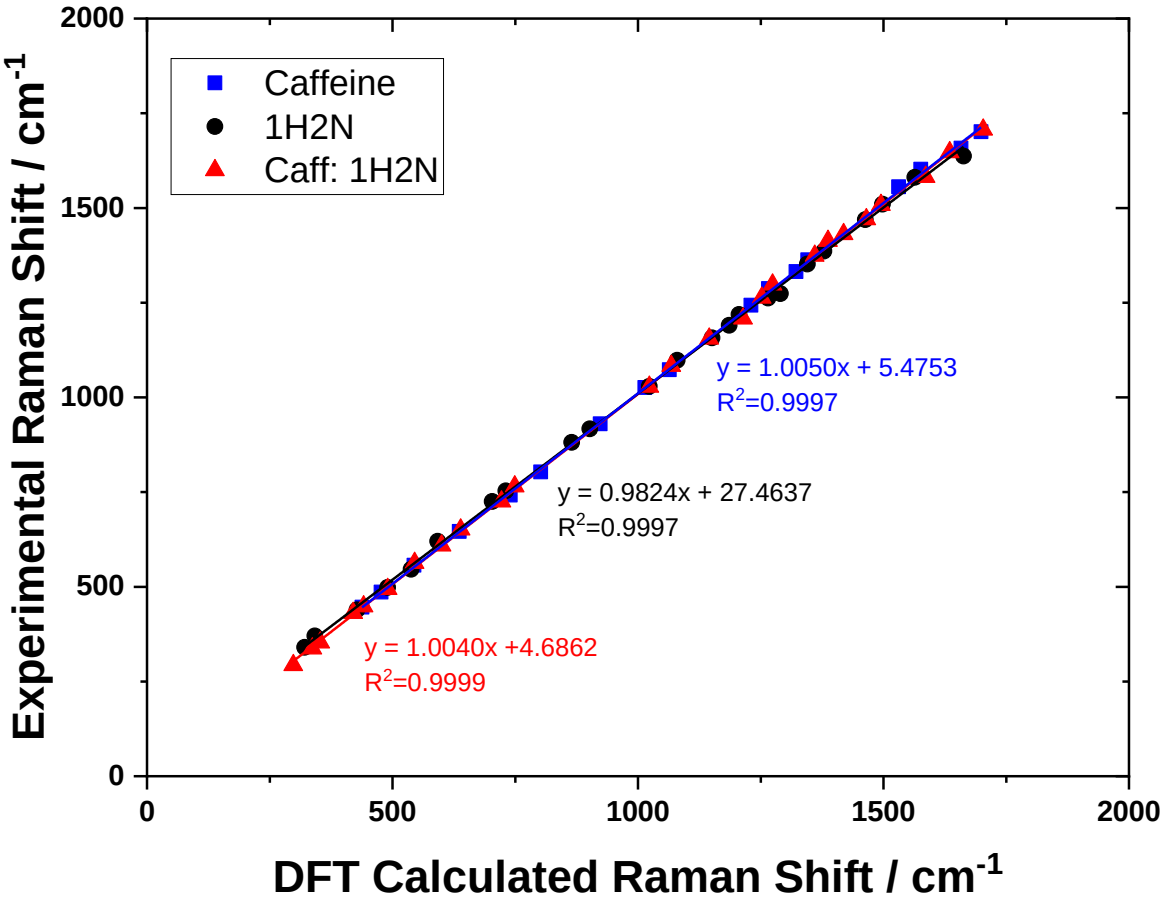

Figure 4.14: Correlation between experimental and DFT calculated Raman shifts.

In the Figure 4.13 we presented the data collected with DFT calculations compared to the experimental results for caffeine (a), 1H2N (b) and Caff: 1H2N cocrystals (c). Calculated and experimental are the spectra obtained for starting materials: caffeine and 1H2N (Fig 4.13 (a and b) are not entirely consistent. In this work DFT calculations were performed for a single molecule in the gas phase, so intermolecular interactions were not considered. Therefore, the experimental and calculated spectra may not be identical[163]. However, experimental peaks for these compounds

corresponds to the peaks reported in the literature[164], [165]. For Caff: 1H2N cocrystals, the peaks between the experimental and calculated spectra are more consistent because H-bonds between two molecules were considered (Fig 4.14). The experimental peaks correspond to the bands with data acquired by means of DFT calculations (Fig 4.13 (c)). The frequencies are basically identical and the differences in the intensity are negligible. Please refer to Tables 4.2 - 4.4 for details on band assignments.

Table 4.2: Assignment for the most characteristic vibrational bands of caffeine[166].

Experimental Raman shifts	Experimental Raman Normalized Intensity	DFT calculated and corrected Raman shifts	DFT Raman Normalized Intensity	Assignement
446	0.143	438	0.064	CH_3 sym. bend + CH_3 rock
486	0.228	477	0.072	Imidazole ring def + O=C–N def + CH bend
557	0.81	544	0.508	CH bend + CH_3 sym. bend + CH_3 rock
646	0.211	636	0.075	midazole ring def + O=C–N def + CH_3 sym. bend
742	0.261	740	0.098	Imidazole ring def + CH_3 sym. bend + CH_3 rock
803	0.149	802	0.028	Imidazole ring def + C=O def + CH_3 rock
930	0.105	923	0.031	Imidazole + CH_3 rock
1026	0.097	1014	0.028	CH_3 rock + C–N stretch + C–N bend
1073	0.15	1064	0.077	H–C=N bending
1243	0.271	1230	0.087	H–C=N bending
1250 (shoulder)	0.217	1238	0.101	C–N stretch
1287	0.361	1266	0.182	C2–N3 sym. str + CH_3 rock
1332	1	1322	0.226	Imidazole trigonal ring stretch
1363	0.374	1346	0.386	C–N str + CH_3 sym. Bending
1410 (broad)	0.178	1410	0.078	CH_3 sym. bend + C14–N7 sym. str
1433 (broad)	0.158	1434	0.147	CH_3 twisting
1470 (broad)	0.184	1469	0.121	CH_3 sym. bending
1556	0.107	1531	0.021	CH_3 sym. bend + CH_3 bend + C–N stretch
1602	0.474	1576	0.245	C=C sym. str + C–N sym. str + CH_3 sym. bend
1658	0.314	1658	0.153	Out-of-phase C=O stretch + C=C sym. Stretch
1701	0.546	1699	0.232	In-phase C=O stretch
2960 (broad)	0.685	2931	1	CH_3 sym. stretch
3030 (broad. multiple)	0.175	2986	0.275	CH_3 asym. stretch
		2996	0.151	CH_3 asym. stretch
		3006	0.128	CH_3 asym. stretch
		3027	0.0674	CH_3 asym. stretch
		3036	0.064	CH_3 asym. stretch
3117	0.301	3103	0.172	imidazole C-H stretch

Table 4.3: Assignment for the most characteristic vibrational bands of 1–hydroxy–2–naphthoic acid[165].

Experimental Raman shifts	Experimental Raman Normalized Intensity	DFT calculated and corrected Raman shifts	DFT Raman Normalized Intensity	Assignement
340	0,523	321	0,214	naphtalene squeletal in plane deformation
370	0,226	342	0,06	
439	0,121	428	0,071	
498	0,415	490	0,064	
546	0,273	538	0,124	naphtalene squeletal in plane deformation
620	0,158	592	0,03	
725	0,694	703	0,403	
753	0,163	731	0,086	
881	0,159	865	0,022	
917	0,219	902	0,027	
1029	0,385	1023	0,253	ring breathing mode
1098	0,158	1080	0,032	
1157	0,161	1151	0,027	
1190	0,14	1186	0,075	
1219	0,768	1206	0,188	naphtalene CCH bend + C=C stretch + C-O-H bend
1262	0,345	1265	0,104	
1274	0,274	1290	0,142	naphtalene CCH bend and C=C stretch
1326 (broad)	0,407			
1352	0,375	1345	1	naphtalene CCH bend + C=C stretch + C-O-H bend
1386	1	1379	0,543	naphtalene CCH bend + C=C stretch + phenolic C-O-H bend
1418 (broad)	0,787	1398	0,475	naphtalene CCH bend + phenolic C-O bending
1469	0,41	1463	0,237	naphtalene CCH bend + phenolic C-O stretch
1510	0,674	1498	0,074	C=C stretch of naphtalene part + phenolic C-O-H bend
1581	0,791	1564	0,117	C=C stretch of naphtalene part + phenolic C-O-H bend
1612 (broad)	0,633	1616	0,276	C=C stretch of naphtalene part
1637	0,784	1663	0,549	C=O stretch of the COOH group
3066	0,775	3033	0,275	aromatic C-H stretch
3075	0,877	3042	0,373	aromatic C-H stretch
3089	0,46	3062	0,315	aromatic C-H stretch
3230	0,153	3195	0,106	phenolic O-H stretch in intra H bond with C=O
		3572	0,17	O-H stretching of COOH group

Table 4.4 Assignment for the most characteristic vibrational bands of Caff: 1H2N cocrystals.

Experimental Raman shifts	Experimental Raman Normalized Intensity	DFT calculated and corrected Raman shifts	DFT Raman Normalized Intensity	Assignement
293	0,0328	298	0,01	
337	0,103	337	0,08	
353	0,02	353	0,027	
431	0,041	420	0,014	
448	0,064	441	0,023	
494	0,073	490	0,021	
537	0,081	538 (shoulder)	0,08	
563	0,145	545	0,118	
609	0,027	600	0,011	
651	0,031	639	0,012	
725	0,166	722	0,106	
765	0,072	749	0,025	
1028	0,116	1023	0,073	
1083	0,063	1068	0,029	
1155	0,06	1145	0,01	
1208	0,31	1214	0,082	
1263	0,146	1252	0,05	
1298	0,108	1274	0,051	
1374	1	1360	1	imidazole C=N stretch + C-O-H carboxylic group bend bonded by H bonds
1413	0,313	1387	0,043	
1431	0,149	1419	0,038	
1461 (shoulder)	0,171	1455	0,07	
1470	0,219	1465	0,055	
1508	0,174	1495	0,035	
1582	0,148	1586	0,048	
1624 (shoulder)	0,189	1618	0,075	
1647	0,462	1635	0,24	C=O stretch of COOH group bonded by H bond to imidazole group
1662 (shoulder)	0,254	1664	0,054	
1707	0,284	1703	0,065	in phase C=O stretchs of caffeine
2956	0,2	2936	0,415	
2995 (shoulder)	0,116	2992	0,032	
3003	0,138	3002	0,028	
3012	0,114	3013	0,025	
3035	0,123	3028	0,029	
3045	0,143	3041	0,087	
3060	0,272	3050	0,106	
3081	0,138	3072	0,071	
3125	0,05	3117	0,032	
3146	0,066	3131	0,053	

4.3.5. Images at the liquid-liquid interface

The images in Figure 4.15a show the changes over time (35 min) occurring in interphase. The procedure and setup are described in the Chapter 2.4.5. The images show the formation of cocrystals when the caffeine-saturated aqueous phase and the almost saturated 1H2N solution in the organic phase were placed together and when a high potential was applied. In the first 3 minutes, we see the caffeine deposited at the water-organic interface. After this time of about 3 minutes, the first cocrystals started to form. Based on visual observation, a shapeless precipitate first appears and then transforms into needle-shaped cocrystals. The Caff:1H2N crystal gradually increases in size over a period of 35 minutes. Figure 4.15b shows the formation of cocrystals in the control experiment. In the absence of potential, the caffeine accumulates on the surface within

the first three minutes and after this time we see the first crystals at the liquid-liquid interface. In the case of the control experiment, we could see more small-sized crystals forming at the interface except of the larger needle-like cocrystals. The process in this case is less rapid than with the positive potential. The positive potential brings caffeine to the interface thus the cocrystals are formed faster. When intermediate and low potential was applied we did not observe caffeine accumulation at the LLI (Fig. 4.15c and d), confirming that the application of a positive interfacial potential difference is responsible for the precipitation of $CaffH^+$ at the ITIES.

(a)

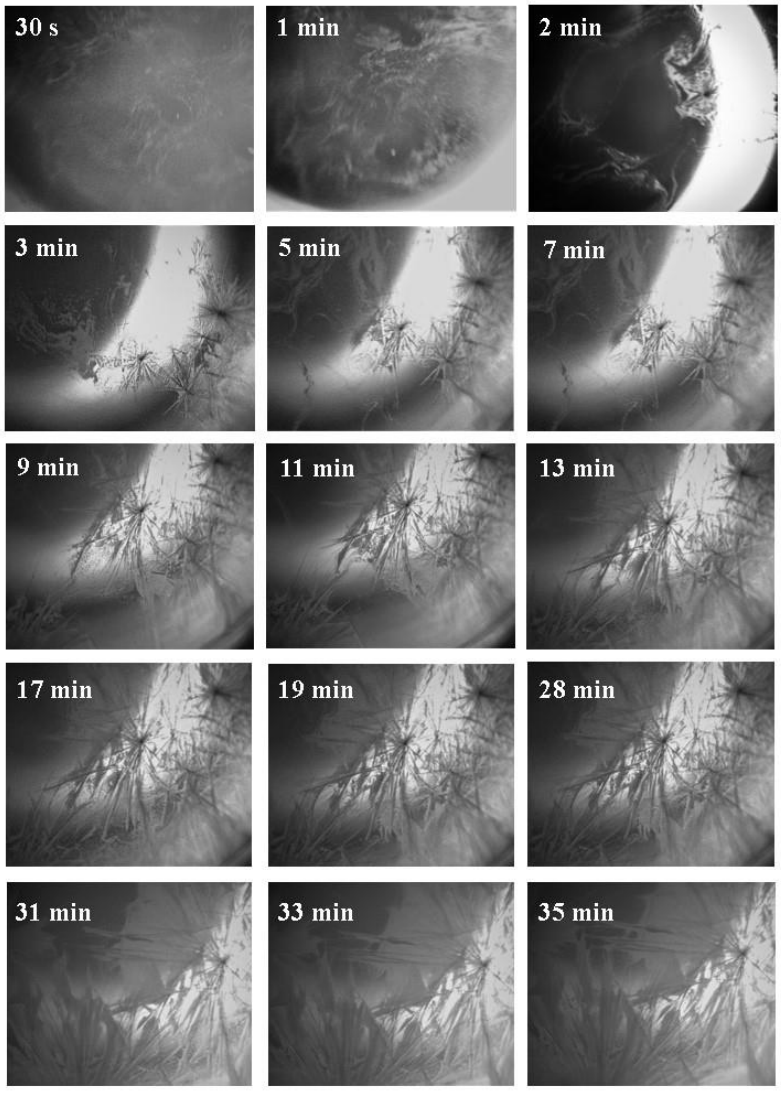

(b)

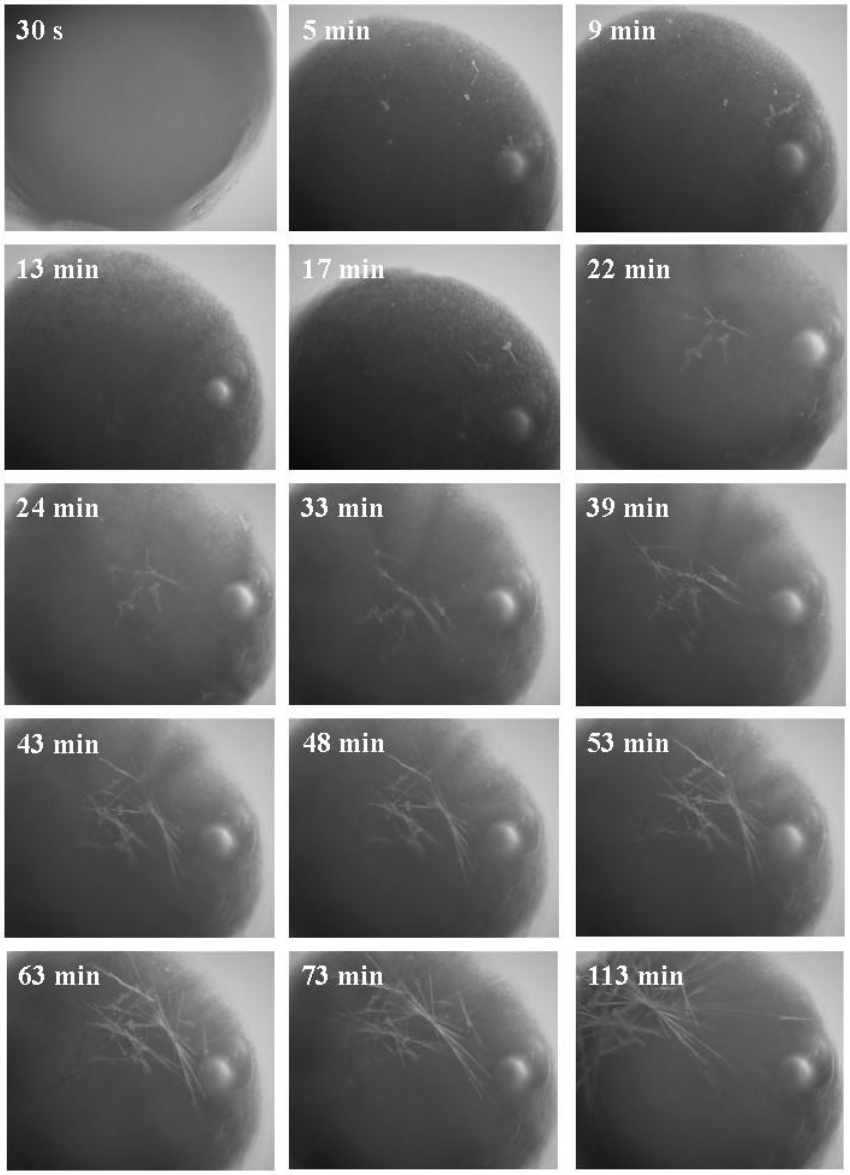
30 s
5 min
9 min
13 min
17 min
22 min
24 min
33 min
39 min
43 min
48 min
53 min
63 min
73 min
113 min

(c)

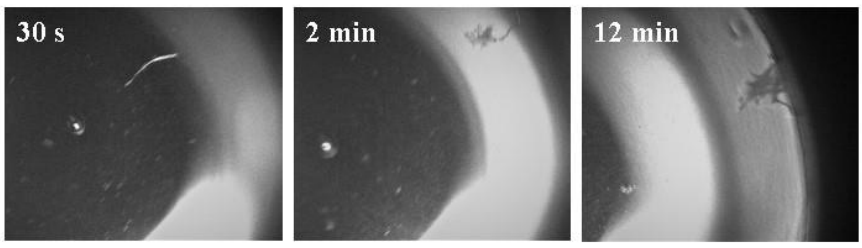
30 s
2 min
12 min

(d)

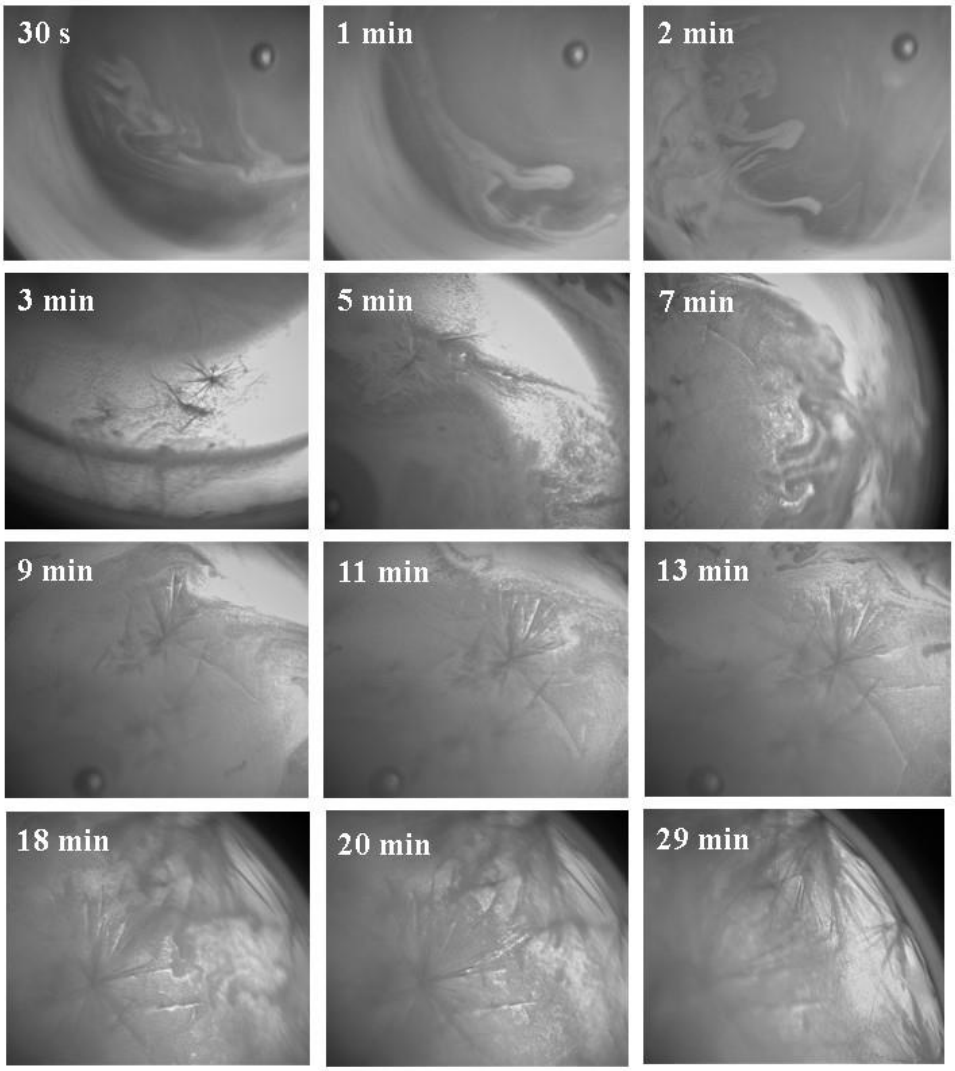

Figure 4.15: In situ images of the cocrystals formed at the liquid-liquid interface (a) at the high interfacial polarization, (b) intermediate interfacial polarization, (c) low interfacial polarization and (d) control experiment.

4.4. Mechanism of Caff:1H2N cocrystal formation

We assumed that in the absence of polarisation, $CaffH^+$ and 1H2N cocrystals are formed through an interfacial process (Fig 4.16). However, when we applied a sufficiently high potential at the interface, $CaffH^+$ was transferred to the organic phase, where a complex with 1H2N was formed.

It was accompanied by proton release, as evidenced by pre- and post-crystallization pH analysis of the aqueous phase (Fig 4.17). Cocrystals of caffeine of Phase I were previously obtained in acetonitrile[39], [40] and ethyl acetate[27]. This may indicate that the use of more polar solvents favoured crystallization of Form I what may confirm the theory that in case of positive potential, the cocrystals are created at the organic side of the interface.

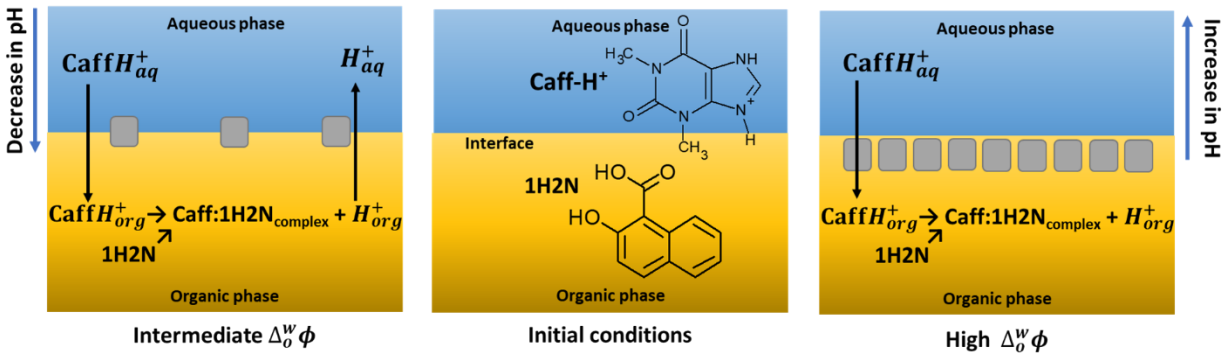

Figure 4.16: Caff:1H2N cocrystallisation at a polarised oil-water interface. Initially, CaffH^+ is dissolved in the aqueous phase whereas 1H2N is present in the organic phase.

The absence of carboxylate peaks (1701 cm^{-1}) in the cocrystals Raman spectrum supports the formation of molecular cocrystals rather than ionic cocrystals of cationic Caff and anionic 1H2N (Fig 2.14). At high $\Delta^w_o\phi$, H^+ is remaining in the organic phase which is supported by an increase in pH after cocrystallisation. This is attributed to an interfacial potential ($\Delta^w_o\phi$) greater than the standard interfacial transfer potential of H^+ ($\Delta^w_o\phi > \Delta^w_o\phi^0_{H^+}$) [167]. On the opposite, in the absence of polarization or when the interfacial potential is low, protons remain in the aqueous phase ($\Delta^w_o\phi < \Delta^w_o\phi^0_{H^+}$), which leads to a decrease in pH.

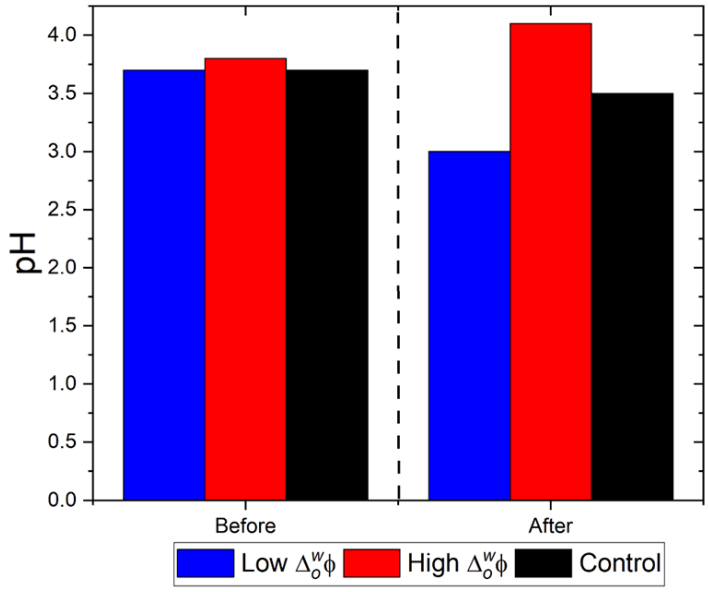

Figure 4.17: Changes in pH before and after the cocrystallization process for caffeine saturated solution.

We demonstrated an indirect evidence of the $CaffH^+$ transfer upon chemical polarization of the interface by analyzing the content of the organic phase by SEM (Fig 4.18b). The procedure is presented on the Figure 4.18a. The experiment was left for 16h as standard. After this time, the aqueous phase was removed with a pipette. Also, with a pipette, the organic phase was collected and placed on the substrate. After evaporation of the solvent, the sample was analysed by SEM. The SEM images (Fig. 4.18b) showed that when the interface was polarized at high potential, large crystals were collected from the organic phase, whereas, almost no deposits were detected on the substrate when the interface was polarized with intermediate or negative potentials. This may provide indirect evidence for the transfer of $CaffH^+$ to the organic phase when the interface is positively polarized.

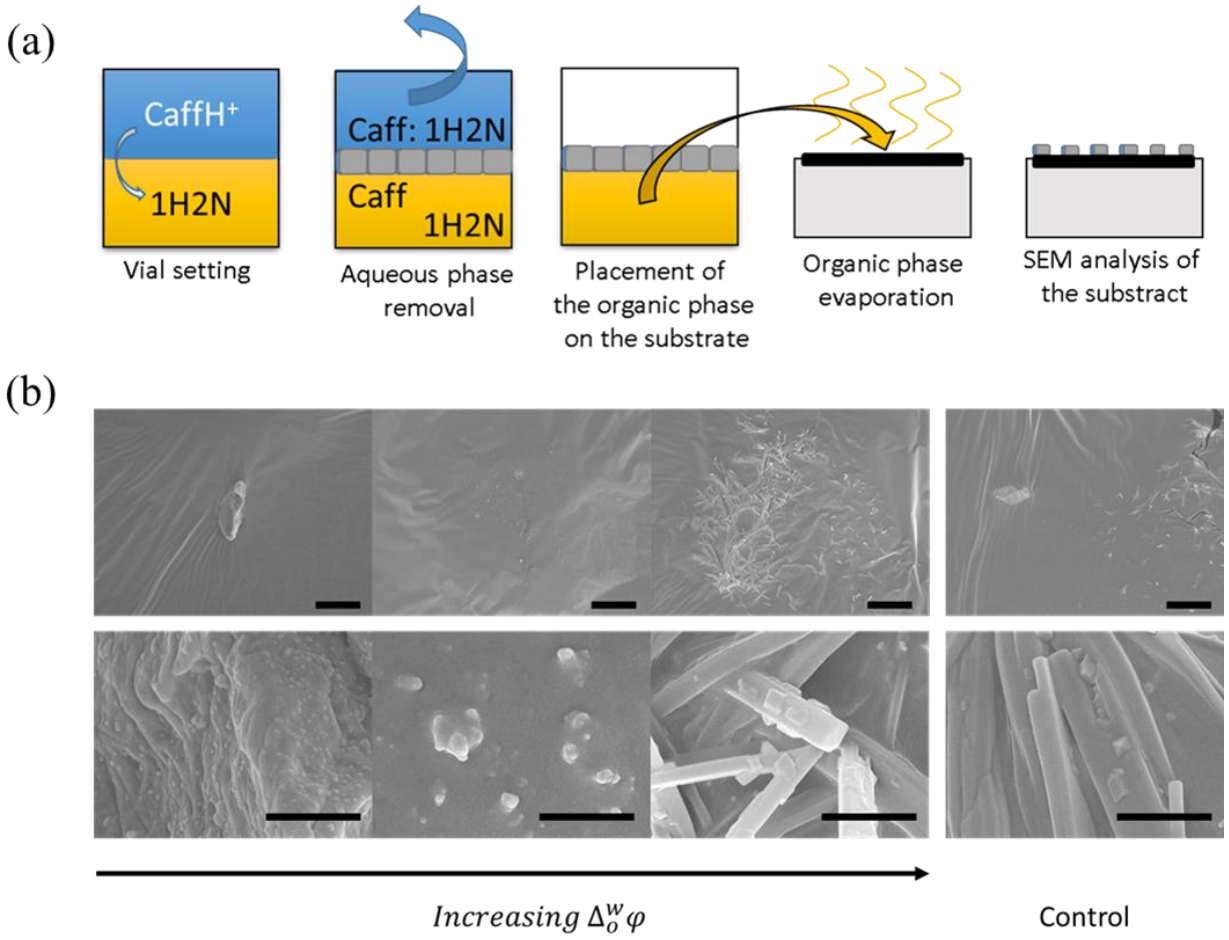

Figure 4.18: (a) procedure of sample preparation for SEM analysis; (b) SEM images of the organic phase after solvent evaporation for low, intermediate and high interfacial polarization and for control experiments. Top images: scale bars: 20µm; bottom images: 1 µm.

4.5. Conclusion

Cocrystals of caff with 1H2N of high purity were formed upon chemical polarisation of the interface between immiscible liquids. Raman spectroscopy confirmed that the products collected at the ITIES were cocrystals of Caff: 1H2N that were free of starting reagents and solvents. By applying low interfacial potential difference, we were able to inhibit the cocrystallisation process. Moreover, manipulation with the applied potential has allowed the formation of a large majority of a polymorphic form. Indeed, XRD analysis showed the two different polymorphs were obtained, depending on the presence of the interfacial polarisation. For non-polarised interfaces (control

experiment), a mixture of cocrystals of phases I and II were obtained, whereas cocrystal of phase I were formed when a high interfacial potential difference was applied. Based on the XRD and Raman spectroscopy, we can clearly state that the compounds obtained at the interface are the cocrystals of caff: 1H2N and not the salts, which was additionally emphasized by the change of pH, before and after the cocrystallisation process. Such cocrystallisation opens up perspectives for better control and understanding of the cocrystallisation process through polarisation changes at the oil-water interface. Further studies of mechanism behind the cocrystals formation was studied in Chapter 5.

5. PROBING INTERFACIAL COCRYSTALLISATION USING SIMULTANEOUS POTENTIAL AND CURRENT MEASUREMENTS AT LIQUID-LIQUID INTERFACES POLARISED BY COMMON ION APPROACH

Electrochemical noise (EN) is a method commonly used, which allows the simultaneous measurement of spontaneous variation of potential and current caused by corrosion events [168], [169]. Indeed, most semi-macroscopic phenomena associated with corrosion are stochastic, which make their study difficult by electrochemical impedance spectroscopy or polarisation curves. Potential electrochemical noise, ΔE, represents the variation of potential around a dc potential value, whereas current electrochemical noise, ΔI, is the stochastic variation of current around a dc current value. These variations, ΔE and ΔI, can be analysed in the time domain based on different parameters such as the shape, amplitude and frequency. Analysis can also be made in the frequency domain by the calculation of the power spectral density of the current and potential fluctuations [169]. Electrochemical noise allows one to determine corrosion rates and to identify different corrosion events: e.g. (i) monitoring of the formation and destruction of corrosion inhibitor films [170], investigating the mechanism of formation of the lithium-based conversion layer [171] or analysing aqueous corrosion inhibition process [172]. Simultaneous measurements of potential and current fluctuation is possible thanks to a zero-resistance ammeter [173].

We propose here to monitor simultaneously current and potential changes associated with cocrystallisation events at a liquid-liquid interface polarised by a common ion dissolved in each phase. Polarised liquid-liquid interfaces have recently been used to produce cocrystals of caffeine and 1-hydroxy-2-naphthoic acid [174]. XRD analysis of the cocrystals showed two crystallographic phases. These phases were formed under specific conditions: there is a majority of phase I when the interface was positively polarised; a majority of phase II in the case of a non-polarised interface, this is the natural potential of the cell. We proposed the mechanism of cocrystallisation: in case of positive polarization, the caffeine transfers to the organic phase and

the cocrystals are created in the organic side of the interface. However, when no potential is applied the cocrystals are formed in an interfacial process. In order to determine the role of the interfacial potential in the cocrystallisation process, simultaneous measurement of both potential and current at the liquid-liquid interface may provide important information. The electrochemical cells were assembled with various concentrations of tetraalkylammonium cations (TAA^+) in the organic and aqueous phases and the potential and current were tracked by the adaptation of the EN method to the ITIES. The electrochemical noise data were analysed based on several parameters used in corrosion studies: the power spectral density (PSD) plots, the current root mean square (I_{rms}) values of PSD of current (PSD_I) and the low frequency noise impedance R_{sn}. This approach provides a new way to monitor and understand events at the ITIES.

5.1. Description of the experimental set-up

The Electrochemical Noise (EN) technique was applied to measure the potential and the current synchronously. EN is usually used in the corrosion studies[175] however here it was applied to four-electrodes system at the liquid/liquid interface. The potentiostat VSP-300 Biologic (Electrochemical Applications/Corrosion) was used to measure the electrochemical potential and current noise.

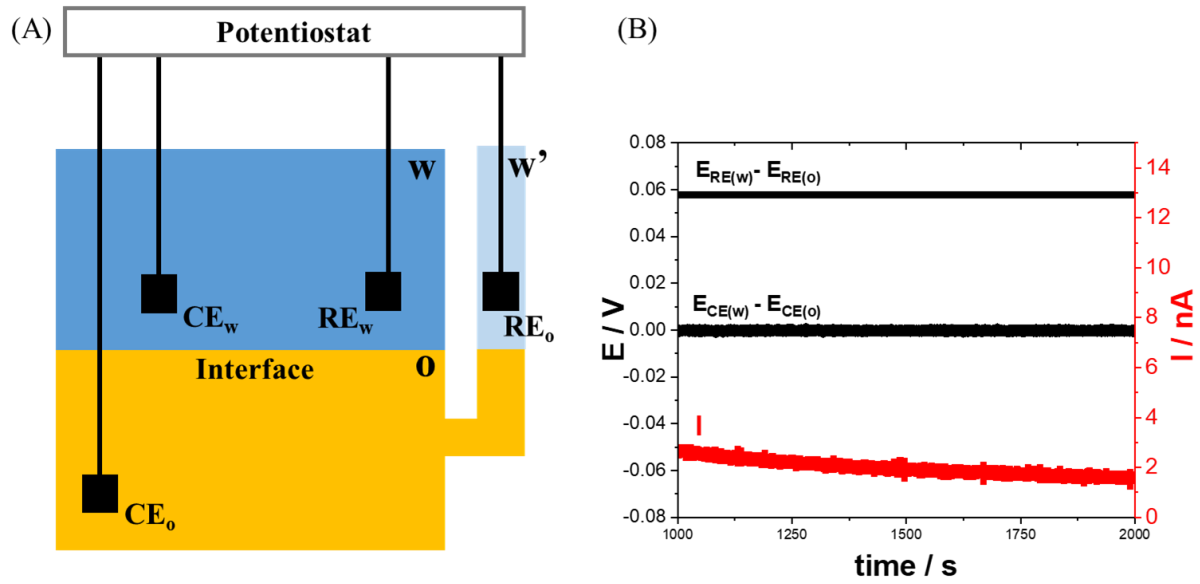

Figure 5.1: (A) Schematic representation of the electrochemical cell used for the simultaneous current and potential measurements. CE: counter electrode, RE: Reference electrode, o: organic phase, and w: aqueous phase. (B) Simultaneous potential (black) and current (red) measurement as a function of time. $E_{RE(w)} - E_{RE(o)}$ represents the potential measured between the two reference electrodes and $E_{CE(w)} - E_{CE(o)}$ shows the potential of 0 V (Mean ± SD: -0.00028±.00033V) imposed between the two counter electrodes. I is the current measured through the electrochemical cell.

It allows the application of 0 V between the counter electrodes in the organic phase (CE_o) and in the aqueous phase (CE_w) [169]. The potential is measured between the RE_w and REo and the current between CE_w and CE_o (Fig. 5.1). The electrochemical cells were placed in a grounded Faraday cage.

The equilibrium potential differences at the Ag ($RE_{w'}$)/w, w/o, o/w' and w'/Ag (RE_w) interfaces can be described by the corresponding Nernst equations:

$$E = \phi_{Ag/AgCl} - \phi_{Ag/AgCl'} = \Delta_w^{Ag/AgCl}\phi + \Delta_o^w\phi - \Delta^{w'}{}_o\phi - \Delta_{w'}^{Ag/AgCl'}\phi \quad (5.1)$$

Where the different potentials are defined as follows:

$$\Delta_w^{Ag/AgCl}\phi = \Delta_w^{Ag/AgCl}\phi^0 + \frac{RT}{F} ln \frac{1}{c_{Cl^-}^w} \quad (5.2)$$

$$\Delta_{w'}^{Ag/AgCl'}\phi = \Delta_{w'}^{Ag/AgCl}\phi^0 + \frac{RT}{F} ln \frac{1}{c_{Cl^-}^{w'}} \quad (5.3)$$

$$\Delta_o^w\phi = \Delta_o^w\phi_{TAA^+}^0 + \frac{RT}{F} ln \frac{c_{TAA^+}^o}{c_{TAA^+}^w} \quad (5.4)$$

$$\Delta^{w'}{}_o\phi = \Delta^{w'}{}_o\phi_{TAA^+}^0 + \frac{RT}{F} ln \frac{c_{TAA^+}^o}{c_{TAA^+}^{w'}} \quad (5.5)$$

where $c_{TAA^+}^w$, $c_{TAA^+}^o$, $c_{TAA^+}^{w'}$ represents the concentration of TAA^+ in the aqueous phase, organic phase and aqueous phase for organic reference electrode, respectively, $c_{Cl^-}^w, c_{Cl^-}^{w'}$ represent the concentration of Cl^- in the aqueous phase and aqueous phase for organic reference electrode and $\Delta_o^w\phi_{TAA^+}^{o'}$ is the formal ion transfer potential difference for TAA^+.

By combining equations (5.1) and (5.2-5.5):

$$E = \frac{RT}{F} ln \frac{c_{Cl^-}^{w'}}{c_{Cl^-}^{w}} + \frac{RT}{F} (\ln \frac{c_{TAA^+}^{o}}{c_{TAA^+}^{w}} - ln \frac{c_{TAA^+}^{o}}{c_{TAA^+}^{w'}}) \quad (5.6)$$

To simplify this equation, if we keep $[c_{Cl^-}^{w} = c_{Cl^-}^{w'}]$ and $[c_{TAA^+}^{o} = c_{TAA^+}^{w'}]$ in which case the potential measured will depend solely on $\frac{c_{TAA^+}^{o}}{c_{TAA^+}^{w}}$.

$$E = \frac{RT}{F} \ln \frac{c_{TAA^+}^{o}}{c_{TAA^+}^{w}} \quad (5.7)$$

This is true if[100]:

$$\Delta_o^w \phi_{TAA^+}^{0'} - \Delta_o^w \phi_{Cl^-}^{0'} \gg \frac{RT}{F} ln[4 \frac{c_{TAA^+}^{w}}{c_{TAA^+}^{o}} \left(1 + \frac{c_{TAA^+}^{w}}{c_{TAA^+}^{o}}\right)] \quad (5.8)$$

Based on the above-mentioned equations the four-electrode cell comprising liquid/liquid interface was prepared according to Scheme 1:

Scheme 5.1: Description of the electrochemical cells used:

Electrochemical cell:	**Ref 1:**	**(w)**	**(o)**	**(w')**	**Ref 2:**	**Information:**
1	Ag/AgCl	1 mM TAACl 9 mM LiCl	x mM TAATPBCl	x mM TAACl (10 – x) mM LiCl	AgCl/Ag	x = 0.1, 0.5, 1, 5, 10
2	Ag/AgCl	X 0.01 mM TMACl	Y 10 mM TMATPBCl	10 mM TMACl 10 mM LiCl	AgCl/Ag	X = -, Caff SAT Y = -, 1H2N

		9.995 mM LiCl 9.995 mM HCl					
3	Ag/AgCl	X mM Caff x mM TMACl 10-(x/2) mM LiCl 10-(x/2) mM HCl	10 mM 1H2N y mM TMATPBCl	Y mM TMACl 20 – y mM LiCl	AgCl/Ag	X = 40, SAT x = 0.01, 0.1, 1, 10 y = 0.01, 0.1, 1, 10	
4	Ag/AgCl	X mM Caff x mM TMACl 10-(x/2) mM LiCl	10 mM 1H2N y mM TMATPBCl	Y mM TMACl 10 – y mM LiCl	AgCl/Ag	X = 40, SAT x = 0.01, 0.1, 1, 10 y = 0.01, 0.1, 1, 10	
5	Ag/AgCl	X mM Caff	10 mM 1H2N	Y mM TMACl	AgCl/Ag	X = 40, SAT	

		x mM TMACl 10-(x/2) mM LiCl 10 mM LiOH	y mM TMATPBCl	10 – y mM LiCl			x = 0.01, 0.1, 1, 10 y = 0.01, 0.1, 1, 10
6	Ag/AgCl	Caff SAT 10 mM X 10 mM HCl	10 mM 1H2N 1 mM Y	5 mM BACl	AgCl/Ag		X = LiCl, Li_2SO_4 Y = KTPBCl, KTB, LiTB

The volumes of the aqueous (w) and organic (o) phases were both 2.5 mL. The delay between the preparation of the cells and the start of the experiment was 45 s. The same time was kept in each experiment to allow comparison between experiments. The measurements were carried out for 60 min to allow the electrochemical cell to reach equilibrium. The change in potential and current is a result of ions transferring at the liquid/liquid interface and allows changes on the interface to be followed during the establishment of equilibrium on this interface. The potential and the current were recorded at room temperature every 0.01 s, sufficiently frequent to observe current and potential spikes.

Since EN has been employed to monitor the type of corrosion and find the corrosion rate, in this work we have used similar parameters to explain the processes taking place at the LLI. The recorded experimental potential and current data were then used to analyse the electrochemical noise via Microsoft Excel.[176] Power spectral density (PSD) in the frequency domain is used to predict the corrosion mechanism and can be used to compare processes taking place at LLI. Our data have a large number of points and repeated signals, so PSD plots can be calculated using Fast Fourier Transform (FFT).

Before the results could be analysed, the trend line had to be removed. This was done using Origin® software and the polynomial removal procedure. To do this, we constructed graphs of potential or current over time, adding the trend line that provides the best fit to the data. The results were divided into ten sections of 20 seconds each, consisting of exactly 2048 points. In these time sections, PSD_E and PSD_I in the frequency domains were calculated. In this work, the following are used to calculate the PSD:

$$PSD_x(f) = |X_T(f)|^2 = \left[Re\left(X_T(f)\right)\right]^2 + \left[Im\left(X_T(f)\right)\right]^2 \quad (5.9)$$

Where $X_T(f)$ is the Fourier transform of x(t), T is the experimental time, Re and Im correspond to real and imaginary part, respectively and the number 2 means that only positive frequencies are concerned[176].

Root mean square (rms) was calculated as the ratio of standard deviation of current PSD (PSD_I).

$$I_{rms} = \sqrt{\frac{\sum_i^n PSD_I}{n}} \quad (5.10)$$

Where n was the number of experimental data points.

The low frequency noise impedance (R_{sn}) was determined as the ratio of the standard deviations of experimental potential (δV) and current (δI) after the trend removal.[168], [171]

$$R_{sn} = \left|\frac{PSD_E(f)}{PSD_I(f)}\right|^{\frac{1}{2}} \quad (5.11)$$

Where $PSD_E(f)$ and $PSD_I(f)$ are the power spectral density of the potential ΔE, and the current density (I), respectively, in the frequency domain f.

5.2. Measurement of the potential difference

A first series of experiments was designed to check that the potential measured is consistent with the potential expected from equation (5.7). Several configurations of electrochemical cells (9) were prepared with the different ratio of tetraalkylammonium (TAA^+) in organic and aqueous phase.

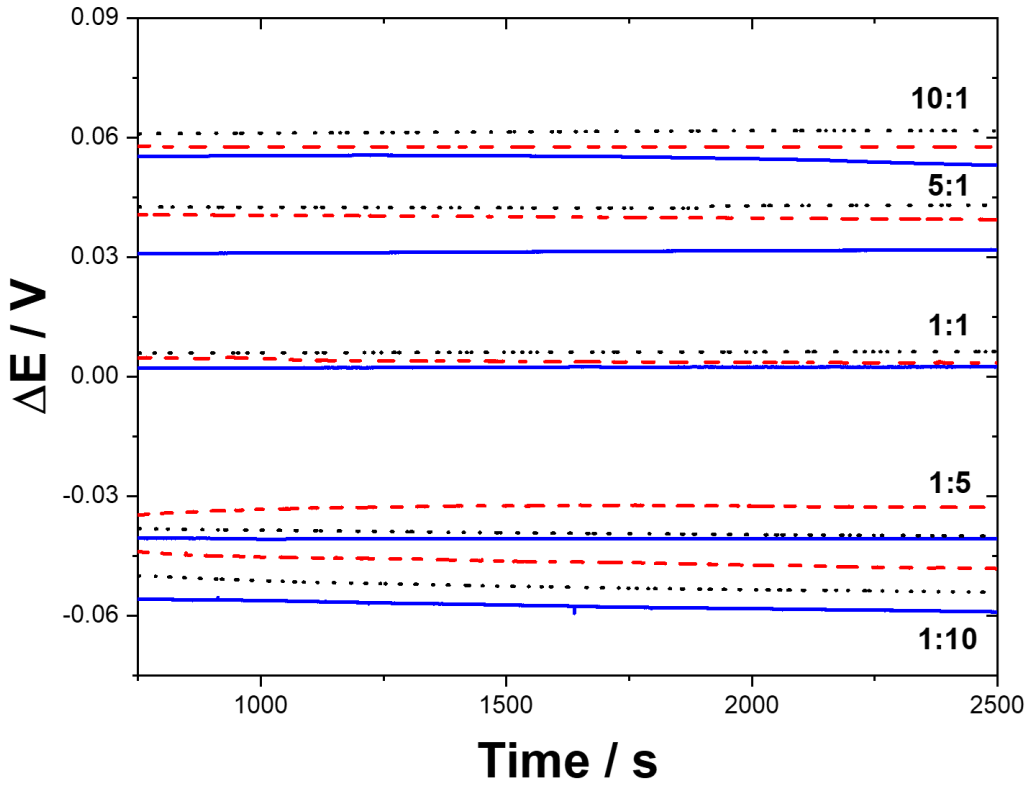

Figure 5.2: Change of potential as a function of time in the various configurations according to cell 1 Table 1. TMA^+ (···), TEA^+ (---) and TPA^+ (——). The presented ratio corresponds to $\frac{c^o_{TAA^+}}{c^w_{TAA^+}}$ *ratio.*

In these experiments, the interface is polarised by the distribution of a common TAA^+ ion between the two immiscible phases. The measurements were performed for 1 hour to allow the partition of ions to reach equilibrium at the liquid/liquid interface. The measurements were started right after the electrochemical cells where prepared. The comparison of the change of the potentials in time for three TAA^+ (TMA^+, TEA^+ and TPA^+) and various ratios of concentration in organic and in aqueous phase is shown in Figure 5.2. The potential is stable in time and its value decreases with the $\frac{c^o_{TAA^+}}{c^w_{TAA^+}}$ ratio. Similar results were obtained for the three ions, TMA^+, TEA^+ and TPA^+, which indicated that the transfer is not based on the formal transfer potential, but on the ratio of concentration of TAA^+ in each phase, as expected from equation (5.7).

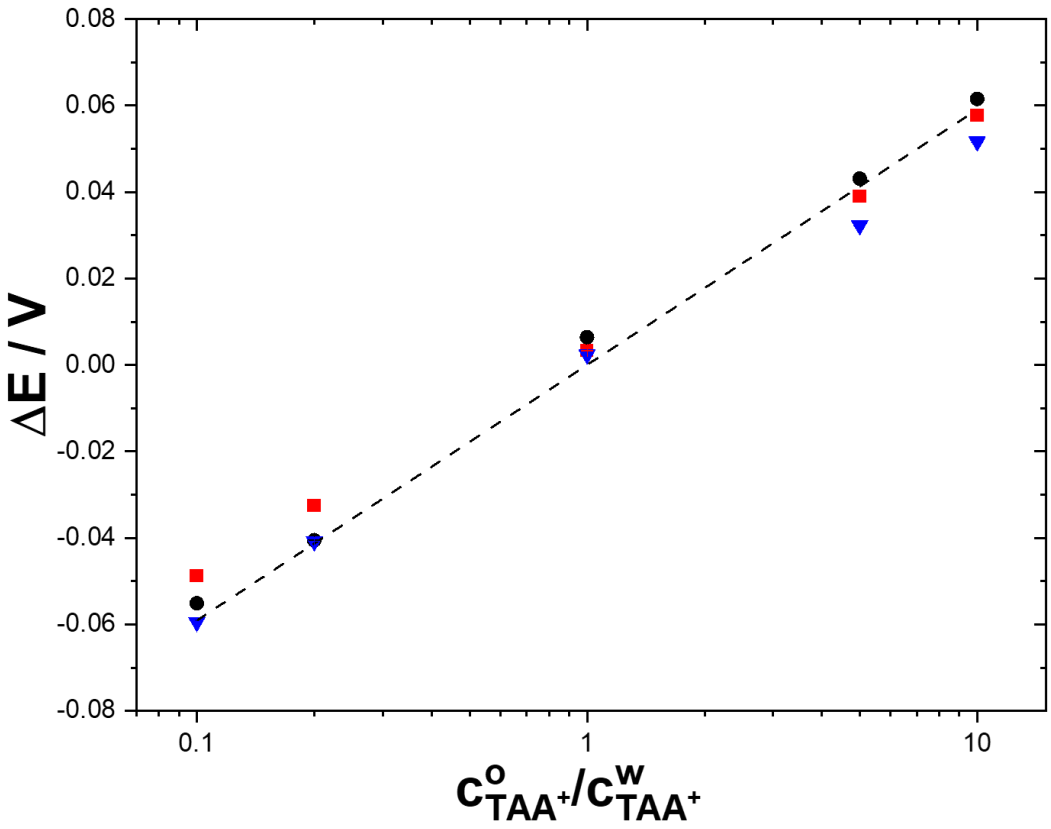

Figure 5.3: Equilibrium potential dependences on the ratio of common ion in organic and aqueous phases $\frac{c^o_{TAA^+}}{c^w_{TAA^+}}$ *. TMA^+ (●), TEA^+ (■) and TPA^+ (▼). Dashed line represents theoretical data calculated according to Eq. (2.15). When not visible, error bars are smaller than symbols.*

In Figure 5.3, we see the dependence of the potential on the ratio of the concentrations in the organic and aqueous phases. The dashed line and crosses represent the theoretical calculations based on Eq. (5.7). We see that the three cations, TMA^+, TEA^+ and TPA^+, fit into the theoretical calculations. When the ratio is 1:1, the potential is around 0 V (Mean ± SD: 3.3 ± 0.06 mV, 6.4 ± 0.02 mV, 2.39 ± 0.02 mV for TMA^+, TEA^+ and TPA^+ respectively). This confirms compliance with theoretical assumptions. The potential is positive when there is the excess of the ion in the organic phase and it takes negative values when the concentration in the aqueous phase is higher than in the organic phase. The potentials for the electrochemical cells built with these three quaternary ammonium salts are very close to the theoretical values calculated (Fig. 5.3) confirming

that this method is suitable to monitor the changes of potential at the liquid-liquid interface. The difference between the theoretical calculations (based on the Eq. 5.7) and experimental results might originate from the moisture content of the TAACl salts or impurities from the self-prepared TAATPBCl salts or small difference in the reference electrodes.

5.3. Simultaneous measurement of potential and current

In the next part of the study, along with the well-defined solutions which comply with theory (Fig. 5.1 and 5.2), we set up the electrochemical cell with saturated solution of caffeine as the aqueous phase and 1-hydroxy-2-naphthoic acid to the organic phase, according to electrochemical cell 2.

In Figure 5.4a, we observe the differences between four experiments: blank (black line, both caffeine and 1H2N are absent from the cell), when only 1H2N was present in the cell (green line), when only caffeine was present in the cell (blue line), and finally when both are present (red line). For the blank electrochemical cell, the potential difference was lower than expected by theory. This might be due to experimental conditions, which do not verify the conditions of Eq. (5.7). The potential signals exhibit a gradual decrease in all cases. In the Caff/1H2N configuration, we were able to follow the potential changes in the potential during the cocrystallisation process. At this ratio of $\frac{c^o_{TMA+}}{c^w_{TMA+}} = \frac{10\ mM}{0.01\ mM}$ and saturated concentration of caffeine we could establish positive potential for the transfer of caffeine. The conditions are sufficient to transfer the caffeine and the formation of cocrystals at the interface is observed. The presence of caffeine has a significant effect on potential. At pH 2, caffeine is present in its cationic form[149] so it is being exchanged with TMA^+ present in the organic phase. The drop in the potential indicate the transfer of caffeine from aqueous phase to the DCE and lowering of the ratio $\frac{c^o_{TMA+}}{c^w_{TMA+}}$. The potential in the presence of caffeine (red and blue line) is noisier and corresponds to the exchange of cations ($Caff^+$ and TMA^+) which takes place at the liquid-liquid interface. The potential of the cell with the presence of only 1H2N comparing with blank is lower due to the presence of H^+ and the facilitated proton transfer. The results shown in Figure 5.4 are carried out according to Scheme 5.1 of cell 2. Here, the pH is equal to 2 and was fixed by adding 10 mM HCl.

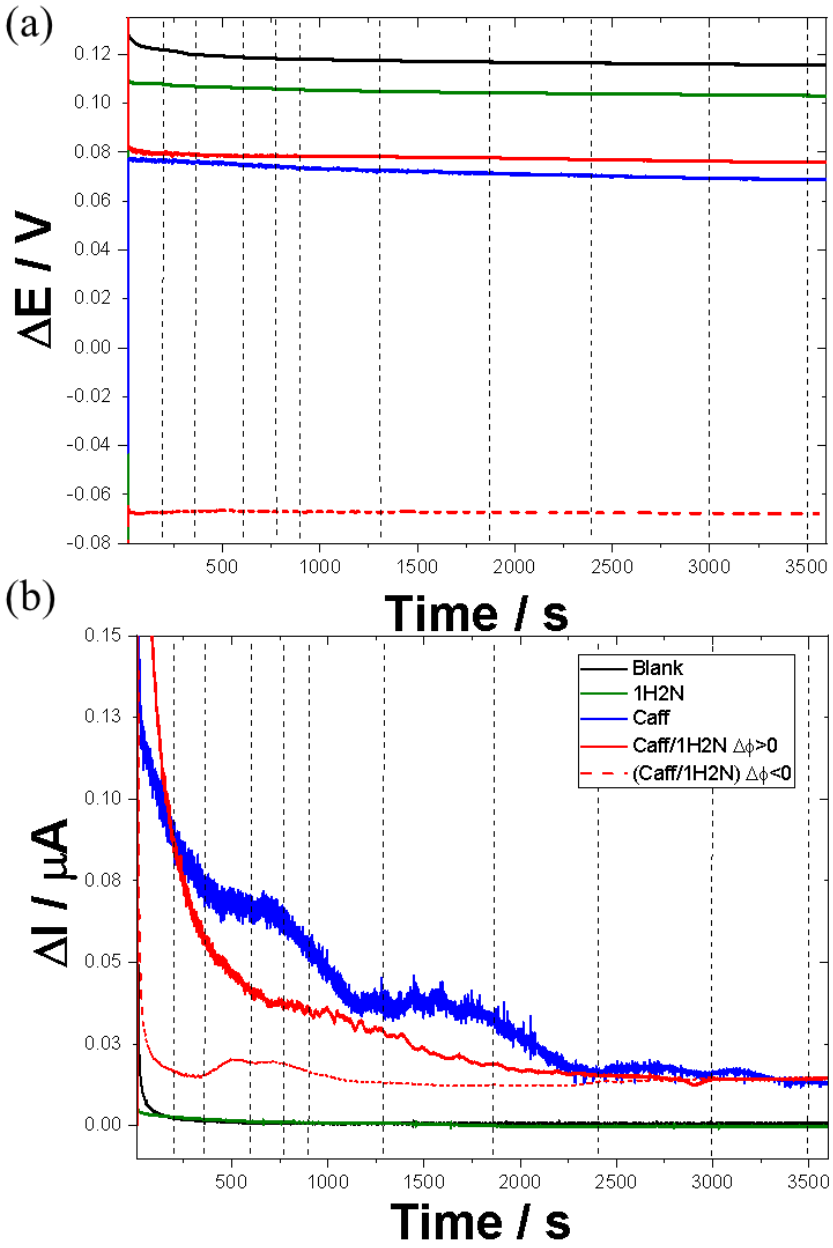

<u>Figure 5.4:</u> Variation of (a) potential and (b) current as a function of time for the various electrochemical cell 2 configurations. $\frac{c^o_{TMA^+}}{c^w_{TMA^+}} = \frac{10\ mM}{0.01\ mM}$ *. Blank: absence of Caff and 1H2N (──), 1H2N: absence of Caff and presence of 1H2N (──), Caff: presence of Caff and absence of 1H2N (──), Caff/1H2N: presence of Caff and 1H2N (──), and Caff/1H2N: presence of Caff and 1H2N (----) negative potential* ($\frac{c^o_{TMA^+}}{c^w_{TMA^+}} = \frac{0.1\ mM}{1\ mM}$)*. Dotted lines represent the times for which* I_{rms} *and the low frequency noise impedance were calculated.*

Potential variation is concomitant with changes in current, as shown to Figure 5.4b. The current signals are close to zero for the cells where there is no caffeine, which indicates that no ion transfer is occurring at the liquid-liquid interface. It can be seen that there is no difference when 1H2N is absent (Figure 5.4b, black line) and present in the system (green line) which confirms that the 1H2N is not transferring at ITIES[174]. However, when caffeine is present in the aqueous phase, a high initial value for current is observed followed by a significant drop with time. The cocrystals are created after 1 minute what corresponds to the change in current (Figure 5.4b red line). This higher current value is attributed to the transfer of caffeine from the aqueous to the organic phase. In the cell with both caffeine and 1H2N present (Fig 5.4b red line), the current decreases over time. The slope is sharp at the beginning and gradually decreases after 900 s until 2000 s, until it reaches a plateau.

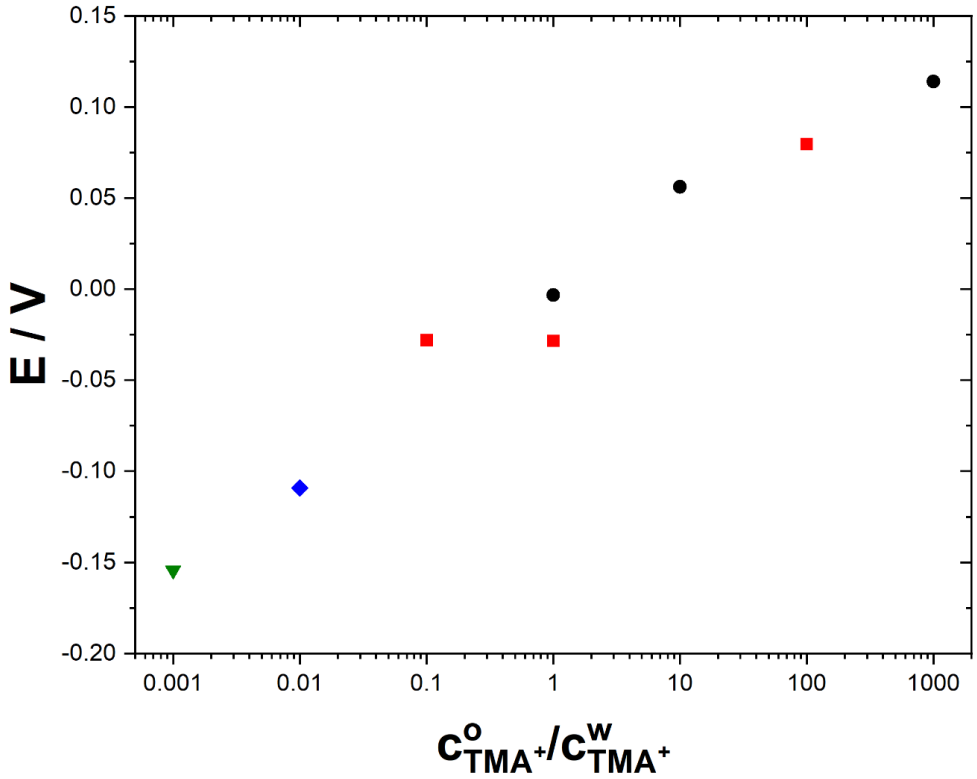

<u>Figure 5.5:</u> Equilibrium potential based on the ratio $\frac{c^o_{TMA^+}}{c^w_{TMA^+}}$ *of electrochemical cell 2 and Caff = 40 mM prepared in the presence of caffeine and 1H2N in the range of time 3000-3600 s. The error bars are shorter than the size of the symbols. The ratio was change by varying the concentration of* $c^o_{TMA^+}$. $c^o_{TMA^+}$ *= 0.01 mM (▼),* $c^o_{TMA^+}$ *= 0.1 mM (♦),* $c^o_{TMA^+}$ *= 1 mM (■),* $c^o_{TMA^+}$ *= 10 mM (●).*

These experiments were followed by the series of experiment with various ratio of $\frac{c^o_{TMA^+}}{c^w_{TMA^+}}$ when aqueous solution of caffeine and organic solution of 1H2N were placed together according to electrochemical cell 2. We can observe in Figure 5.5 that the potential values become higher when we increase the ratio $\frac{c^o_{TMA^+}}{c^w_{TMA^+}}$. With a lower ratio, less caffeine is transferred into the organic phase and less TMA^+ ions transfer to the aqueous phase due to the obtained distribution at the ITIES. It is remarkable that the values of potential are similar for the same ratio $\frac{c^o_{TMA^+}}{c^w_{TMA^+}}$. This is because the changes in the potential do not depend on the concentration of TMA^+ in the organic phase ($c^o_{TMA^+}$) but solely on the ratio $\frac{c^o_{TMA^+}}{c^w_{TMA^+}}$ as indicated in Eq. (5.7).

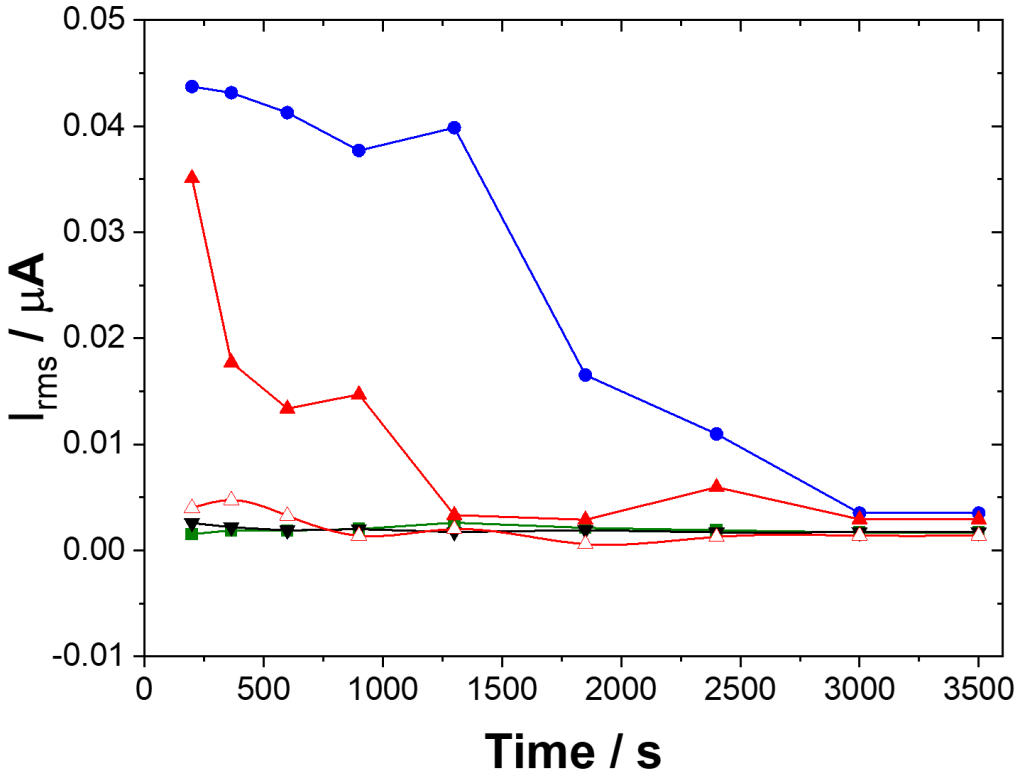

Figure 5.6: Root mean square of PSD_I. Experimental conditions were: absence of Caff and 1H2N (▼); absence of Caff and presence of 1H2N (■); presence of Caff and absence of 1H2N (●); presence of Caff and 1H2N (▲ and Δ). Full symbols represent data collected with positive interfacial potential. Interface potential was negative for hollow symbols.

Figure 5.6 shows the I_{rms} (calculated from the results shown in Figure 5.4b) for the different experimental conditions at various times. For these experiments, the interface is polarised positively. When no caffeine is present (green and black curves on Figure 5.6), I_{rms} values are below 0.005 µA for the whole duration of the experiment, suggesting that no interfacial charge transfer is occurring. When caffeine is present in the aqueous phase, I_{rms} values are higher, whether 1H2N is present (red curve) or not (blue curve) in the organic phase. In the presence of 1H2N, I_{rms} values decrease faster with time. Indeed, after 1250 s, the I_{rms} values reach the same level as for the control experiments, while it takes 3000 s in the absence of 1H2N. As a control experiment, the current and potential were measured in the presence of both caffeine and 1H2N but when the interfacial potential is negative (Figure 5.6), which is unfavourable to the formation of caffeine:1H2N cocrystals [174]. I_{rms} values in these experimental conditions are similar to the ones observed in the absence of caffeine confirming that the high I_{rms} values are linked to caffeine charge transfer, when the interface potential is positive.

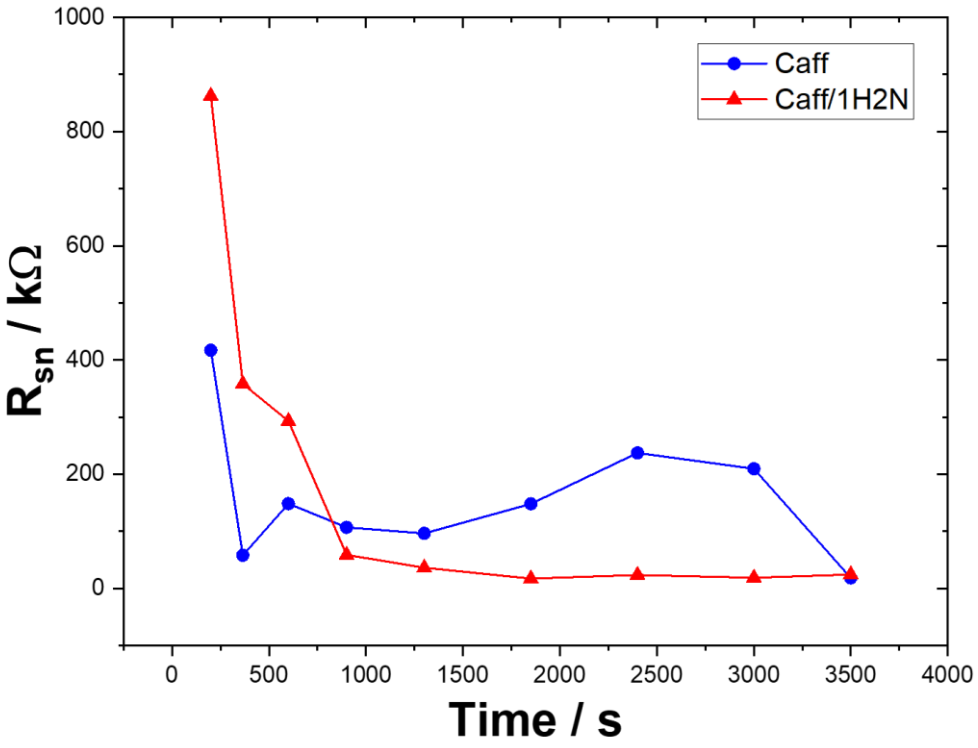

Figure 5.7: The low frequency noise impedance calculated for Scheme 5.1 electrochemical cell 12 in the absence (●) and in the presence (▲) of 1H2N. Caffeine is present for both experiments.

In electrochemical cell when the cocrystals are created the low frequency noise impedance decreases within first 1000s which can be attributed to the creation of the complex Caff/1H2N (Fig 5.7 red line) and low current noise. After these times the resistance flattens, which may be related to the adsorption of complex at the ITIES. In contrast to a cell in which the complex is not formed (Fig. 5.7 blue line), the change in the R_{sn} does not change significantly during the course of an experiment. The noise impedance has lower values at the beginning, because growth or adsorption of the cocrystal on the LLI does not take place - the caffeine is transferred and the current has higher values.

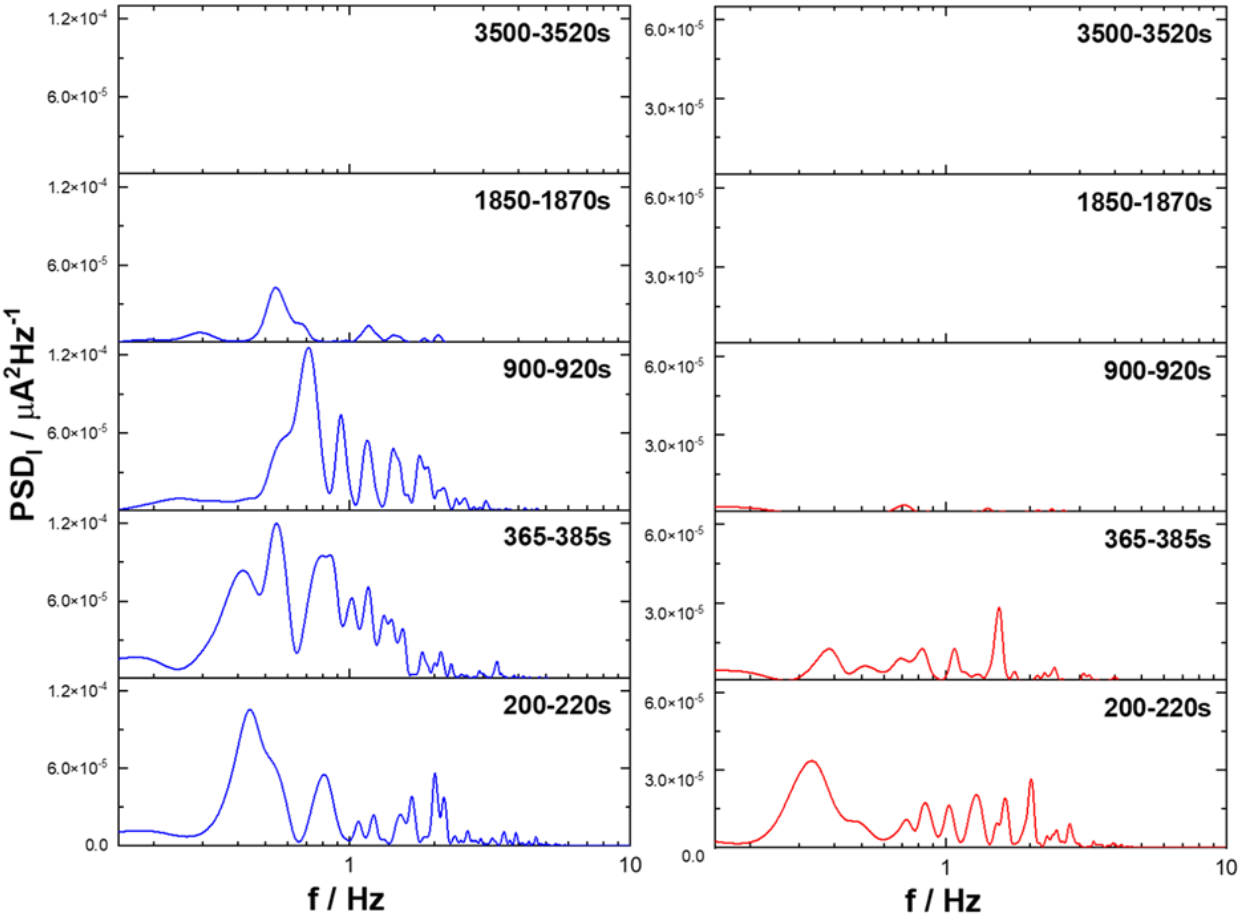

<u>Figure 5.8:</u> PSD spectra of electrochemical current (PSD_I) recorded in the cell (left) in the absence and (right) in the presence of 1H2N (electrochemical cell 11) calculated from different times.

Figure 5.8 presents the comparison of PSD_I as the function of frequency in the absence and in the presence of 1H2N; caffeine is present in both experiments. In the absence of 1H2N, the PSD_I

values are high and for the times: 200, 365 and 900 s they reach values of 1.2×10^{-4} μA^2 Hz^{-1} and the signal decreased at 1850s. In the presence of both caffeine and 1H2N cocrystals are formed at the liquid-liquid interface. The PSD_I values when cocrystals are formed are one order of magnitude lower (4×10^{-5} μA^2 Hz^{-1}) from the beginning of the experiment and is no longer visible after 900 s. Most of the current is cumulated in the region around 1 Hz. However, PSD_I for the formation of crystals appear at slightly lower frequencies than in the sole presence of caffeine. This is due to the complex formation causing the changes at the liquid-liquid interface which hold caffeine transfer. The signal fades out more rapidly (385 s) upon cocrystal formation as the caffeine enters into a reaction with 1H2N and their adsorption at ITIES. In contrast, in the absence of 1H2N, caffeine continues to transfer to the organic phase as the signal becomes less intense after 1870 s. The PSD spectrum of electrochemical current is much less intense (1×10^{-6} μA^2 Hz^{-1}) when a negative potential is applied, although both Caff and 1H2N (Fig. 5.9) are present in the cell. In such conditions, no formation of cocrystals occurred suggesting that caffeine transfer is responsible for the PSD current.

Caffeine is a weak base with a pK_a of 10.4[147], so it is in cationic form in the acidic conditions (pH = 2) at which the cocrystallisation process occurs.[174] As control experiments, experiments were carried out at pH values of 6 and 11. Caffeine transfers at $\Delta_o^w\phi_{Caffeine}^0 = 0.390\ V$ at pH 2 as shown by the transfer peak observed (Figure 5.10). However, caffeine transfer was not observed for pH 6 and 11 as it could be masked by the transfer of background electrolyte. Electrochemical noise was also measured at pH 6 and 11 and the PSD_I at various pHs are shown in Figure 5.10 for the time period 900 - 920 s. At pH 2 and 6, power spectra showed noise with a frequency in the 0.1-10 Hz, whereas the PSD signal was significantly lower at pH 11 in the same frequency region. These observations are consistent with the fact that cocrystals were collected in electrochemical cells at pH 2 and 6 and not at pH 11.

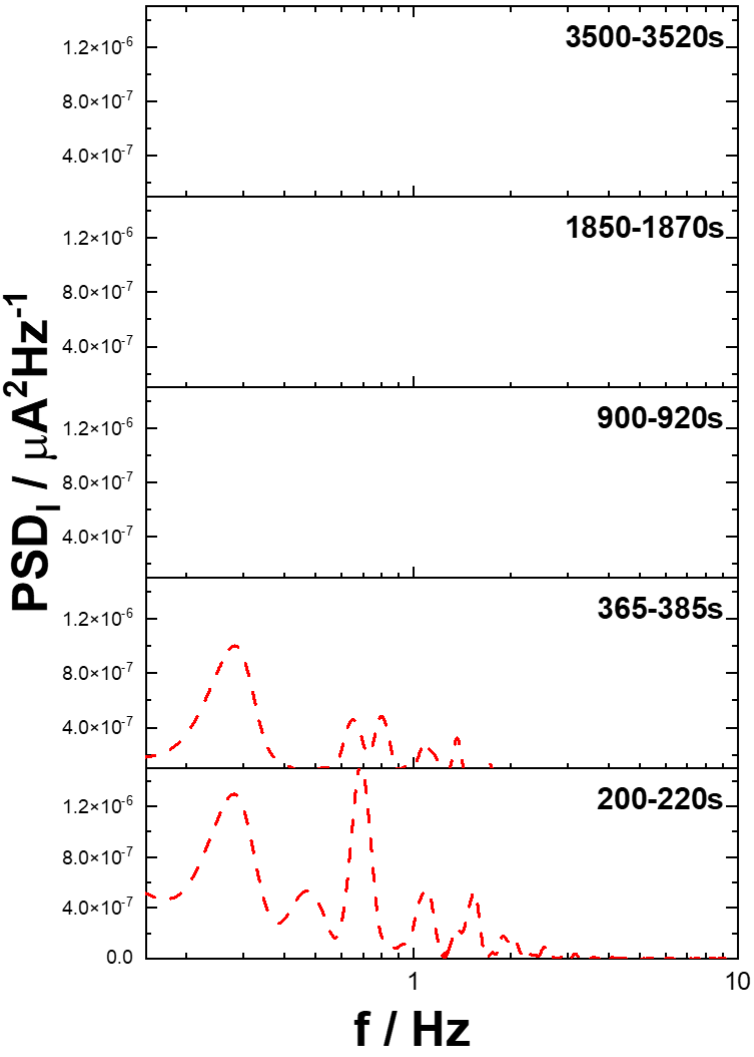

<u>Figure 5.9:</u> The PSD I spectrum of the electrochemical current recorded in the cells under conditions consistent with electrochemical cell 3 Scheme 5.1 and corresponding to a negative potential (x = 1, y = 0.1, X = SAT).

Electrochemical noise analysis shows that, when both caffeine and 1H2N are initially present, interfacial processes of charge transfer are occurring in the first 1000 s of the experiment. During this period, caffeine is transferred across the interface and forms complexes with 1H2N in the organic phase, which then lead to the adsorption of cocrystals at the interface. After 1000 s, electrochemical noise analysis indicates that interfacial charge transfers have ceased, suggesting

the cocrystallisation is a two-step process with (i) a potential-driven nucleation with the transfer of caffeine from the aqueous to the organic phase; (ii) a growth stage where the interfacial potential no longer plays a role.

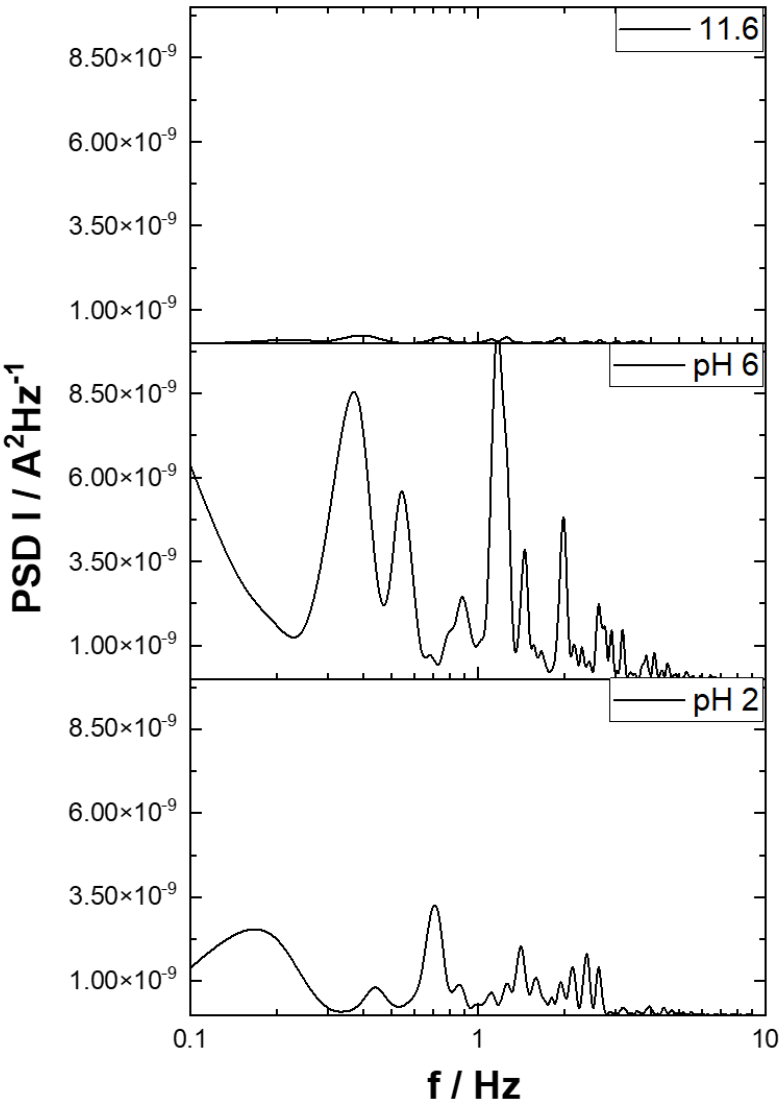

Figure 5.10: PSD spectrum of electrochemical current recorded in the cells in the conditions presented in the electrochemical cell 3, 4 and 5 (Scheme 5.1) and corresponds to the pH 2, 6 and 11.6 respectively. 900 < time < 920 s.

5.4. Conclusions

The potential for the designed electrochemical cells with various ratio of concentration of tetraalkylammonium salts in organic and aqueous phase was monitored. It was found to be in good agreement with the theoretical values based on the Nernst-like equation. The results were similar for three ions: tetramethylammonium, tetraethylammonium and tetrapropylammonium, which indicated that the potential values depend uniquely on the ratio $\frac{c^o_{TAA^+}}{c^w_{TAA^+}}$. Thus, by varying the ratio of concentrations of the selected ion in the organic and aqueous phases, we were able to obtain suitable potential values to drive the cocrystallisation process. Addition of caffeine and 1-hydroxy-2-naphthoic acid to these well-defined electrochemical cells allowed to monitor the potential and current at the liquid-liquid interface. Analysis of the electrochemical current noise showed a clear difference between cells in which cocrystals are formed and those in which cocrystallisation is hindered, either by a negative potential or by a change in pH. Caffeine transfer and cocrystal formation generate different signals with current maxima at frequencies in the 0.1 – 1 Hz range. The EC method is a powerful tool to follow the changes occurring at ITIES in common ion experiments by simultaneous measurement of potential and current.

6. INFLUENCE OF EXPERIMENTAL FACTORS ON INTERFACIAL COCRYSTALLISATION

The goal of this chapter was to investigate the important factors that influence the interfacial cocrystallization. We investigated factors such as drug form, drug concentration, pH, choice of aqueous ($LiCl/Li_2SO_4$) and organic electrolytes (KTPBCl, KTB, LiTB), choice of acids and bases used to change pH or type of solvent (DCE, TFT and a mixture of Anisole and TFT). The differences between the resulting cocrystals were tested using the following methods: XRD, interfacial tension measurements and simultaneous ΔE and I measurements. 16 experiments for each drug, in different conditions, were made to select optimal parameters. The statistical analysis of results was then done to check, which parameters are important for the crystallization/cocrystallization at the liquid-liquid interface and polymorph selection.

Design of experiments (DoE) is the part of applied statistics in which controlled studies are planned, conducted, analysed and interpreted. The aim is to evaluate the factors that control the value of a parameter or group of parameters. DoE is a tool which allows the data collection and analysis in a various experimental condition. With the DoE, we can manipulate a number of input factors and examine their impact on the desired output (response).

To investigate all these factors the DoE function in R software was used with R packages *Rcmdr.Plugin.Doe* [177]. With its help, we were able to reduce the number of experiments to the number which was feasible, e.g. 16 (instead of $4^{\text{nr of factors}}$) and still being able to perform a reliable statistical analysis. To obtain this the regular fractional factorial 2-level design was created. The first attempts were carried out using: piroxicam and sildenafil and their salts and ketoprofen and diclofenac (results presented in APPENDIX 2).

6.1. Materials and methods

The composition of the following vials were projected with Design of experiments by the R software package *RcmdrPlugin.DoE* [177] and *Doe.base* [178]. This tool enabled the design, control and export of experimental conditions. For the purpose of this study the Regular (Fractional) Factorial 2-level design was found to be the more suitable to find the active factor at

two levels (-1, 1) which may influence the interfacial crystallization/cocrystallization. All vials were left for 16h.

The factors that needed to be investigated for their effect on interfacial crystallisation were: (i) solvent, (ii) aqueous phase anion, (iii) organic phase cation and (iv) anion. 4 factors were considered at 2 levels and 16 runs, resulting in the experimental vials in Figure 6.1.

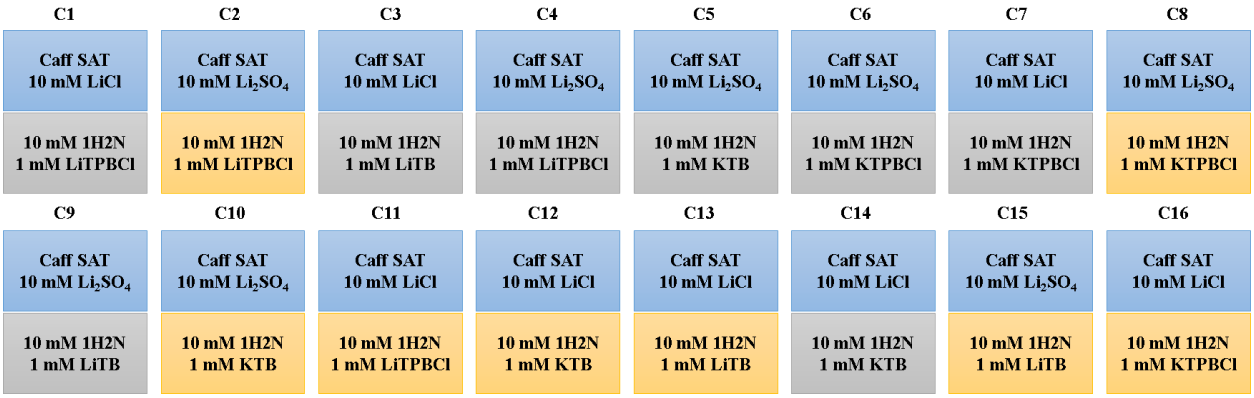

Figure 6.1: Experimental set up presenting chemical polarisation of the interface applied for DoE experiments. KTPBCl - potassium tetrakis(4-chlorophenyl) borate; KTB - potassium tetrakis(pentafluorophenyl)borate; LiTB - lithium tetrakis(pentafluorophenyl)borate.

On the Figure 6.1 the experimental set up is presented. It consisted of two immiscible solutions in order to form the interface. The aqueous phase was an acidic solution of 10 mM LiCl or 10 mM Li_2SO_4 (acidified with HCl or H_2SO_4 down to pH = 2), and saturated solution of caffeine. The organic phase (immiscible with water) was 1H2N in DCE or mixture of Anisole and TFT (2:1). The following salts were added to the organic phase of the biphasic systems in order to chemically apply the high potential: KTPBCl, KTB and LiTB. The ions present in the system are distributed in equilibrium between the aqueous and organic phases, resulting in a change of interfacial potential ($\Delta_o^w\phi$)[156], [157]. The standard transfer potential of K^+ and Li^+ ($\Delta_o^w\phi_{K^+}^0$=0.53 V and $\Delta_o^w\phi_{Li^+}^0$=0.61 V)[91] is higher than the one of caffeine($\Delta_o^w\phi_{Caff^+}^0$= 0.39V) so there is an ion exchange. An additional biphasic system without salt imposing potential in organic phase was prepared as a control sample (Fig 6.2).

Table 6.1: The various properties of selected organic solvents.

Solvent	Static relative permittivity (ε)	Solubility in water	Dipole moment (μ)	Interfacial tension (ϒ)	Density	Viscosity
Unit	**$F \cdot m^{-1}$**	**g per 100 g of water**	**D**	**$mN \cdot m^{-1}$**	**g/cm^{-3}**	**10^{-3} Pa·s**
DCE	10.42 [67]	0.852	1.83	30.5 [121]	1.250 [67]	0.779 [67]
TFT	9.18 [66]	< 0.100	2.86	38	1.190 [66]	0.750
Anisole (A)	4.33 [67]	0.171	1.36	35	0.995 [67]	0.895 [67]

In the Table 6.1 are listed the properties of the selected organic solvent. These differences in their features may lead to the changes in the cocrystals formed at the liquid-liquid interface. The mixture of A: TFT (2:1) was used as a second organic phase solvent. These chemicals were mixed due to the two factors (i) anisole has a lower density than water (Table 6.1), so it did not form a bottom layer. Beside 1H2N is not well soluble in TFT and is well soluble in anisole. The ratio A: TFT – 2:1 was calculated to be enough to form a bottom phase after the vial establishment. Density of this mixture was lower (1.056 g/cm^{-3}, measured with pycnometer) than the density of DCE.

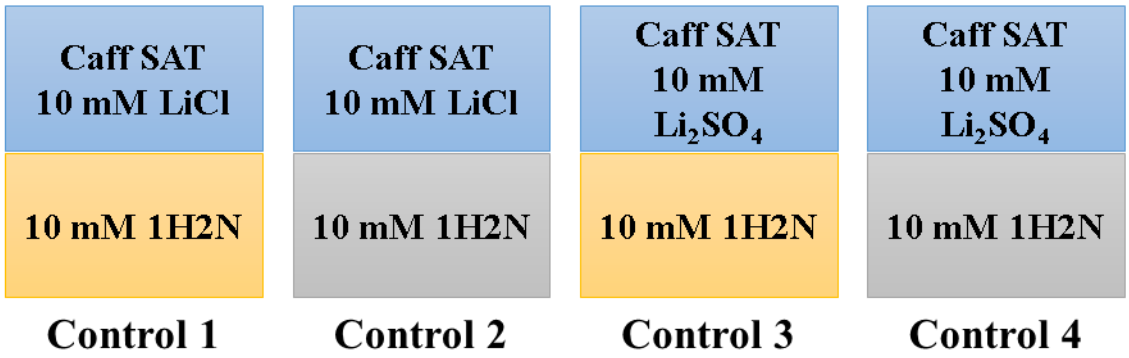

Figure 6.2: Experimental set up presenting control experiments applied for DoE experiments.

The cocrystallisation of caff/1H2N was further investigated through shake-flask experiments. The factors that were considered were:

- aqueous phase electrolyte (LiCl, Li_2SO_4)
- organic phase electrolyte cation for interfacial polarization (K^+, Li^+)
- organic phase electrolyte anion for interfacial polarization ($TPBCl^-$, TB^-)
- choice of solvent (DCE, mixture of Anisole:TFT)

Numerical values for the analysis carried out with R software have been converted to (-) for minimum values and (+) for maximum values (Table 6.2). The full factorial 2-level design was created. The number of factors was four and the number of runs were chosen as 16. The results are presented in Figure 6.1:

Table 6.2: Numerical values converted to (-) for minimum values and (+).

Parameters	-	+
Solvent	A: TFT	DCE
Aqueous phase anion	Li_2SO_4	LiCl
Organic phase cation	Li^+	K^+
Organic phase anion	TB^-	$TPBCl^-$

6.2. Shake-flask experiment of caffeine: 1H2N in various conditions

In this chapter the influence of various factors (organic solvent, aqueous phase acid/anion, organic phase cation and anion) on cocrystallization process at the liquid-liquid interface were studied. It was proven that these factor can change and influence the interfacial interactions which leads to various polymorphic outcome of cocrystals formed at liquid-liquid interface[27], [30]. Solvents used for the cocrystallization at the liquid-liquid interface had an influence on the polymorphic forms that were found at the water-oil interface. The use of more polar solvent favoured the creation of form I [27] when in other work the use of solvent with high dielectric constant tended to create the form II and non-polar solvents gave the form I [179]. The use of different solvents has resulted in different polymorphic phases. Therefore, in this study, it was decided to change the organic solvent. This was the first factor used for DoE, which can affect the cocrystals formed at the phase interface.

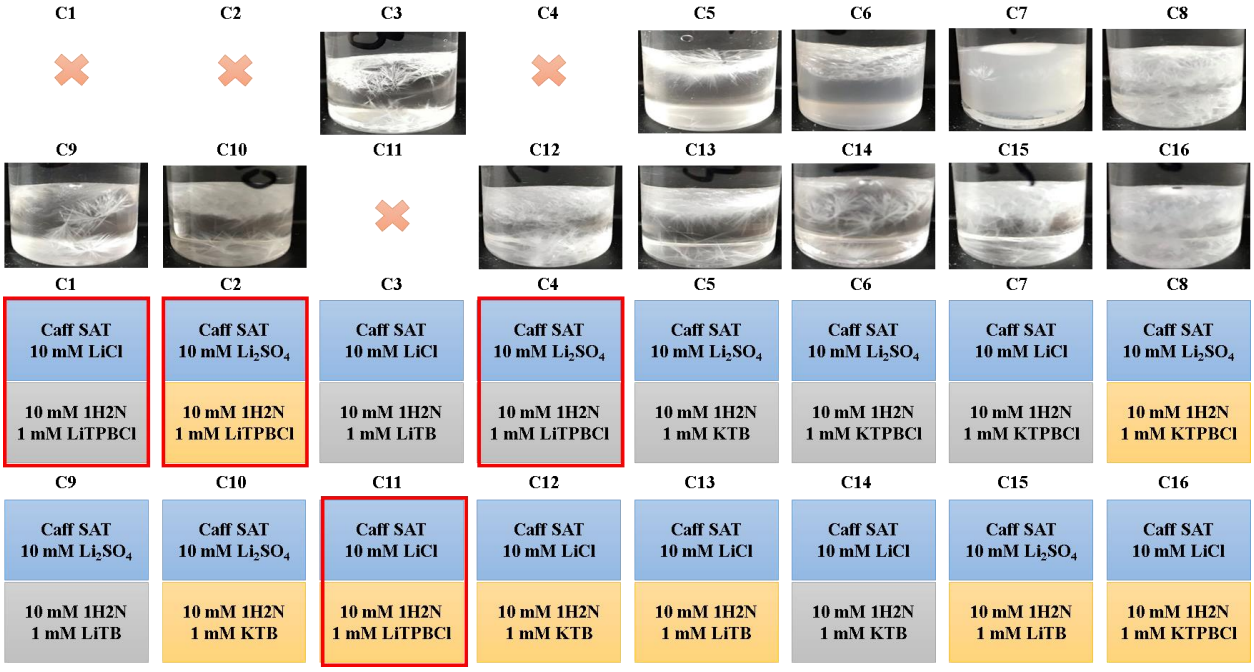

Figure 6.3: Photographs of aqueous-organic biphasic systems for various aqueous phase electrolytes and different organic phase salts with corresponding experimental conditions below. Images were taken after the vials had been left at room temperature for 16 hours. Grey – A: TFT (2:1), yellow – 1.2-DCE. The vials with the red frame were not possible to perform.

The formation of Caff: 1H2N cocrystals at a water-oil interface was investigated by preparing a series of vials of varying experimental conditions according to the description in Chapter 6.1. Figure 6.3 shows biphasic system consisting of aqueous caffeine solution and organic solution of 1H2N, respectively, and polarised by the addition of salts with corresponding experimental conditions. The aqueous phase consisted of 10 mM solution of LiCl (Figure 6.3 vials C1, C3, C7, C12, C13, C14 and C16) or 10 mM solution of Li_2SO_4 (Figure 6.3 vials C5, C6, C8, C9, C10 and C15). The aqueous solution was acidified with HCl or H_2SO_4 to reach pH 2, respectively. In the organic phase we tested two solvents: DCE and the mixture of A: TFT (2:1). The interfacial potential was imposed by addition of KTPBCl, KTB and LiTB to the organic phase. Control experiment vials were prepared in the absence of potential-imposing salts in the organic phase

(Fig. 6.2). Four conditions could not be fulfilled because the salt LiTPBCl does not exist so the vials C1, C2, C4 and C11 on the Figure 6.1 should be eliminated before starting the experiments.

Figure 6.3 shows the images of the cocrystals obtained at the LLI. Cocrystals were obtained in all vials. Control experiment vials (Control 1, 2, 3 and 4 Fig. 6.2) were prepared in the absence of potential-imposing salts in the organic phase. When the aqueous solution was saturated with $CaffH^+$, differences in the number and shape of cocrystals forming at the interface were observed. In some vials (Fig. 6.3 vials C5, C6, C7) the cocryatls remained at the liquid-liquid interface where in the other vials we saw the cocrystals at the bottom. It suggested that the size was too big to remain adsorbed at the interface and they fell at the bottom of the vials. In some vials (Figure 6.3 vials C6, C7 and C16) the organic phase was blurred due to the smaller particles (cocrystals with smaller size) suspended in the organic solvent.

The cocrystals were collected from the interface, air-dried and analysed by XRD to check the differences in the content of the phase I and II (Chapter 4.3.2).

6.3. XRD of Caff/1H2N cocrystals obtained under different conditions

The cocrystals obtained at the liquid-liquid interface (Figure 6.5) were collected and analysed by PXRD. All peaks presented in the diffractograms were thus well fitted and indexed only by phase I or phase II (explained in Chapter 4.3). We proposed semi-quantitative calculations to compare the phase ratios of the samples. The PXRD diagrams of a phase I and II mixture was simulated based on the CCDC files from the known structures of pure single-phase material. Then we calculated the proportions of phases present in the cocrystals. The intensities of the peaks in the analyzed samples were normalized and compared with the normalized intensities of the pure single phases from the simulated phase I and II diffractograms. The results for various conditions are presented on Figure 6.5. None of the compounds initially present in the vials (LiCl, KTPBCl, KTB, LiTB) were visible in the PXRD diagram, as there were no 1H2N residues. In all vials the interface was positively polarized however involving different salts imposing high potential (KTPBCl, KTB and LiTB) and various solvents in organic phase (DCE and A: TFT mixture). The combination of other salts and solvents (Figure 6.5) did not result in a significant advantage of phase I, in contrast to the previous experiment when KTPBCl and DCE (here Fig. 6.4 C16) were used in the organic

phase (Chapter 4.3). In all vials except of C16 we observed the predominance of phase II. In the vial C9 on Figure 6.5 there is almost pure phase II. Thus, we also found the conditions to obtain cocrystals forming only phase II. The diffractograms of cocrystals of pure phase I (red) and pure phase II (black) are presented on Figure 6.4. The conditions applied in the vial C9 are very different from the conditions where only phase I was found (C16). In vial C9, Li_2SO_4 was the aqueous phase electrolyte and LiTB dissolved in A: TFT was the organic phase electrolyte. Mixture of these two solvents have lower relative permittivity than DCE (10.42, 9.18 and 4.33 $F \cdot m^{-1}$ for DCE, TFT and A, respectively). Lower permittivity so the use of less polar solvent (diisopropyl ether – DIPE) was found to promote the formation of form II in case of Caff:1H2N cocrystals [27].

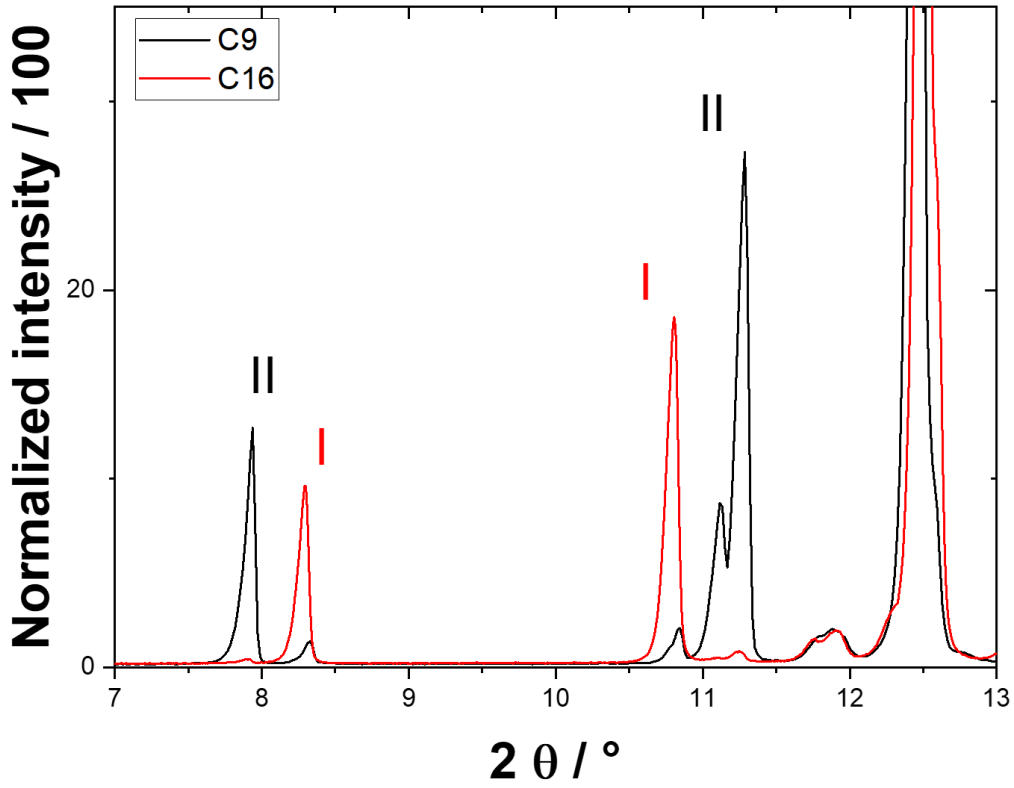

Figure 6.4: Diffractograms of cocrystal (Caff: 1H2N) powders obtained at the liquid-liquid interface for the C9 (Li_2SO_4/LiTB/A: TFT) and C16 (LiCL/KTPBCl/DCE). Roman numbers attributed the different peaks to the corresponding crystallographic phase.

On the Figure 6.5 no trend favoring a particular solvent or aqueous salt was observed. Therefore, further analyses need to be carried out.

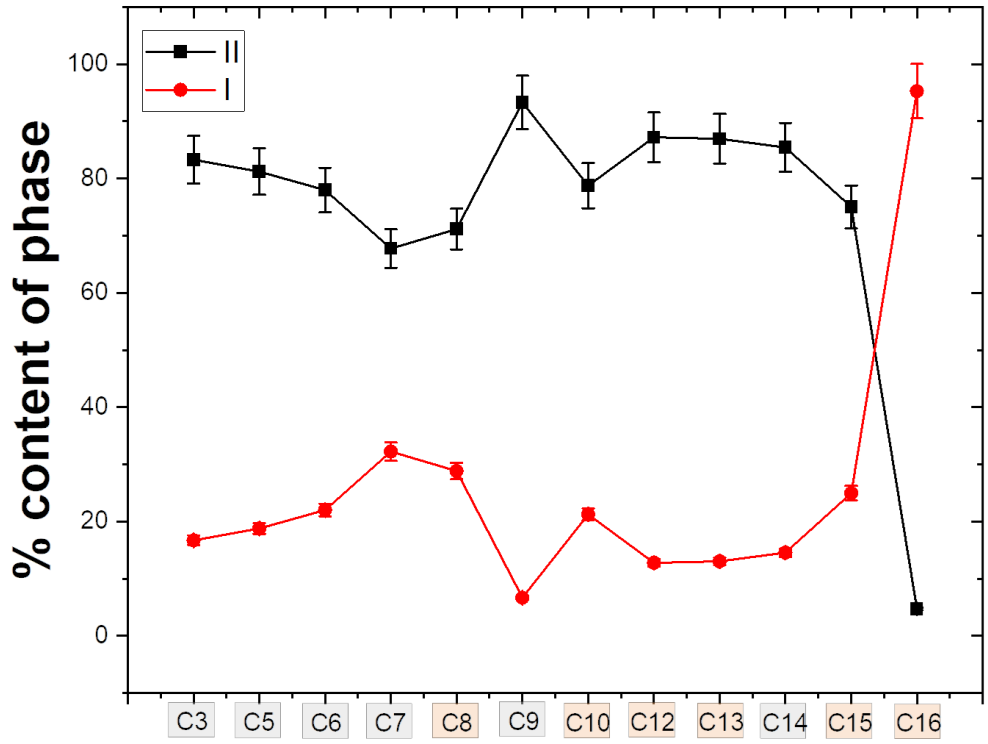

Figure 6.5: The Phase I % (–●–) and II % (–■–) content dependence on various conditions applied for cocrystallization of Caff:1H2N according to vials in Figure 6.3. Cocrystals caff: 1H2N obtained at the liquid-liquid interface for solution saturated with caffeine and different salts and solvents in organic phase. Error bars with the default 5% value. Grey – A: TFT, orange – DCE.

6.4. Simultaneous measurements of ΔE and I during the formation of Caff/1H2N cocrystals

Simultaneous measurements of ΔE and I was carried out according to scheme 5.1 and electrochemical cell 6. The potential and current were measured simultaneously during 3600 s (5.1) and the graphs ΔE(t) and I(t) are presented on Figure 6.6a and b, respectively. The organic phase solvent was DCE. The conditions correspond to the vials in Figure 6.3. The experiments

were carried out with KTPBCl (vials C8 and C16), KTB (vials C10 and C12) and LiTB (vials C13 and C15) which were the salts applying positive potential. In all the experimental vials the cocrystals were formed at the ITIES.

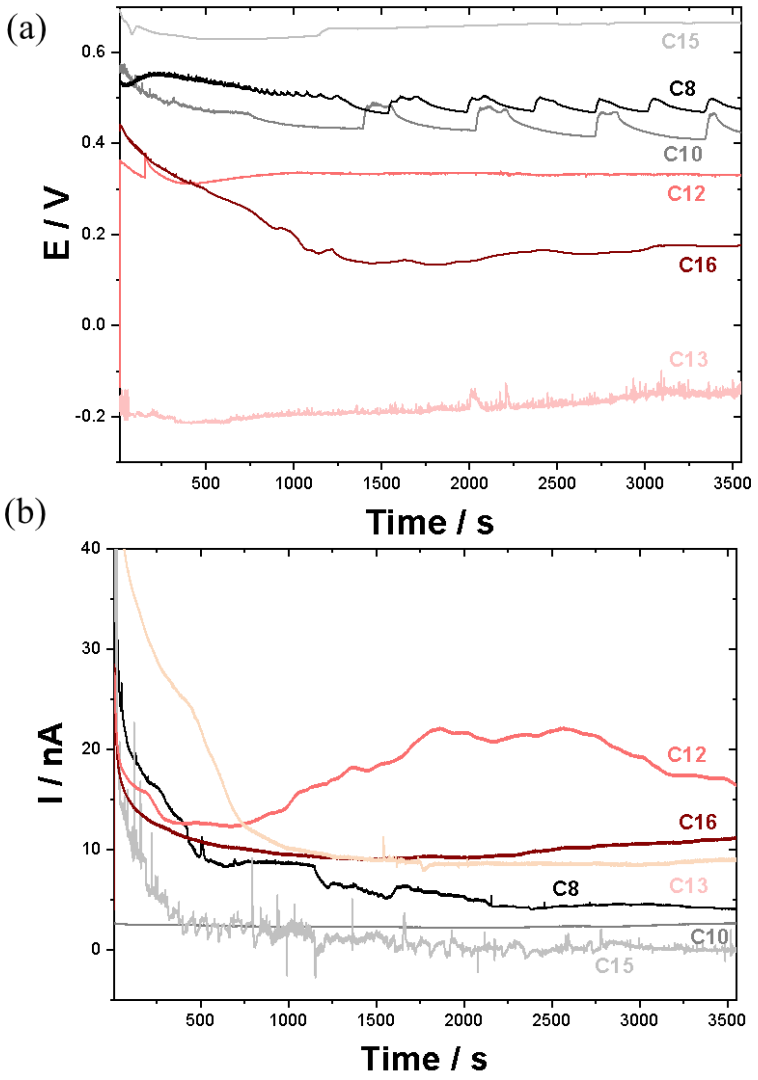

<u>Figure 6.6:</u> Variation of (a) potential and (b) current as a function of time for DCE as organic solvent and the various electrochemical cell 6 (Scheme 5.1) configurations. C8 – Li_2SO_4/KTPBCl (——), C10 – Li_2SO_4/KTB (——), C15 – Li_2SO_4/LiTB (——), C12 – LiCl/KTB (——), C13 – LiCl/LiTB (——) andC16 – LiCl/KTPBCl (——).

The potential in vials C13, C15 is stable in time and the potential for C12 and C16 is higher at the at the start of the experiment and decreased after 1000 s. After this time, the cocrystals are already formed. The potential in vials C8 and C10 seem to drift with time initially until repetitive events of potential variation appear after 1500 s. It should be noted that the vials, for which the potential are most stable, have a common cation in both the aqueous and the organic phase. The variation in potential for the other cells could be induced by the incessant transfer of K^+ and Li^+ between the two phases. For all the vials at Figure 6.6 the potential had positive values except of C13 where LiTB was a part of organic phase. The current in the vials C8, C10, C13, C15 and C16 decreased to a time of 1000 s and after that time it took a constant value. The current for the vial C12 was not stable over 3600 s and is significantly different from the others. The current decreased at first before increasing slowly after 800 s. The potential and current were not stable as in the experiments with the ratio $\frac{c^o_{TMA^+}}{c^w_{TMA^+}}$ (Chapter 5). Here, we were not able to fulfil the equation 5.7. The concentration of Li^+ and K^+ in w and w' and o was not equal (Scheme 5.1 electrochemical cell 6). Additionally, KTPBCl is not fully soluble in DCE and it was not possible to maintain the same $c^{w'}_{Li^+} = c^w_{Li^+}$. Therefore, 5 mM BACl was the w' phase. Furthermore, K^+ and especially Li^+ are hydrophilic cations which may not be stable in organic phase which result in potential and current signals.

The simultaneous measurements of ΔE and I were carried out for A: TFT as an organic phase according to scheme 5.1 and electrochemical cell 6. The potential and current were measured simultaneously during 3600 s (description in Chapter 5.1) and the graphs ΔE(t) and I(t) are presented on Figure 6.7a and b, respectively. The conditions correspond to the vials in Figure 6.3. The experiments were carried out with KTPBCl (vials C6 and C7), KTB (vials C5 and C14) and LiTB (vials C3 and C9) which were the salts applying positive potential. In all the experimental vials the cocrystals were formed at the ITIES.

The potential and current vs. time graphs are less stable than for the vials with DCE (Figure 6.6). The potential in vials C3, C7 and C9 were stable in time and C5, C6 and C14 were very unstable during the whole experiment. For all the vials shown in Figure 6.7, the potential difference had positive values. However, for the three latter vials the potential difference values drop off significantly. The current in the vials C3, C5, C7 and C14 increased over time, and the current in

vial C9 was constant. The current in the vial C6 was not stable over 3600 s and is significantly different from the others.

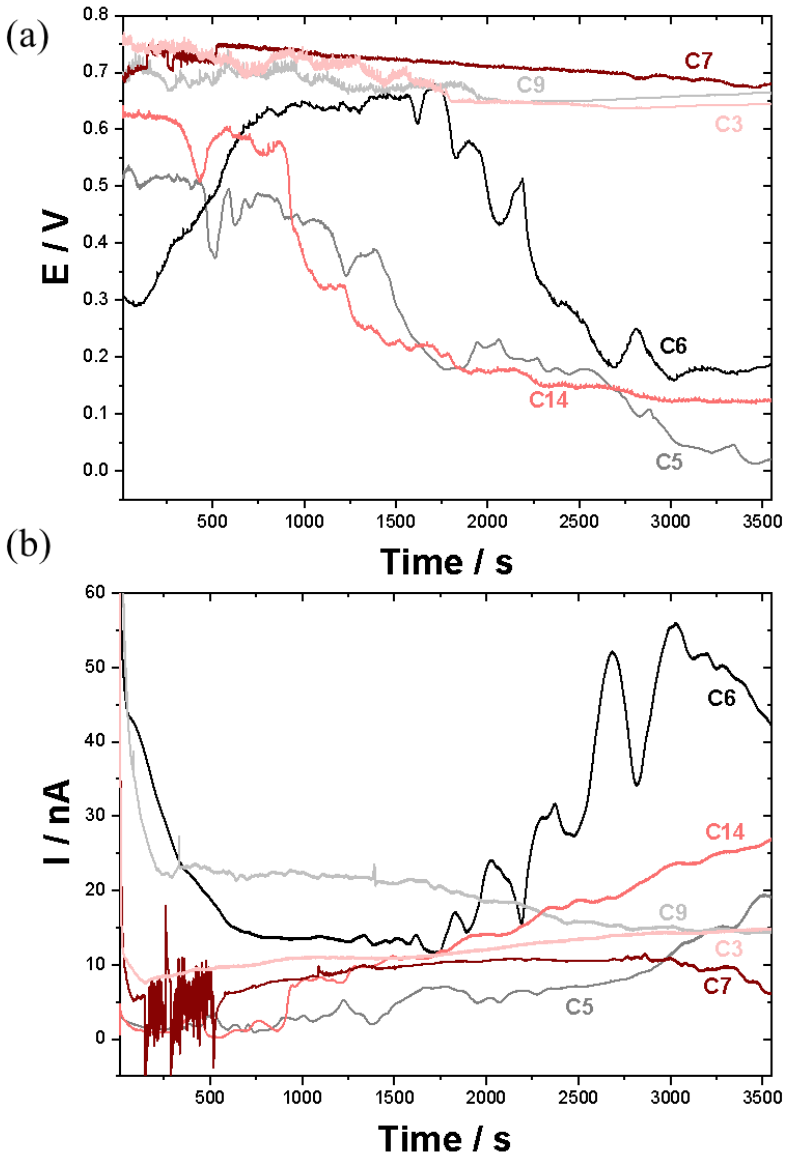

<u>Figure 6.7</u>: Variation of (a) potential and (b) current as a function of time for A: TFT mixture as organic solvent and the various electrochemical cell 6 configurations. C6 – Li_2SO_4/KTPBCl (——), C5 – Li_2SO_4/KTB (——), C9 – Li_2SO_4/LiTB (——), C7 – LiCl/KTPBCl (——), C14 – LiCl/KTB (——) and C3 – LiCl/LiTB (——).

Interestingly, local ΔE maxima seem to correspond to local i minima (and vice versa) in the 1500 – 3000 s time frame (Fig. 6.8). A similar observation can be made for C5 (to a lesser extent). These inverted variations of current and potential difference could be explained by the formation / desorption of Caff: 1H2N crystals at the ITIES. Indeed, when the potential is increasing, more $CaffH^+$ is transferring to the organic phase, which results in crystal growth at the interface. As a consequence, mass transfer to the interface might be impeded and interfacial surface area available is decreasing, leading to a drop in current. During the cocrystal formation, protons are released and could contribute to the decrease of potential difference. The current increase could also be associated with cocrystals desorbing from the interface and hence leaving a larger interfacial surface area. Supposedly, K^+ and especially Li^+ are hydrophilic cations which may not be stable in organic phase which result in noisy potential and current signals. In addition, it was noted that in the case of the solvent mixture (A: TFT), one of the solvents evaporated faster than the other, leading to a separation of the mixture and the boundary between the layers began to be visible.

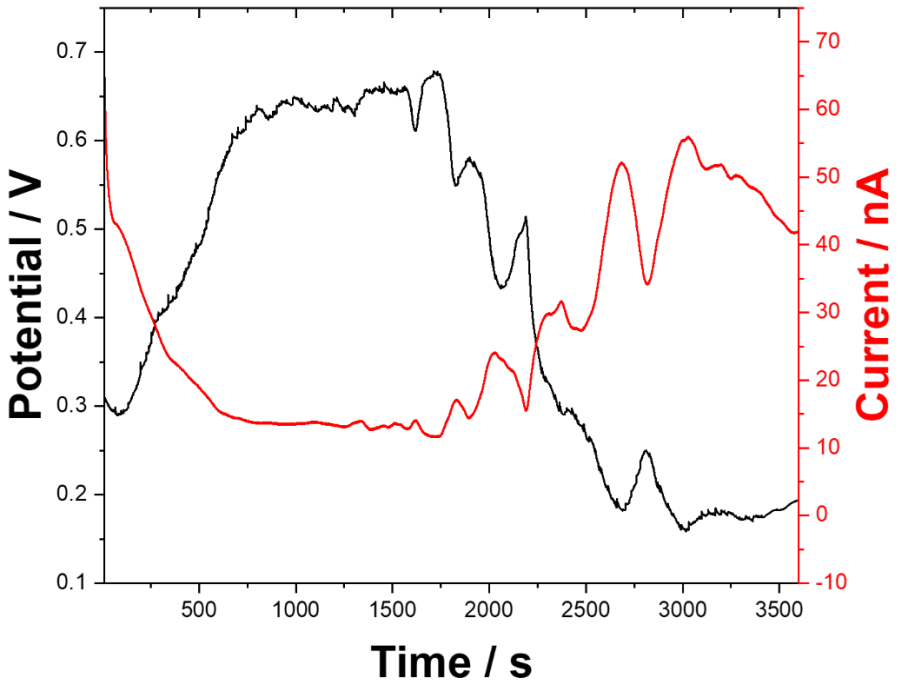

Figure 6.8: Potential and current versus time for C6 experiment (Li_2SO_4/KTPBCl/A: TFT).

6.5. Interfacial tension measurements of Caff/1H2N cocrystals obtained under different conditions

Interfacial tension (γ) at the molecular level, is the energy difference between molecules at the liquid interface. It describes how much energy is necessary to create the interface between two solvents [180]. Interface between at immiscible liquids depends on the nature of these phases, their chemical structure, and flow dynamics. It is therefore important to study the interactions at the phase interface to understand the behaviour of these liquids. Interfacial tension (IFT) is the energy per unit area of the liquid-liquid interface.

6.5.1. Drop shape analysis

The pendant drop method coupled with computer image analysis is fast, inexpensive and accurate method to measure the interfacial tension[181]. The pendant drop tensiometry involves a liquid drop realised from a needle.[180] Geometrical dimension used for the surface tension analysis are explained in Figure 6.9a. S is the distance along the droplet profile from the apex of the droplet, and θ is the angle between the horizontal and the tangent to the profile of the droplet at a point defined by the x and y coordinates[181].

The drop shape was automatically analysed by data fitting using the Laplace–Young equation.

$$\gamma\left(\frac{1}{R_1}+\frac{1}{R_2}\right) = \Delta\mathrm{P} = \Delta P_0 - \Delta\rho g z$$

Where R_1 and R_2 are the curvature radii, $\Delta\mathrm{P} = P_{in} - P_{out}$ and it is the Laplace pressure across the interface, Δρ is the difference between the density of the drop and surrounding liquid ($\Delta\rho = \rho_d - \rho$), Δp_0 is the difference of the pressure at droplet's apex, z is vertical distance from origin, and g is the gravitational acceleration.[182] In Figure 6.9b a capture of pendant drop during the interfacial tension measurement is presented.

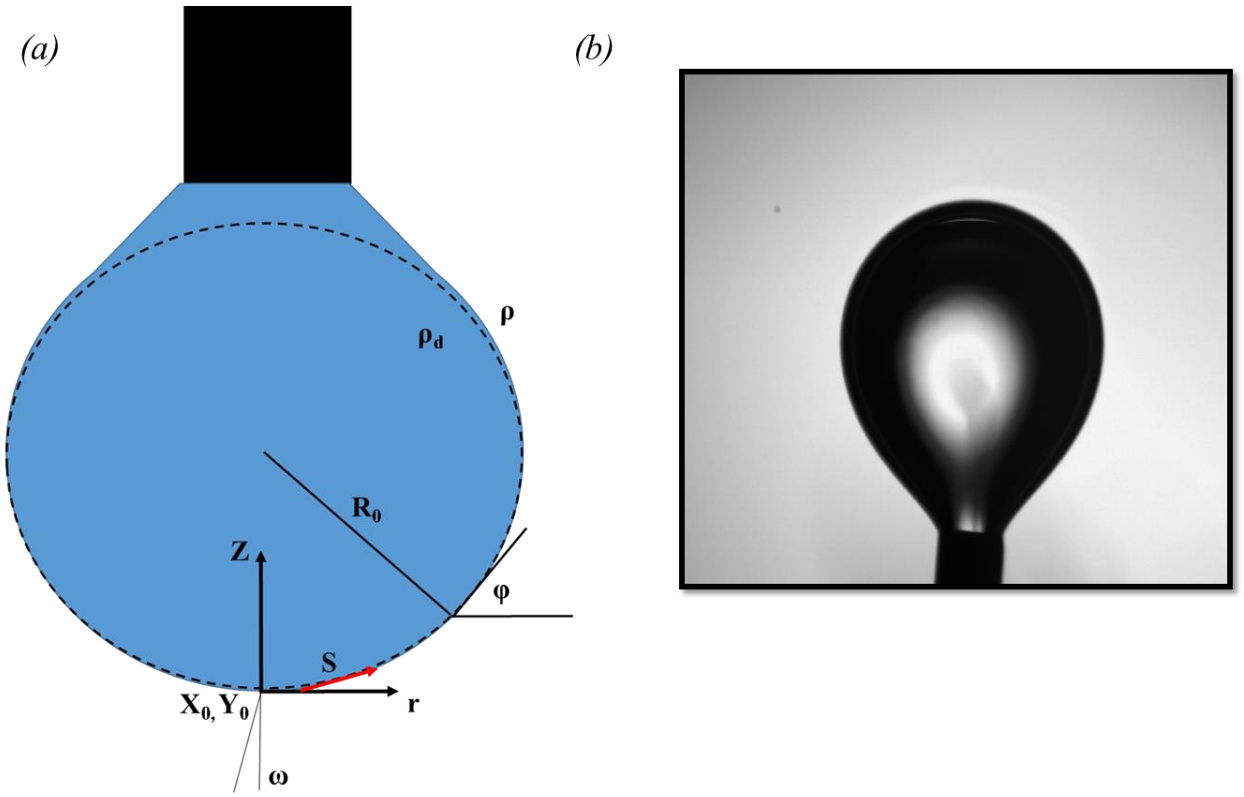

<u>Figure 6.9:</u> Schematic showing (a) a capture of pendant drop using the Attension Theta Optical Tensiometer taken at 0 s. Figure is based off of figures appearing in the One Attension experiment report. (b) an illustration the geometrical dimensions of the pendant drop method.

The experimental setup for the pendant drop analysis is presented on Figure 6.9. The drop shape analysis was performed using Attension Theta Optical Tensiometer (T200 from Biolin Scientific) operated by One Attension Software Version 3.2. Measurements were made by means of surface tension measurements. In this method the shape of the droplet is automatically analyzed by fitting the data with the Laplace-Young equation. The duration of the measurement was 30 s - 30 minutes. The experimental liquid was loaded into a 10.0 mL syringe. The drop of experimental liquid was formed in the second experimental liquid through a vertical stainless-steel needle in U-shape (Hooked needle for C205 and C205A/C201, gauge 22 (C210-22)). The needle stayed attached to the droplet to allow the volume of the droplet to be changed. The drop was illuminated from behind. Drop image acquisition was performed by USB3 digital camera (2680 fps max) and it was calibrated with a tungsten carbide ball (4.0 ± 1.0 um). The temperature was always 298K to maintain a constant solvent density. Density of all the solvents was checked before each

measurement. The needle was cleaned by sonication in acetone and ultrapure water and the syringe was rinsed with the same solvents.

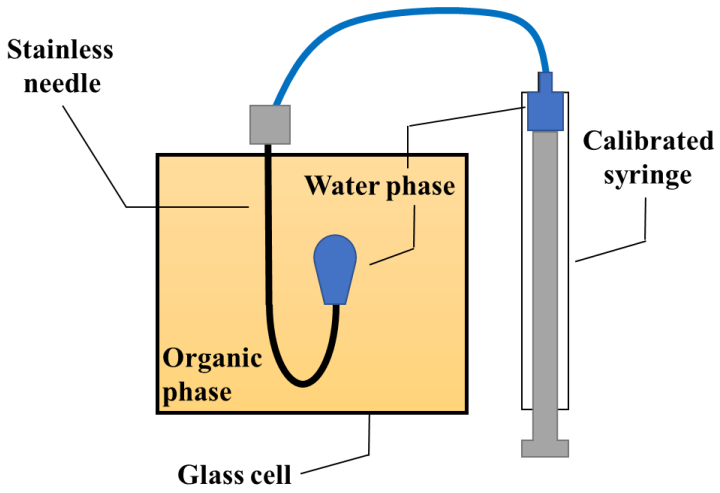

<u>Figure 6.10:</u> Experimental set up of drop shape analysis.

On the Figure 6.10 the scheme of the experimental set up for pendant drop analysis is presented. The organic solution was in the cubic vial. The volume of organic phase was 30 mL. All experimental conditions are presented in Figure 6.11. Two solvents were tested: DCE and the mixture of anisole: TFT (2:1). The pH of the aqueous phase was always 2 to favour the conditions for cocrystal formation. An aqueous phase consisted of water with 10 mM LiCl and 10 mM Li_2SO_4 saturated with caffeine. Two solvents were used as an organic phase: DCE and the mixture of A: TFT (2:1). In addition, the organic phase comprised 10 mM 1H2N and the salts changing the potential at ITIES (1 mM KTPBCl, 1 mM KTB and 1 mM LiTB). The control experiments were carried out without the potential imposing salts (Figure 6.2). Each solvent was analysed with the 5 aqueous phase compositions according to Figure 6.11: water *(——)*, 10 mM LiCl *(——)*, 10 mM Li_2SO_4 *(——)* and the solutions of 10 mM LiCl *(——)*, 10 mM Li_2SO_4 *(——)* saturated with caffeine.

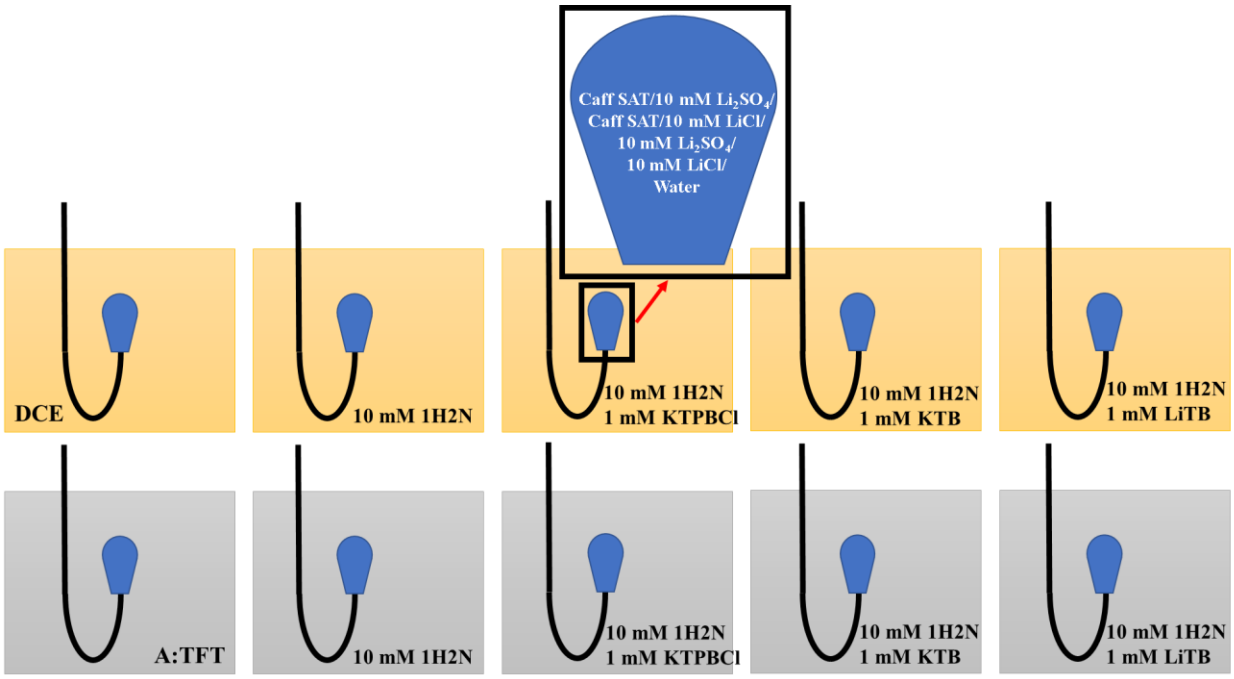

Figure 6.11: Experimental conditions for pendant drop analysis.

6.5.2. Interpretation of interfacial tension measurements

Interfacial tension was proven to provide important information about the nature of the solvents and electrolytes used for measurements and its impact on the kinetics that govern processes occurs at ITIES.[108], [154] The pendant drop analysis is able to measure the interfacial tension at ITIES. The differential capacitance (measured by AC Voltammetry in Chapter 3.3) of the water/DCE interface was shown to vary with the change in the ionic composition of the aqueous and organic solvent phases. The changes were due to the specific ions adsorption at ITIES and by ion pairs formed between ions present in both phases.[153], [183] However, the differential capacitance measurements had to be supplemented with interfacial tension measurements. The purpose of this study was to check the differences in the salts presents in both phases and to distinguish an impact of organic solvents. All the average values are calculated for the time 250-300 s.

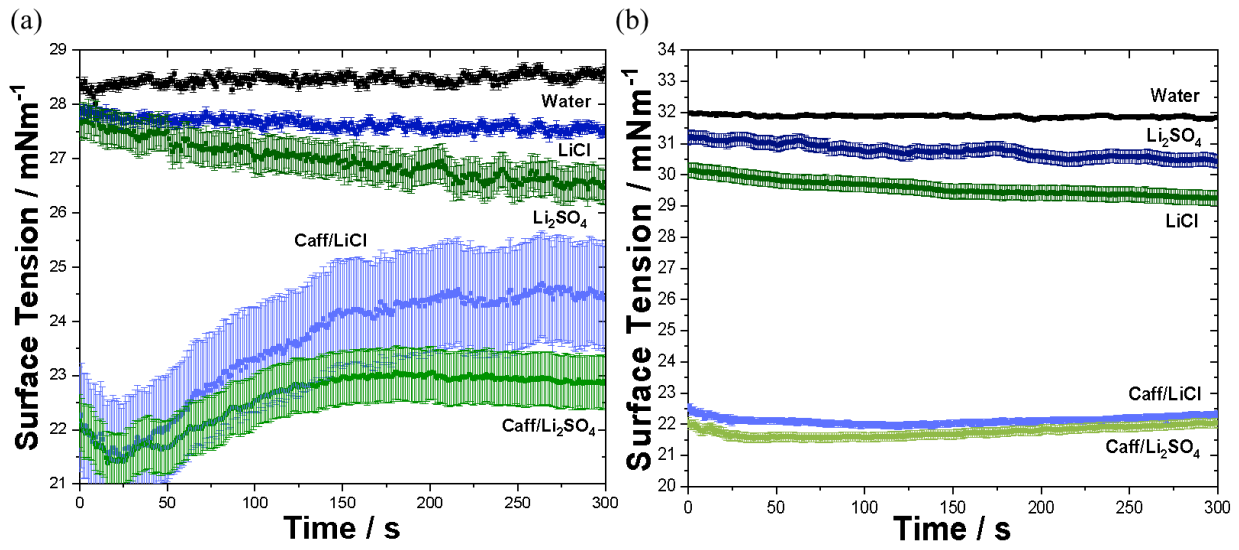

Figure 6.12: Surface tension as a function of time for the vials with water (──), LiCl (──), Li_2SO_4 (──), Caff/LiCl (──) and Caff/ Li_2SO_4 (──) containing (a) DCE and (b) Anisole: TFT as the organic phase. The error bars are based on the standard deviation with 95% of confidence interval.

On the Figure 6.12 was presented surface tension dependence as a function of time when no additional component was added to the organic phase. On Figure 6.12a DCE was used as a solvent in organic phase. Here, the differences in surface tension when no additional component was present in organic phase was verified. The value 28.46 ± 0.09 mNm^{-1} at water/DCE interface was found to be in agreement with previous studies[154], [184]. The surface tension was constant in time when 10 mM LiCl and 10 mM Li_2SO_4 were in the droplet and has high average values 27.64 ± 0.10 mNm^{-1} and 26.98 ± 0.33 mNm^{-1}, respectively. The measurements were shorter for 10 mM LiCl and 10 mM Li_2SO_4 because it was difficult to maintain the good size of the drop to obtain valuable results for longer time [154]. Addition of caffeine caused an initial drop of the interfacial tension. When caffeine is present in the system, the surface tension is not constant over time. It decreases at the beginning of the process and increases until 200 s, when it starts to stabilise. The cells with caffeine had the γ values: Caff/LiCl (24.52 ± 0.08 mNm^{-1}) and Caff/ Li_2SO_4 (21.75 ± 0.15 mNm^{-1}). On Figure 6.12b we verified the differences in surface tension when no additional componet was present in organic phase consisted of A: TFT. The surface tension had notably higher values and it was constant in time with all aqueous solutions. The interfacial tension is higher for this mixture of solvents (Fig. 6.12b) than for the DCE (Fig. 6.12a). This is consistent

with the surface tension measurement of TFT (38 mNm^{-1}) and anisole (38 mNm^{-1}) which was a lot higher than the one of DCE.[121] The tension decresed as follows: water (31.87 ± 0.04 mNm^{-1}), 10 mM LiCl (30.76 ± 0.21 mNm^{-1}) and 10 mM Li_2SO_4 (29.58 ± 0.24 mNm^{-1}) and in the cells with caffeine: Caff/LiCl (22.11 ± 0.11 mNm^{-1}) and Caff/ Li_2SO_4 (22.90 ± 0.03 mNm^{-1}).

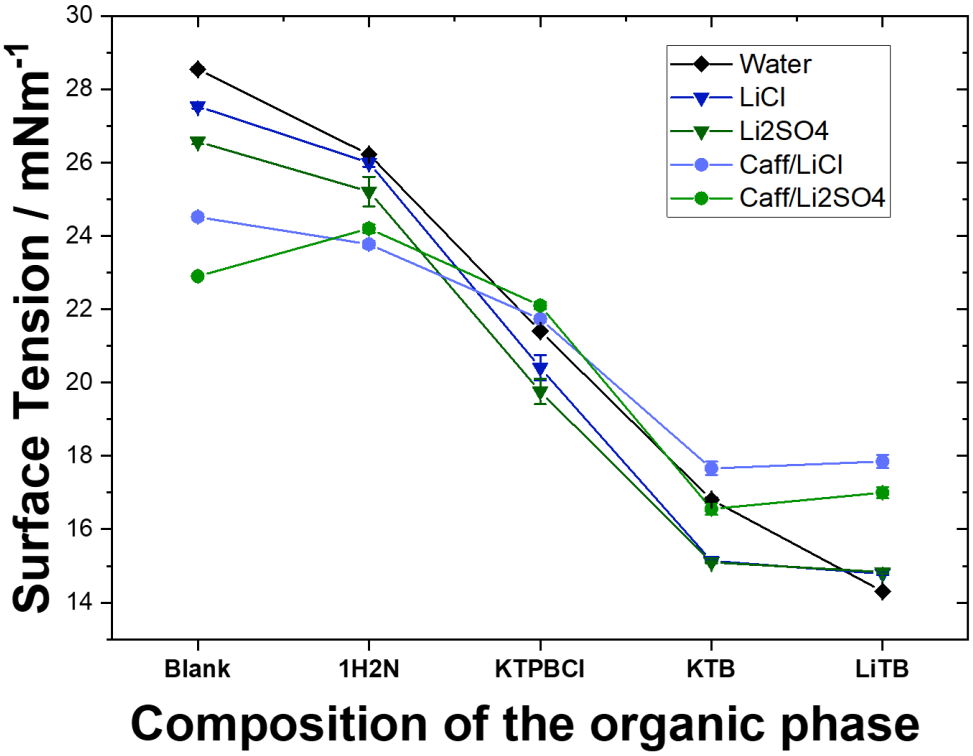

Figure 6.13: Comparison of surface tension for various composition of organic phase consisted of DCE and aqueous phase: water (—), LiCl (—), Li_2SO_4 (—), Caff/LiCl (—) and Caff/ Li_2SO_4 (—). The error bars are based on the standard deviation with 95% of confidence interval.

The comparison of the surface tension for various conditions is presented in Figure 6.13. First of all, we concluded that the addition of 1H2N to the organic phase decreased the interfacial tension. In the vials when DCE, 10 mM 1H2N and 1 mM KTPBCl were part of the organic phase the addition of caffeine caused the drop off the surface tension. Where in the vials with 1 mM KTB and 1 mM LiTB its value increased (Figure 6.13 light blue and light green line). The surface tension took on increasingly smaller values when the following components were added to the

organic phase: 10 mM 1H2N and 1 mM KTBCl, 1 mM KTB and 1 mM LiTB (together with acid), respectively. There was no particular difference when 10 mM LiCl and 10 mM Li_2SO_4 constituted the aqueous phase (Figure 6.13 dark blue and green line) when the same organic phase composition was in the vial. However, there is a difference in interfacial tension when the organic phase contained various cations and anions. It suggested that the interaction between cations and anions in organic phase and their interactions with $CaffH^+$ or change of the interface structure had the most impact on interfacial tension.

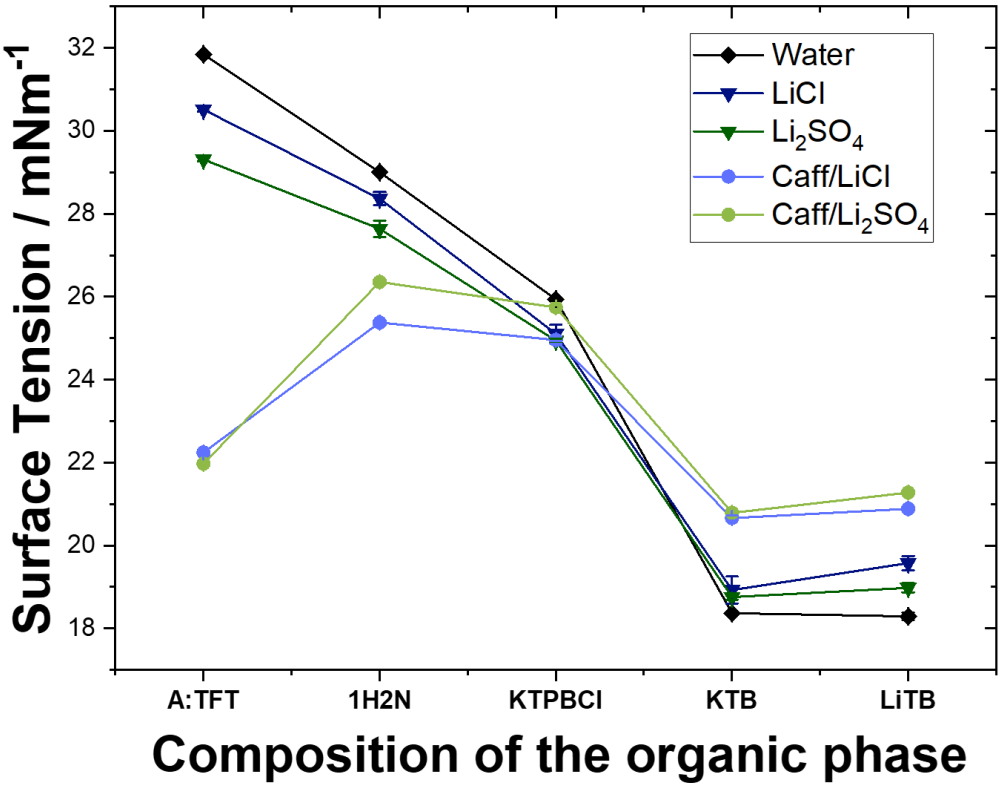

Figure 6.14: Comparison of surface tension for various composition of A: TFT organic phase and aqueous phase: water (—), LiCl (—), Li_2SO_4 (—), Caff/LiCl (—) and Caff/ Li_2SO_4 (—). The error bars are based on the standard deviation with 95% of confidence interval.

The differences in interfacial tension values between DCE and A:TFT suggested that not only the composition of phases plays role in surface tension but also the choice of the solvent.[185] Therefore, the comparison of the surface tension when a mixture A: TFT was a solvent in organic

phase is showed on the Figure 6.14. First of all, we concluded that the addition of 1H2N to the organic phase lowered the interfacial tension. Similarly, to the experiments with DCE, in the vials with A: TFT, 10 mM 1H2N and 1 mM KTPBCl the addition of caffeine caused the drop off the surface tension. Where in the vials with 1 mM KTB and 1 mM LiTB its value increased. When the aqueous solution was saturated with caffeine so in the vials where the cocrystals are formed at the liquid-liquid interface (light blue and light green line) the surface tension values change for various salts in the organic phase. The surface tension drops off after the addition of 1H2N comparing to the vials with only A: TFT and it did not change a lot after the addition of KTPBCl. However, the interfacial tension decreased in the vials with KTB and LiTB, which was already a case where DCE was used as a solvent. There is no particular difference when LiCl and Li_2SO_4 constituted the aqueous phase (Fig. 6.14 blue and green lines).

Figure 6.15 presented the conditions used in cells presented on Figure 6.3. In all of these vials the cocrystals were found on the liquid-liquid interface after 16h (Chapter 6.2). The experiment was conducted for 1200 s to check the change in surface tension during the formation of cocrystals. The comparision of the surface tension was drawn for the experiments where 10 mM LiCl (Fig. 6.15 a and c) and 10 mM Li_2SO_4 (Fig. 6.15 b and d) solution was saturated with caffeine and organic phase consisted of DCE (Fig. 6.15 a and b) and A: TFT (Fig.6.15 c and d) and various salts: KTPBCl (C16, C8, C7 and C6), KTB (C12, C10, C14 and C5) and LiTB (C13, C15, C3 and C9). In all the experiments the interfacial tension was lower when KTB and LiTB. The average values was estimated between 100-1200 s. The values of interfacial tension were lower for DCE than for TFT. Furthermore, different bevaiour is noticible during the 1200 s of experiments. In the experiments where DCE was in the organic phase, the interfacial tension was increasing for the first 300 s and after it was decreasing till 800 s. After this time it stabilised. In the experiments where A: TFT was in organic phase, the surface tension was increasing till 900 s and stabilized after this time.

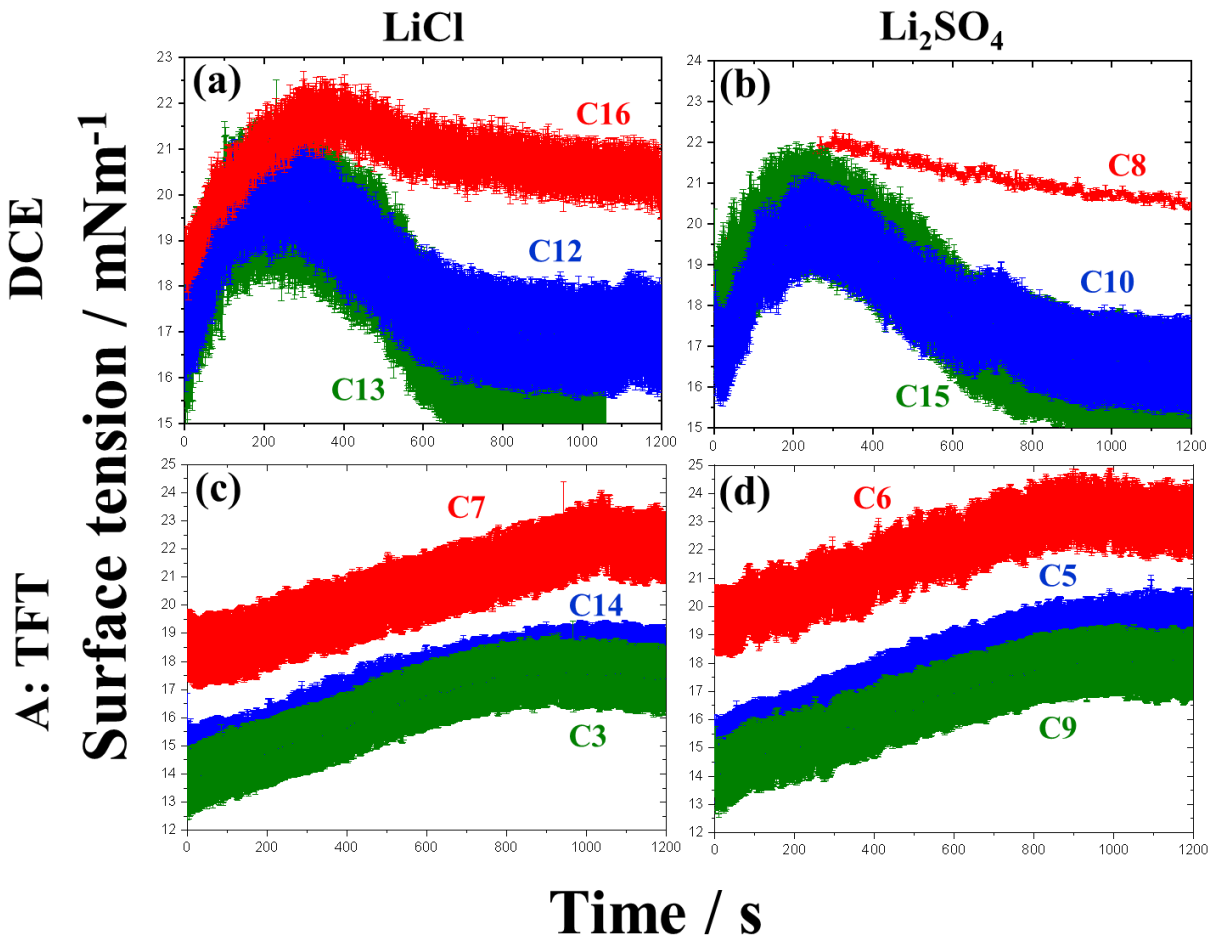

Figure 6.15: The surface tension as a function of time for Caff SAT in aqueous phase and KTPBCl (—), KTB (—), LiTB (—) in organic phase consisted of DCE (LiCl (aq) – (a) and Li_2SO_4 (aq) – (b)) and a: TFT (LiCl (aq) – (c) and Li_2SO_4 (aq) – (d)) according to experimental vial Figure 6.10. The error bars are based on the standard deviation with 95% of confidence interval.

In the experiments with 10 mM LiCl in the aqeous phase, the average value were 20.55 ± 0.11 mNm^{-1} for the cell with KTPBCl/DCE (C16) versus 22.22 ± 3.4 mNm^{-1} for the cell with KTPBCl/A: TFT (C8), 16.88 ± 0.09 mNm^{-1} for the cell with KTB/DCE (C12) versus 18.15 ± 0.07 mNm^{-1} for the cell with KTB/A: TFT (C14) and 15.24 ± 0.11 mNm^{-1} for the cell with LiTB/DCE (C13) versus 17.46 ± 0.09 mNm^{-1} for the cell with KTB/A: TFT (C3). The values did not vary a lot when 10 mM Li_2SO_4 was used as the electrolyte in the aqueous phase as mentioned in the description of Figures 6.13 and 6.14. In the experiments with 10 mM Li_2SO_4 in the aqeous phase,

the average value were very similar: 20.73 ± 0.10 mNm^{-1} for the cell with KTPBCl/DCE (C8) versus 23.13 ± 3.5 mNm^{-1} for the cell with KTPBCl/A: TFT (C6), 18.15 ± 0.07 mNm^{-1} for the cell with KTB/DCE (C10) versus 19.11 ± 0.12 mNm^{-1} for the cell with KTB/A: TFT (C5) and 17.46 ± 0.11 mNm^{-1} for the cell with LiTB/DCE (C15) versus 17.96 ± 0.09 mNm^{-1} for the cell with KTB/A: TFT (C9). The interfacial tension decreased with the increase of the hydrophobicity of the organic cation (TB^- > $TPBCl^-$)[154]. The presence of Li^+ and Cl^- or SO_4^{2-} did not change the interfacial tension significantly comparing to blank but did make the changes in differential capacitance was already observed before.[186] Another important point is that like in the case of impedance measurements, the differences are more visible when 1H2N and $CaffH^+$ are in the vials. It suggested that there are interfacial interactions between these components and electrolytes present in both phases.

Comparing the results from surface tension measurements to those obtained by XRD analysis (Section 6.3), we see that where pure phase I was obtained (Vial C16 Fig.6.15a, $\gamma = 20.55 \pm 0.11$ mNm^{-1}), the surface tension is much higher than when pure phase II was obtained (Figure 6.15d vial C9 17.96 ± 0.09 mNm^{-1}). The cocrystals of phase I was formed in the cell C16. Then we had LiCl in aqueous phase and KTPBCl in organic phase. Both of the cations Li^+ and K^+ and anion Cl^- have chaotropic properties. They caused the mixing of the solvents at ITIES which leaded to easier access of $CaffH^+$ to 1H2N and creation of the cocrystals at the organic side of the interface. When in other cases the anions and cations present in aqueous and organic phase created more kosmotropic conditions.[187], [188] There is an important correlation between surface tension and capacitance measurements.[186] Increase in capacitance in the LiCl may be caused by the presence of more chaotropic Cl^- in the aqueous phase. It expanded the width layer of the mixed solvents (water/DCE) and the $CaffH^+$ penetrated the interface. Also $CaffH^+$ itself can act as the chaotrop in aqueous phase due to the increase of the capacitance and pzc shift towards negative values.[187] The hydrophobicity of the interphase increased and it was followed by the rise of solvents miscibility. Additionally, the higher interfacial tension in the vials with KTPBCl than KTB and LiTB might have promoted the cocrystallization of phase I rather than phase II.

6.6. Analysis of DoE experiments of Caff/1H2N cocrystals obtained under different conditions

The **unrepx** package in R was used as a tool to experiments analysis. It is suitable for the analysis of basic unreplicated screening experiments such as two-level factorial designs and fractal factorial designs. Here, we have a set of independent effect estimates, but no degrees of freedom for error. The analyses are based on these basic assumptions about effect estimates: (i) the effects are independent, (ii) they all have the same variance, (iii) they are normally distributed, (iv) minority of effects is non-negligible (active) and many of effects are negligible (inactive)[189]–[191]. The function *yates ()* which implement Yates's algorithm was used to estimate the effects. The results were at first ranged in standard order.

As the LiTPBCl salt is not commercially available, the number of experiments was narrowed down. A new DoE design was performed using R with 3 factors and 8 replicates. The factor that were analysed are presented in Table 6.3.

Table 6.3: Numerical values converted to (-) for minimum values and (+).

Parameters	-	+
Solvent	A: TFT	DCE
Aqueous phase anion	Li_2SO_4	LiCl
Organic phase salt	LiTB	KTPBCl

The experiment involved 3 factors: solvent (DCE, A: TFT), aqueous phase acid (HCl, H_2SO_4) and organic phase anion (KTPBCl, LiTB). Each factor had two levels, which were attributed to -1, 1 value, respectively. In this method, we estimate the impact of these factors on the performance of the process, giving the response values in a standardised order (from the negative to positive). The experiments from which the reaction yields were determined were: the % content of phase I according to XRD analysis and the values of interfacial tension. Based on these results the yield was calculated and assigned to the experimental vials listed in Table 6.4.

Table 6.4: Table of data used for data output analysis by R. The yellow and grey colour correspond to the vials where DCE and the mixture of A: TFT were organic phase solvents respectively.

No	Solvent	Acid	Organic Cation	Yield
3	LiCl	TFT	LiTB	1.18
6	Li2SO4	TFT	KTPBCl	1.47
7	LiCl	TFT	KTPBCl	1.54
8	Li2SO4	DCE	KTPBCl	1.32
9	Li2SO4	TFT	LiTB	1.1
13	LiCl	DCE	LiTB	1.01
15	Li2SO4	DCE	LiTB	1.1
16	LiCl	DCE	KTPBCl	1.96

The package **unrepx** provide graphical analysis of the data output to identify important effects. Figure 6.16 showed (a) the half-normal plot and (b) pareto plot from which the active effects were determined. Half-normal plot was drawn by *hnplot ()*. The labels are added to the values that crossed value 0.2282 (Fig. 6.16a). The reference line was added by the default Zahn method (black line). It is based on the slope of a line fitted to the lowest two-thirds of the points in the half-normal plot. The blue dots correspond to positive effects (DCE, LiCl, and KTPBCl). It seemed that KTPBCl is the most important active factor, as it had the largest values, exceeding reference SD = 0.2282.

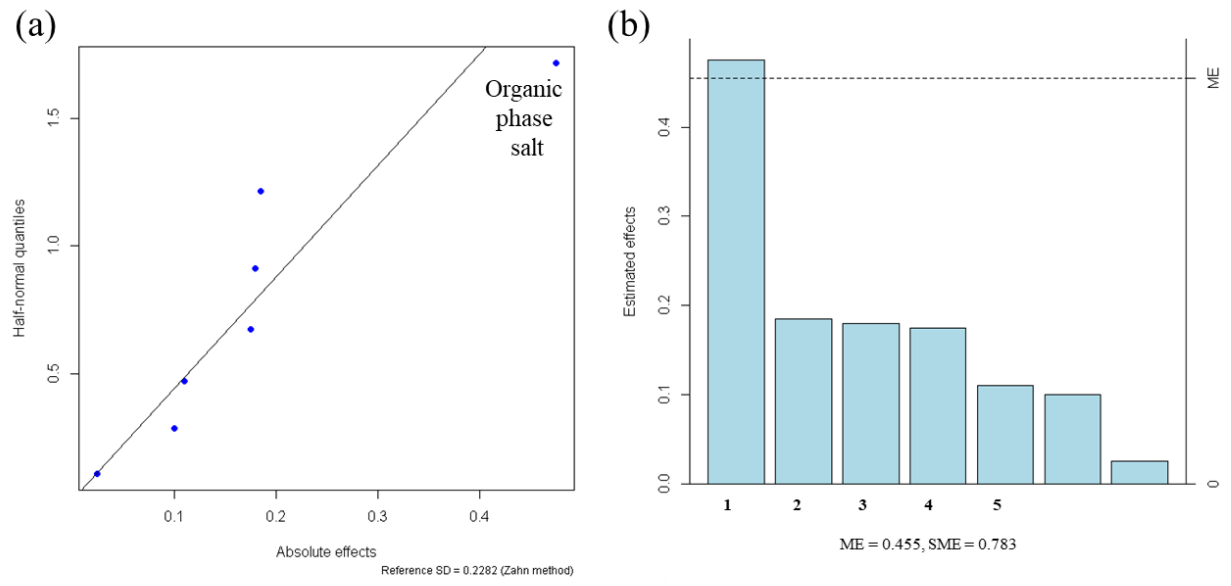

Figure 6.16: Graphic tools to identify active effects (a) the half-normal plot and (b) pareto plot. The blue ones to positive effects (DCE, LiCl, K^+, $TPBCl^-$). 1 - Organic phase salt, 2 - Organic phase salt - Aqueous phase electrolyte, 3 - Aqueous phase electrolyte, 4 - Organic phase salt – Solvent, 5 – Solvent.

The pareto graphs were drawn using the *parplot ()* function. This is a bar chart with bars organised by effect size. The graph has been marked with the margin of error (ME) and the simultaneous margin of error SME of the effects, which is larger than the effect size. The auxiliary lines in the Figure 6.16b (reference SD (a), ME and SME (b)) are done via a *pseudo-standard-error* estimate. It was assumed that the sparsity-of-effects and equal variances allowed the standard error of effects to be estimated by looking at the variability of smaller effects. The *PSE ()* command was used to calculate them. There is a linked *reference distribution*, which can be estimated through the simulation of the t-statistic for independent inactive effects. The 95th percentile of the reference distribution |t| represents the critical value. Multiplying this critical value by the PSE, gives the margin of error (ME) for assessing effects. Simultaneous margin of error (SME) is based on the max |t| from every effect. Unfortunately, any of the effect did not exceed this value so the effects can be not truly active. However, these active effects are consistent with the results obtained in the

AC voltammetry and interfacial tension studies. It was proven that mainly the cations and anions present in organic phase were influencing the changes between the vials.

6.7. Conclusions

In the shake-flask experiments of poorly water-soluble drugs i.e. piroxicam, sildenafil, diclofenac and ketoprofen the crystals were not formed at the liquid-liquid interface. The DoE analysis did not find as well the factor that could improve this crystallization due to the few materials for further analysis that was present at the liquid-liquid interface. A perspective for these experiments would be to add a coformer to the aqueous phase and to increase their concentration so as to obtain an almost saturated solution.

The shake-flask experiments of the caffeine and 1H2N supplemented and summarised previous knowledge of cocrystals formed at the liquid-liquid interface. In all experimental vials the Caff:1H2N cocrystals with acceptable amount and size were found at ITIES. These complexes were analysed by XRD to find the quantity of phase I and II and were followed by the simultaneous measurements of ΔE and I at ITIES and interfacial tension measurement. XRD shows that most of the experimental conditions give an 80:20 mixture of phase II: phase I with two exceptions. For cell C16 (LiCl//KTPBCl in DCE) a large majority of phase I is observed (95 %) and for cell C9 (Li2SO4//LiTB in A: TFT), 92 % of phase II was collected. In both vials we used completely different components, with the exception of caffeine and 1H2N. The conditions to obtain almost pure Phase I and Phase II were found.

Next, ΔE and I were measured simultaneously for all conditions described. Lower ΔE values were measured for C16 (ΔE = 0.18 V after 3600 s) against ΔE = 0.65 V for C9 (after 3600 s too). This lower potential for C16, along with lower current values, suggested slower transfer kinetics of $CaffH^+$ from aqueous to organic. This means that much more species transferred in the cell C9 than C16 and the applied potential influences the kinetics of the process, as crystals of different phases were obtained. However, this analysis would have to be supplemented in EN analysis, thus the programming of the calculation should be developed.

Pendant drop measurements showed that the addition of 1H2N and caffeine had an influence of the interfacial tension. However, when the interface was polarised, there was significant influence

of the aqueous electrolyte anion or of the nature of the solvent, unlike the nature of the organic electrolyte anion. Addition of KTPBCl, KTB and LiTB to the oil phase decreased the interfacial tension in comparison with the control experiment. The decrease in surface tension was especially visible for KTB and LiTB salts because these salts are more hydrophilic. Also, Li^+ is more hydrophilic than K^+ so it transfers more easily to the aqueous phase. Chaotropic effects from Cl^-, $CaffH^+$ and $TPBCl^-$ might favour the preferential phase I polymorph.

Summarising the results by means of a DoE analysis made it possible to find factors that actively influence the cocrystallisation process. DoE analysis indicated that mainly the salt of organic phase was an active factor that influence the differences between the cocrystals formed at liquid-liquid interface. Therefore, the interfacial cocrystallization was indeed controlled by the chemical polarization which is proven also by statistical analysis.

7. General conclusions

The research was focus on the interrogation of the cocrystals formation at liquid-liquid interface and the influence of the interface polarization and phase composition on the cocrystallization process.

Electrochemical measurements by the means of cyclic voltammetry study proved that caffeine turned out to be the best candidate for the electrochemically driven cocrystallization. It is transferred across the ITIES and it is highly soluble in water. Caffeine was studied at various pH; pH 2 was chosen as the most suitable for cocrystals formation. 1H2N did not transfer at ITIES and it was chosen as the cocrystal conformer. AC Voltammetry showed big difference in pzc and capacitance in presence and absence of $CaffH^+$ and 1H2N. The results suggested that these two molecules are interfacially active. Mainly, the effect of the anion in the organic phase was identified as the one that most altered pzc and capacitance.

Cocrystals of Caff with 1H2N of high purity were formed upon chemical polarisation of the ITIES. Raman spectroscopy confirmed that the products collected at the ITIES were cocrystals of Caff: 1H2N and that they were free of starting reagents and solvents. By applying low interfacial potential difference, we were able to inhibit the cocrystallisation process. Moreover, manipulation with the applied potential has allowed the formation of a large majority of a polymorphic form. Indeed, XRD analysis showed the two different polymorphs were obtained, depending on the presence of the interfacial polarisation. For non-polarised interfaces (control experiment), a mixture of cocrystals of phases I and II were obtained, whereas cocrystal of phase I were formed when a high interfacial potential difference was applied. Based on the XRD and Raman spectroscopy, we can clearly state that the compounds obtained at the interface are the cocrystals of caff: 1H2N and not the salts, which was additionally emphasized by the change of pH, before and after the cocrystallisation process. Such cocrystallisation opens up perspectives for better control and understanding of the cocrystallisation process through polarisation changes at the oil-water interface.

To further investigate the mechanism behind the cocrystals formation simultaneous analysis of potential and current was performed. The potential for the designed electrochemical cells with various ratio of concentration of tetraalkylammonium salts in organic and aqueous phase was

monitored. It was found to be in good agreement with the theoretical values based on the Nernst-like equation. The results were similar for three ions: tetramethylammonium, tetraethylammonium and tetrapropylammonium, which indicated that the potential values depend uniquely on the ratio $\frac{c^o_{TAA^+}}{c^w_{TAA^+}}$. Thus, by varying the ratio of concentrations of the common ion to the organic and aqueous phases, we were able to obtain suitable potential values to drive the cocrystallisation process. Addition of Caff and 1H2N to these well-defined electrochemical cells allowed the monitoring of the potential and current at the liquid-liquid interface. Analysis of the electrochemical current noise showed a clear difference between cells in which cocrystals are formed and those in which cocrystallisation is hindered, either by a negative potential or by a change in pH. Caffeine transfer and cocrystal formation generate different signals with current maxima at frequencies in the 0.1 – 1 Hz range. The EC method is a powerful tool to follow the changes occurring at ITIES in common ion experiments by simultaneous measurement of potential and current. Such a method could be used to follow other processes at the ITIES e.g. catalytic reactions, NPs assemblies etc.

The shake-flask experiments of the caffeine and 1H2N with modified aqueous and organic phase composition supplemented and summarised previous knowledge of cocrystals formed at the liquid-liquid interface. In all experimental vials, the Caff:1H2N cocrystals with acceptable amount and size were found at ITIES. These complexes were analysed by XRD to find the quantity of phase I and II and were followed by the simultaneous measurements of ΔE and I at ITIES and interfacial tension measurement. XRD shows that most of the experimental conditions give an 80:20 mixture of phase II: phase I with two exceptions. For cell containing LiCl in aqueous phase and KTPBCl in DCE a large majority of phase I is observed (95 %) and for cell with Li_2SO_4 in aqueous phase and LiTB in A: TFT, 92 % of phase II was collected. In both vials we used completely different components, with the exception of caffeine and 1H2N. The conditions to obtain almost pure Phase I and Phase II were found. Next, ΔE and I were measured simultaneously for all conditions described. Lower ΔE values were measured for the cell when Phase I was found. This lower potential for first cell, along with lower current values, suggested that less species of $CaffH^+$ from aqueous to organic are transferred in this cell. This means that the applied potential influences the kinetics of the process, as crystals of different phases were obtained. Pendant drop measurements showed that the addition of 1H2N and caffeine had an influence of the interfacial tension. However, when the interface was polarised, there was a significant influence of the aqueous

electrolyte anion or of the nature of the solvent, unlike the nature of the organic electrolyte anion. Addition of KTPBCl, KTB and LiTB to the oil phase decreased the interfacial tension in comparison with the control experiment. The decrease in surface tension was especially visible for KTB and LiTB salts because these salts are more hydrophilic. Also, Li^+ is more hydrophilic than K^+ so it transfers more easily to the aqueous phase. Chaotropic effects from Cl^-, $CaffH^+$ and $TPBCl^-$ might favour the preferential phase I polymorph. DoE analysis indicated that mainly the nature of organic phase was an active factor that influence the differences between the cocrystals formed at liquid-liquid interface. Therefore, the interfacial cocrystallization was indeed controlled by the chemical polarization which was proven also by the statistical analysis.

8. Future work

This research provided a lot of interesting information on the mechanism of cocrystal formation and the electrochemical control of the cocrystallisation process. However, many topics in this work require further investigation. The chemical polarization of the liquid-liquid interface allowed to control formation of caff: 1H2N cocrystals. The application of negative potential inhibited the cocrystallization and the application of positive potential leaded to the formation of cocrystals of Phase I. 1. As the manuscript is based on a novel strategy of cocrystallization in order to validate the method it needs to explore more examples. It was a proof-of-concept study and it demand to be extended for other coformers of caffeine such as 3-hydroxy-2-naphthoic acid and 6-hydroxy-2-naphthoic acid which created various polymorphic form via interfacial cocrystallization in previous studies.[27] The next step would be to investigate other coformers for caffeine like organic acids and other drugs that form cocrystals with cofomers of opposite solubility. The research could be interesting in protein crystallization because applied potential at liquid-liquid interface changed the cocrystals size and quantity at water-oil interface.[126] Except of the pharmaceutical and biological use the control of crystallization at liquid-liquid interface could be used in the oil industry to stop the formation of undesirable inorganic salts.[3]

The simultaneous analysis of potential (ΔE) and current (I) has produced a system that works in accordance with the theoretical assumptions, but needs refinement. Mainly because of the delay between the time t_0, i.e. the time of cell establishment, and the time at which the measurement starts. In our experimental set-up, there is a delay of approximately 30 s. And the work of other groups has shown that this can be an important time in the study of the mechanism at the liquid-liquid interface[102]. A set-up was used that allowed measurements from time t_0. The equipment presented on Figure 8.1 should be used for simultaneous measurement of potential and current. The aqueous and organic phase are separated by an air-bubble inside of the tip of the capillary. The bubble can be removed by the syringe connected with the capillary and the phases made contact.

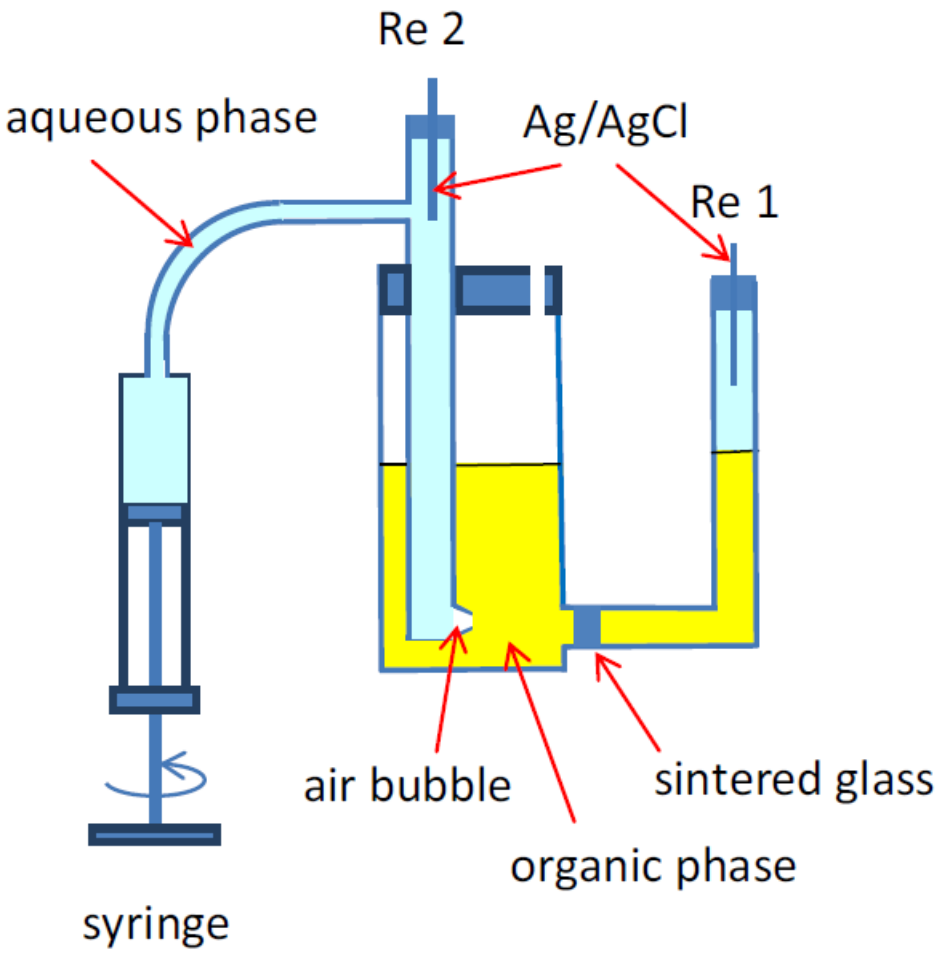

Figure 8.1: Schematic diagram of the electrochemical set-up allowing to start measurements at time t_0 [102]

Another solution to encounter this problem would be the use of the microfluidics channels. They were already applied at ITIES.[192] Here, the aqueous and organic phase undergo simultaneous laminar flow. The microfluidic crystallizers were also applied in pharmaceutical industry to increase the performance and control of the crystallization process.[193], [194]

The electrochemical noise analysis (EN) proved to be the powerful tool to examine the differences between the various conditions and under the different polarizations applied. The analysis and background subtraction were made manually in Excel calculations as explained in Chapter 5.1. The programming of the calculation e.g. by using Matlab software would be necessary to analyse bigger set of data which was proven for example in Chapter 6.4. Programmed calculations, would allow the input of experimental values from which we would automatically obtain the parameters

of interest described in section 5.3. Such probing interfacial cocrystallisation using simultaneous potential and current measurements at liquid-liquid interfaces polarised by common ion approach could be extended to other shake-flask experiments where the tracking changes at the liquid-liquid interface was not previously possible *in vivo* and in real time.

The design of experiments (DoE) analysis provided a lot of valuable information on the main factors influencing the formation of phase I and phase II cocrystals. However, more sophisticated statistical analysis would be needed for a broader analysis of the data obtained. Designing a test with more than two factors, i.e. a 3-level general full factorial experiments rather than a 2-level regular (fractional) factorial design, would allow more salts in the organic phase and more organic solvents to be tested. Also the analysis of the data could have been extended to include, among other things, the response surface method or ANOVA in order to better understand the influence of the factors tested.

This research provided many experimental results. Undoubtedly, an important next step would be to combine experimental and theoretical results through the molecular dynamics (MD) simulations.

Bibliography:

[1] J. Lu, Z. Li, and X. Jiang, "Polymorphism of pharmaceutical molecules: Perspectives on nucleation," *Front. Chem. Eng. China*, vol. 4, no. 1, pp. 37–44, 2010, doi: 10.1007/s11705-009-0294-2.

[2] D. M. Croker *et al.*, "Demonstrating the Influence of Solvent Choice and Crystallization Conditions on Phenacetin Crystal Habit and Particle Size Distribution," *Org. Process Res. Dev.*, vol. 19, no. 12, pp. 1826–1836, 2015, doi: 10.1021/op500308x.

[3] C. Dai, A. G. Stack, A. Koishi, A. Fernandez-Martinez, S. S. Lee, and Y. Hu, "Heterogeneous Nucleation and Growth of Barium Sulfate at Organic-Water Interfaces: Interplay between Surface Hydrophobicity and Ba2+ Adsorption," *Langmuir*, vol. 32, no. 21, pp. 5277–5284, 2016, doi: 10.1021/acs.langmuir.6b01036.

[4] J. Chen, B. Sarma, J. M. B. Evans, and A. S. Myerson, "Pharmaceutical crystallization," *Cryst. Growth Des.*, vol. 11, no. 4, pp. 887–895, Apr. 2011, doi: 10.1021/cg101556s.

[5] S. Rohani, "Applications of the crystallization process in the pharmaceutical industry," *Front. Chem. Eng. China*, vol. 4, no. 1, pp. 2–9, 2010, doi: 10.1007/s11705-009-0297-z.

[6] M. Solares-Briones *et al.*, "Mechanochemistry: A green approach in the preparation of pharmaceutical cocrystals," *Pharmaceutics*, vol. 13, no. 6, pp. 1–49, 2021, doi: 10.3390/pharmaceutics13060790.

[7] D. P. Elder, R. Holm, and H. L. De Diego, "Use of pharmaceutical salts and cocrystals to address the issue of poor solubility," *Int. J. Pharm.*, vol. 453, no. 1, pp. 88–100, Aug. 2013, doi: 10.1016/j.ijpharm.2012.11.028.

[8] W. Jones, W. D. S. Motherwell, and A. V. Trask, "Pharmaceutical cocrystals: An emerging approach to physical property enhancement," *MRS Bull.*, vol. 31, no. 11, pp. 875–879, 2006, doi: 10.1557/mrs2006.206.

[9] N. Schultheiss and A. Newman, "Pharmaceutical cocrystals and their physicochemical properties," *Cryst. Growth Des.*, vol. 9, no. 6, pp. 2950–2967, 2009, doi: 10.1021/cg900129f.

[10] A. Karagianni, M. Malamatari, and K. Kachrimanis, “Pharmaceutical cocrystals: New solid phase modification approaches for the formulation of APIs,” *Pharmaceutics*, vol. 10, no. 1, pp. 1–30, 2018, doi: 10.3390/pharmaceutics10010018.

[11] A. M. Healy, Z. A. Worku, D. Kumar, and A. M. Madi, “Pharmaceutical solvates, hydrates and amorphous forms: A special emphasis on cocrystals,” *Adv. Drug Deliv. Rev.*, vol. 117, pp. 25–46, 2017, doi: 10.1016/j.addr.2017.03.002.

[12] A. V. Trask, W. D. Samuel Motherwell, and W. Jones, “Pharmaceutical cocrystallization: Engineering a remedy for caffeine hydration,” *Cryst. Growth Des.*, vol. 5, no. 3, pp. 1013–1021, May 2005, doi: 10.1021/cg0496540.

[13] A. M. Belenguer, G. I. Lampronti, N. De Mitri, M. Driver, C. A. Hunter, and J. K. M. Sanders, “Understanding the Influence of Surface Solvation and Structure on Polymorph Stability: A Combined Mechanochemical and Theoretical Approach,” *J. Am. Chem. Soc.*, vol. 140, no. 49, pp. 17051–17059, Dec. 2018, doi: 10.1021/JACS.8B08549/SUPPL_FILE/JA8B08549_SI_001.PDF.

[14] T. C. Farmer, C. L. Carpenter, and M. F. Doherty, “Polymorph selection by continuous crystallization,” *AIChE J.*, vol. 62, no. 9, pp. 3505–3514, Sep. 2016, doi: 10.1002/AIC.15343.

[15] L. Nicoud, F. Licordari, and A. S. Myerson, “Polymorph control in batch seeded crystallizers. A case study with paracetamol,” *CrystEngComm*, vol. 21, no. 13, pp. 2105–2118, Mar. 2019, doi: 10.1039/C8CE01428K.

[16] N. Javid, T. Kendall, I. S. Burns, and J. Sefcik, “Filtration suppresses laser induced nucleation of glycine in aqueous solutions.”

[17] A. T. M. Serajuddin, “Salt formation to improve drug solubility,” *Adv. Drug Deliv. Rev.*, vol. 59, no. 7, pp. 603–616, 2007, doi: 10.1016/j.addr.2007.05.010.

[18] A. Berziņš, E. Skarbulis, T. Rekis, and A. Actiņš, “On the formation of droperidol solvates: Characterization of structure and properties,” *Cryst. Growth Des.*, vol. 14, no. 5, pp. 2654–2664, May 2014, doi: 10.1021/CG5003447/SUPPL_FILE/CG5003447_SI_008.CIF.

[19] E. H. Lee, “A practical guide to pharmaceutical polymorph screening & selection,” *Asian J. Pharm. Sci.*, vol. 9, no. 4, pp. 163–175, 2014, doi: 10.1016/j.ajps.2014.05.002.

[20] Z. Gao, S. Rohani, J. Gong, and J. Wang, “Recent Developments in the Crystallization Process: Toward the Pharmaceutical Industry,” *Engineering*, vol. 3, no. 3, pp. 343–353, 2017, doi: 10.1016/J.ENG.2017.03.022.

[21] G. Bolla, B. Sarma, and A. K. Nangia, “Crystal Engineering of Pharmaceutical Cocrystals in the Discovery and Development of Improved Drugs,” *Chemical Reviews*, vol. 122, no. 13. American Chemical Society, pp. 11514–11603, Jul. 13, 2022, doi: 10.1021/acs.chemrev.1c00987.

[22] N. Qiao, M. Li, W. Schlindwein, N. Malek, A. Davies, and G. Trappitt, “Pharmaceutical cocrystals: An overview,” *Int. J. Pharm.*, vol. 419, no. 1–2, pp. 1–11, 2011, doi: 10.1016/j.ijpharm.2011.07.037.

[23] E. Grothe, H. Meekes, E. Vlieg, J. H. Ter Horst, and R. De Gelder, “Solvates, Salts, and Cocrystals: A Proposal for a Feasible Classification System,” *Cryst. Growth Des.*, vol. 16, no. 6, pp. 3237–3243, Jun. 2016, doi: 10.1021/acs.cgd.6b00200.

[24] P. Verma, A. Srivastava, K. Srivastava, P. Tandon, and M. R. Shimpi, “Molecular Structure, Spectral Investigations, Hydrogen Bonding Interactions and Reactivity-Property Relationship of Caffeine-Citric Acid Cocrystal by Experimental and DFT Approach,” *Front. Chem.*, vol. 9, no. July, pp. 1–13, 2021, doi: 10.3389/fchem.2021.708538.

[25] T. Friščič and W. Jones, “Recent advances in understanding the mechanism of cocrystal formation via grinding,” *Cryst. Growth Des.*, vol. 9, no. 3, pp. 1621–1637, 2009, doi: 10.1021/cg800764n.

[26] M. Karimi-Jafari, L. Padrela, G. M. Walker, and D. M. Croker, “Creating cocrystals: A review of pharmaceutical cocrystal preparation routes and applications,” *Cryst. Growth Des.*, vol. 18, no. 10, pp. 6370–6387, Oct. 2018, doi: 10.1021/acs.cgd.8b00933.

[27] S. J. Diez *et al.*, “Crystallization at Solvent Interfaces Enables Access to a Variety of Cocrystal Polymorphs and Hydrates,” *Cryst. Growth Des.*, vol. 18, no. 6, pp. 3263–3268, 2018, doi: 10.1021/acs.cgd.8b00114.

[28] N. Schultheiss and A. Newman, “Pharmaceutical cocrystals and their physicochemical properties,” *Cryst. Growth Des.*, vol. 9, no. 6, pp. 2950–2967, Jun. 2009, doi: 10.1021/cg900129f.

[29] S. Aitipamula, P. S. Chow, and R. B. H. Tan, “Polymorphism in cocrystals: A review and assessment of its significance,” *CrystEngComm*, vol. 16, no. 17, pp. 3451–3465, 2014, doi: 10.1039/c3ce42008f.

[30] M. K. Corpinot *et al.*, “On the predictability of supramolecular interactions in molecular cocrystals-the view from the bench,” *CrystEngComm*, vol. 18, no. 29, pp. 5434–5439, 2016, doi: 10.1039/c6ce00293e.

[31] Santra, “Ertugliflozin co-crystals and process for their preparation,” May 24, 2016.

[32] I. A. Alsarra, M. Al-Omar, and F. Belal, “Valproic Acid and Sodium Valproate: Comprehensive Profile,” *Profiles Drug Subst. Excipients Relat. Methodol.*, vol. 32, pp. 209–240, Jan. 2005, doi: 10.1016/S0099-5428(05)32008-9.

[33] W. T. A. Harrison, H. S. Yathirajan, S. Bindya, H. G. Anilkumar, and Devaraju, “Escitalopram oxalate: Co-existence of oxalate dianions and oxalic acid mol-ecules in the same crystal,” *Acta Crystallogr. Sect. C Cryst. Struct. Commun.*, vol. 63, no. 2, pp. 129–131, 2007, doi: 10.1107/S010827010605520X.

[34] C. Almansa, R. Mercè, N. Tesson, J. Farran, J. Tomàs, and C. R. Plata-Salamán, “Co-crystal of Tramadol Hydrochloride-Celecoxib (ctc): A Novel API-API Co-crystal for the Treatment of Pain,” *Cryst. Growth Des.*, vol. 17, no. 4, pp. 1884–1892, 2017, doi: 10.1021/acs.cgd.6b01848.

[35] S. A. Pan, Y. Sun, M. Li, W. W. Deng, and Z. Z. Zhang, “Guanine deaminase provides evidence of the increased caffeine content during the piling process of pu’erh tea,” *RSC Adv.*, vol. 9, no. 62, pp. 36136–36143, 2019, doi: 10.1039/c9ra05655f.

[36] N. Mou, Z. Duan, P. Ma, R. Fu, and D. Fan, “Study on the hypnotic effect of rare protopanaxadiol-type and protopanaxatriol-type ginsenosides,” *RSC Adv.*, vol. 9, no. 35, pp. 20483–20491, 2019, doi: 10.1039/c9ra01549c.

[37] E. Zylber-Katz, L. Granit, and M. Levy, “Relationship between caffeine concentrations in plasma and saliva,” *Clin. Pharmacol. Ther.*, vol. 36, no. 1, pp. 133–137, 1984, doi: 10.1038/clpt.1984.151.

[38] R. Thakuria *et al.*, “Cocrystal Dissociation under Controlled Humidity: A Case Study of Caffeine-Glutaric Acid Cocrystal Polymorphs,” *Org. Process Res. Dev.*, vol. 23, no. 5, pp. 845–851, 2019, doi: 10.1021/acs.oprd.8b00422.

[39] D. K. Bučar *et al.*, “Co-crystals of caffeine and hydroxy-2-naphthoic acids: Unusual formation of the carboxylic acid dimer in the presence of a heterosynthon,” *Mol. Pharm.*, vol. 4, no. 3, pp. 339–346, Jun. 2007, doi: 10.1021/mp070004b.

[40] D. K. Bučar, R. F. Henry, R. W. Duerst, X. Lou, L. R. MacGillivray, and G. G. Z. Zhang, “A 1:1 cocrystal of caffeine and 2-hydroxy-1-naphthoic acid obtained via a slurry screening method,” *J. Chem. Crystallogr.*, vol. 40, no. 11, pp. 933–939, 2010, doi: 10.1007/s10870-010-9766-y.

[41] D. K. Bučar, R. F. Henry, X. Lou, T. B. Borchardt, and G. G. Z. Zhang, “A ‘hidden’ co-crystal of caffeine and adipic acid,” *Chem. Commun.*, no. 5, pp. 525–527, 2007, doi: 10.1039/b611749j.

[42] D. Hasa *et al.*, “Mechanochemical Formation and ‘disappearance’ of Caffeine-Citric-Acid Cocrystal Polymorphs,” *Cryst. Growth Des.*, vol. 20, no. 2, pp. 1119–1129, Feb. 2020, doi: 10.1021/acs.cgd.9b01431.

[43] T. Friščić, L. Fábián, J. C. Burley, W. Jones, and W. D. S. Motherwell, “Exploring cocrystal-cocrystal reactivity via liquid-assisted grinding: The assembling of racemic and dismantling of enantiomeric cocrystals,” *Chem. Commun.*, no. 48, pp. 5009–5011, 2006, doi: 10.1039/b613073a.

[44] L. H. do Amaral *et al.*, “Development and Characterization of Dapsone Cocrystal Prepared by Scalable Production Methods,” *AAPS PharmSciTech*, vol. 19, no. 6, pp. 2687–2699, 2018, doi: 10.1208/s12249-018-1101-5.

[45] D. Mellah *et al.*, “New Cocrystallization Method: Non-photochemical Laser-Induced Nucleation of a Cocrystal of Caffeine-Gallic Acid in Water,” *Cryst. Growth Des.*, 2022,

doi: 10.1021/ACS.CGD.2C00624/SUPPL_FILE/CG2C00624_SI_001.PDF.

[46] A. V. Trask, W. D. S. Motherwell, and W. Jones, “Solvent-drop grinding: green polymorph control of cocrystallisation,” *Chem. Commun.*, vol. 4, no. 7, pp. 890–891, 2004, doi: 10.1039/b400978a.

[47] M. K. Mishra, K. Mishra, A. Narayan, C. M. Reddy, and V. R. Vangala, “Structural Basis for Mechanical Anisotropy in Polymorphs of a Caffeine-Glutaric Acid Cocrystal,” *Cryst. Growth Des.*, vol. 20, no. 10, pp. 6306–6315, 2020, doi: 10.1021/acs.cgd.0c01033.

[48] A. Mukherjee, R. D. Rogers, and A. S. Myerson, “Cocrystal formation by ionic liquid-assisted grinding: case study with cocrystals of caffeine,” *CrystEngComm*, vol. 20, no. 27, pp. 3817–3821, 2018, doi: 10.1039/C8CE00859K.

[49] D. K. Bučar, R. F. Henry, X. Lou, R. W. Duerst, L. R. MacGillivray, and G. G. Z. Zhang, “Cocrystals of caffeine and hydroxybenzoic acids composed of multiple supramolecular heterosynthons: Screening via solution-mediated phase transformation and structural characterization,” *Cryst. Growth Des.*, vol. 9, no. 4, pp. 1932–1943, 2009, doi: 10.1021/cg801178m.

[50] T. Leyssens, N. Tumanova, K. Robeyns, N. Candoni, and S. Veesler, “Solution cocrystallization, an effective tool to explore the variety of cocrystal systems: Caffeine/dicarboxylic acid cocrystals,” *CrystEngComm*, vol. 16, no. 41, pp. 9603–9611, 2014, doi: 10.1039/c4ce01495b.

[51] T. Leyssens, G. Springuel, R. Montis, N. Candoni, and S. Veesler, “Importance of solvent selection for stoichiometrically diverse cocrystal systems: Caffeine/maleic acid 1:1 and 2:1 cocrystals,” *Cryst. Growth Des.*, vol. 12, no. 3, pp. 1520–1530, 2012, doi: 10.1021/cg201581z.

[52] R. Mohite, P. Mehta, S. Arulmozhi, R. Kamble, A. Pawar, and C. Bothiraja, “Synthesis of fisetin co-crystals with caffeine and nicotinamide using the cooling crystallization technique: Biopharmaceutical studies,” *New J. Chem.*, vol. 43, no. 34, pp. 13471–13479, 2019, doi: 10.1039/c9nj01848d.

[53] T. Koide *et al.*, “Quantification of a cocrystal and its dissociated compounds in solid dosage

form using transmission Raman spectroscopy," *J. Pharm. Biomed. Anal.*, vol. 177, p. 112886, 2020, doi: 10.1016/j.jpba.2019.112886.

[54] V. Titapiwatanakun, A. W. Basit, and S. Gaisford, "A New Method for Producing Pharmaceutical Co-crystals: Laser Irradiation of Powder Blends," *Cryst. Growth Des.*, vol. 16, no. 6, pp. 3307–3312, 2016, doi: 10.1021/acs.cgd.6b00289.

[55] T. Friščić, A. V. Trask, W. Jones, and W. D. S. Motherwell, "Screening for Inclusion Compounds and Systematic Construction of Three-Component Solids by Liquid-Assisted Grinding," *Angew. Chemie*, vol. 118, no. 45, pp. 7708–7712, 2006, doi: 10.1002/ange.200603235.

[56] P. Macfhionnghaile, C. M. Crowley, P. McArdle, and A. Erxleben, "Spontaneous Solid-State Cocrystallization of Caffeine and Urea," *Cryst. Growth Des.*, vol. 20, no. 2, pp. 736–745, 2020, doi: 10.1021/acs.cgd.9b01152.

[57] K.-W. Jeong, J.-M. Ku, M.-W. Park, S.-M. Park, J.-E. Yang, and T.-G. Nam, "Hydroxynaphthoic Acids Identified in a High Throughput Screening Potently Ameliorate Endoplasmic Reticulum Stress as Novel Chemical Chaperones," *Chem. Pharm. Bull*, vol. 61, no. 7, pp. 740–746, 2013.

[58] F. Reymond, D. Fermín, H. J. Lee, and H. H. Girault, "Electrochemistry at liquid/liquid interfaces: Methodology and potential applications," *Electrochim. Acta*, vol. 45, no. 15–16, pp. 2647–2662, 2000, doi: 10.1016/S0013-4686(00)00343-1.

[59] G. Herzog, "Recent developments in electrochemistry at the interface between two immiscible electrolyte solutions for ion sensing," *Analyst*, vol. 140, no. 12, pp. 3888–3896, 2015, doi: 10.1039/c5an00601e.

[60] P. S. Toth and R. A. W. Dryfe, "Novel organic solvents for electrochemistry at the liquid/liquid interface," *Analyst*, vol. 140, no. 6, pp. 1947–1954, 2015, doi: 10.1039/c4an02250e.

[61] Y. Cheng and D. J. Schiffrin, "A study of 2-heptanone and 2-octanone as solvents for two-phase electrochemistry. Part 1. Simple ion transfers," *J. Electroanal. Chem.*, vol. 409, no. 1–2, pp. 9–14, Jun. 1996, doi: 10.1016/0022-0728(95)04441-8.

[62] T. Solomon, H. Alemu, and B. Hundhammer, “Standard Gibbs energies of transfer of ions across the water-acetophenone interface,” *J. Electroanal. Chem.*, vol. 169, no. 1–2, pp. 303–309, 1984, doi: 10.1016/0022-0728(84)80091-1.

[63] H. Katano, H. Tatsumi, and M. Senda, “Ion-transfer voltammetry at 1,6-dichlorohexane|water and 1,4-dichlorobutane|water interfaces,” *Talanta*, vol. 63, no. 1, pp. 185–193, 2004, doi: 10.1016/j.talanta.2003.10.044.

[64] B. Hundhammer, C. Müller, T. Solomon, H. Alemu, and H. Hassen, “Ion transfer across the water-o-dichlorobenzene interface,” *J. Electroanal. Chem.*, vol. 319, no. 1–2, pp. 125–135, 1991, doi: 10.1016/0022-0728(91)87072-C.

[65] N. Nishi, “Ionic Liquid|Water Interface As an Electrochemical Reaction Field for the Formation of Novel Metal Nanostructure,” *ECS Meet. Abstr.*, vol. MA2016-02, no. 46, pp. 3357–3357, Sep. 2016, doi: 10.1149/ma2016-02/46/3357.

[66] A. J. Olaya, P. Ge, and H. H. Girault, “Ion transfer across the water|trifluorotoluene interface,” *Electrochem. commun.*, vol. 19, no. 1, pp. 101–104, 2012, doi: 10.1016/j.elecom.2012.03.010.

[67] M. Kasuno, K. Wakabayashi, Y. Matsuyama, and R. Yamamura, “Ion transfer voltammetry at the interface of water and low dielectric constant organic solutions,” *Electrochim. Acta*, vol. 343, p. 136069, 2020, doi: 10.1016/j.electacta.2020.136069.

[68] R. Chen, K. Xu, and M. Shen, “Avocado oil, coconut oil, walnut oil as true oil phase for ion transfer at nanoscale liquid/liquid interfaces,” *Electrochim. Acta*, vol. 357, p. 136788, 2020, doi: 10.1016/j.electacta.2020.136788.

[69] C. M. Alder *et al.*, “Updating and further expanding GSK’s solvent sustainability guide,” *Green Chem.*, vol. 18, no. 13, pp. 3879–3890, 2016, doi: 10.1039/c6gc00611f.

[70] Z. Samec, “Electrochemistry at the interface between two immiscible electolyte solutions (IUPAC technical report),” *Pure Appl. Chem.*, vol. 76, no. 12, pp. 2147–2180, Jan. 2004, doi: 10.1351/pac200476122147.

[71] D. W. M. Arrigan, E. A. De Eulate, and Y. Liu, “Electroanalytical Opportunities Derived

from Ion Transfer at Interfaces between Immiscible Electrolyte Solutions," *Aust. J. Chem.*, vol. 69, no. 9, pp. 1016–1032, 2016, doi: 10.1071/CH15796.

[72] P. Vanýsek and L. B. Ramírez, "Interface between two immiscible liquid electrolytes: A review," *Journal of the Chilean Chemical Society*, vol. 53, no. 2. Sociedad Chilena de Química, pp. 1455–1463, 2008, doi: 10.4067/S0717-97072008000200002.

[73] A. J. Bard and C. G. Zoski, "Electroanalytical chemistry," *Electroanal. Chem.*, vol. 23, pp. 1–315, Jan. 2010, doi: 10.1201/9781420084863/ELECTROANALYTICAL-CHEMISTRY-ALLEN-BARD-CYNTHIA-ZOSKI.

[74] G. Herzog and V. Beni, "Stripping voltammetry at micro-interface arrays: A review," *Anal. Chim. Acta*, vol. 769, no. 2010, pp. 10–21, 2013, doi: 10.1016/j.aca.2012.12.031.

[75] L. Poltorak, E. J. R. Sudhölter, and L. C. P. M. de Smet, "Effect of charge of quaternary ammonium cations on lipophilicity and electroanalytical parameters: Task for ion transfer voltammetry," *J. Electroanal. Chem.*, vol. 796, no. April, pp. 66–74, 2017, doi: 10.1016/j.jelechem.2017.04.051.

[76] Y. Shao, M. D. Osborne, and H. H. Girault, "Assisted ion transfer at micro-ITIES supported at the tip of micropipettes," *J. Electroanal. Chem.*, vol. 318, no. 1–2, pp. 101–109, 1991, doi: 10.1016/0022-0728(91)85297-3.

[77] F. Reymond, P. A. Carrupt, and H. H. Girault, "Facilitated ion transfer reactions across oil|water interfaces. Part I. Algebraic development and calculation of cyclic voltammetry experiments for successive complex formation," *J. Electroanal. Chem.*, vol. 449, no. 1–2, pp. 49–65, Jun. 1998, doi: 10.1016/S0022-0728(97)00430-0.

[78] J. Koryta, "Electrochemical polarization phenomena at the interface of two immiscible electrolyte solutions," *Electrochim. Acta*, vol. 24, no. 3, pp. 293–300, 1979, doi: 10.1016/0013-4686(79)85048-3.

[79] P. J. Greenawalt, M. B. Garada, and S. Amemiya, "Voltammetric Characterization of Ion-Ionophore Complexation Using Thin Polymeric Membranes: Asymmetric Thin-Layer Responses," *Anal. Chem.*, vol. 87, no. 16, pp. 8564–8572, 2015, doi: 10.1021/acs.analchem.5b02355.

[80] F. Reymond, G. Steyaert, A. Pagliara, P. A. Carrupt, B. Testa, and H. Girault, “141. Transfer mechanism of ionic drugs: Piroxicam as an agent facilitating proton transfer,” *Helv. Chim. Acta*, vol. 79, no. 6, pp. 1651–1669, 1996, doi: 10.1002/hlca.19960790616.

[81] T. Solomon and A. J. Bard, “Reverse (uphill) electron transfer at the liquid/liquid interface,” *J. Phys. Chem.*, vol. 99, no. 49, pp. 17487–17489, 1995, doi: 10.1021/j100049a002.

[82] Z. Ding, P. F. Brevet, and H. H. Girault, “Heterogeneous electron transfer at the polarised water/1,2-dichloroethane interface studied by in situ UV-VIS spectroscopy and differential cyclic voltabsorptometry,” *Chem. Commun.*, no. 21, pp. 2059–2060, 1997, doi: 10.1039/a705156e.

[83] R. A. W. Dryfe, Z. Ding, R. G. Wellington, P. F. Brevet, A. M. Kuznetzov, and H. H. Girault, “Time-resolved laser-induced fluorescence study of photoinduced electron transfer at the water/1,2-dichloroethane interface,” *J. Phys. Chem. A*, vol. 101, no. 14, pp. 2519–2524, 1997, doi: 10.1021/jp9630434.

[84] G. C. Gschwend, A. Olaya, P. Peljo, and H. H. Girault, “Structure and reactivity of the polarised liquid–liquid interface: what we know and what we do not,” *Curr. Opin. Electrochem.*, vol. 19, pp. 137–143, 2020, doi: 10.1016/j.coelec.2019.12.002.

[85] Z. Samec, V. Mareček, and J. Weber, “Detection of an electron transfer across the interface between two immiscible electrolyte solutions by cyclic voltammetry with four-electrode system,” *J. Electroanal. Chem.*, vol. 96, no. 2, pp. 245–247, 1979, doi: 10.1016/S0022-0728(79)80382-4.

[86] P. Peljo, E. Smirnov, and H. H. Girault, “Heterogeneous versus homogeneous electron transfer reactions at liquid–liquid interfaces: The wrong question?,” *J. Electroanal. Chem.*, vol. 779, pp. 187–198, Oct. 2016, doi: 10.1016/j.jelechem.2016.02.023.

[87] E. Smirnov, P. Peljo, M. D. Scanlon, and H. H. Girault, “Interfacial Redox Catalysis on Gold Nanofilms at Soft Interfaces,” *ACS Nano*, vol. 9, no. 6, pp. 6565–6575, 2015, doi: 10.1021/acsnano.5b02547.

[88] E. Smirnov, P. Peljo, and H. H. Girault, “Self-assembly and redox induced phase transfer of gold nanoparticles at a water-propylene carbonate interface,” *Chem. Commun.*, vol. 53,

no. 29, pp. 4108–4111, 2017, doi: 10.1039/c6cc09638g.

[89] R. A. Lehane *et al.*, “Electrosynthesis of Biocompatible Free-Standing PEDOT Thin Films at a Polarized Liquid|Liquid Interface,” *J. Am. Chem. Soc.*, vol. 144, no. 11, pp. 4853–4862, Mar. 2022, doi: 10.1021/jacs.1c12373.

[90] M. N. Jajuli, M. H. Hussin, B. Saad, A. A. Rahim, M. Hébrant, and G. Herzog, “Electrochemically Modulated Liquid-Liquid Extraction for Sample Enrichment,” *Anal. Chem.*, vol. 91, no. 11, pp. 7466–7473, Jun. 2019, doi: 10.1021/acs.analchem.9b01674.

[91] S. M. Ulmeanu, H. Jensen, Z. Samec, G. Bouchard, P. A. Carrupt, and H. H. Girault, “Cyclic voltammetry of highly hydrophilic ions at a supported liquid membrane,” *J. Electroanal. Chem.*, vol. 530, no. 1–2, pp. 10–15, 2002, doi: 10.1016/S0022-0728(02)01002-1.

[92] J. W. Robinson, E. S. Frame, and G. M. Frame II, “Electroanalytical Chemistry,” *Undergrad. Instrum. Anal.*, vol. 23, pp. 1074–1167, Jan. 2021, doi: 10.1201/b15921-19.

[93] G. Luo *et al.*, “Ion distributions at the nitrobenzene-water interface electrified by a common ion,” *J. Electroanal. Chem.*, vol. 593, no. 1–2, pp. 142–158, Aug. 2006, doi: 10.1016/j.jelechem.2006.03.051.

[94] R. A. Hartvig *et al.*, “Interfacial complexes between a protein and lipophilic ions at an oil-water interface,” *Anal. Chem.*, vol. 82, no. 18, pp. 7699–7705, Sep. 2010, doi: 10.1021/ac101528r.

[95] A. Berduque and D. W. M. Arrigan, “Selectivity in the coextraction of cation and anion by electrochemically modulated liquid-liquid extraction,” *Anal. Chem.*, vol. 78, no. 8, pp. 2717–2725, 2006, doi: 10.1021/ac0521192.

[96] F. Li, M. Edwards, J. Guo, and P. R. Unwin, “Silver particle nucleation and growth at liquid/liquid interfaces: A scanning electrochemical microscopy approach,” *J. Phys. Chem. C*, vol. 113, no. 9, pp. 3553–3565, Mar. 2009, doi: 10.1021/jp809165t.

[97] P. Peljo *et al.*, “Biomimetic oxygen reduction by cofacial porphyrins at a liquid-liquid Interface,” *J. Am. Chem. Soc.*, vol. 134, no. 13, pp. 5974–5984, Apr. 2012, doi: 10.1021/ja3004914.

[98] L. Rivier *et al.*, “Decamethylruthenocene Hydride and Hydrogen Formation at Liquid|Liquid Interfaces,” *J. Phys. Chem. C*, vol. 119, no. 46, pp. 25761–25769, Nov. 2015, doi: 10.1021/acs.jpcc.5b08148.

[99] R. Partovi-Nia *et al.*, “Dioxygen reduction by cobalt(II) octaethylporphyrin at liquid &vbar; liquid interfaces,” *ChemPhysChem*, vol. 11, no. 13, pp. 2979–2984, 2010, doi: 10.1002/cphc.201000200.

[100] K. Holub, Z. Samec, and V. Mareček, “Role of water in the mechanism of the salt extraction to the organic solvent,” *Electrochim. Acta*, vol. 306, pp. 541–548, 2019, doi: 10.1016/j.electacta.2019.03.096.

[101] A. Trojánek, Z. Samec, and V. Mareček, “Self-perturbation of the salt partition at the water/1,2-dichloroethane interface,” *Electrochim. Acta*, vol. 361, pp. 1–7, 2020, doi: 10.1016/j.electacta.2020.137059.

[102] V. Mareček, “Electrochemical monitoring of the co-extraction of water with hydrated ions into an organic solvent,” *Electrochem. commun.*, vol. 88, no. January, pp. 57–60, 2018, doi: 10.1016/j.elecom.2018.01.017.

[103] E. Laborda, A. Molina, V. F. Espín, F. Martínez-Ortiz, J. García de la Torre, and R. G. Compton, “Single Fusion Events at Polarized Liquid–Liquid Interfaces,” *Angew. Chemie - Int. Ed.*, vol. 56, no. 3, pp. 782–785, 2017, doi: 10.1002/anie.201610185.

[104] A. Trojánek, V. Mareček, and Z. Samec, “Open circuit potential transients associated with single emulsion droplet collisions at an interface between two immiscible electrolyte solutions,” *Electrochem. commun.*, vol. 86, pp. 113–116, Jan. 2018, doi: 10.1016/j.elecom.2017.11.026.

[105] D. P. August *et al.*, “Self-assembly of a layered two-dimensional molecularly woven fabric,” *Nature*, vol. 588, no. 7838, pp. 429–435, 2020, doi: 10.1038/s41586-020-3019-9.

[106] P. Y. Gu *et al.*, “Stabilizing Liquids Using Interfacial Supramolecular Polymerization,” *Angew. Chemie - Int. Ed.*, vol. 58, no. 35, pp. 12112–12116, 2019, doi: 10.1002/anie.201906339.

[107] B. Qin, S. Zhang, Z. Huang, J. F. Xu, and X. Zhang, "Supramolecular Interfacial Polymerization of Miscible Monomers: Fabricating Supramolecular Polymers with Tailor-Made Structures," *Macromolecules*, vol. 51, no. 5, pp. 1620–1625, 2018, doi: 10.1021/acs.macromol.8b00289.

[108] M. D. M. D. Scanlon, E. Smirnov, T. J. Stockmann, and P. Peljo, "Gold Nanofilms at Liquid-Liquid Interfaces: An Emerging Platform for Redox Electrocatalysis, Nanoplasmonic Sensors, and Electrovariable Optics," *Chem. Rev.*, vol. 118, no. 7, pp. 3722–3751, 2018, doi: 10.1021/acs.chemrev.7b00595.

[109] T. J. Stockmann, J. M. Noël, A. Abou-Hassan, C. Combellas, and F. Kanoufi, "Facilitated Lewis Acid Transfer by Phospholipids at a (Water|CHCl3) Liquid|Liquid Interface toward Biomimetic and Energy Applications," *J. Phys. Chem. C*, vol. 120, no. 22, pp. 11977–11983, 2016, doi: 10.1021/acs.jpcc.6b02354.

[110] L. Poltorak, G. Herzog, and A. Walcarius, "Electrochemically assisted generation of silica deposits using a surfactant template at liquid/liquid microinterfaces," *Langmuir*, vol. 30, no. 38, pp. 11453–11463, Sep. 2014, doi: 10.1021/la501938g.

[111] A. F. Molina-Osorio *et al.*, "Self-Assembly of Porphyrin Nanostructures at the Interface between Two Immiscible Liquids," *J. Phys. Chem. C*, vol. 124, no. 12, pp. 6929–6937, 2020, doi: 10.1021/acs.jpcc.0c00437.

[112] I. Robayo-Molina, A. F. Molina-Osorio, L. Guinane, S. A. M. Tofail, and M. D. Scanlon, "Pathway Complexity in Supramolecular Porphyrin Self-Assembly at an Immiscible Liquid-Liquid Interface," *J. Am. Chem. Soc.*, vol. 143, no. 24, pp. 9060–9069, Jun. 2021, doi: 10.1021/jacs.1c02481.

[113] A. F. Molina-Osorio, J. A. Manzanares, A. Gamero-Quijano, and M. D. Scanlon, "Electrochemically controlled ion dynamics in porphyrin nanostructures," *J. Phys. Chem. C*, vol. 124, no. 33, pp. 18346–18355, Aug. 2020, doi: 10.1021/acs.jpcc.0c04976.

[114] A. Gamero-Quijano *et al.*, "Modulating the pro-apoptotic activity of cytochrome c at a biomimetic electrified interface," *Sci. Adv.*, vol. 7, no. 45, p. eabg4119, Nov. 2021, doi: 10.1126/sciadv.abg4119.

[115] A. Gamero-Quijano, M. Dossot, A. Walcarius, M. D. Scanlon, and G. Herzog, "Electrogeneration of a Free-Standing Cytochrome c - Silica Matrix at a Soft Electrified Interface," *Langmuir*, vol. 37, no. 13, pp. 4033–4041, Apr. 2021, doi: 10.1021/acs.langmuir.1c00409.

[116] G. Herzog, V. Kam, and D. W. M. Arrigan, "Electrochemical behaviour of haemoglobin at the liquid/liquid interface," *Electrochim. Acta*, vol. 53, no. 24, pp. 7204–7209, 2008, doi: 10.1016/j.electacta.2008.04.072.

[117] K. Kowalewska, K. Sipa, A. Leniart, S. Skrzypek, and L. Poltorak, "Electrochemistry at the liquid–liquid interface rediscovers interfacial polycondensation of nylon-6,6," *Electrochem. commun.*, vol. 115, no. March, p. 106732, Jun. 2020, doi: 10.1016/j.elecom.2020.106732.

[118] B. Su *et al.*, "Reversible Voltage-Induced Assembly of Au Nanoparticles at Liquid|Liquid Interfaces," *J. Am. Chem. Soc.*, vol. 126, no. 3, pp. 915–919, Jan. 2004, doi: 10.1021/ja0386187.

[119] L. Hu, M. Chen, X. Fang, and L. Wu, "Oil–water interfacial self-assembly: A novel strategy for nanofilm and nanodevice fabrication," *Chem. Soc. Rev.*, vol. 41, no. 3, pp. 1350–1362, Jan. 2012, doi: 10.1039/c1cs15189d.

[120] Z. Yang, J. Wei, Y. I. Sobolev, and B. A. Grzybowski, "Systems of mechanized and reactive droplets powered by multi-responsive surfactants," *Nature*, vol. 553, no. 7688, pp. 313–318, Jan. 2018, doi: 10.1038/nature25137.

[121] E. Smirnov, P. Peljo, M. D. Scanlon, F. Gumy, and H. H. Girault, "Self-healing gold mirrors and filters at liquid-liquid interfaces," *Nanoscale*, vol. 8, no. 14, pp. 7723–7737, 2016, doi: 10.1039/c6nr00371k.

[122] M. K. Bera *et al.*, "Interfacial localization and voltage-tunable arrays of charged nanoparticles," *Nano Lett.*, vol. 14, no. 12, pp. 6816–6822, 2014, doi: 10.1021/nl502450j.

[123] L. Poltorak, K. Morakchi, G. Herzog, and A. Walcarius, "Electrochemical characterization of liquid-liquid micro-interfaces modified with mesoporous silica," *Electrochim. Acta*, vol. 179, pp. 9–15, Oct. 2015, doi: 10.1016/j.electacta.2015.01.129.

[124] E. R. Ravenhill, P. M. Kirkman, and P. R. Unwin, “Microscopic Studies of Calcium Sulfate Crystallization and Transformation at Aqueous-Organic Interfaces,” *Cryst. Growth Des.*, vol. 16, no. 10, pp. 5887–5895, 2016, doi: 10.1021/acs.cgd.6b00941.

[125] D. Perry, A. S. Parker, A. Page, and P. R. Unwin, “Electrochemical Control of Calcium Carbonate Crystallization and Dissolution in Nanopipettes,” *ChemElectroChem*, vol. 3, no. 12, pp. 2212–2220, 2016, doi: 10.1002/celc.201600547.

[126] B. R. Silver, V. Fülöp, and P. R. Unwin, “Protein crystallization at oil/water interfaces,” *New J. Chem.*, vol. 35, no. 3, pp. 602–606, 2011, doi: 10.1039/c0nj00822b.

[127] P. D. Morris, I. J. McPherson, M. A. Edwards, R. J. Kashtiban, R. I. Walton, and P. R. Unwin, “Electric Field-Controlled Synthesis and Characterisation of Single Metal–Organic-Framework (MOF) Nanoparticles,” *Angew. Chemie - Int. Ed.*, vol. 59, no. 44, pp. 19696–19701, Oct. 2020, doi: 10.1002/anie.202007146.

[128] C. N. R. Rao and K. P. Kalyanikutty, “The liquid-liquid interface as a medium to generate nanocrystalline films of inorganic materials,” *Acc. Chem. Res.*, vol. 41, no. 4, pp. 489–499, 2008, doi: 10.1021/ar700192d.

[129] F. M. Maddar, D. Perry, and P. R. Unwin, “Confined crystallization of organic materials in nanopipettes: Tracking the early stages of crystal growth and making seeds for unusual polymorphs,” *Cryst. Growth Des.*, vol. 17, no. 12, pp. 6565–6571, 2017, doi: 10.1021/acs.cgd.7b01224.

[130] Š. Komorsky-Lovrić, M. Lovrić, and F. Scholz, “Cyclic voltammetry of decamethylferrocene at the organic liquid aqueous solution graphite three-phase junction,” *J. Electroanal. Chem.*, vol. 508, no. 1–2, pp. 129–137, 2001, doi: 10.1016/S0022-0728(01)00527-7.

[131] A. Berduque, A. Sherburn, M. Ghita, R. A. W. Dryfe, and D. W. M. Arrigan, “Electrochemically Modulated Liquid-Liquid Extraction of Ions between two immiscible electrolyte solutions is discussed . potentiostatic extraction of non-redox-active species from,” *Anal. Chem.*, vol. 77, no. 22, pp. 7310–7318, 2005.

[132] G. Bouchard, P. A. Carrupt, B. Testa, V. Gobry, and H. H. Girault, “The apparent

lipophilicity of quaternary ammonium ions is influenced by galvani potential difference, not ion-pairing: A cyclic voltammetry study," *Pharm. Res.*, vol. 18, no. 5, pp. 702–708, 2001, doi: 10.1023/A:1011001914685.

[133] T. Wandlowski, V. Mareček, and Z. Samec, "Galvani potential scales for water-nitrobenzene and water-1,2-dichloroethane interfaces," *Electrochim. Acta*, vol. 35, no. 7, pp. 1173–1175, 1990, doi: 10.1016/0013-4686(90)80035-M.

[134] L. J. Sanchez Vallejo, J. M. Ovejero, R. A. Fernández, and S. A. Dassie, "Simple Ion Transfer at Liquid|Liquid Interfaces," *Int. J. Electrochem.*, vol. 2012, pp. 1–34, 2012, doi: 10.1155/2012/462197.

[135] A. J. Olaya, M. A. Méndez, F. Cortes-Salazar, and H. H. Girault, "Voltammetric determination of extreme standard Gibbs ion transfer energy," *J. Electroanal. Chem.*, vol. 644, no. 1, pp. 60–66, 2010, doi: 10.1016/j.jelechem.2010.03.030.

[136] G. Herzog, W. Moujahid, J. Strutwolf, and D. W. M. Arrigan, "Interactions of proteins with small ionised molecules: Electrochemical adsorption and facilitated ion transfer voltammetry of haemoglobin at the liquidliquid interface," *Analyst*, vol. 134, no. 8, pp. 1608–1613, Jul. 2009, doi: 10.1039/b905441n.

[137] C. B. Aakeröy, A. B. Grommet, and J. Desper, "Co-crystal screening of diclofenac," *Pharmaceutics*, vol. 3, no. 3, pp. 601–614, 2011, doi: 10.3390/pharmaceutics3030601.

[138] S. L. Childs and K. I. Hardcastle, "Cocrystals of chlorzoxazone with carboxylic acids," *CrystEngComm*, vol. 9, no. 5, pp. 364–367, Jul. 2007, doi: 10.1039/b703292g.

[139] M. Žegarac *et al.*, "A sildenafil cocrystal based on acetylsalicylic acid exhibits an enhanced intrinsic dissolution rate," *CrystEngComm*, vol. 16, no. 1, pp. 32–35, 2014, doi: 10.1039/c3ce42013b.

[140] M. D. Eddleston, R. Thakuria, B. J. Aldous, and W. Jones, "An investigation of the causes of cocrystal dissociation at high humidity," *J. Pharm. Sci.*, vol. 103, no. 9, pp. 2859–2864, 2014, doi: 10.1002/jps.23865.

[141] Y. Wicaksono, D. Setyawan, and Siswandono, "Formation of ketoprofen-malonic acid

cocrystal by solvent evaporation method," *Indones. J. Chem.*, vol. 17, no. 2, pp. 161–166, 2017, doi: 10.22146/ijc.24884.

[142] G. L. Perpétuo *et al.*, "A combined approach using differential scanning calorimetry with polarized light thermomicroscopy in the investigation of ketoprofen and nicotinamide cocrystal," *Thermochim. Acta*, vol. 651, pp. 1–10, 2017, doi: 10.1016/j.tca.2017.02.014.

[143] P. Panzade, G. Shendarkar, S. Shaikh, and P. B. Rathi, "Pharmaceutical Cocrystal of Piroxicam: Design, formulation and evaluation," *Adv. Pharm. Bull.*, vol. 7, no. 3, pp. 399–408, 2017, doi: 10.15171/apb.2017.048.

[144] V. Gobry, G. Bouchard, P. A. Carrupt, B. Testa, and H. H. Girault, "Physicochemical characterization of sildenafil: Ionization, lipophilicity behavior, and ionic-partition diagram studied by two-phase titration and electrochemistry," *Helv. Chim. Acta*, vol. 83, no. 7, pp. 1465–1474, 2000, doi: 10.1002/1522-2675(20000705)83.

[145] F. Reymond *et al.*, "Ionic partition diagrams of ionisable drugs: PH-lipophilicity profiles, transfer mechanisms and charge effects on solvation," *J. Electroanal. Chem.*, vol. 462, no. 2, pp. 235–250, 1999, doi: 10.1016/S0022-0728(98)00418-5.

[146] G. Bouchard, P. A. Carrupt, B. Testa, V. Gobry, and H. H. Girault, "Lipophilicity and solvation of anionic drugs," *Chem. - A Eur. J.*, vol. 8, no. 15, pp. 3478–3484, 2002, doi: 10.1002/1521-3765(20020802)8.

[147] A. Karnjanapiboonwong, A. N. Morse, J. D. Maul, and T. A. Anderson, "Sorption of estrogens, triclosan, and caffeine in a sandy loam and a silt loam soil," *J. Soils Sediments*, vol. 10, no. 7, pp. 1300–1307, 2010, doi: 10.1007/s11368-010-0223-5.

[148] P. D. Beattie, R. G. Wellington, and H. H. Girault, "Cyclic voltammetry for assisted ion transfer at an ITIES," *J. Electroanal. Chem.*, vol. 396, no. 1–2, pp. 317–323, 1995, doi: 10.1016/0022-0728(94)03734-K.

[149] L. Poltorak, I. Eggink, M. Hoitink, E. J. R. Sudhölter, and M. De Puit, "Electrified Soft Interface as a Selective Sensor for Cocaine Detection in Street Samples," *Anal. Chem.*, vol. 90, no. 12, pp. 7428–7433, 2018, doi: 10.1021/acs.analchem.8b00916.

[150] C. Yufei, V. J. Cunnane, D. J. Schiffrin, L. Mutomäki, and K. Kontturi, “Interfacial capacitance and ionic association at electrified liquid/liquid interfaces,” *J. Chem. Soc. Faraday Trans.*, vol. 87, no. 1, pp. 107–114, 1991, doi: 10.1039/FT9918700107.

[151] H. Jensen, D. J. Fermín, J. E. Moser, and H. H. Girault, “Organization and reactivity of nanoparticles at molecular interfaces. Part I. Photoelectrochemical responses involving TiO2 nanoparticles assembled at polarizable water|1,2-dichloroethane junctions,” *J. Phys. Chem. B*, vol. 106, no. 42, pp. 10908–10914, 2002, doi: 10.1021/jp0261253.

[152] M. F. Suárez-Herrera and M. D. Scanlon, “On the non-ideal behaviour of polarised liquid-liquid interfaces,” *Electrochim. Acta*, vol. 328, pp. 1–28, 2019, doi: 10.1016/j.electacta.2019.135110.

[153] C. M. Pereira, A. Martins, M. Rocha, C. J. Silva, and F. Silva, “Differential capacitance of liquid/liquid interfaces: Effect of electrolytes present in each phase,” *J. Chem. Soc. Faraday Trans.*, vol. 90, no. 1, pp. 143–148, 1994, doi: 10.1039/FT9949000143.

[154] M. C. Martins, C. M. Pereira, H. H. Girault, and F. Silva, “Specific adsorption of tetraalkylammonium cations on the 1,2-dicloroethane/water interface,” *Electrochim. Acta*, vol. 50, no. 1, pp. 135–139, 2004, doi: 10.1016/j.electacta.2004.07.023.

[155] L. Poltorak, G. Herzog, and A. Walcarius, “In-situ formation of mesoporous silica films controlled by ion transfer voltammetry at the polarized liquid-liquid interface,” *Electrochem. commun.*, vol. 37, pp. 76–79, 2013, doi: 10.1016/j.elecom.2013.10.018.

[156] L. Quoc Hung, “Electrochemical properties of the interface between two immiscible electrolyte solutions. Part I. Equilibrium situation and galvani potential difference,” *J. Electroanal. Chem.*, vol. 115, no. 2, pp. 159–174, Dec. 1980, doi: 10.1016/S0022-0728(80)80323-8.

[157] T. Iwata, H. Nagatani, and T. Osakai, “Determination of the electrostatic potential of oil-in-water emulsion droplets by combined use of two membrane potential-sensitive dyes,” *Anal. Sci.*, vol. 33, no. 7, pp. 813–819, 2017, doi: 10.2116/analsci.33.813.

[158] C. R. Groom, I. J. Bruno, M. P. Lightfoot, and S. C. Ward, “The Cambridge structural database,” *Acta Crystallogr. Sect. B Struct. Sci. Cryst. Eng. Mater.*, vol. 72, no. 2, pp. 171–

179, 2016, doi: 10.1107/S2052520616003954.

[159] A. B. M. Buanz, G. N. Parkinson, and S. Gaisford, “Characterization of carbamazepine-nicatinamide cocrystal polymorphs with rapid heating DSC and XRPD,” *Cryst. Growth Des.*, vol. 11, no. 4, pp. 1177–1181, Apr. 2011, doi: 10.1021/cg101377u.

[160] A. B. Singaraju, D. Bahl, C. Wang, D. C. Swenson, C. C. Sun, and L. L. Stevens, “Molecular Interpretation of the Compaction Performance and Mechanical Properties of Caffeine Cocrystals: A Polymorphic Study,” *Mol. Pharm.*, vol. 17, no. 1, pp. 21–31, Jan. 2020, doi: 10.1021/acs.molpharmaceut.9b00377.

[161] F. Ucun, A. Sağlam, and V. Güçlü, “Molecular structures and vibrational frequencies of xanthine and its methyl derivatives (caffeine and theobromine) by ab initio Hartree-Fock and density functional theory calculations,” *Spectrochim. Acta - Part A Mol. Biomol. Spectrosc.*, vol. 67, no. 2, pp. 342–349, Jun. 2007, doi: 10.1016/j.saa.2006.07.029.

[162] M. Inoue *et al.*, “Solid-State Quantification of Cocrystals in Pharmaceutical Tablets Using Transmission Low-Frequency Raman Spectroscopy,” *Anal. Chem.*, vol. 91, no. 21, pp. 13427–13432, Nov. 2019, doi: 10.1021/acs.analchem.9b01895.

[163] C. Sui *et al.*, “Raman spectroscopy of seized drugs and density functional theory interpretation,” *Spectrosc. Lett.*, vol. 51, no. 8, pp. 403–413, Sep. 2018, doi: 10.1080/00387010.2018.1501703.

[164] A. Hédoux, A. A. Decroix, Y. Guinet, L. Paccou, P. Derollez, and M. Descamps, “Low- and high-frequency raman investigations on caffeine: Polymorphism, disorder and phase transformation,” *J. Phys. Chem. B*, vol. 115, no. 19, pp. 5746–5753, May 2011, doi: 10.1021/jp112074w.

[165] A. Eşme, “Experimental (FT-IR, FT-Raman, and UV-Vis) and quantum chemical calculations on monomer and dimer structures of l-hydroxy-2-naphthoic acid using the DFT and TD-DFT methods,” *Indian J. Pure Appl. Phys.*, vol. 57, no. 11, pp. 822–835, 2019.

[166] J. Kang, H. Gu, L. Zhong, Y. Hu, and F. Liu, “The pH dependent Raman spectroscopic study of caffeine,” *Spectrochim. Acta - Part A Mol. Biomol. Spectrosc.*, vol. 78, no. 2, pp. 757–762, 2011, doi: 10.1016/j.saa.2010.11.055.

[167] I. Hatay *et al.*, “Hydrogen evolution at liquid-liquid interfaces,” *Angew. Chemie - Int. Ed.*, vol. 48, no. 28, pp. 5139–5142, 2009, doi: 10.1002/anie.200901757.

[168] F. Mansfeld and H. Xiao, “Electrochemical Noise Analysis of Iron Exposed to NaCl Solutions of Different Corrosivity,” *J. Electrochem. Soc.*, vol. 140, no. 8, pp. 2205–2209, 1993, doi: 10.1149/1.2220796.

[169] D.-H. Xia *et al.*, “Review—Electrochemical Noise Applied in Corrosion Science: Theoretical and Mathematical Models towards Quantitative Analysis,” *J. Electrochem. Soc.*, vol. 167, no. 8, p. 081507, 2020, doi: 10.1149/1945-7111/ab8de3.

[170] Y. J. Tan, S. Bailey, and B. Kinsella, “The monitoring of the formation and destruction of corrosion inhibitor films using electrochemical noise analysis (ENA),” *Corros. Sci.*, vol. 38, no. 10, pp. 1681–1695, 1996, doi: 10.1016/S0010-938X(96)00061-3.

[171] Z. Li, A. Homborg, Y. Gonzalez-Garcia, A. Kosari, P. Visser, and A. Mol, “Evaluation of the formation and protectiveness of a lithium-based conversion layer using electrochemical noise,” *Electrochim. Acta*, vol. 426, no. June, p. 140733, 2022, doi: 10.1016/j.electacta.2022.140733.

[172] A. M. Homborg *et al.*, “Application of transient analysis using Hilbert spectra of electrochemical noise to the identification of corrosion inhibition,” *Electrochim. Acta*, vol. 116, pp. 355–365, 2014, doi: 10.1016/j.electacta.2013.11.084.

[173] R. A. Cottis, “CRITICAL REVIEW OF CORROSION SCIENCE AND ENGINEERING Interpretation of Electrochemical Noise Data,” *Corrosion*, vol. 57, no. 3, pp. 265–285, 2001.

[174] M. Kaliszczak *et al.*, “Electrochemically controlled cocrystallisation of caffeine:1-hydroxy-2-naphthoic acid,” *CrystEngComm*, vol. 24, no. 1, pp. 48–51, 2022, doi: 10.1039/d1ce01281a.

[175] I. B. Obot, I. B. Onyeachu, A. Zeino, and S. A. Umoren, “Electrochemical noise (EN) technique: review of recent practical applications to corrosion electrochemistry research,” *J. Adhes. Sci. Technol.*, vol. 33, no. 13, pp. 1453–1496, 2019, doi: 10.1080/01694243.2019.1587224.

[176] S. Barrozo, R. N. Peres, M. J. Witzler, A. V. Benedetti, and C. S. Fugivara, "Electrochemical noise analysis to obtain the Rsn value via FFT using Excel," *Eclet. Quim.*, vol. 45, no. 4, pp. 71–75, 2020, doi: 10.26850/1678-4618EQJ.V45.4.2020.P57-70.

[177] U. Grömping, *Tutorial for designing experiments using the R package RcmdrPlugin.DoE*. 2011, pp. 1–54.

[178] P. Doe, "Package 'DoE.base,'" 2022.

[179] M. D. Eddleston, S. Sivachelvam, and W. Jones, "Screening for polymorphs of cocrystals: A case study," *CrystEngComm*, vol. 15, no. 1, pp. 175–181, Nov. 2013, doi: 10.1039/c2ce26496j.

[180] J. D. Berry, M. J. Neeson, R. R. Dagastine, D. Y. C. Chan, and R. F. Tabor, "Measurement of surface and interfacial tension using pendant drop tensiometry," *J. Colloid Interface Sci.*, vol. 454, pp. 226–237, 2015, doi: 10.1016/j.jcis.2015.05.012.

[181] W. Alnoush, A. Sayed, and N. Alyafei, "Optimization of contact angle and interfacial tension measurements for fluid/rock systems at ambient conditions," *MethodsX*, vol. 6, no. March, pp. 1706–1715, 2019, doi: 10.1016/j.mex.2019.07.009.

[182] S. Mhatre, S. Simon, and J. Sjöblom, "Experimental Evidence of Enhanced Adsorption Dynamics at Liquid-Liquid Interfaces under an Electric Field," *Anal. Chem.*, vol. 92, no. 19, pp. 12860–12870, 2020, doi: 10.1021/acs.analchem.0c01287.

[183] C. M. Pereira, W. Schmickler, F. Silva, and M. J. Sousa, "Ion association at liquid|liquid interfaces," *J. Electroanal. Chem.*, vol. 436, no. 1–2, pp. 9–15, Oct. 1997, doi: 10.1016/S0022-0728(97)00283-0.

[184] H. H. J. Girault, D. J. Schiffrin, and B. D. V. Smith, "The measurement of interfacial tension of pendant drops using a video image profile digitizer," *J. Colloid Interface Sci.*, vol. 101, no. 1, pp. 257–266, 1984, doi: 10.1016/0021-9797(84)90026-2.

[185] G. C. Gschwend and H. H. Girault, "Discrete Helmholtz charge distribution at liquid-liquid interfaces: Electrocapillarity, capacitance and non-linear spectroscopy studies," *J. Electroanal. Chem.*, vol. 872, 2020, doi: 10.1016/j.jelechem.2020.114240.

[186] Z. Samec, A. Lhotský, H. Jänchenová, and V. Mareček, “Interfacial tension and impedance measurements of interfaces between two immiscible electrolyte solutions,” *J. Electroanal. Chem.*, vol. 483, no. 1, pp. 47–56, 2000, doi: 10.1016/S0022-0728(00)00051-6.

[187] A. Gamero-Quijano *et al.*, “On the origin of chaotrope-modulated electrocatalytic activity of cytochrome c at electrified aqueous|organic interfaces,” *Chem. Commun.*, vol. 58, no. 20, pp. 3270–3273, 2022, doi: 10.1039/d1cc05293d.

[188] M. F. Suárez-Herrera, P. A. Cazade, D. Thompson, and M. D. Scanlon, “Monitoring transient changes in the structure of water at a polarised liquid-liquid interface using electrocapillary curves,” *Electrochem. commun.*, vol. 109, no. September, p. 106564, 2019, doi: 10.1016/j.elecom.2019.106564.

[189] R. V. Lenth, “Quick and easy analysis of unreplicated factorials,” *Technometrics*, vol. 31, no. 4, pp. 469–473, 1989, doi: 10.1080/00401706.1989.10488595.

[190] S. Addelman, “Statistics for Experimenters,” *Technometrics*, vol. 21, no. 3. pp. 387–388, 1979, doi: 10.1080/00401706.1979.10489788.

[191] C. Daniel, “Use of Half-Normal Plots in Interpreting Factorial Two-Level Experiments,” *Technometrics*, vol. 1, no. 4, pp. 311–341, 1959, doi: 10.1080/00401706.1959.10489866.

[192] A. Berduque, J. O’Brien, J. Alderman, and D. W. M. Arrigan, “Microfluidic chip for electrochemically-modulated liquid|liquid extraction of ions,” *Electrochem. commun.*, vol. 10, no. 1, pp. 20–24, 2008, doi: 10.1016/j.elecom.2007.10.023.

[193] M. Ildefonso, E. Revalor, P. Punniam, J. B. Salmon, N. Candoni, and S. Veesler, “Nucleation and polymorphism explored via an easy-to-use microfluidic tool,” *J. Cryst. Growth*, vol. 342, no. 1, pp. 9–12, 2012, doi: 10.1016/j.jcrysgro.2010.11.098.

[194] M. Ildefonso, N. Candoni, and S. Veesler, “A cheap, easy microfluidic crystallization device ensuring universal solvent compatibility,” *Org. Process Res. Dev.*, vol. 16, no. 4, pp. 556–560, Apr. 2012, doi: 10.1021/op200291z.

[195] M. Sairi, J. Strutwolf, R. A. Mitchell, D. S. Silvester, and D. W. M. Arrigan, “Chronoamperometric response at nanoscale liquid-liquid interface arrays,” *Electrochim.*

Acta, vol. 101, pp. 177–185, 2013, doi: 10.1016/j.electacta.2012.11.062.

[196] S. C. S. Lai *et al.*, "Effects of electrolyte pH and composition on the ethanol electro-oxidation reaction," *Catal. Today*, vol. 154, no. 1–2, pp. 92–104, 2010, doi: 10.1016/j.cattod.2010.01.060.

[197] V. D. Nikolić *et al.*, "Photostability of piroxicam in the inclusion complex with 2-hydroxypropyl-β-cyclodextrin," *Hem. Ind.*, vol. 68, no. 1, pp. 107–116, 2014, doi: 10.2298/HEMIND130306034N.

[198] D. Di Leo, F. Berrettini, and R. Cini, "Synthesis of platinum(II)-piroxicam compounds. Crystal structure of trans-dichloro(η2-ethene)(piroxicam)platinum(II)," *J. Chem. Soc. - Dalt. Trans.*, vol. 0, no. 12, pp. 1993–2000, Jan. 1998, doi: 10.1039/a709280f.

[199] K. Takács-Novák *et al.*, "Microscopic Protonation/Deprotonation Equilibria of the Anti-Inflammatory Agent Piroxicam," *Helv. Chim. Acta*, vol. 78, no. 3, pp. 553–562, 1995, doi: 10.1002/hlca.19950780304.

[200] X. Y. Song, Y. P. Shi, and J. Chen, "A novel extraction technique based on carbon nanotubes reinforced hollow fiber solid/liquid microextraction for the measurement of piroxicam and diclofenac combined with high performance liquid chromatography," *Talanta*, vol. 100, pp. 153–161, 2012, doi: 10.1016/j.talanta.2012.08.042.

APPENDIX 1

Instruments and methods

High Performance Liquid Chromatography (HPLC)

Chromatograms were recorded using a Shimadzu HPLC with UV/Vis detector. The used column was commercially available Chromolith® RP-18e by Merck. The solutions of drugs were filtered by a syringe filter, before injecting into the HPLC. Chromatograms were recorded at 254 and 275 nm for piroxicam, diclofenac and KTPBCl. Mobile phase flow rate was optimized 2.0 $mLmin^{-1}$ and all the experiments were performed at room temperature.

Chronoamperometry

The chronoamperometry measurements were run with an Autolab potentiostat PGSTAT302N controlled by NOVA software (Version 2.1). All measurements were performed in a custom made four-electrode glass cell with an interface area of ~1.13 cm^2. Platinum mesh was used as the counter electrodes. Ag/AgCl were the reference electrodes in both phases. Examined compounds were dissolved in aqueous and/or organic phase electrolyte solution before filling the cell. Water was used as an aqueous phase and 1.2 - DCE was used as an organic solvent in each experiment. The volume added to the cell in each phase was always exactly 2.5 mL.

Chronoamperometry allows the application of the potential difference across the interface from a region where there is no Faradaic process to a potential where a Faradaic process appears and the control of the mass transport is possible. The response of the electrochemical system of potential change is tracked in time, which results in current versus time I=f (t) graphs[195].

In classical electrochemistry a Faradaic process is a charge (electron) transfer between electrode-electrolyte interfaces which take place at the surface of the electrode. Such reactions are the subject to Faraday's law:

$$I_F = \frac{dQ}{dt} = n_e F \frac{dN}{dt} \quad (1)$$

Where, Q is the charge which passes through the working electrode, N is the amount of reactant, n_e is the number of electrons exchanged and F is the Faraday constant[196].

By measuring the variation of the current with time, we can calculate the load. Indeed we obtain the load from the following relation:

$$Q = It \quad (2)$$

Taking into consideration that in electrochemistry at ITIES the charge being transferred across the interface and give rise to a current, hence we can apply the Faraday's law for such systems:

$$Q=z_iFN \quad (3)$$

Where z_i is the charge of ion is transferred, and N is the number of moles of transferred ion.

In this chapter, cyclic voltammetry was used to determine the ion transfer from an organic phase to an aqueous phase and to initiate precipitation of cocrystals. Electrochemical experiments at the ITIES were carried out to monitor the transfer behaviour of drug's cations and anions across the LLI. The effect of pH on the ion transfer at the ITIES was studied to understand the processes occurring at the polarised LLI. In order to achieve electrochemically controlled cocrystallisation of drugs, it was important to verify that ions are transferred at the interface.

The ITIES allows the application of an external potential that can induce the transfer of the ionic species through the interface[58]. Preceding the preparation of co-crystals, it was necessary to perform the screening of the API and coformers, which comply with both: (i) the regulations of the creation of pharmaceutical cocrystals as well as with (ii) the rules governing the electrochemistry at ITIES. The studied drugs were already examined in the topic of pharmaceutical cocrystals formation[27], [40], [137]–[143]. For the purpose of the study, four drugs with low solubility in water (piroxicam, sildenafil, diclofenac and ketoprofen) and one with high solubility in water (caffeine) and chemical structure proper for creation of cocrystals were selected. Features that were mainly considered were: (i) water solubility, (ii) amphiphylic properties with $0 < \log P < 3$, (iii) electrical charge and (iv) selected chemical groups to create cocrystals.

Characterisation of the product of the metathesis reaction - piroxicamH^+-tetrakis (4-chlorophenylborate).

^{1}H NMR

In order to prove formation of PH^+TPBCl^- the ^{1}H NMR spectrum was used and the results are presented in Table 1. The marking protons are given in Figure 1.

Table 1: Chemical shifts for the 1H NMR spectrum of piroxicam, PH^+ ($C_{15}H_{13}N_3O_4S$), K^+ $TPBCl^-$ ($C_{24}H_{16}BCl_4K$). 1 proton = 0.19-unit area and PH^+ $TPBCl^-$. 1 proton = 0.75-unit area.

Chemical shift [ppm]	Shape	Area	Theoretical number of protons	Assignation
PH^+				
13.5	singlet	0.78	1	OH(1)
9.1	singlet	0.42	1	[NH(9)]
8.4	singlet	0.77	1	H(11)
8.1	doublet	1.20	2	H(14), H(2), H(5)
7.9	triplet	3.63	4	H(3), H(4), H(13)
7.2	doublet	0.95	1	H(12)
2.95	singlet	3.00	3	H(6), H(7), H(8)
1,9-2,2	triplet	1.51	3	Impurity (?)
Total		12.26	13	
K^+ $TPBCl^-$				
7.14-7.22	Multiplet (septet)	0.99	5	H(1), H(4)
7.02-7.1	doublet	1.00	5	H(2), H(3)
1.8-2.4	Triplet	0.96	5	Impurity, solvent

2.5-2.6	Singlet	0.02	0	Impurity, solvent
Total		2.97	16	
PH^+ $TPBCl^-$				
9.6	Doublet	0.95	1	H[N(10)]
9.4	doublet	0.96	1	H[N(9)]
8.5-8.6	doublet	0.95	1	H(11)
8.4	Multiplet	0.96	1	H(2)
7.9-8.1	multiplet	5.11	5	H(14), H(3), H(4), H(13), H(12)
7.7-7.8	doublet	0.51	1	H(5)
7.45-7.55	Doublet	4.39	4	$TPBCl^-$
7.35-7.45	multiplet	1.51	2	$TPBCl^-$
7.2-7.35	doublet	4.11	4	$TPBCl^-$
1.5	singlet	3.00	3	H(6), H(7), H(8)
Total	22.45	30		

Following the calculations 1 proton = 0.94-unit area, it was possible to assign protons and compare the theoretical number with the spectrum. The signals in the region of chemical shift 8.4-7.2ppm were assigned to the aromatic pyridine and benzothiazine rings [197]. The spectrum present characteristic signal of protons at 2.95 ppm, which corresponds to the methyl group and we could observe the signal at 13.5 ppm, which was for the result of the OH group.[198]

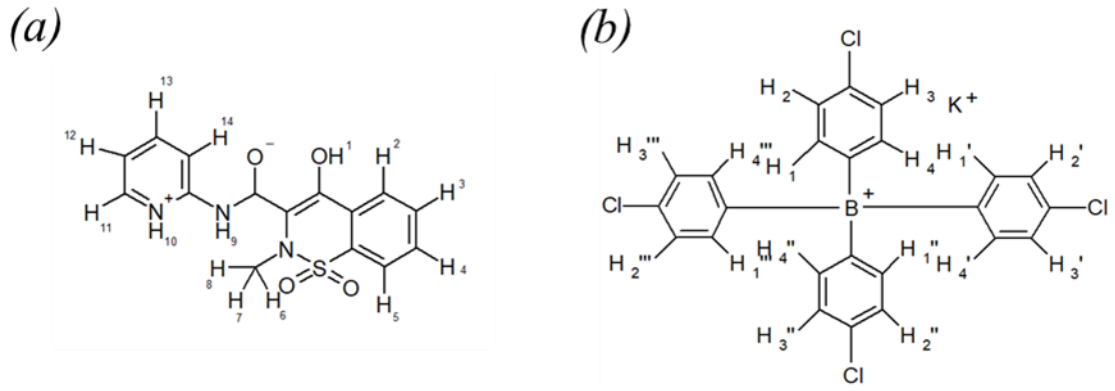

Figure 1: Assigned hydrogens in the structure of piroxicam (a) and KTPBCl (b).

The ^{1}H NMR spectrum of PH^{+} $TPBCl^{-}$ showed variation of chemical shifts of some protons comparing to the spectrum of piroxicam alone. It occurred due to the various electric states upon protonation and deprotonation of piroxicam. With decrease of pH, the protonated form of piroxicam showed up, and the differences in aromatic rings could be observed. Aromatic rings protons were up field shifted at 8.6 – 7.8 ppm upon metathesis reaction. The chemical shifts of pyridyl protons were susceptible to protonation [199]. The chemical shift could correspond to the non-covalent interaction with $TPBCl^{-}$ [197]. Between 7.55 and 7.35 ppm were the doublets and multiplets which correspond to $TPBCl^{-}$ rings. The number of protons did not correspond to the theoretical one, since the OH group vanished but the new signal at 9.6 ppm occurred which was assigned to the protonation of pyridine group and the large shift for the H (9) was be present.

Mass spectrometry

Mass spectra were used to confirm the structure of the salt of $PirH^{+}$-TPBCl. According to Table 2, the mass determined for the sample corresponded to the calculated mass. So, the mass spectrometry experiment confirmed the presence of the salt after the metathesis experiment.

Table 2: Mass determined for the PH^{+} $TPBCl^{-}$ salt prepared by metathesis.

Ion	Theoretical molecular weight [g mol^{-1}]	Control molecular weight [g mol^{-1}]	Salt molecular weight [g mol^{-1}]
PH^{+}	332.35	332.08	332.08
$TPBCl^{-}$	457.09	458.01	457.01

Total	879.57	880.09	879.09

Evidence of the absence transfer of $PirH^+$ from organic to aqueous by ionolysis followed by HPLC analysis.

Chronoamperometry

To investigate the transfer of $PirH^+$ from organic to aqueous phase the chronoamperometry experiment were performed. The initial concentration 5mM of $PirH^+$-$TPBCl^-$ in 1,2 –DCE were placed in the cell as organic phase and water were used as aqueous phase and left for approximately 5h at ΔE= -0.3 V. The applied potential assured us that $PirH^+$ should be transferred, according to the rules governing electrochemistry at the ITIES[59]. The solution after the chronoamperometry experiment was further analysed by HPLC due to determine the concentration of Pir in the aqueous solution.

In order to determinate the concentration of $PirH^+$ in the aqueous phase after the chronoamperometry process, the 500 µL of aqueous phase was collected in close proximity to the interface. Next, the 20 µl samples were injected to the HPLC to check the presence of transferred $PirH^+$ and $TPBCl^-$ in aqueous phase.

HPLC

In order to further investigate the transfer of cationic form of $PirH^+$ high performance liquid chromatography (HPLC) was used.

The mobile phase used in HPLC was acetic acid (pH 2.0, 0.05 M): methanol, and the gradient elution, initially 20:80, 10 min. 80:20, 20 min 20:80 v/v [200]. Aqueous acetic acid solution was prepared by diluting 20 mL acetic acid (100%, Sigma Aldrich) in 1000 mL highly pure water. To perform the salt effect, the small amount of $NaNO_3$ were added to the solution. In order to prepare piroxicam stock solution, 20.0 mg piroxicam was accurately weighed, dissolved and diluted to 50.0 mL in methanol. Six standard solutions ranging from 0.001 to 0.08 mM were prepared. Firstly, it was necessary to measure the retention time and peak area of piroxicam, K^+TPBCl^- and to create the calibration curve for both compounds. The retention times are presented in Table 3.

The one of piroxicam corresponds to the one found in the literature [200]. The calibration curves are presented in Figure 2.

Table 3: Retention time of piroxicam and KTPBCl.

Compound	Retention time [min]
Piroxicam	2.7
KTPBCl	6.9

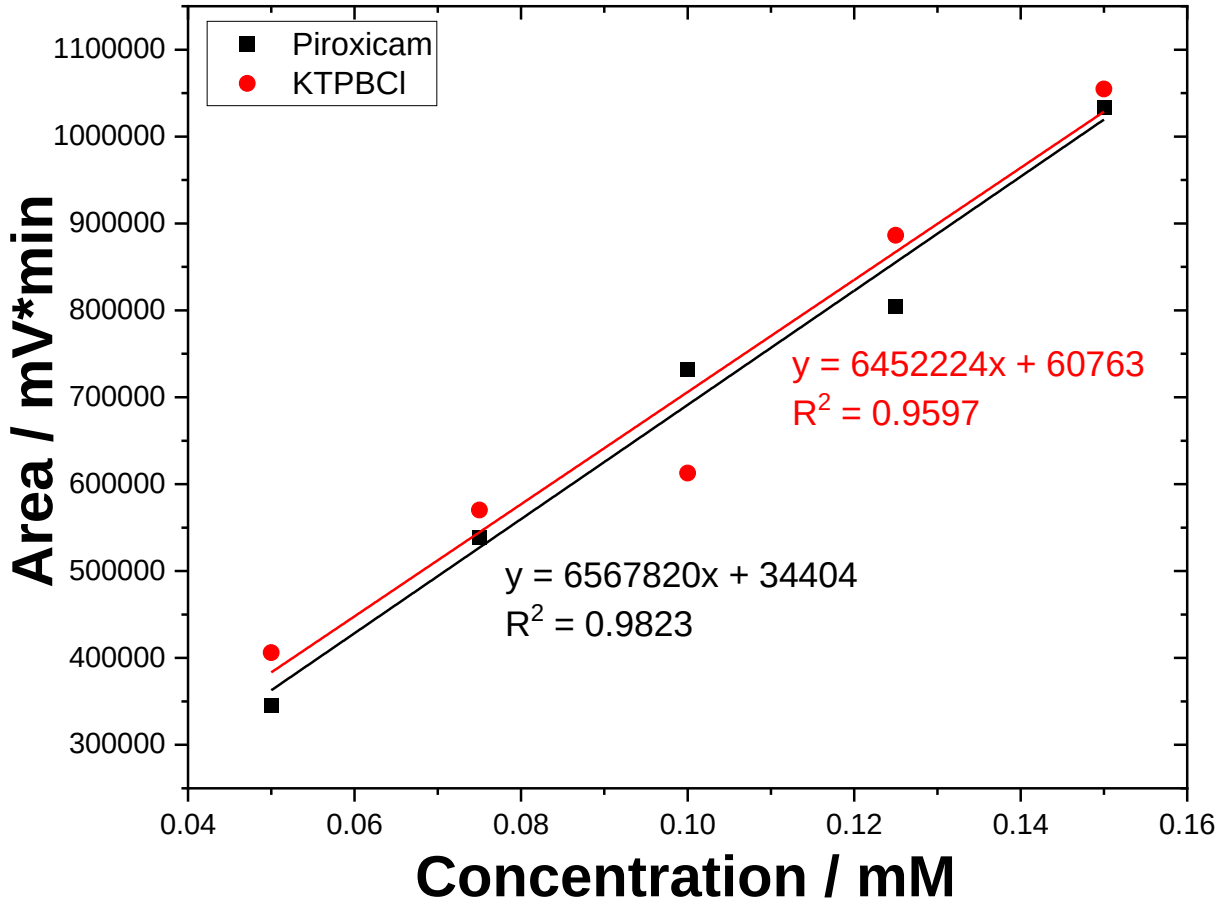

Fig 2: Calibration curve of piroxicam (black) and KTPBCl (red).

The concentration of transferred piroxicam was presented in Table 4. The concentration of transferred piroxicam was not equal in every experiment and that there was not clear analogy with time and the concentration of transferred $PirH^+$. The average concentration of piroxicam 0.000145mM (Table 4) did not correspond to the concentration calculated based on Eq. 1 and initial concentration of Pir 5 mM. The fault can derive from absence of piroxicam in the sample due to sample taking too far from interface. However, in the chromatogram on Figure 4, there is no peak of $TPBCl^-$. This is logical, because such hydrophobic anions are not transferred at ITIES.

<u>Table 4:</u> Concentration of piroxicam transferred during chronoamperometry ΔE= -0.3V based on Faraday's law.

I [A]	t [s]	Q [C]	n [mol]	c [M]
4.33E-07	1.09E+04	4.72E-03	4.89E-08	1.95E-05
3.66E-05	1.65E+04	6.04E-01	6.26E-06	2.50E-03
1.93E-06	1.72E+04	3.32E-02	3.44E-07	1.38E-04
8.97E-07	2.00E+04	1.79E-02	1.86E-07	7.44E-05

Based on the results of cyclic voltammetry and chronoamperometry, the $PirH^+$ cation was not transferred at ITIES and cocrystals formed with it cannot be electrochemically controlled. These salts proved not to be good candidates for electrochemical control of cocrystal formation at the LLI. Although, it indicated that it may be interesting to create the cocrystals of piroxicam by dissolving cocrystaling agent in aqueous phase and limit the scale of experiment to avoid the diffusion limit.

APPENDIX 2

DoE Experiments

Shake-flask experiments of selected drugs

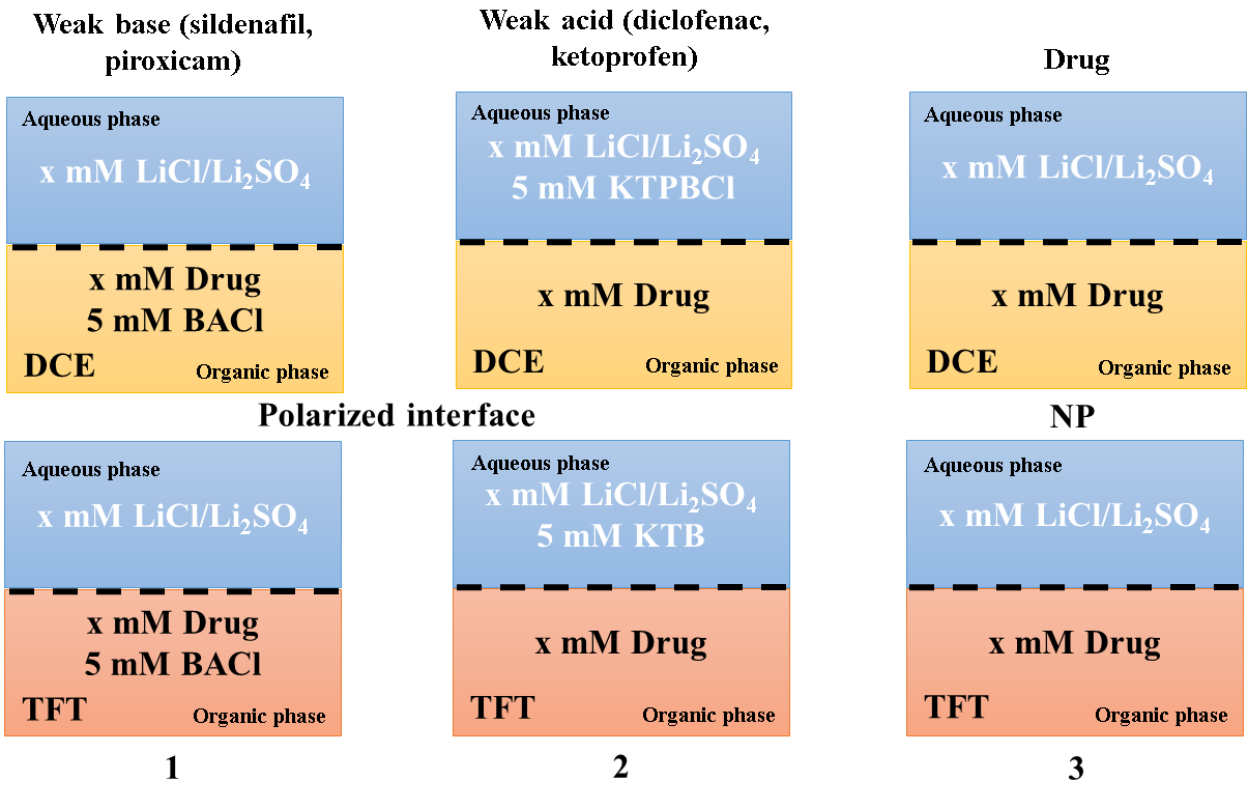

Figure 3: Experimental set up presenting chemical polarisation of the interface. BACl - Bis (triphenylphosphoranylidene) ammonium chloride; KTPBCl - potassium tetrakis (4-chlorophenyl) borate; KTB – potassium tetrakis (pentafluorophenyl) borate. The dashed line indicates the liquid-liquid interface. NP – non-polarized.

On the Figure 3 the experimental set up is presented. It consisted of two immiscible solutions in order to form the interface. The aqueous phase was a solution of 10 mM LiCl or Li_2SO_4 (Fig 3 Vial 1) and KTPBCl or KTB (Fig 3 Vial 2). The organic phase (immiscible with water) was various concentrations of tested drug in DCE (yellow) or TFT (red). Following salts were added to the organic phase of the two-phase systems to chemically polarize the interface: BACl for a low potential and KTPBCl (DCE) or KTB (TFT) for high potential. The ions present in the system are distributed in equilibrium between the aqueous and organic phases, resulting in a change of

interfacial potential ($\Delta_o^w\phi$)[156], [157]. In case of negative potential (Fig. 3 Vial 1 and 2), the standard transfer potential of BA^+ ($\Delta_o^w\phi_{BA^+}^0$ = -0.67V) is lower than the standard positive potential of lithium ($\Delta_o^w\phi_{Li^+}^0$ = 0.610 V)[91] so lithium will not transfer to the organic phase. However, when in the cell we placed KTPBCl (Fig. 3 Vial 2 DCE) or KTB (Fig. 3 Vial 2 TFT) standard transfer potential of K^+ is higher than the one of the drugs presents in the organic phase ($\Delta_o^w\phi_{K^+}^0$=0.53V) so there is an ion exchange. An additional biphasic system without salt imposing potential in organic phase was prepared as a control sample (Fig. 3 Vials 3 NP). The vials were left for 16h.

Crystallisation of drugs was investigated through shake-flask experiments. The factors that were considered were:

- form of drug (cationic, anionic, neutral)
- drug concentration
- pH
- selection of acid
- selection of aqueous electrolyte (LiCl, Li_2SO_4)
- Li^+ concentration
- interface polarization
- choice of solvent (DCE, TFT)

The composition of the following vials were projected with Design of experiments by the R software package *RcmdrPlugin.DoE*[177] and *Doe.base*[178]. This tool enabled the design, control and export of experimental conditions. For the purpose of this study the Regular (Fractional) Factorial 2-level design was found to be the more suitable to find the active factor at two levels (-1, 1) which may influence the interfacial crystallization/cocrystallization. All vials were left for 16h. Table 5 lists the factors that needed to be investigated for their effect on interfacial crystallisation. For piroxicam and sildenafil, 8 factors were considered at 2 levels and 16 runs, resulting in the experimental vials in Figure 5a and b. For ketoprofen and DFA, 7 agents were considered over 2 levels and 16 runs, resulting in the experimental vials in Figure 5c and d.

Table 5: Factors and assigned variables for DoE experiments for piroxicam.

Piroxicam				
No	Reaction condition	-1	1	Unit
1	Form of drug	Neutral	Cationic	-
2	Concentration of drug	0.5	2	mM
3	pH	0.5	1.5	-
4	Acid	HCl	HNO_3	-
5	Salt	Li_2SO_4	LiCl	-
6	Concentration of Li^+	5	10	mM
7	Polarized	no	yes	-
8	Solvent	1.2-DCE	TFT	-
Sildenafil				
1	Form of drug	Neutral	Cationic	-
2	Concentration of drug	0.5	2	mM
3	pH	0.5	2.5	-
4	Salt	Li_2SO_4	LiCl	-
5	Concentraton of Li^+	5	10	mM
6	Acid	HCl	H_2SO_4	-
7	Polarized	no	yes	-
8	Solvent	1,2-DCE	TFT	-
Ketoprofen				
1	Concentration of drug	0.5	2	mM
2	pH	7	12	-

3	Salt	Li_2SO_4	LiCl	-
4	Concentraton of Li^+	5	10	mM
5	Polarized	no	yes	-
6	Solvent	1,2-DCE	TFT	-
7	Base	LiOH	NaOH	-
Diclofenac Free Acid				
1	Concentration of drug	0.5	2	mM
2	pH	7	12	-
3	Salt	Li_2SO_4	LiCl	-
4	Concentration of Li^+	5	10	mM
5	Polarized	no	yes	-
6	Solvent	1.2-DCE	TFT	-
7	Base	LiOH	NaOH	-

(a)

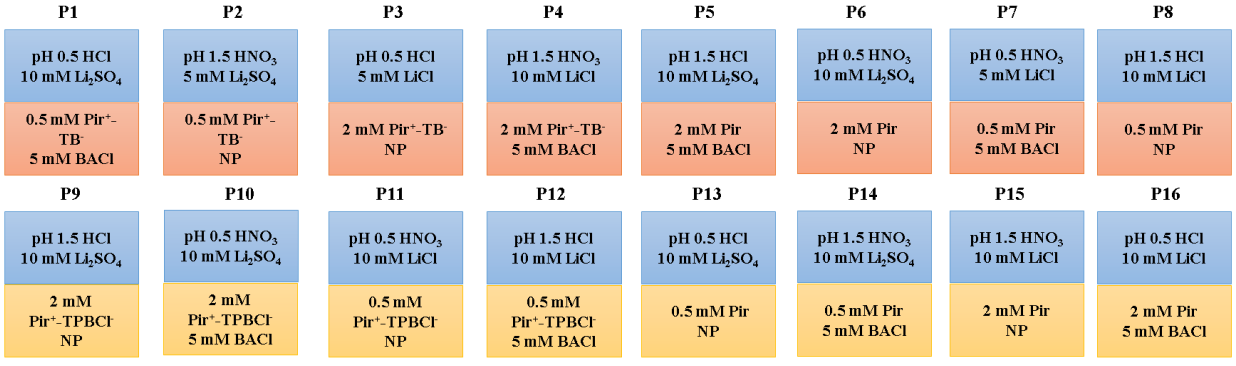

(b)

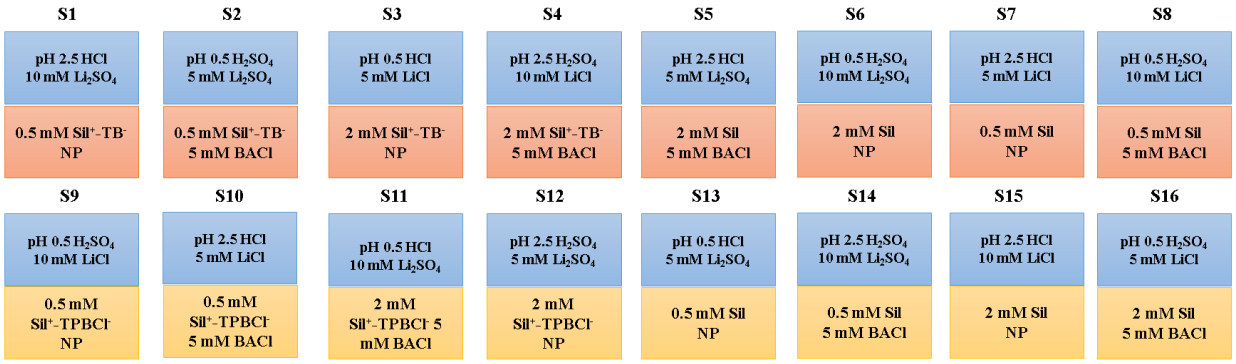

(c)

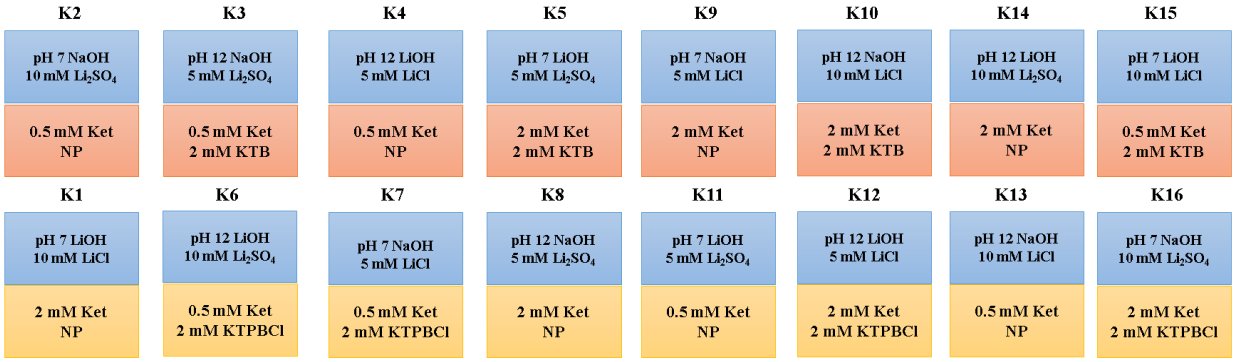

(d)

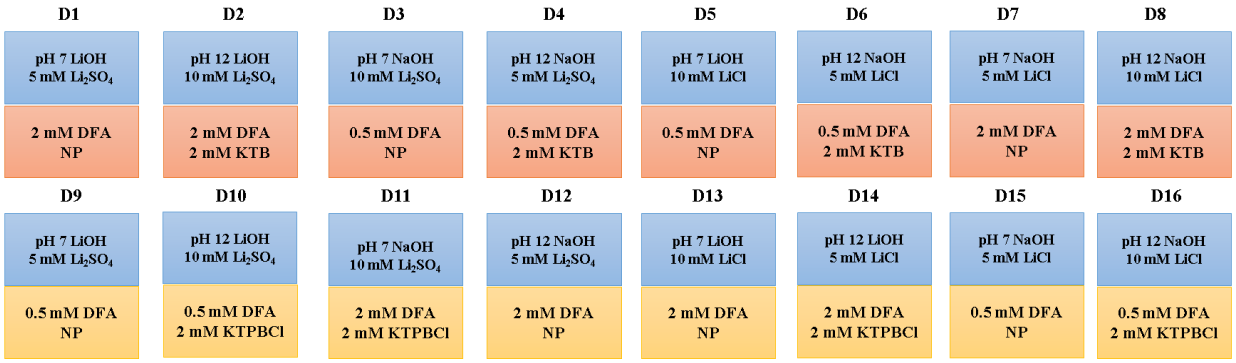

Figure 5: Experimental set up presenting chemical polarisation of the interface applied for DoE experiments of poorly water soluble drugs: piroxicam, sildenafil, ketoprofen and DHA. BACl - Bis (triphenylphosphoranylidene) ammonium chloride; KTPBCl - potassium tetrakis (4-chlorophenyl) borate; KTB – potassium tetrakis (pentafluorophenyl) borate. The dashed line indicates the liquid-liquid interface. NP – none polarized.

Shake-flask experiments of weak bases – piroxicam and sildenafil

In Table 5 are listed the factors and assigned variables for DoE experiments for piroxicam and its salt Pir^+-$TPBCl^-$. The factors that were verified are (i) drug form, that is the difference between the neutral and the cationic salt, (ii) concentration of drug between 0.5 mM and 2 mM (iii) pH of the aqueous phase 0.5 or 1.5 which favours the piroxicam protonation, (iv) acid used to change the pH, (v) aqueous phase electrolyte (vi) Li^+ concentration in aqueous phase, (vii) if the interface will be polarized or not and (viii) impact of DCE and TFT. Interface was polarized with the 5 mM concentration of BACl. This cation in organic phase cause the negative polarization which is a suitable potential for weak bases transfer.

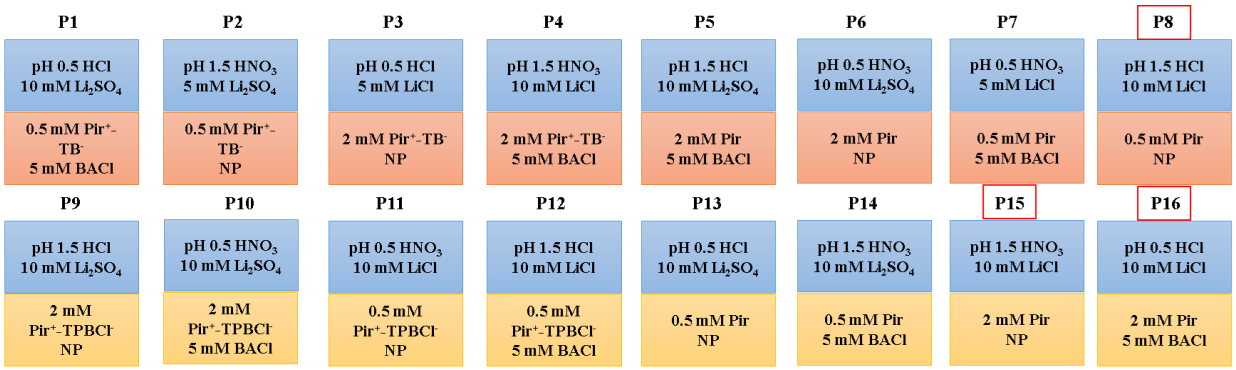

<u>Figure 6:</u> Biphasic system of piroxicam. Orange – TFT, yellow – 1.2-DCE; NP – non-polarized.

After 16 hours of experiment only in three vials (Figure 6 vials P8, P15 and P16) there were crystals found at the liquid-liquid interface. However, there was not enough precipitate to collect from the phase interface and to check the structure in Raman spectroscopy or XRD.

In Table 5 are listed the factors and assigned variables for DoE experiments for sildenafil and its salt Sil^+-$TPBCl^-$. The factors that were verified are (i) drug form, that is the difference between the neutral and the cationic salt, (ii) concentration of drug between 0.5 mM and 2 mM (iii) pH of the aqueous phase 0.5 or 2.5 which favours the sildenafil protonation, (iv) aqueous phase electrolyte (v) Li^+ concentration in aqueous phase, (vi) acid used to change the pH, (vii) if the interface will be polarized or not and (viii) impact of DCE and TFT. Interface was polarized with the 5 mM

concentration of BACl. This cation in organic phase cause the negative polarization which is a suitable potential for weak bases transfer.

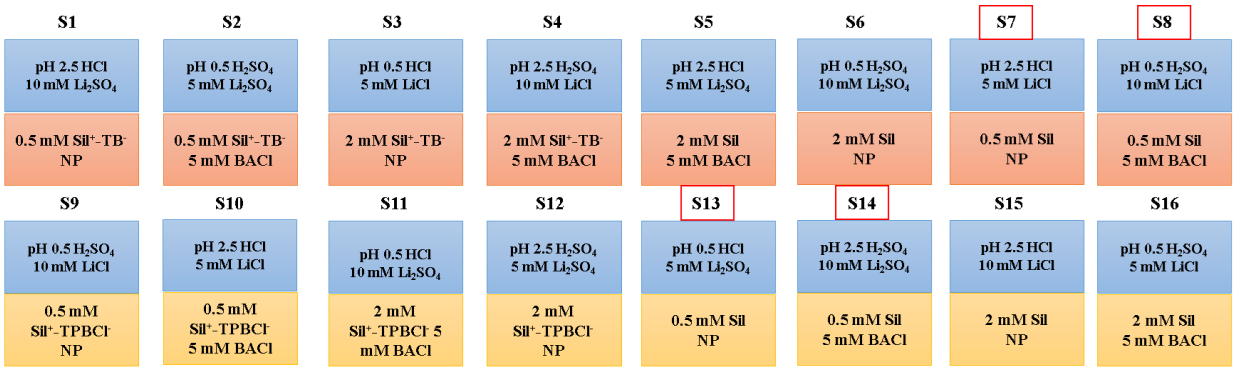

Figure 7: Biphasic system of sildenafil its salts. Orange – TFT, yellow – 1.2-DCE; NP – non-polarized.

After 16 hours of experiment only in four vials (Figure 7 vials S7, S8, S13 and S14) there were crystals found at the liquid-liquid interface. However, as with piroxicam, there was not enough precipitate to collect it from the phase boundary and check the structure by Raman spectroscopy or XRD.

Shake-flask experiments of weak acids – ketoprofen and diclofenac

In Table 5 are listed the factors and assigned variables for DoE experiments for ketoprofen. The factors that were verified are (i) concentration of drug between 0.5 mM and 2 mM (ii) pH of the aqueous phase 7 or 12 which favours the ketoprofen deprotonation, (iii) aqueous phase electrolyte (iv) Li^+ concentration in aqueous phase, (v) if the interface will be polarized or not and (vi) impact of DCE and TFT, (vii) the bases used to adjust pH of the aqueous solution. Interface was polarized with the 5 mM concentration of KTPBCl in case of DCE and KTB when TFT was the solvent of organic phase. This salt in aqueous phase caused the positive polarization which was a suitable potential for weak acid transfer.

After 16 hours of experiment some precipitation was found at the liquid-liquid interface in all the following vials on Figure 8: K2, K4, K9, K10, K6, K8, K12, K13 and K16. The deposit was present in the vials with DCE as well as TFT. The most of the deposit was found in three vials (Figure 8 vials K9 and K16). We collected small amount of product to make the analysis in Raman spectroscopy. In all the Raman spectra was found a peak characteristic for ketoprofen (1000cm^{-1}).

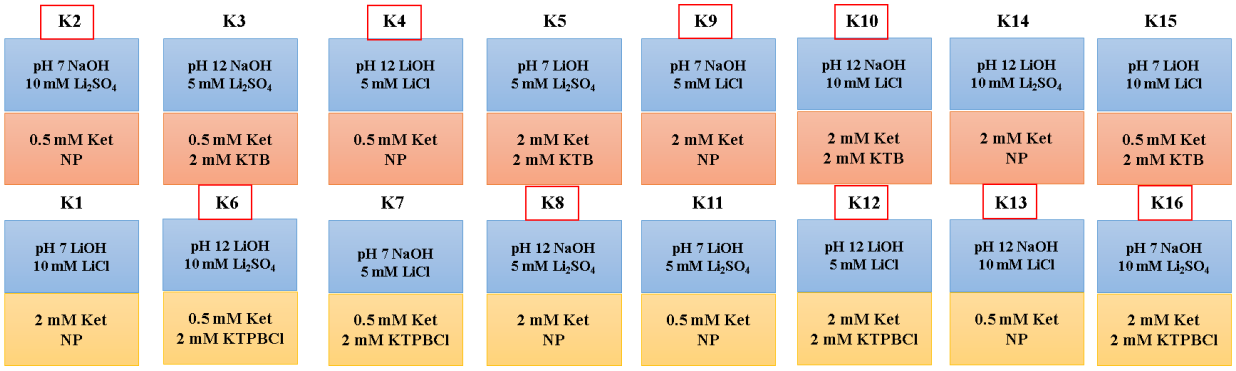

Figure 8: Biphasic system of ketoprofen. Orange – TFT, yellow – 1.2-DCE; NP – non-polarized.

In Table 5 are listed the factors and assigned variables for DoE experiments for DFA. The factors that were verified are (i) concentration of drug between 0.5 mM and 2 mM (ii) pH of the aqueous phase 7 or 12 which favours the diclofenac deprotonation, (iii) aqueous phase electrolyte (iv) Li^+ concentration in aqueous phase, (v) if the interface will be polarized or not and (vi) impact of DCE and TFT, (vii) the bases used to adjust pH of the aqueous solution. Interface was polarized with the 5 mM concentration of KTPBCl in case of DCE and KTB when TFT was the solvent of organic phase. The K^+ in aqueous phase caused the positive polarization which was a suitable potential for weak acid transfer.

After 16 hours of experiment some precipitation was found at the liquid-liquid interface in all the following vials on Figure 9: D2, D4, D5, D6, D7, D8, D9, D11, D12, D13 and D16. The deposit was present in the vials with DCE as well as TFT. The most of the deposit was found in three vials (Figure 6.4 vials D4, D8 and D11).

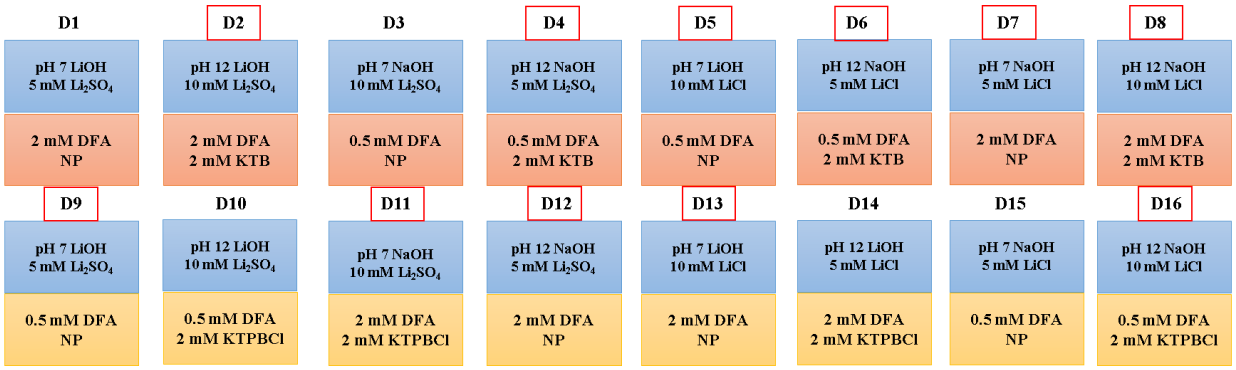

Figure 9: Biphasic system of diclofenac. Orange – TFT, yellow – 1.2-DCE; NP – non-polarized

The output results were analysed by R software however the active factors were not statistically significant.